

**Characterisation of the Role of VPS33B in Vesicular
Trafficking in Polarised Epithelial Cells.**

By

Andrew Robert Cullinane

A thesis submitted to
The University of Birmingham
for the degree of
DOCTOR OF PHILOSOPHY

College of Medicine & Dentistry
The University of Birmingham
July 2009

UNIVERSITY OF
BIRMINGHAM

University of Birmingham Research Archive

e-theses repository

This unpublished thesis/dissertation is copyright of the author and/or third parties. The intellectual property rights of the author or third parties in respect of this work are as defined by The Copyright Designs and Patents Act 1988 or as modified by any successor legislation.

Any use made of information contained in this thesis/dissertation must be in accordance with that legislation and must be properly acknowledged. Further distribution or reproduction in any format is prohibited without the permission of the copyright holder.

Abstract

Arthrogryposis, Renal dysfunction, and Cholestasis (ARC) syndrome is a multisystem disorder associated with abnormal localisation of some polarised membrane transporter proteins. Distinct apical and basolateral poles are essential for epithelial function and organ development but the molecular pathways determining the biogenesis of polarised membranes are not fully characterised. Mutations in *VPS33B*, a Sec1-Munc18 protein, account for 75% of ARC patients. Reduced expression of *VPS33B* at both the RNA and protein level was demonstrated in all ARC syndrome patients, even if mutations were not identified in *VPS33B*. A novel protein POLARIN (*PLRN*) was identified that interacts with *VPS33B*, and is crucial for *VPS33B* function. Pathogenic mutations in *PLRN* occur in ARC patients without *VPS33B* mutations. Decreased Polarín and Vps33b expression in mouse renal collecting duct cells led to abnormal localisation of specific apical membrane proteins and to disordered apical junction complex formation. In an *in vivo* model, knockdown of polarin in zebrafish resulted in defects in biliary tract development. These findings establish that a *VPS33B*-POLARIN-Rab11a intracellular trafficking pathway is functionally distinct from another *VPS33*-related pathway (*VPS33A/VPS16*) and is required for (a) normal epithelial polarisation and apical junction complex formation, and (b) normal liver and kidney development and function.

Acknowledgments

I would like to thank all the members of the Medical and Molecular Genetics Department at the University of Birmingham, with special thanks to Ania Straatman-Iwanowska and Chris Bruce for their continued help throughout the project. I would also like to thank Andreas Zaucker and Ferenc Mueller for their introduction to the zebrafish model, and Joshua Rappoport for his help with the co-localisation studies. Thanks also go to Paul Gissen and Deirdre Kelly for supervising the project, and the Children's Liver Disease Foundation (CLDF) for funding the research. I am grateful to Yoshiyuki Wakabayashi, Irwin Arias, Rachid Sougrat and Jennifer Lippincott Schwartz from the National Institutes of Child Health and Development, NIH, for allowing me work in their laboratory and their help with advanced microscopy techniques. Thanks also to Alex Knisely (King's College Hospital London), and Hartwig Wolburg (University of Tübingen) for supplying data. Finally I would like to thank my family and friends for their continued support and encouragement throughout this project, without which things would have been much more difficult.

Table Of Contents

List of Figures	VII
List of Tables.....	X
Abbreviations.....	XI
 CHAPTER 1 - INTRODUCTION	 1
1.1 – ARC Syndrome.....	2
1.2 – VPS33B	3
1.3 – Pathology of ARC Syndrome	5
1.4 – Vesicular Trafficking.....	7
1.4.1 – The Biosynthetic Pathway	9
1.4.2 – The Endocytic Pathway	9
1.4.2.1 – The ESCRT Complexes.....	10
1.5 – SNARE Proteins	12
1.6 – SNARE Interacting Proteins.....	16
1.6.1 – SM Proteins	16
1.6.2 – Rab GTPases	19
1.6.2.1 – Structural Features	19
1.6.2.2 – Localisation and Function	20
1.6.2.3 – Rab Effectors	26
1.7 – Vesicle Budding and Fusion.....	26
1.8 – The HOPS Complex	29
1.9 – The CORVET Complex	33
1.10 – Polarised Epithelia.....	35
1.11 – The Apical Junction Complex	35
1.11.1 – Adherens Junctions.....	36
1.11.2 – Tight Junctions	37
1.11.3 – The Adhesion To Polarity Model	38
1.11.4 – The Polarity To Adhesion Model	40
1.12 – Polarised Protein Trafficking.....	41
1.12.1 – Basolateral Protein Sorting.....	44
1.12.2 – Apical Protein Sorting	45
1.12.3 – The Cytoskeleton.....	46
1.13 – Summary.....	48
 CHAPTER 2 – MATERIALS AND METHODS	 50
2.1 – Materials	51
2.1.1 – DNA and RNA Analysis	51
2.1.2 – Cell Culture	52
2.1.3 – Protein Reagents	52
2.1.4 – Cloning	53
2.1.5 – Antibodies and Stains	53
2.1.6 – Zebrafish Reagents	54
2.1.7 – General Chemicals.....	54
2.2 – Methods	55
2.2.1 – Sequencing Analysis of ARC Patients	55
2.2.1.1 – Polymerase Chain Reaction.....	55

2.2.1.2 – Agarose Gel Electrophoresis	56
2.2.1.3 – Exo-SAP Reaction	56
2.2.1.4 – Sequencing	57
2.2.1.5 – Sequencing Precipitation	58
2.2.1.6 – Sequencing Analysis	58
2.2.2 – Cell Culture	58
2.2.2.1 – Transfection	59
2.2.2.2 – Collagen Culture	60
2.2.3 – RNA Analysis	60
2.2.3.1 – RNA Extraction	60
2.2.3.2 – RNA Concentration Quantification	61
2.2.3.3 – cDNA Synthesis	61
2.2.3.4 – Quantitative Real Time PCR	62
2.2.4 – Protein Analysis	64
2.2.4.1 – Protein Extraction	64
2.2.4.2 – Protein Concentration Quantification	65
2.2.4.3 – Co – Immunoprecipitation	65
2.2.4.3.1 – Antibody Conjugation	66
2.2.4.3.1 – Immunoprecipitation	67
2.2.4.4 – Membrane Protein Biotinylation	67
2.2.4.5 – Western Blotting	69
2.2.4.5.1 – SDS – PAGE	69
2.2.4.5.2 – Transfer	70
2.2.4.5.3 – Immunodetection	71
2.2.4.5.4 – Membrane Stripping and Re-probing	71
2.2.4.5.5 – Densitometry	72
2.2.4.6 – Yeast – 2 – Hybrid Screen	72
2.2.5 – Cloning	72
2.2.5.1 – IMAGE Clones	72
2.2.5.2 – Cloning Strategy	73
2.2.5.3 – Proofreading PCR	74
2.2.5.4 – Agarose Gel Extraction	75
2.2.5.5 – Restriction Digestion	75
2.2.5.6 – Ligation	77
2.2.5.7 – Transformation	77
2.2.5.8 – Site Directed Mutagenesis	78
2.2.5.9 – Colony Screening	78
2.2.5.10 – Plasmid Sequencing	79
2.2.5.11 – Plasmid Purification	80
2.2.5.12 – DNA Concentration Quantification	81
2.2.6 – Cell Analysis	81
2.2.6.1 – Immunofluorescence Confocal Microscopy	81
2.2.6.1.1 – Co-localisation Analysis	82
2.2.6.1.2 – Live Cell Imaging	83
2.2.6.2 – Pulse Chase Experiments	83
2.2.6.3 – shRNA	84
2.2.6.4 – Trans-Epithelial Resistance Assay	84
2.2.6.5 – Paracellular Diffusion Assay	85

2.2.6.6 – Calcium Switch Experiments	85
2.2.7 – Zebrafish Experiments.....	85
2.2.7.1 – In-Situ Hybridisation	86
2.2.7.1.1 – Probe Synthesis	86
2.2.7.1.2 – Hybridisation	87
2.2.7.1.3 – Detection.....	89
2.2.7.2 – Morpholino Oligonucleotide Injections	90
2.2.7.2.1 – mRNA Rescue	90
2.2.7.3 – PED-6 Treatment.....	92
2.2.7.4 – Immunostaining	92
CHAPTER 3 – MOLECULAR INVESTIGATIONS OF ARC SYNDROME PATIENTS AND DEVELOPMENTAL EXPRESSION OF VPS33 HOMOLOGUES	94
3.1 – Introduction and Overview	95
3.1.1 – ARC Patients	95
3.1.2 – Developmental Expression of VPS33 Homologues.....	96
3.2 – Aims.....	96
3.3 – Results	97
3.3.1 – Mutation Analysis of VPS33B in ARC Patients	97
3.3.2 – ARC Patient Expression of VPS33A and VPS33B.....	98
3.3.2.1 – Patient 21	100
3.3.3 – ARC Patients’ Cellular Phenotype	103
3.3.4 – Developmental Expression of VPS33 Homologues.....	103
3.3.4.1 – Human Expression.....	103
3.3.4.2 – Mouse Expression	108
3.4 – Discussion.....	111
3.4.1 – ARC Patients	111
3.4.2 – Developmental Expression	112
CHAPTER 4 – VPS33B INTERACTING PROTEINS	115
4.1 – Introduction and Overview	116
4.2 – Aims.....	117
4.3 – Methodologies	117
4.3.1 – Yeast–2–Hybrid System.....	117
4.3.2 – Live Cell Imaging.....	120
4.3.3 – FRET	121
4.4 – Results	125
4.4.1 – Yeast – 2 – Hybrid Screen.....	125
4.4.2 – In-silico Analysis of POLARIN	127
4.4.3 – Confirmation of Interaction	130
4.4.4 – Co-localisation of VPS33B-POLARIN Clusters with Organelle Markers	134
4.4.5 – The VPS33B-POLARIN Complex Interacts with Rab11a	137
4.4.6 – POLARIN Interacts with the HOPS Complex Proteins	141
4.4.7 – PLRN Mutation Analysis of ARC Syndrome Patients.....	149
4.5 – Discussion.....	151

CHAPTER 5 – EFFECT OF VPS33B AND POLARIN KNOCKDOWN ON AN EPITHELIAL CELL LINE.....	155
5.1 – Introduction and Overview	156
5.2 – Aims.....	157
5.3 – Results	158
5.3.1 – Polarin and Vps33b shRNA in mIMCD-3 cells	158
5.3.3 – Apical Junction Complex Defects	162
5.3.4 – Abnormal mIMCD-3 Cell Differentiation and Growth.....	175
5.4 – Discussion.....	179
 CHAPTER 6 – USE OF MORPHOLINOS AGAINST PLRN IN ZEBRAFISH EMBRYOS MIMICS THE ARC SYNDROME LIVER DISEASE.....	183
6.1 – Introduction and Overview	184
6.1.1 – Zebrafish as a Model Organism	184
6.1.2 – ARC Syndrome Zebrafish Model Using vps33b.....	186
6.1.2.1 – Expression Pattern of vps33b	186
6.1.2.2 – Effect of vps33b Knockdown on Zebrafish Development	188
6.2 – Aims.....	191
6.3 – Results	191
6.3.1 – Expression Pattern of polarin	192
6.3.2 – Effect of polarin Knockdown in Zebrafish.....	192
6.4 – Discussion.....	198
 CHAPTER 7 – DISCUSSION	202
7.1 – VPS33B Interacts with a Novel Protein POLARIN	203
7.2 – Deficiencies of VPS33B or POLARIN in Development and Disease.	204
7.3 – VPS33B and POLARIN Function Through a Rab4-Rab11 Pathway	208
7.4 – Conclusions	210
7.5 – Future Experiments.....	211
7.5.1 – Molecular and Cellular Experiments	211
7.5.2 – Animal Models	213
 APPENDICES.....	215
Appendix 1	216
Appendix 2	219
Appendix 3	220
Appendix 4	224
Appendix 5	225
 REFERENCES	228
 PEER REVIEWED PUBLICATIONS.....	241

List of Figures

Chapter 1

Figure 1.1 – The predicted structure of the VPS33B protein.	4
Figure 1.2 – Immunostaining of ARC patient biopsies.	6
Figure 1.3 – Schematic diagram of vesicular trafficking.	8
Figure 1.4 – An overview of the endocytic pathway.	11
Figure 1.5 – Schematic diagram demonstrating the domain structure of SNARE proteins.	14
Figure 1.6 – The SNARE cycle.	16
Figure 1.7 – Proposed mechanisms of binding of SM protein to the SNARE complex.	18
Figure 1.8 – The Rab GTPase cycle.	21
Figure 1.9 – Intracellular vesicular pathways and localisation of selected Rab proteins.	23
Figure 1.10 – The Rab GTPase nucleotide and membrane attachment cycle.	25
Figure 1.11 – Steps of vesicle budding and fusion.	29
Figure 1.12 – Rab5 to Rab7 conversion on early to late endosomes.	31
Figure 1.13 – The HOPS and CORVET complexes and models for their intermediates.	34
Figure 1.14 – The adhesion to polarity model of epithelial polarisation.	39
Figure 1.15 – Protein trafficking pathways in polarised epithelial cells.	43

Chapter 3

Figure 3.1 – Quantitative Real Time PCR (qRT-PCR) of VPS33A and VPS33B in ARC syndrome patients' fibroblasts.	101
Figure 3.2 – Immunoblotting of VPS33B in control and ARC patients' fibroblasts.	102
Figure 3.3 – Cellular phenotype of ARC patient fibroblasts.	104
Figure 3.4 – Expression of VPS33A in human foetal and adult kidney, liver and brain samples.	105
Figure 3.5 – Expression of VPS33B in human foetal and adult kidney, liver and brain samples.	106
Figure 3.6 – Analysis of VPS33B expression in human foetal kidneys, liver and brain by immunoblotting.	107
Figure 3.7 – Mouse embryonic expression of Vps33a and Vps33b at E14.5.	109
Figure 3.8 – Expression of Vps33a and Vps33b in individual mouse embryonic tissues at E14.5.	110

Chapter 4

Figure 4.1 – Yeast-2-hybrid method of identifying putative protein-protein interactions.	119
Figure 4.2 – Live cell imaging techniques.	122
Figure 4.3 – FRET analysis of protein interactions.	124
Figure 4.4 – Species alignment of POLARIN.	128
Figure 4.5 – Amino acid alignment of POLARIN and VPS16 C- terminal domain.	129
Figure 4.6 – Co-immunoprecipitation of VPS33 homologues with VPS16 and POLARIN.	131
Figure 4.7 – Confocal fluorescence photomicrographs of VPS33 homologues with POLARIN.	132

Figure 4.8 – YFP-VPS33B FLIP confocal live-cell microscopy.	133
Figure 4.9 – Negative co-localisation of VPS33B-POLARIN clusters with organelle markers.	135
Figure 4.10 – Positive co-localisation of VPS33B-POLARIN clusters with organelle markers.	136
Figure 4.11 – Endogenous co-localisation of VPS33B and Rab11a.	138
Figure 4.12 – Co-localisation of the VPS33B-POLARIN clusters with the transferrin receptor.	139
Figure 4.13 – FRET analysis of VPS33B-POLARIN complex and Rab11a.	142
Figure 4.14 - Reciprocal co-immunoprecipitation of endogenous VPS33B and Rab11a.	143
Figure 4.15 – Co-immunoprecipitation of the VPS33B-POLARIN complex and Rab11a. ..	144
Figure 4.16 – Co-immunoprecipitation of POLARIN with the HOPS complex.	145
Figure 4.17 – Confocal immunofluorescence of POLARIN with the HOPS complex.	146
Figure 4.18 – POLARIN interaction with VPS18.	148
Figure 4.19 – Model for conventional HOPS complex and VPS33B-POLARIN complex.	153

Chapter 5

Figure 5.1 – Assessment of Polarin or Vps33b knockdown in mIMCD-3 cells.	159
Figure 5.2 – Endogenous Vps33b staining in Control-, Polarin- and Vps33b-shRNA cells.	160
Figure 5.3 – Abnormal localisation of apical markers in Polarin- and Vps33b-shRNA cells.	163
Figure 5.4 – Reduced expression of membrane CEA in Polarin- and Vps33b-shRNA cells.	164
Figure 5.5 – Co-localisation of apical membrane markers with Polarin-Vps33b clusters in mIMCD-3 cells.	165
Figure 5.6 – Trans Epithelial Resistance (TER) in Control-, Polarin- and Vps33b-shRNA cells.	167
Figure 5.7 – Paracellular diffusion in Control-, Polarin- and Vps33b-shRNA cells.	168
Figure 5.8 – Paracellular diffusion in Control-, Polarin- and Vps33b-shRNA cells grown in low calcium medium.	169
Figure 5.9 – Immunostaining of tight and adherens junction proteins in Control-, Polarin-, Vps33b-shRNA and dominant negative Rab11a cells.	171
Figure 5.10 – Western blots of tight and adherens junction proteins in wild type, Control-, Polarin-, and Vps33b-shRNA cells.	173
Figure 5.11 – Freeze fracture electron micrographs of Control-, Polarin- and Vps33b-shRNA cells.	174
Figure 5.12 – Immunostaining of ARC syndrome patient liver biopsies for E-Cadherin.	176
Figure 5.13 – Abnormal cell growth of Polarin- and Vps33b-shRNA cells.	177
Figure 5.14 – Abnormal cell proliferation in Polarin-, and Vps33b-shRNA cells.	178

Chapter 6

Figure 6.1 – In-situ hybridisation of vps33b in zebrafish embryos and larvae.	187
Figure 6.2 – vps33b knockdown disrupts zebrafish intrahepatic biliary development.	189
Figure 6.3 – vps33b knockdown disrupts biliary ultrastructure.	190
Figure 6.4 – In-situ hybridisation of plrn in zebrafish embryos and larvae.	193
Figure 6.5 – Knockdown of plrn in the zebrafish does not cause any morphological abnormalities detectable by light microscopy.	195
Figure 6.6 – plrn deficiency causes a decreased gall bladder size.	196
Figure 6.7 – Quantification of gall bladder size in plrn deficient zebrafish larvae.	197
Figure 6.8 – Immunofluorescence confocal micrographs of E-Cadherin in sections of 5 dpf larvae livers.	199

List of Tables

Chapter 1

Table 1.1 – Localisation, expression and function of selected Rab GTPases.	22
---	----

Chapter 3

Table 3. 1 – Mutations in VPS33B identified in ARC Patients.	99
---	----

Chapter 4

Table 4.1 – Yeast – 2 – Hybrid results.	126
Table 4.2 – PLRN is mutated in ARC syndrome.	150

Abbreviations

AJ – Adherens Junction

AJC – Apical Junction Complex

AOBS – Acousto-Optical Beam Splitter

AP – Adaptor coat Protein

ARC – Arthrogryposis, Renal dysfunction and Cholestasis (syndrome)

ARE – Apical Recycling Endosome

ATP – Adenosine Tri-Phosphate

BFP – Blue Fluorescent Protein

BLAST – Basic Local Alignment Search Tool

BP – Base Pairs

BSA – Bovine Serum Albumin

BSEP – Bile Salt Export Protein

CCD – Charge-Coupled Device

CCV – Clathrin Coated Vesicle

CFP – Cyan Fluorescent Protein

CV – Constitutive secretory Vesicles

CEA – Carcino-Embryonic Antigen

CMV – CytoMegalovirus

CNS – Central Nervous System

COP – COat Protein

CORVET – class C cORE Vacuole Endosome Tethering

CRB – CRumB (complex)

CRE – Common Recycling Endosome

DIG – DIGoxigenin

dHPLC – denaturing High Performance Liquid Chromatography

DMEM – Dulbecco’s Modified Eagle’s Medium

DMSO – DiMethyl SulfOxide

DN – Dominant Negative

DPF – Days Post Fertilisation

EC – Extracellular Cadherin

ECL – Enhance ChemiLuminescence

EDTA – Ethylene Diamine Tetraacetic Acid

EE – Early Endosome

EEA1 – Early Endosome Antigen 1

(E)GFP – (Enhanced) Green Fluorescence Protein

EGTA – Ethylene Glycol Tetraacetic Acid

EMT – Epithelial-to-Mesenchymal Transition

ER – Endoplasmic Reticulum

ES – Embryonic Stem (cells)

ESCRT – Endosomal Sorting Complex Required for Transport

EtBr – Ethidium Bromide

(E)YFP – (Enhanced) Yellow Fluorescent Protein

FBS – Foetal Bovine Serum

FITC – Fluorescein IsoThioCyanate

FLIP – Fluorescence Loss In Photobleaching

FRAP – Fluorescence Recovery After Photobleaching

FRET – Förster (or Fluorescence) Resonance Energy Transfer

GAP – Rab GTP Activating Proteins

GDP – Guanosine Di-Phosphate

GDI – Rab GDP Dissociation Inhibitor

GEF – Guanine nucleotide Exchange Factors

GFP – Green Fluorescence Protein

γ GT – Gamma Glutamyl Transpeptidase

GM130 – Golgi Marker of 130 kDa

GPI-AP – GlycosylPhosphatidyl-Inositol Anchored Protein

GTP – Guanosine Tri-Phosphate

HA – HemAgglutinin

HEK293 – Human Embryonic Kidney 293 (cells)

HEPES – HydroxyEthyl-1-PiperazineEthaneSulfonic acid

HOPS – HOmotypic fusion and vacuole Protein Sorting

HPF – Hours Post Fertilisation

HPS – Hermansky-Pudlak Syndrome

HRP – Horse Radish Peroxidase

IgG – Immunoglobulin G

IP – ImmunoPrecipitation

IVS – InterVening Sequence

LAMP-1 – Lysosome Associated Membrane Protein 1

LDL – Low Density Lipoprotein

LE – Late Endosome

MDCK – Madin-Darby Canine Kidney

MESAB – MEthylSulfonate ethyl-3-AminoBenzoate

mIMCD-3 – Murine Inner Medullary Collecting Duct -3 (cells)

MO – Morpholino Oligonucleotide

MPR – Mannose-6-Phosphate Receptor

MRP2 – Multidrug Resistance Protein 2

NSF – N-ethylmalamide Sensitive Factor

MVB – Multi-Vesicular Body

NISCH – Neonatal Ichthyosis associated with Sclerosing CHolangitis (syndrome)

OD – Optical Density

PAR – Partitioning defective (complex)

PBS – Phosphate Buffered Saline

PBST – Phosphate Buffered Saline with 0.1% Tween-20

PCR – Polymerase Chain Reaction

PFAM – Protein FAMilies

PFIC – Progressive Familial Inter-hepatic Cholestasis

Pi – Inorganic Phosphate

PM – Plasma Membrane

PTU – Phenyl-2-ThioUrea

PVDF – PolyVinylidene DiFluoride

qRT-PCR – Quantitative Real Time PCR

RE – Recycling Endosome

REP – Rab Escort Protein

RFP – Red Fluorescent Protein

RPM – Revolutions Per Minute

RV – Regulated secretory Vesicles

SDS – Sodium Dodecyl Sulfate

SDS PAGE – Sodium Dodecyl Sulfate PolyAcrylamide Gel Electrophoresis

shRNA – Short Hairpin RNA

SM – Sec1/Munc18

SNARE – Soluble N-ethylmaleimide sensitive Receptors

SNP – Single Nucleotide Polymorphism

SSC – Saline Sulphate Citrate

SV – Synaptic Vesicle

TCS – True Confocal System

TEM – Transmission Electron Microscopy

TEMED – TetraMethylEthyleneDiamine

TER – Trans Epithelial Resistance

TGN – Trans-Golgi Network

TJ – Tight Junction

TRITC – Tetramethyl Rhodamine IsoThioCyanate

VAMP – Vacuole Associated Membrane Protein

VPS – Vacuole Protein Sorting

vWF – von Willebrand factor

WB – Western Blot

WT – Wild Type

ZO – Zonula Occludens

CHAPTER 1 - INTRODUCTION

1.1 – ARC Syndrome

Arthrogryposis, Renal dysfunction and Cholestasis (ARC) syndrome (MIM:208085) is a severe disorder affecting multiple organ systems with an autosomal recessive mode of inheritance [1]. The cardinal features of the syndrome are congenital neurogenic arthrogryposis, renal tubular dysfunction and neonatal cholestasis with bile duct hypoplasia and low gamma glutamyl transpeptidase (γ GT) activity. Platelet dysfunction is also common, to the extent that half of the patients that undergo diagnostic biopsy have a life-threatening haemorrhage as a result. Other features include ichthyosis, mild dysmorphic features, absent corpus callosum and recurrent infections resulting in severe metabolic acidosis and worsening nephrogenic diabetes insipidus [2]. Children born with ARC syndrome are often small at birth and fail to thrive. Death usually occurs during the first year of life despite medical intervention. The affected individuals usually die due to an infection leading to dehydration and acidosis [3].

In 2004, the genetic locus for ARC syndrome was mapped to chromosome 15q26.1 using autozygosity mapping on 6 affected consanguineous families. Nine different germline mutations were identified in the *VPS33B* gene in 14 supposed unrelated families [1]. Subsequent mutation screening identified further mutations in *VPS33B* in around 75% of ARC syndrome patients [2;4]. Furthermore, several families with no detectable *VPS33B* mutations did not link to the 15q26.1 locus, thus suggesting locus heterogeneity and other causative gene(s) for ARC syndrome.

1.2 – VPS33B

The *VPS33B* gene contains 23 coding exons with a transcript length of 2,488 base pairs. The transcript encodes the VPS33B protein comprising of 617 amino acids with a predicted unglycosylated weight of 70.6 kDa [5]. In multicellular organisms there are 2 homologues of the yeast Vps33 gene and protein, VPS33A and VPS33B. There is only 31% identity and 51% similarity between VPS33A and VPS33B, suggesting different functions for the 2 proteins. However, both contain a Sec1 like domain that belongs to the Sec1/Munc18 (SM) family of proteins. SM proteins are thought to tightly bind to members of the syntaxin family of target SNAREs (Soluble N-ethylmaleimide sensitive REceptors) and may alter interdomain interactions and influence vesicle-to-target SNARE complex formation [6]. The predicted structure of VPS33B in complex with syntaxin-1 is shown in Figure 1.1.

The function of VPS33B has not been extensively studied in mammals, however, the yeast homologue, Vps33, is a Class C vacuole protein sorting protein and is required for vacuole biogenesis [7]. Mutations in the genes encoding Class C VPS complex proteins (Vps11, Vps16, Vps18, Vps33 or Vps39) all have the same phenotype, and hence the reason why they belong to the same group of VPS proteins. The phenotype comprises of severe intracellular acid-base imbalance, amino acid pool deficiency, and temperature sensitive growth failure [7]. In *Drosophila melanogaster* the yeast Vps33 homologue, *Car*, localises to the endosomal compartment. However, it has been shown that this protein is a homologue of human VPS33A and not VPS33B [8]. A hypomorphic allele of *Carnation* causes the carnation eye colour mutant believed to be due to abnormal lysosome delivery and pigment granule biogenesis [9;10].

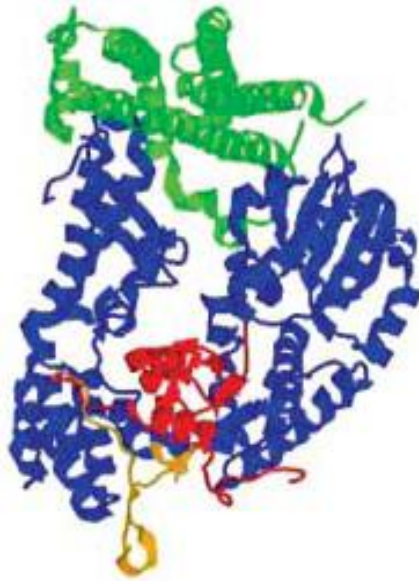


Figure 1.1 – The predicted structure of the VPS33B protein.

VPS33B is shown in blue, red and orange and in complex with the t-SNARE, Syntaxin-1 (green). Red region demonstrates C-terminal region of the protein and the orange shows the sequence absent in VPS33A. [8]

1.3 – Pathology of ARC Syndrome

The identification of mutations in *VPS33B* in ARC syndrome patients, and the protein products' putative function implicates a disorder of vesicular trafficking in the pathogenesis of the condition [1]. Indeed, immunostaining of ARC patients' liver biopsies with antibodies against CEA (Carcino Embryonic Antigen), CD13 (alanyl aminopeptidase) and γ GT, all of which should be restricted to the apical or canalicular membrane, revealed mislocalisation to the basolateral membrane (Figure 1.2). These findings were not observed in age-matched controls or in patients diagnosed with PFIC (Progressive Familial Inter-hepatic Cholestasis), a group of conditions with cholestasis and low γ GT as a feature. Immunostaining of kidney biopsies with CD26 (dipeptidyl peptidase) also revealed disordered localisation of the apical antigen to the basolateral membrane [1;11].

As mentioned previously, patients with ARC syndrome may have a bleeding tendency leading to life-threatening haemorrhage even if clotting studies and platelet counts are normal. In 2005 Lo et al. characterised the platelets from ARC patients and observed reduced aggregation, abnormal morphology, elevated numbers of δ -granules and completely absent α -granules [12]. The α -granules are a principal storage site for proteins involved in haemostasis and wound healing including fibrinogen, von Willebrand factor (vWF), thrombospondin and factor V [13]. However, *VPS33B* is expressed in megakaryocytes and not in platelets, suggesting a role in intracellular vesicular trafficking and platelet granule biogenesis. Therefore, *VPS33B* is essential for the development of platelet α -granules but not for their subsequent secretion [12].

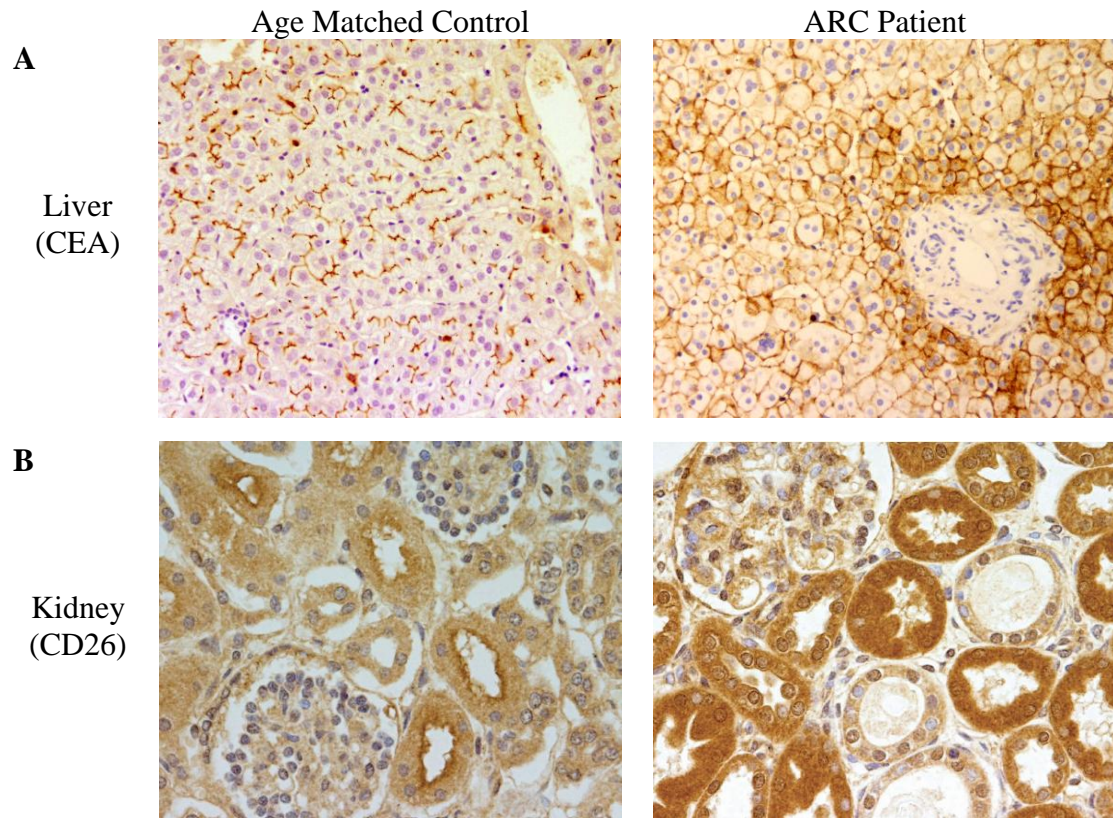


Figure 1.2 – Immunostaining of ARC patient biopsies.

A, CEA staining of an ARC patient liver biopsy compared to an age matched control sample. Staining is limited to the canalicular (apical) membrane in the control but mislocalised to all membranes in the patient. **B**, A similar effect is seen in the ARC patient's kidney biopsy when stained with CD26. [1]

1.4 – Vesicular Trafficking

VPS33B has a predicted but undefined function in vesicular trafficking pathways. In eukaryotic cells, vesicular trafficking and membrane fusion plays an essential role in maintaining physiological integrity and function of distinct intra-cellular organelles [14;15]. A well-studied example is the delivery of protein cargo vesicles from the secretory pathway to the lysosome, or vacuole in yeast, allowing for appropriate lipid and protein composition of the lysosomal membrane and their luminal content [16].

Vesicular trafficking ultimately leads to the delivery of cargo from one compartment or organelle to another via membrane-bound vesicle intermediates (Figure 1.3). The process involves a vesicle that buds off the donor organelle and eventually fuses with the correct target organelle through the interaction of vesicle and target-SNAREs (called v- and t-SNAREs respectively) [17]. The specificity of the delivery is enforced by specific SNARE interactions, and is also mediated by SNARE interacting proteins such as SM and Rab GTPase proteins, which modulate the interaction [6;18]. Further details of vesicle budding and fusion will be discussed later in section 1.7 after the necessary protein complexes have been introduced in the following sections.

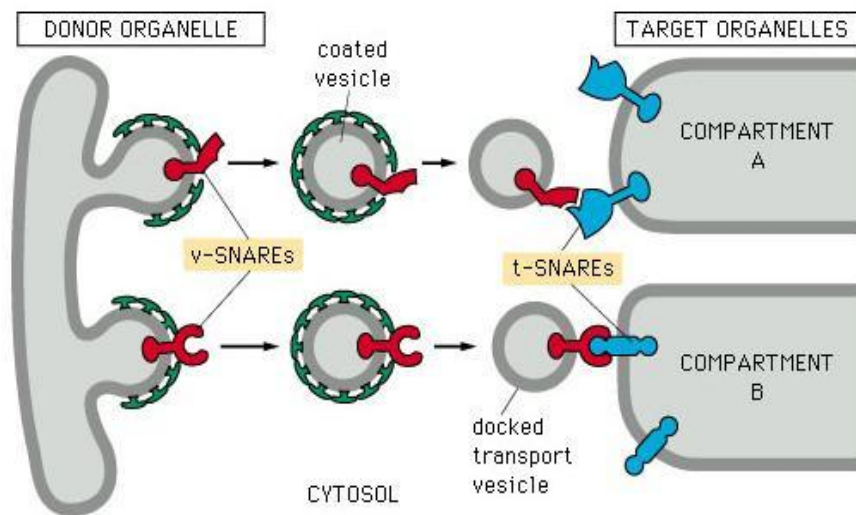


Figure 1.3 – Schematic diagram of vesicular trafficking.

Carrier or transport vesicles bud off the donor organelle and fuse with the correct target organelle. Vesicular trafficking is cargo specific, which is regulated in part by vesicle or v-SNARE and target or t-SNARE molecules. [19]

In general, there are two major routes of vesicular traffic within non-polarised cells depending on the direction of flow in relation to the plasma membrane. These are termed the biosynthetic and endocytic routes. Vesicular trafficking pathways in polarised epithelial cells are discussed later in section 1.12.

1.4.1 – The Biosynthetic Pathway

The biosynthetic route deals with the trafficking of *de novo* proteins synthesised in the cytosolic ribosomes to their final required destination. In the endoplasmic reticulum (ER), the synthesised polypeptides are folded and sometimes can undergo oligomerisation to form multi-subunit protein complexes. When these necessary events have occurred the proteins are sorted into transport vesicles by the cargo-sorting machinery and are transported to the cis side of the Golgi apparatus, where post-translational modifications tend to occur. The proteins travel through the Golgi apparatus and emerge at the trans-Golgi network (TGN) where they are again sorted into vesicles for trafficking to their final destination [20].

1.4.2 – The Endocytic Pathway

The endocytic route is used to internalise molecules from the extracellular space and plasma membrane. They are carried from their original location to peripheral early sorting endosomes where they are either recycled back to their original location via recycling endosomes, or degraded through the late endosome and lysosome pathway (Figure 1.4) [21;22].

Early endosomes play a crucial role in co-ordinating vesicular transport between the plasma membrane, the TGN and the lysosome [23]. They have a pleiomorphic structure composed of vesicular and tubular domains that are physically connected, but maintain their separate identity due to their specific complement of Rab GTPases (see section 1.6.2) [24]. Over time, endocytosed proteins concentrate on intraluminal vesicles that accumulate in the vesicular structures of the early endosomes, giving rise to Multi-Vesicular Bodies (MVBs) [24].

Accompanying the physical MVB maturation process, the MVB also moves towards the cell centre from the cell periphery. Proteins that are not ubiquitinated, and hence destined for recycling back to the plasma membrane are removed from the MVB into the tubular structures of early endosomes [24]. Once all recycling proteins have been removed, all remaining ubiquitinated proteins are degraded by the MVB fusing with late endosomes and in turn lysosomes [25]. These fusion steps release the contents of the MVB vesicle into the lumen of lysosomes, where the vesicles and protein cargo are degraded by the action of lysosomal hydrolases (proteases and lipases) [23].

1.4.2.1 – The ESCRT Complexes

In both yeast and mammalian cells, proteins that function in the MVB pathway are referred to as class E VPS proteins [23]. Deletion of any of the Class E VPS components results in the mislocalisation of MVB cargoes to the lysosome or vacuole and the accumulation of endosomal cargoes in large aberrant structures adjacent to the vacuole, called the class E compartment [26;27].

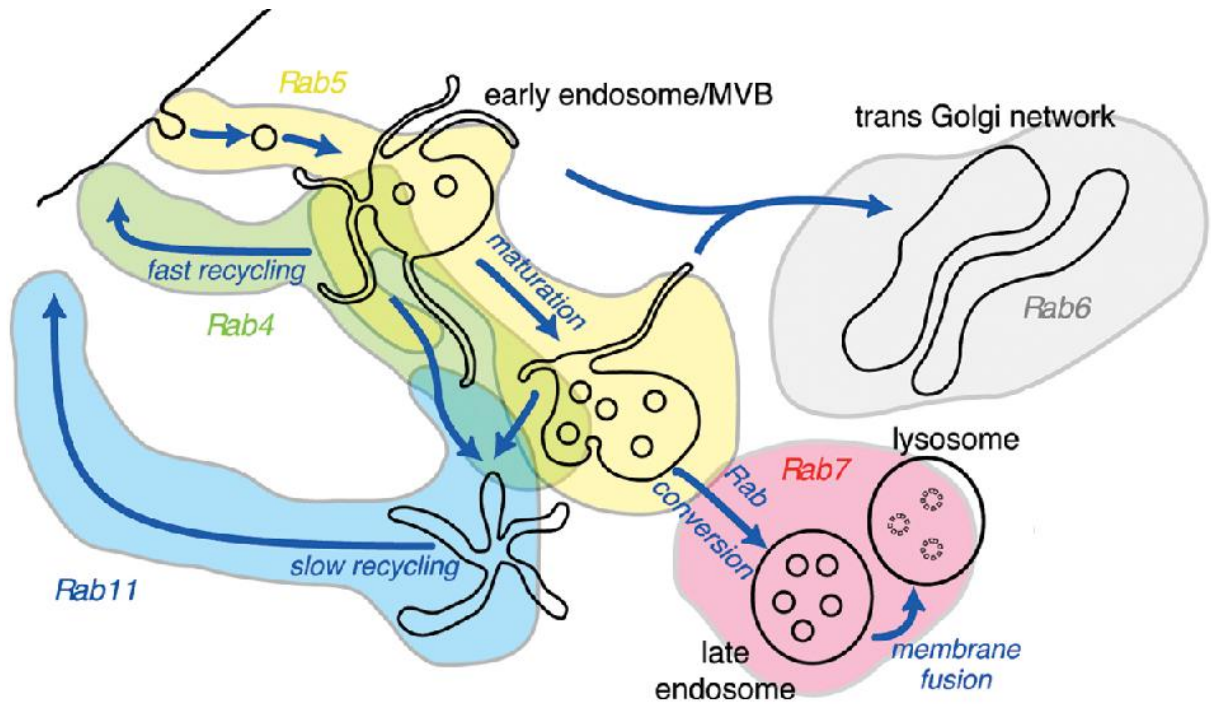


Figure 1.4 – An overview of the endocytic pathway.

Proteins are endocytosed from the plasma membrane into Rab5 positive early endosomes. Over time, endocytosed proteins concentrate on intraluminal vesicles that accumulate in the vesicular structures of the early endosomes, giving rise to Multi-Vesicular Bodies (MVBs).

The movement of the MVB from the cell periphery to the cell centre accompanies the maturation of the MVB. Non-ubiquitinated proteins are removed from the MVB into tubular structures and are either recycled back to the plasma membrane through Rab4 or Rab11 positive endosomes, or trafficked to the TGN. Ubiquitinated proteins remain in the MVB, which fuse with late endosomes and in turn lysosomes, for degradation of the cargo. [Adapted from 24]

The majority of the class E VPS proteins form three distinct complexes called the Endosomal Sorting Complex Required for Transport (ESCRT) –I, -II and –III [23]. These complexes function sequentially in sorting endocytosed proteins into the MVB pathway and MVB vesicle formation [28;29]. Ubiquitinated proteins, destined for lysosomal degradation are recruited into the MVB by the direct interaction with ubiquitin binding domains within the ESCRT-I and -II complexes.

The human homologues of the yeast class E VPS proteins have been identified and seem to function in the ESCRT complexes in the same manner as their yeast counterparts [23;28]. This suggests that mechanism of endocytic trafficking is conserved from yeast to humans.

1.5 – SNARE Proteins

Söllner and Rothman first suggested the concept and the name of SNARE proteins over 15 years ago [30;31]. There are 25 members of the protein superfamily in yeast, and 36 in humans. SNARE proteins are central to the fusion of lipid membranes [32]. All SNARE proteins are formed by domain structures, which includes a central evolutionary conserved SNARE motif comprised of a stretch of between 60 and 70 hydrophobic amino acids arranged in heptad repeats [33]. SNARE proteins were first characterised by their preferred location on either vesicle (v-) or on target (t-) membranes, however over time this was proven to be too simplistic, as it did not take into account homotypic fusion and that SNARE proteins can have multiple sites of action [34]. An *in-silico* amino acid search and alignment of the SNARE proteins revealed that most v-SNAREs had an arginine (R) residue in the middle of the SNARE domain, and are now called R-SNAREs accordingly. The other members of the

SNARE family (predominantly t-SNARES) have either a glutamine (Q) or aspartate residue present, and are now called Q-SNAREs [35]. Further classification of the latter group gave the Q_a-, Q_b- and Q_c- sub groups (Figure 1.5).

Upon membrane contact SNARE proteins form trans-SNARE complexes, also called SNAREpins [36]. Several groups have solved the crystal structure of trans-SNARE complexes, and in all cases it has been shown that the complex comprises of four SNARE domains forming helical coiled coils with each other [37;38]. Moreover the complex is made up of one R-SNARE and one of each of the Q-SNAREs. It was first believed that formation of the trans-SNARE complex lead to lipid membrane fusion through the action of NSF (N-ethylmaleimide Sensitive Factor). However, in a cell-free system where full-length SNARE proteins were reconstituted onto liposome membranes, fusion still occurs [39]. Nevertheless NSF greatly enhanced fusion *in vivo*, and was shown to be involved with the disassembly and recycling of the complex [40]. Taken together these findings suggest that the assembly of the complex drives fusion and NSF disassembles the complex so that it can function again, completing the cycle (Figure 1.6).

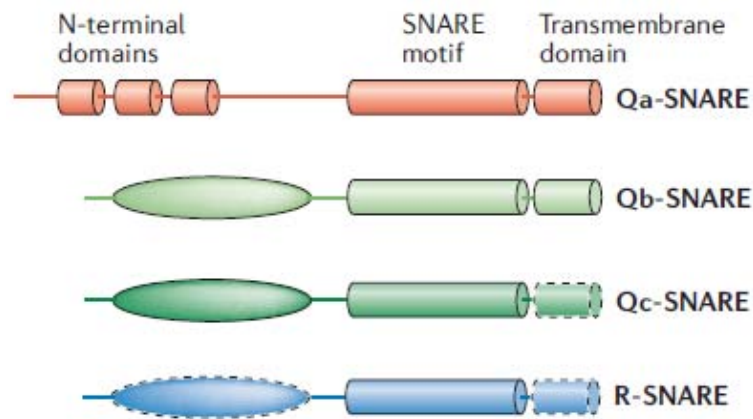


Figure 1.5 – Schematic diagram demonstrating the domain structure of SNARE proteins. Each SNARE protein has a characteristic SNARE domain with a variable N-terminal region. Dashed lines surrounding domains represent domains that are missing in some subfamily members. Q_a SNAREs have three antiparallel helix bundles in the N-terminal region. The variable N terminal regions of Q_b , Q_c and R- SNAREs are represented as oval shapes. A SNARE complex is formed by one of each of these sub-families. [Adapted from 33]

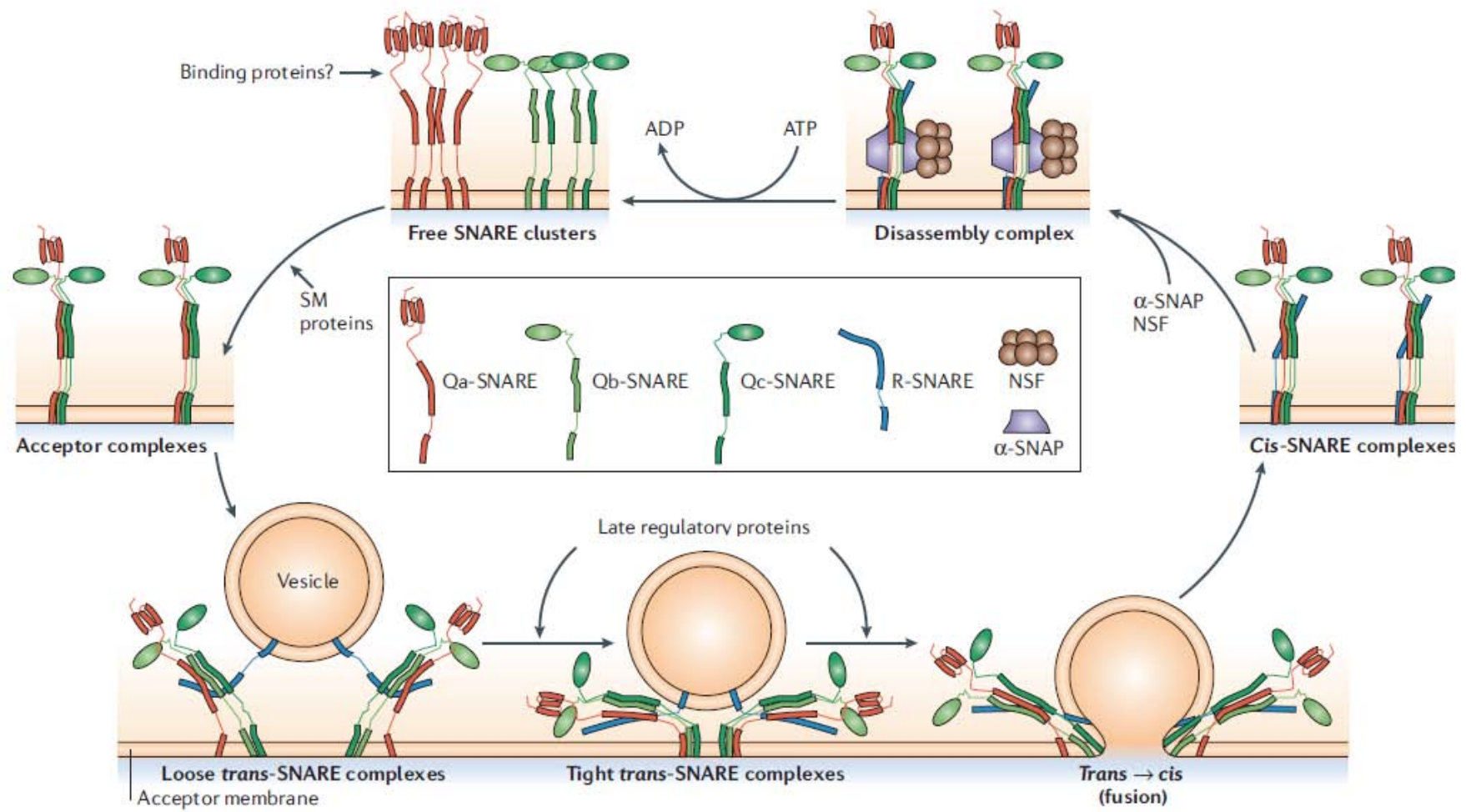


Figure 1.6 – The SNARE cycle.

In this example Q-SNAREs can be found on the target membrane and the R-SNARE on the vesicle. Firstly, the acceptor complex is formed on the target membrane, from one of each of the Q-SNAREs, by the proposed action of SM proteins. This now interacts with the R-SNARE by making coiled coils and forming the loose then tight trans-SNARE complex. The free energy obtained by this conformational change drives membrane fusion. After fusion NSF and α -SNAP disassemble the cis-SNARE complex, and through ATP hydrolysis returns the SNARE proteins to their original free state. [33]

1.6 – SNARE Interacting Proteins

The original hypothesis by Rothman et al. in 1994, suggested that SNARE proteins alone controlled the specificity of vesicle fusion, however, it was shown in the liposome system that SNARE proteins are much more promiscuous *in vitro* than they are *in vivo* [34;41]. Several families of proteins have now been suggested to both facilitate and regulate SNARE interactions, and the best characterised families are the SM proteins and small Rab GTPases [6;42;43].

1.6.1 – SM Proteins

There are seven members of the SM (Sec1/Munc18) family of cytosolic proteins in vertebrates and these include munc18-1, munc18-2, munc18-3, Sly1, VPS45, VPS33A and VPS33B. The exact function of SM proteins remains unclear, despite the crystal structure of some members being resolved [44]. There have been various mechanisms of action proposed depending on the family member. Nevertheless, all are believed to bind either directly or indirectly to the Q-SNARE complex (predominantly t-SNAREs) in different states throughout the cycle [45].

Based on structural information and biochemical studies, there are currently four different ways that SM proteins are proposed to bind SNARE proteins. These include binding of SM proteins to the closed conformation of syntaxin, the assembled SNARE complex, the N-terminal region of syntaxin and through a multi sub-unit complex [46]. See Figure 1.7 for more information and examples. Binding of yeast Vps33 to its cognate syntaxin, Vamp3 is mediated by a 6-member protein complex, called the HOmotypic fusion and vacuole Protein Sorting (HOPS) Complex (see section 1.8 for more details) [47].

SM proteins were initially thought to exert an inhibitory effect on SNARE complex formation because of the binding pattern of SM proteins to monomeric SNARE molecules (Figure 1.7 - A, C and D). This was certainly the case when these proteins were over-expressed alone in cells. For example, when Munc18-2 was over expressed in Caco-2 cells, a polarised epithelial cell line, there was inhibition of the syntaxin 3 based SNARE complex formation and transport of P75, an apical membrane marker [48]. However, further experiments where the SM protein was co-over expressed with its' cognate syntaxin released the inhibition [49]. These findings suggest that there is a delicate stoichiometric balance required for normal membrane trafficking, and that SM proteins are likely to exert a regulatory as opposed to purely an inhibitory effect.

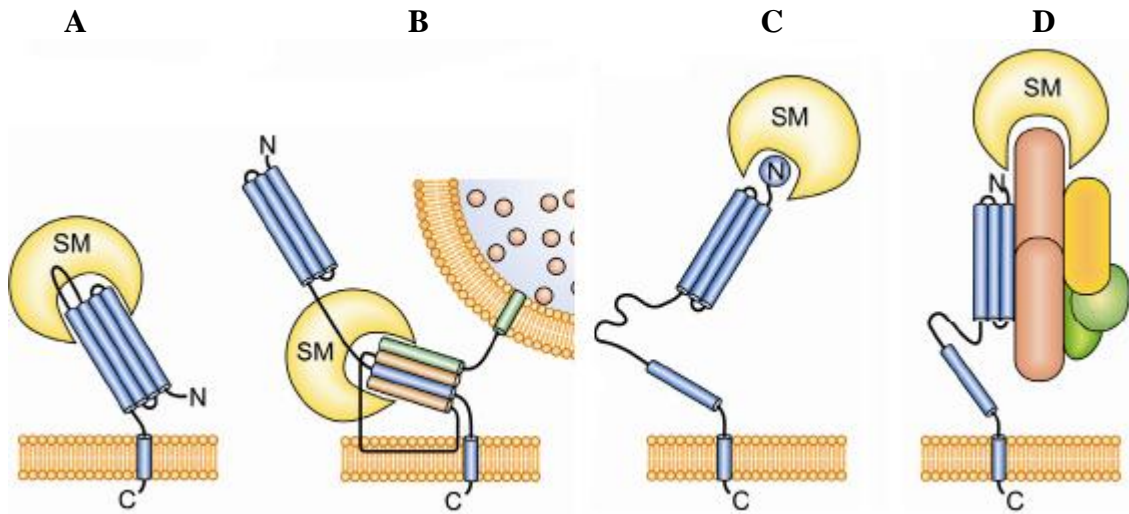


Figure 1.7 – Proposed mechanisms of binding of SM protein to the SNARE complex. The syntaxin is shown in blue and SM proteins in yellow. An example for each is given in brackets. **A:** The SM protein binds to the closed conformation of syntaxin (Munc18-1 and syntaxin 1a). **B:** Binding of the SM protein to the assembled SNARE complex (yeast Sec1 with a complex of Sso, Snc and Sec9). **C:** Binding to the N-terminal regions of syntaxin (Vps45 and Tlg2). This mode of binding allows for interaction with SNARE molecules that are in and out of complex. **D:** An indirect association of the SM protein with the SNARE molecule (Vps33 and Vamp3). [Adapted from 46]

1.6.2 – Rab GTPases

These small GTPases are the largest family of the known membrane trafficking proteins. In yeast there are 11 Rab isoforms, 29 in *C. elegans* and *D. melanogaster* and more than 60 variants in humans. Interestingly there are only 5 isoforms that are conserved from yeast to human which are Rab1 (Ypt1), Rab5 (Ypt5), Rab6 (Ypt6), Rab7 (Ypt7) and Rab11/Ypt31, suggesting an essential and conserved function for these proteins [50]. Furthermore, in several cases a mammalian Rab protein can functionally replace its' yeast homologue demonstrating conserved functions of the proteins [51].

1.6.2.1 – Structural Features

It is believed that the majority of different Rab proteins are a result of gene duplication, as sub-families of Rab isoforms have been identified with between 75% and 95% DNA sequence identity and overlapping protein functions [51]. Rab GTPases differ the most in their C termini, which have been shown to be involved in subcellular targeting, allowing for greater specificity between the Rab proteins [52]. In contrast, the GDP and GTP binding regions are highly conserved.

The crystal structures for several Rab proteins, including mouse Rab3 [53], *Plasmodium falciparum* Rab6 [54] and yeast Ypt5 [55], have been solved. These identified a fold that is essentially present in all Ras superfamily members, and is the region of the protein involved in GDP or GTP binding. This region comprises of a six-stranded β -sheet, consisting of 5 parallel and 1 antiparallel strands, surrounded by 5 α -helices [53-55]. Furthermore, the

crystal structures of GDP- and GTP bound forms of yeast Sec4, revealed 2 different conformations of the proteins depending on the nucleotide status, giving rise to the first idea of a Rab GTPase cycle (Figure 1.8) [56].

Similar to that of other small Ras-like GTPases, Rab proteins function as a molecular switch by cycling between a GTP bound active form to a GDP bound inactive form (Figure 1.8) [20]. There needs to be a delicate regulation between these 2 forms to achieve successful trafficking, and this is accomplished by 2 families of proteins. These are called Rab Guanine nucleotide Exchange Factors (Rab GEFs) and Rab GTP Activating Proteins (Rab GAPs). The GTP bound form recruits specific effector proteins, which usually links the vesicle and target membranes to the cytoskeleton [57;58]. Rab proteins and their tethers add another layer of complexity, specificity and regulation to SNARE mediated membrane fusion [59].

1.6.2.2 – Localisation and Function

The majority of Rab proteins have a ubiquitous pattern of expression in all cells and tissues, however some have a tissue specific localisation, such as Rab3a and Rab27 (Table 1.1) [51]. Within cells, Rab proteins are localised to the cytoplasmic surface of various distinct organelles (Table.1.1 and Figure 1.9) allowing specificity in vesicular trafficking.

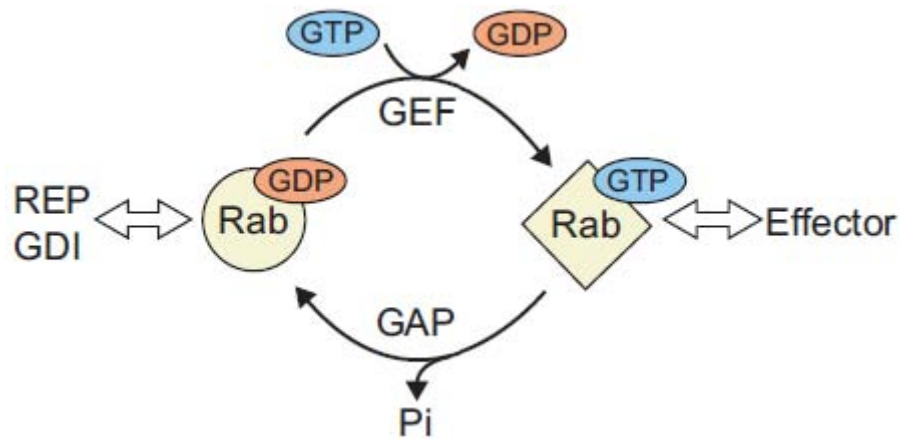


Figure 1.8 – The Rab GTPase cycle.

The Rab GTPase switches between GDP- and GTP- bound forms, which have different conformations. Conversion from the GDP- to the GTP- bound form is caused by nucleotide exchange, catalysed by a GDP/GTP Exchange Factor (GEF). Conversion from the GTP- to the GDP- bound form occurs by GTP hydrolysis, facilitated by a GTPase activating protein (GAP). The GTP-bound form interacts with effector molecules, whereas the GDP bound form interacts with Rab escort proteins (REP) and GDP dissociation inhibitor (GDI). Pi = inorganic phosphate. [51]

Name	Localisation	Expression	Function
Rab1a	ER + cis-Golgi	Ubiquitous	ER to Golgi transport
Rab2a	ER + cis-Golgi	Ubiquitous	Golgi to ER retrograde transport
Rab3a	SV	Neuronal	Regulation of neurotransmitter release
Rab4a	EE	Ubiquitous	Endocytic recycling
Rab5a	EE, CCV + PM	Ubiquitous	Budding, motility and fusion in endocytosis
Rab6a	Golgi	Ubiquitous	Retrograde Golgi traffic
Rab7a	LE	Ubiquitous	Late endocytic traffic
Rab8a	TGN + PM	Ubiquitous	TGN to PM traffic
Rab9a	LE	Ubiquitous	LE to TGN traffic
Rab11a	RE + TGN	Ubiquitous	Endocytic recycling via RE and TGN
Rab27	Melanosomes Granules	Melanocytes Platelets Lymphocytes	Movement of lytic granules and melanosomes towards PM

Table 1.1 – Localisation, expression and function of selected Rab GTPases.

Abbreviations: ER – endoplasmic reticulum, SV – synaptic vesicle, EE – early endosome, CCV – clathrin coated vesicle, PM – plasma membrane, LE – late endosome, TGN – trans Golgi network and RE – recycling endosome. [42;51;60;61] See Figure 1.8 for a schematic diagram.

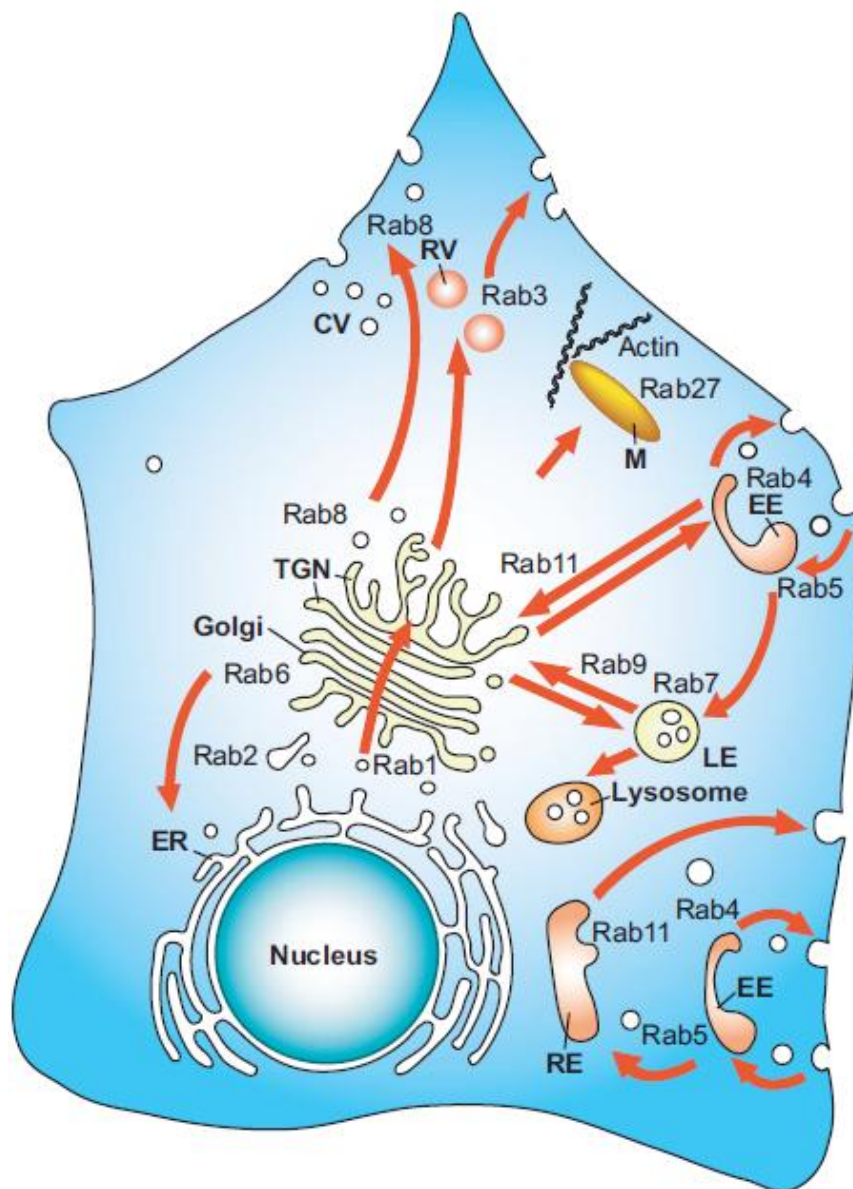


Figure 1.9 – Intracellular vesicular pathways and localisation of selected Rab proteins. The biosynthetic pathway transports proteins from the endoplasmic reticulum (ER) through the Golgi complex to the cell surface. In the trans-Golgi Network (TGN), molecules can enter either constitutive secretory vesicles (CV) or regulated secretory vesicles (RV). In the endocytic pathway, material internalised from outside the cell reaches the early endosomes (EE) first and can be recycled back to the surface, either directly or via a perinuclear recycling endosome (RE) compartment. Proteins that are internalised can also be delivered to late endosomes (LE) and lysosomes for degradation. The localisation of selected mammalian Rab proteins in the membrane compartments participating in these transport processes are indicated. [51]

Rab GTPases' reversible membrane localisation is dependent on post-translational modifications of a cysteine motif at the extreme C termini. These cysteine motifs include CXXX, CC, CXC or CCXXX, where X is any amino acid, with 1 or 2 highly hydrophobic geranyl-geranyl groups [62]. Rab Escort Proteins (REPs) present the newly synthesised Rab protein to geranyl-geranyl transferase, allowing the post-translational modification to occur [63]. REPs also chaperone the modified Rab proteins to their correct membrane, which is thought to involve membrane receptors that recognise the specific Rab-REP complexes [63;64]. Rab GTPases that are in complex with REPs are in the inactive GDP bound form, whereas insertion into the membrane and dissociation with the REP is associated with the exchange of GDP to GTP, catalysed by a Rab GEF (Figure 1.10) [63]. Upon GTP hydrolysis, which is catalysed by a Rab GAP, the Rab GTPase is released from the membrane. A Rab GDP Dissociation Inhibitor (GDI) mediates the retrieval of geranyl-geranylated GDP bound form Rab proteins from the intracellular membranes [65]. GDI can also present geranyl-geranylated GDP bound Rab proteins to specific membranes, and thus serves as a recycling factor that allows several rounds of membrane association and dissociation of the Rab protein [66].

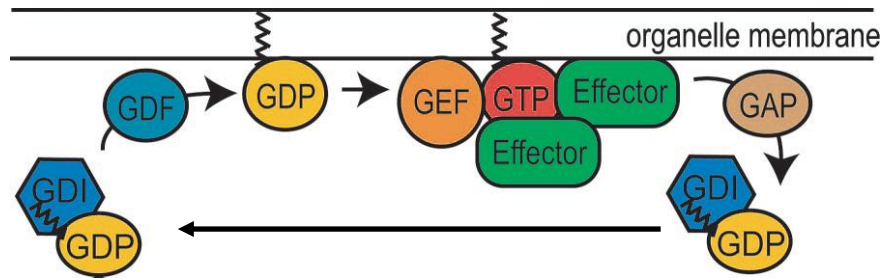


Figure 1.10 – The Rab GTPase nucleotide and membrane attachment cycle. Inactive, GDP-bound Rab GTPases are bound to GDI, which prevents membrane attachment and maintains cytoplasmic solubility. Membrane attachment of Rab GTPases requires the function of GDF (GDI Displacement Factor), which dissociates the Rab from the GDI. Subsequently, a specific GEF exchanges the bound GDP for GTP on the Rab molecule. This leads to its' activation and allows the Rab GTPase to fulfil its function in membrane trafficking by binding to specific effector proteins. Finally, a specific GAP inactivates the Rab GTPase by accelerating the hydrolysis of GTP to GDP. The inactive GDP bound form dissociates from the membrane and re-binds to GDI and the process starts again. [Adapted from 59]

1.6.2.3 – Rab Effectors

Rab GTPases function as regulators of specific intracellular trafficking pathways, and the key to their function is the recruitment of effector molecules that bind exclusively to their GTP bound form [42]. Rab effector molecules are a very heterogeneous group of proteins, of which some are coiled coil proteins involved in membrane tethering or docking, whilst others are enzymes or cytoskeleton-associated proteins [51]. The role of the yeast Vps33 homologue, and the complexes in which it forms, as Rab effector molecules will be discussed in sections 1.8 and 1.9.

Rab effector molecules can also have protein sorting functions. The best-characterised example is the retrograde trafficking of the Mannose-6-Phosphate Receptors (MPRs) from late endosomes to the TGN [59]. TIP47, a Rab9 effector, directly binds to MPRs, thus leading to the accumulation of MPRs on late endosomes, and allowing their transport back to the TGN using the appropriate Rab GTPase (Table 1.1) [67].

1.7 – Vesicle Budding and Fusion

The budding of transport vesicles off the donor compartment and the selective incorporation of cargo into the forming vesicle are both mediated by coat proteins [68]. These protein coats are macromolecular structures that are assembled from monomeric coat proteins located in the cytosol of cells [69]. The coat proteins recognise sorting signals in the cytosolic domains of transmembrane cargo proteins, with examples of such proteins being clathrin, and members of the COPI and COPII complexes [69]. The polymerised coat proteins deform flat regions of

membrane into round buds, eventually leading to the formation of transport vesicles, which contain the protein cargo and a R-SNARE (Figure 1.11) [70].

Once the vesicle has fully formed and closed, the coat proteins are disassembled and recycled back to the cytosol for future use. The vesicle is then targeted to the appropriate acceptor compartment, using specific Rab proteins and their effectors for movement along the cytoskeleton [51]. The specific Rab protein also binds to tethering factors that are present on the acceptor compartment, and thus physically links the transport vesicle to the acceptor compartment [51]. The close proximity of the 2 compartments now allows the R- and Q-SNAREs to interact with each other from their N- to their C-termini, creating a zippering action, bringing the 2 membranes closer together [33]. The formation of the trans-SNARE complex generates enough energy for the membranes to fuse and the cargo to be delivered to the acceptor compartment [33].

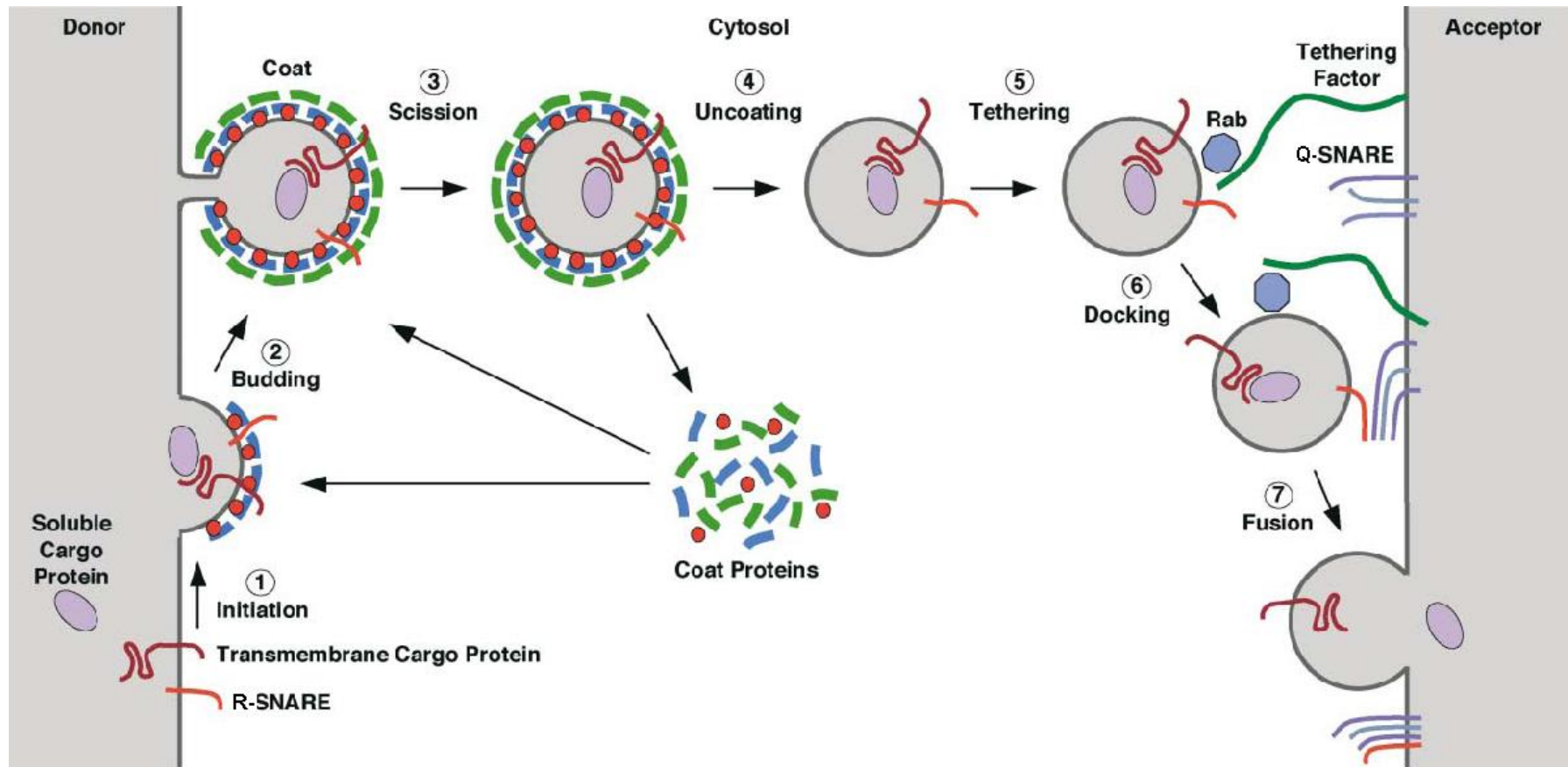


Figure 1.11 – Steps of vesicle budding and fusion.

(1) Initiation of coat assembly: The membrane-proximal coat components (blue) are recruited to the donor compartment by binding to a membrane-associated GTPase (red). Transmembrane cargo proteins and SNAREs begin to gather at the assembling coat. (2) Budding: The membrane-distal coat components (green) are added and polymerise into a mesh-like structure. Cargo becomes concentrated and membrane curvature increases. (3) Scission: The neck between the vesicle and the donor compartment is severed either by direct action of the coat or by accessory proteins. (4) Uncoating: The vesicle loses its coat due to various events including inactivation of the small GTPase, and the action of uncoating enzymes. Cytosolic coat proteins are then recycled for additional rounds of vesicle budding. (5) Tethering. The “naked” vesicle moves to the acceptor compartment, possibly guided by the cytoskeleton, and becomes tethered to the acceptor compartment by the combination of a GTP bound Rab and a tethering factor. (6) Docking: The Q- and R-SNAREs assemble into a four-helix bundle. (7) This “trans-SNARE complex” promotes fusion of the vesicle and acceptor lipid bilayers. Cargo is transferred to the acceptor compartment, and the SNAREs are recycled as shown in Figure 1.5. [69]

1.8 – The HOPS Complex

The yeast class C VPS proteins (Vps11, Vps16, Vps18 and Vps33) combined with Vps39 and Vps41 form the HOMotypic vacuole Proteins Sorting (HOPS) complex. Studies in yeast showed that this complex binds Ypt7 (Rab7), which in turn initiates vesicle tethering or docking [47]. The HOPS complex is found in a larger cis-SNARE complex, until Sec18 (NSF) primes the un-paired SNARE molecules, which then releases the HOPS proteins. This then allows the HOPS complex to interact with the GTP bound Rab protein Ypt7, and causes vesicle transport to the vacuole or homotypic fusion of two vacuoles [47;71-73]. Therefore the probable function of the HOPS complex, which includes the SM protein Vps33, is to form a link between the Rab based tethering apparatus and SNARE based docking and fusion apparatus.

A recent study by Rink et al. [74] using fast, quantitative, live-cell imaging observed that over time Rab5 positive early endosomes grew in size and moved towards the centre of the cell. The movement of these vesicles was accompanied by the gradual and eventual complete loss of Rab5 and its' effector molecule EEA1, and a gradual increase in Rab7 and its' effector molecules (Figure 1.12) [74]. Proteins associated with the late endosome appeared within the same time scale as Rab exchange, and the late endosomes acquired typical degradative properties [74]. Vps11 has been shown to bind to GTP-bound Rab5 on early endosomes, and therefore has Rab5 effector properties [75]. Another member of the HOPS complex, Vps39, has been shown to have Rab7 GEF activity on late endosomes [73]. Thus a Rab5 – Rab7 cascade is formed, with the HOPS complex possibly playing a key role in the conversion of early to late endosomes as demonstrated in Figure 1.12.

Another recent finding suggests that the HOPS complex may also proofread the trans-SNARE complex, by not allowing fusion to occur if the SNARE complex is incorrect [76]. As mentioned in section 1.5, a trans-SNARE complex requires three Q-SNAREs and one R-SNARE for optimal fusion to occur [33]. Alterations in this central layer greatly reduced membrane fusion. This was shown to be due to the action of the HOPS complex, which firstly inhibited the trans-SNARE complex formation and secondly suppressed membrane fusion of altered central layers [76].

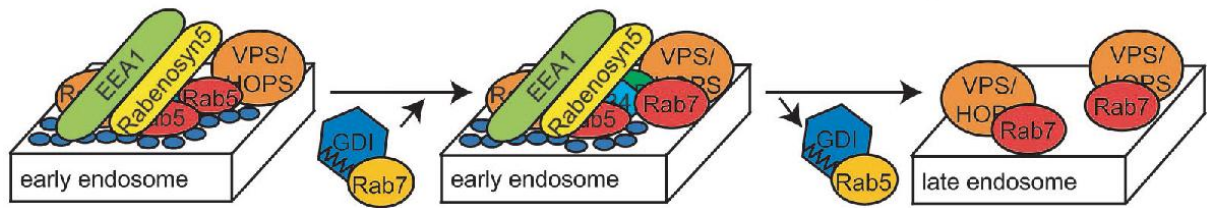


Figure 1.12 – Rab5 to Rab7 conversion on early to late endosomes.

Early endosomes are partially marked by the presence of Rab5 and its effectors, one of which is Vps11, a HOPS complex member. A second subunit of this complex, Vps39, displays GEF activity towards the yeast Rab7 orthologue (Ypt7) on late endosomes. Therefore, Rab5, the HOPS complex and Rab7 appear to form a Rab cascade on early endosomes. There is a gradual inactivation and replacement of Rab5 and its effectors and concordant activation of Rab7 and its effectors as early endosomes mature to late endosomes. [Adapted from 59]

The mammalian HOPS complex counterpart is much less well characterised. The human homologues (VPS11, VPS16, VPS18, VPS33A, VPS39 and VPS41) have been shown to localise to the late endosome and lysosome compartments of cells, and to interact with syntaxin-7 [77;78]. Kinchen et al. in 2008 showed that the HOPS complex is required for phagosome maturation and engulfment of apoptotic cells in *C. elegans* and mammalian cells [79]. Interestingly they suggested that the HOPS complex functions downstream of the Rab5 to Rab7 endosome conversion in this system [79]. However, it was not specified which Vps33 homologue was used in this study, despite both VPS33A and VPS33B being present in *C. elegans*. Therefore, whether or not VPS33B is a member of the mammalian HOPS complex remains unknown. However, over-expression of either VPS18, VPS33B or VPS39 all cause clustering of LAMP-1 positive late endosomes and lysosomes, suggesting that this maybe the case [1;80;81].

The naturally occurring *buff* (*bf*) mouse was identified as having a missense mutation (p.Glu251Asp) in *Vps33a*, and is the only known mammalian HOPS complex mutant to date. The phenotype of the *bf* mouse was suggested as a model for Hermansky-Pudlak syndrome (HPS), which is characterised by oculocutaneous hypopigmentation, a platelet aggregation defect, and in some cases pulmonary fibrosis [82]. The platelet defect was shown to be due to abnormalities in δ -granules, as opposed to α -granule defects in ARC syndrome [83]. Taken together these findings suggest that VPS33A and VPS33B might be part of the same complex, but ultimately have a different function in cells.

1.9 – The CORVET Complex

A novel complex was recently identified in yeast called the class C cORe Vacuole Endosome Tethering (CORVET) complex, which was shown to interact with the Rab GTPase Vps21 the yeast homologue of human Rab5 [84]. Both the HOPS and CORVET complexes contain the class C VPS proteins. The CORVET complex additionally has Vps3 (a homologue of VPS39) and Vps8 (a homologue of VPS41). The complex was shown to have Rab5 effector properties, whereas the authors suggest that the traditional HOPS complex is a Rab7 effector due to its preferential binding of specific GTP bound Rab molecules [84].

Peplowska et al. in 2007 showed that the HOPS and CORVET complexes could inter-convert, and also identified two intermediates depending on which proteins had been exchanged (Figure 1.13) [84]. Two models for the conversion have been postulated. The first model (Figure 1.13A) assumes that the intermediates can assemble *de novo* and bind to different Rab GTPases on endocytic membranes. The second model (Figure 1.13B) links the observed order of intermediates to the Rab GTPase cycle, displacing and recruiting Rab GEFs and Rab effectors as necessary [84].

The identification of the CORVET complex further demonstrates the maturation process of early to late endosomes associated with the conversion of the yeast homologues of Rab5 to Rab7. The function of the complex has been suggested to be for the retrograde trafficking of material from late to early endosomes [84].

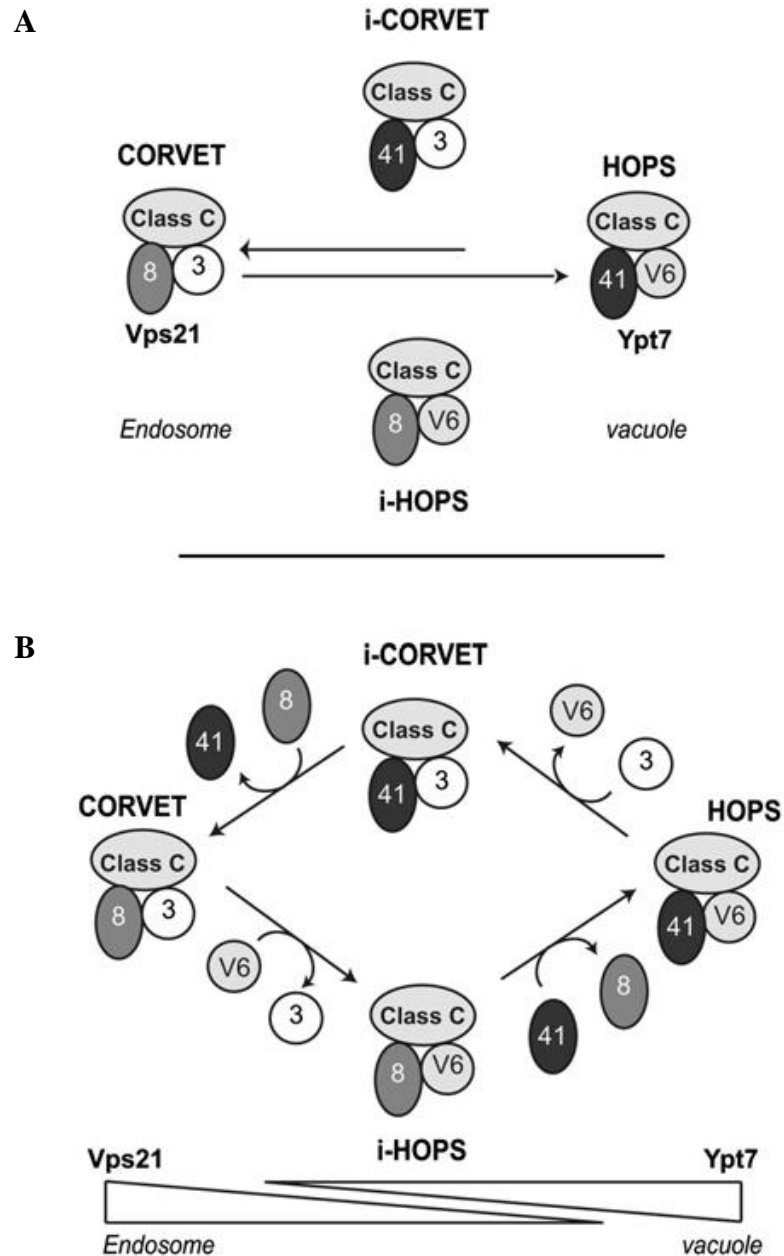


Figure 1.13 – The HOPS and CORVET complexes and models for their intermediates. Two models for the conversion have been postulated, each with the same 2 intermediates, i-CORVET and i-HOPS. Both intermediates are where only one protein has been exchanged. **A**, The first model assumes that the intermediates can assemble de novo and bind to different Rab GTPases on endocytic membranes. **B**, The second model links the observed order of intermediates to the Rab GTPase cycle, displacing and recruiting Rab GEFs and Rab effectors as necessary. [Adapted from 84]

1.10 – Polarised Epithelia

Nearly all cell types in multi-cellular organisms are said to be polarised, a quality of the cells which is characterised by the generation of functionally distinct membrane domains.

Epithelial cells are no exception and require distinct apical and basolateral plasma membrane domains to perform their various epithelial functions, including directional roles in absorption and secretion [85;86]. Generation of these distinct domains is termed polarisation, and requires complex sorting machinery in the cell to deliver proteins and lipids to the correct domain [87]. ARC syndrome patients seem to have abnormally polarised epithelial cells in their kidneys and liver as evidenced by the presence of apical membrane proteins found in the basolateral surface. However, basolateral membrane proteins are not found in the apical surface [1;11]. These findings suggest a role of VPS33B in establishing polarity in epithelial cells.

1.11 – The Apical Junction Complex

Epithelial cells form a protective ion-selective barrier to the external environment. The basolateral membrane contacts neighbouring cells and the underlying tissues, whereas the apical surface faces the lumen of an internal organ. The apical junction complex (AJC) separates the two membrane domains, and is comprised of adherens junctions (AJs) and tight junctions (TJs). This barrier function is highly dependent on the integrity of these two types of junctions, which link adjacent epithelial cells [88;89]. Many human disorders (including cancer, autoimmune diseases, asthma and neurodegeneration) have been associated with abnormalities of the AJC proteins [90-93].

1.11.1 – Adherens Junctions

The adhesion between epithelial cells is primarily generated by the adherens junction, forming an adhesive belt that encircles the cell just below the apical surface, but more basal to the TJ [94]. The AJ has numerous and varied functions including the initiation and stabilisation of cell-cell adhesion, regulation of the actin cytoskeleton, intracellular signalling and transcriptional regulation [89]. The proteins that constitute an AJ are members of the cadherin superfamily, such as E-Cadherin in epithelial cells, and the catenin superfamily, including p120-, α - and β -catenin.

E-Cadherin is a single membrane spanning glycoprotein, with five characteristic extracellular cadherin (EC) domains. These domains interact with E-Cadherin molecules from the neighbouring cell. E-Cadherin trans-dimerisation is calcium dependent, as the EC domain needs to bind Ca^{2+} ions to create the correct protein conformation to allow for trans-dimerisation, initiating a weak cell-cell adhesion [95].

The correct localisation of E-Cadherin to the lateral membrane is critical to epithelial cell polarisation, and the continuous delivery of newly synthesised protein is essential to ensure the dynamic nature of AJs [96]. E-Cadherin is trafficked from the TGN to the Rab11 positive Apical Recycling Endosomes (ARE) before being delivered to the lateral membrane [97]. It is proposed that formation of the AJ leads to the formation, but not the maintenance of the TJ [98]. It has recently been shown that the dimerisation of VE-Cadherin in vascular endothelial cells mediates the transcriptional upregulation of Claudin-5, through activation of

transcription factors and β -catenin [99]. However HepG2 cells engineered not to have AJs still form functional tight junctions, but much more slowly than if AJs are present [100].

1.11.2 – Tight Junctions

Epithelial cells form a cohesive layer of cells capable of physical and ion-selective barrier functions, known as the fence and gate functions respectively [88]. The former function is also responsible for the prevention of intermixing of apical and basolateral membrane lipids and proteins. These functions are for the most part due to the TJ proteins, which are comprised of two types of transmembrane proteins, occludins and claudins, and their associated cytoplasmic proteins that link the TJ to the actin-cytoskeleton and AJs [89]. An important group of these scaffolding proteins are the zonula occludens proteins, ZO-1, ZO-2 and ZO-3, which also interact with the AJ.

Similar to E-Cadherin in the AJ, both the occludin and claudin family of proteins homodimerise with each other, however this interaction is much stronger and generates very tight cell-cell adhesion. Reduction of occludin expression by RNAi failed to reduce either the fence or the gate function in epithelial cells, but a reduced communication of apoptosis to neighbouring cells was evident [101]. This indicated that the claudin family is the key member of the tight junction complex that regulates the paracellular permeability.

Furthermore, each one of the 24 members of the claudin family of proteins has a different expression and permeability pattern, allowing different tissues and cell types to fulfil their different functions [102].

Interestingly both ZO-1 and ZO-2, but not ZO-3, determine where the Claudin family of proteins are dimerised with each other, and hence where functional tight junctions are formed [103]. Therefore this group of proteins maybe the link between the sequential formation of AJs and TJs, as the ZO group of proteins also interact with the AJ. However, these ZO deficient, and in turn functional TJ deficient cells retained their apical basolateral polarity of membrane proteins [104;105].

1.11.3 – The Adhesion To Polarity Model

The apical junction complex plays a complicated role in epithelial cell polarity, and is widely thought as the driving process for the generation of apical basolateral polarity (Figure 1.14). The classic model begins with the dimerisation of E-Cadherin between adjacent cells, which through the action of α -, β - and γ - catenin, reorganises the actin network to form an actin belt that surrounds the apical surface [106]. Meanwhile the TJ protein components are recruited to the AJ, forming spot-like adherens junctions. The TJ components then migrate to a more apical position, and intracellular vesicles fuse with the lateral membrane leading to the vertical extension of the epithelial cells [94;107].

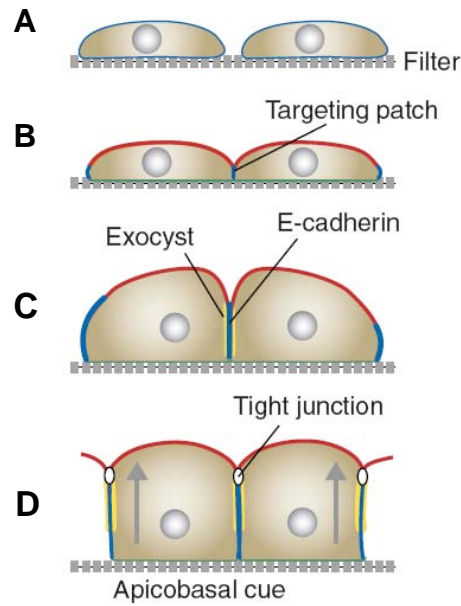


Figure 1.14 – The adhesion to polarity model of epithelial polarisation.

A, Initially the epithelial cells grown on filter supports are not in contact with each other and are relatively unpolarised. **B,** After contact occurs, cells form initial cell-cell junctions, which function as a targeting patch for further junctions to form. **C,** E-Cadherin is trafficked to the lateral membrane, which in turn recruits the exocyst complex. **D,** The lateral membrane then extends and tight junctions concentrate at the most apical region of the lateral surface. The cells then fully polarise along the apical-basolateral axis (grey arrows).
[Adapted from 108]

The co-operation of two independent protein complexes, CRB (crumbs) and PAR (partitioning defective) regulate several steps of the epithelial polarisation process. Activation of the PAR complex and the correct localisation of the CRB complex to the apical and sub-apical region, are essential for apical membrane determination [94]. It has recently been identified that there is an asymmetric distribution of phosphoinositide molecules in the apical and basolateral membrane. The apical membrane is rich in phosphatidylinositol 4,5-bisphosphate (PI(4,5)P₂), whereas the basolateral membrane has phosphatidylinositol 3,4,5-trisphosphate (PI(3,4,5)P₃) [109]. This difference was shown to be due the apical localisation of the enzyme PTEN which converts PI(3,4,5)P₃ to PI(4,5)P₂ [110]. The PAR complex has been linked with the asymmetric distribution of the lipid molecules, but at the present time it is unclear which asymmetry occurs first [111].

1.11.4 – The Polarity To Adhesion Model

Although the classic adhesion to polarity model is favoured by most, recent evidence suggests that this might not necessarily be entirely correct, and that polarisation could occur independent of adhesion. Activation of the PAR complex in contact naïve epithelial cells is sufficient to cause the remodelling of the actin cytoskeleton to a polarised state. Furthermore, these cells formed an apical brush border and began to form primary TJs at single spots on the membrane [112]. Knockdown of the CRB complex proteins causes serious defects in TJ, and also AJ formation, as E-Cadherin fails to reach the membrane. This was shown to be partially due to the mislocalisation of the exocyst complex [113]. The octomeric exocyst complex is an evolutionary conserved complex required for the tethering of exocytic vesicles with the

target membrane, and is proposed to selectively tether cargo vesicles directed towards the basolateral surface [114;115].

Taken all together these findings suggest that there is an intimate and intricate interaction between adhesion and polarity complexes to establish and maintain polarity in epithelial cells. It is most likely that there is an increasingly stronger cyclic relationship between adhesion and polarity. Early adhesion events cause the activation of the polarity proteins, which then reinforces adhesion, which in turn promotes further polarisation. This process continues until the cells become fully polarised.

1.12 – Polarised Protein Trafficking

The protein and lipid content of the apical and basolateral domains of epithelial cells needs to be tightly controlled so that the cells can undertake their correct function. For example, inserting basolateral proteins into the apical domain in kidney epithelial cells would destroy the normal steep electro-chemical gradient across the cells, and also allow for the re-absorption of waste products. Similarly in hepatocytes, the delivery of basolateral unsaturated phospholipids to the apical membrane could disturb the normal resistance of the membrane to bile acid detergents [87].

In epithelial cells, there are three pathways that generate the polarised distribution of apical and basolateral membrane proteins. These are the biosynthetic, endocytic and transcytosis pathways. Until the newly synthesised proteins enter the TGN the steps in the biosynthetic pathway for polarised epithelial cells are the same as shown in section 1.4 for non-polarised

cells. Whilst in the TGN a vast majority of proteins are sorted by the sorting machinery into apical and basolateral vesicles, which deliver the proteins to the correct surface [116]. The mechanisms of sorting at this level are discussed later in this section. Some proteins exit the TGN unsorted and are put into common recycling endosomes (CREs), where they are then sorted into apical and basolateral cargo and delivered to the correct surface through apical or basolateral recycling endosomes [117-119]. Proteins that are not retained at the surface, usually through interaction of the C-terminal region with PDZ domain containing proteins, are rapidly endocytosed and delivered to early endosomes [120]. From here the proteins can be recycled back to the previous membrane, sent to the late endosome and lysosome compartments for degradation, or delivered to the opposite surface through the CRE [121]. The latter process is termed transcytosis and is extensively used by hepatocytes, which first deliver some apical membrane proteins to the basolateral surface, and then transfer them to the apical membrane [122]. A diagram demonstrating the above pathways is given below in Figure 1.15.

Proteins containing PDZ domains help anchor transmembrane proteins to the cytoskeleton and hold signaling complexes together. The domain was named after the three original proteins shown to contain this domain, which were Post synaptic density protein (PSD95), *Drosophila* disc large tumor suppressor (DlgA), and Zonula occludens-1 (ZO-1). The domain is also referred to as the GLGF domain, due to the importance of these amino acids to its' function [123].

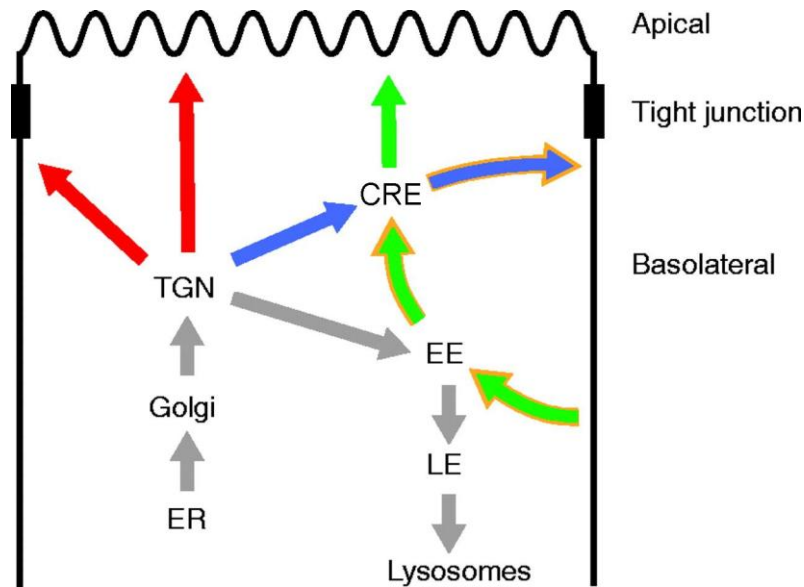


Figure 1.15 – Protein trafficking pathways in polarised epithelial cells.

From the TGN, protein cargo can be sorted directly to the apical and basolateral surface (red arrows). Proteins can also reach their correct surface through sorting at the common recycling endosome (CRE, blue and green arrows). After initial trafficking of apical proteins to the basolateral surface, apical cargo can be delivered to the apical membrane through the transcytosis route (green arrows). The basolateral recycling pathway is shown with gold outlined arrows. The apical recycling and apical to basolateral transcytosis pathways are omitted for clarity (EE – early endosomes, ER – endoplasmic reticulum, LE – late endosomes, and TGN – trans-Golgi network). [Adapted from 87]

1.12.1 – Basolateral Protein Sorting

Basolateral membrane proteins are sorted to their correct surface by having short amino acid sorting signals in their cytoplasmically exposed regions. In 1986 Mostov and co-workers demonstrated that deletion of this sorting signal in the polymeric immunoglobulin-A receptor caused the apical localisation of the basolateral protein, and suggested that apical trafficking was the default pathway [124]. This group went on further and showed in 1991 that if this signal was transplanted into apical membrane proteins the protein was delivered to the basolateral membrane [125]. Since the identification of the basolateral sorting signal, numerous groups have pinpointed the actual amino acids that are required for correct trafficking. These include tyrosine, leucine and dileucine motifs that are often found in close proximity to acidic amino acids, as well as other uncharacterised motifs [126-128].

Several groups realised that the basolateral sorting signals shared a striking resemblance to sequences found in the receptors that were endocytosed from the plasma membrane through clathrin coated pits, or transported to the lysosome [126;129]. All the sorting signals are recognised by adaptor coat proteins, or adaptins, of which there are five, AP-1A, -1B, -2, -3 and -4, each having an organelle specific localisation [130]. In polarised epithelial cells basolateral sorting signals are recognised by AP-1B and AP-4, which can be found in the TGN and endosomal compartments [131;132]. Transfection of the μ 1B sub-unit of the adaptor protein AP-1B complex into μ 1B deficient LLC-PKI cells restores the correct basolateral localisation of the LDL and transferrin receptors [131]. This suggests that these two adaptin proteins are responsible for the correct sorting of basolateral cargo in the biosynthetic and recycling endocytic pathways.

1.12.2 – Apical Protein Sorting

In contrast to the basolateral sorting signals and receptors, the apical sorting signals and machinery are much less well understood. It was first believed that delivery of membrane proteins to the apical membrane was the default process and that only proteins with basolateral sorting signals were directly trafficked to the basolateral surface, however this was shown not be strictly true [133].

Apical sorting signals are found in the exoplasmic, membrane and cytoplasmic regions of the sorted proteins. It was noticed that glycosylphosphatidyl-inositol anchored proteins (GPI-APs) were for the most part localised to the apical surface of polarised epithelial cells, and that translocation of this region onto secreted cargo resulted in an apical localisation [134;135]. The transfer of a GPI moiety onto a protein is a post-translational modification and results in the protein being anchored to the outer membrane leaflet.

A second group of the apical sorting signals are the N- and O-glycans, another post-translational modification, but these were shown to be recessive to basolateral sorting signals [136;137]. Therefore, if a protein contained a basolateral sorting signal and had N- or O-glycans attached, it would still be trafficked to the basolateral membrane. Experiments carried out imply that there are apical sorting receptors similar to that of the basolateral system, as high-level expression of an apical membrane protein saturated the system, and could be out competed by a second apical protein [138]. Glycoproteins acquire their N-linked glycans whilst the polypeptide is being synthesised. The 14-saccharide core is transferred to an asparagine (N) residue within a consensus sequence of N-X-T/S, where X is any amino

acid except proline (P) [139]. However, receptors for these apical sorting signals remain elusive, with only a couple of carbohydrate-binding proteins (lectins) being suggested with currently no direct evidence [139]. These two proteins are VIP36 and galectin-3, but their exact role in apical membrane protein trafficking remains unknown. [140].

In 1988 van Meer and Simons presented an alternative to the conventional sorting receptor model for apical protein sorting in epithelial cells, which they termed the lipid-raft hypothesis. The hypothesis postulates that many proteins are sorted to the apical surface because they have an affinity for micro-domains of glycosphingolipids and cholesterol (lipid-rafts), which are assembled at the Golgi [133;141;142]. The apical membrane was known to be rich in sphingolipids and cholesterol, and depletion of these two molecules caused the mis-sorting of apical proteins [143]. However, very little more is known about how lipid rafts function due to a lack of suitable methods and the fact that they are very difficult to visualise using light microscopy because of their size and dynamic nature [87].

1.12.3 – The Cytoskeleton

Vesicular trafficking relies heavily on the cytoskeleton of cells and in particular the microtubule and actin filament networks. Microtubules are comprised of polymerised α and β tubulin molecules, and in polarised epithelial cells the fast growing plus end faces the basolateral surface, whereas the slow growing minus end faces the apical surface [144]. The microtubule motor protein families of kinesins and dyneins are involved in anterograde (towards the plus end) and retrograde (towards the minus end) transport respectively [145]. The polarised nature of the microtubule network and different directions of motor protein

transport allows for specificity of apical and basolateral trafficking. Polymers of globular actin form actin microfilaments with their barbed end toward the cell membrane and the pointed end toward the cell interior. Unconventional myosin motor proteins, such as myosin-V and -VI are involved in vesicular transport of cargo towards the barbed end and the pointed end respectively [146].

There is increasing evidence to support the idea that the cytoskeleton plays an important role in generating and maintaining apical and basolateral polarity in epithelial cells. The cytoskeleton has been shown to be important at the sorting organelles, the TGN and recycling endosomes; however the function of different systems have different functions in polarity. It seems that microtubules are essential for organisation of the apical membrane, whereas the actin cytoskeleton has a role in basolateral polarity [133].

In polarised epithelial cells the SNARE protein syntaxin-3 is localised to the sub-apical, or upper third of the cell, and syntaxin-4 is found in the lateral areas of cells. However in non-polarised cells this is not the case and both syntaxin molecules are found throughout the cell [133]. This apical basolateral polarisation of these two syntaxin proteins provides a possible mechanism of differential apical and basolateral membrane protein delivery. Furthermore, depolymerisation of the microtubule network in epithelial cells results in the depolarisation of syntaxin-3 and the basolateral delivery of GFP-P75 in MDCK cells, with no change in the basolateral protein trafficking [116]. Similarly depolymerisation of the actin cytoskeleton cause the depolarisation of syntaxin-4 from the lateral surface and leads to apical delivery of basolateral proteins and deficiencies in the basolateral recycling [147]. The exact mechanisms of how both the actin and microtubule cytoskeleton and the polarised distribution

of syntaxin-3 and -4 have an effect on apical-basolateral membrane protein polarity remains poorly understood.

1.13 – Summary

Arthrogyrosis Renal dysfunction and Cholestasis (ARC) syndrome is caused by mutations in *VPS33B* in around 75% of patients [1;2;4]. No detectable mutations have been identified in the remaining patients, and furthermore some consanguineous families with ARC syndrome do not link to the *VPS33B* 15q26.1 locus. Thus suggesting locus heterogeneity and other causal genes for ARC syndrome, which are yet to be identified.

The *VPS33B* gene encodes the VPS33B protein, which in multicellular organisms is one of two homologues of the yeast Vps33 gene and protein. Both the VPS33A and VPS33B proteins contain a Sec1/Munc18 (SM) like domain throughout. SM proteins are thought to tightly bind to members of the syntaxin family of target SNAREs (Soluble N-ethylmaleimide sensitive REceptors) and may alter interdomain interactions and influence vesicle to target SNARE complex formation [6].

Yeast Vps33 alongside Vps11, Vps16, Vps18, and Vps39 belong to the class C vacuole protein sorting (VPS) group of proteins and is required for vacuole biogenesis [7]. The class C VPS proteins with VPS41 form the HOPS complex, which in yeast has been shown to be involved in the maturation of Rab5 positive early endosomes to Rab7 positive late endosomes [74]. The mammalian HOPS complex counterpart is much less well characterised. The human homologues (VPS11, VPS16, VPS18, VPS33A, VPS39 and VPS41) have been shown

to localise to the early endosome, late endosome and lysosome compartments of cells, and to interact with syntaxin-7 [77;78]. Whether or not VPS33B is a member of this mammalian complex remains unknown, however, preliminary data suggests that this might be the case [1;80;81].

The function of VPS33B has not been extensively studied in mammals. However, the identification of mutations in *VPS33B* in ARC syndrome patients might give an insight into the function of VPS33B. ARC syndrome patients seem to have mislocalisation of apical membrane markers in polarised epithelial cells, predominantly in the liver and kidney [1;11]. Taken together with the predicted function of VPS33B in vesicular trafficking, this suggests a function of VPS33B in the trafficking of these proteins to the correct pole of polarised cells. However, the intracellular action of VPS33B and how mutations in *VPS33B* lead to the pathogenicity of ARC syndrome remains unknown. Elucidation of the role of VPS33B in polarised protein trafficking in epithelial cells will not only further the knowledge of how epithelial cells establish and maintain their polarity but may also reveal mechanisms for potential therapeutics for ARC syndrome patients.

CHAPTER 2 – MATERIALS AND METHODS

2.1 – Materials

2.1.1 – DNA and RNA Analysis

Patients that presented with a classical ARC phenotype including arthrogryposis multiplex congenita, renal tubular dysfunction and cholestasis with low γ GT activity were included in the study. DNA was extracted from blood samples using standard protocols and stored at 500 ng μ l⁻¹ at -80°C until required. Protein and RNA samples obtained at different stages of human foetal development were provided by Prof. M. Kilby (University of Birmingham, UK). The study was approved by the local research ethics committee.

Standard PCR reagents (Taq DNA polymerase, buffer, MgCl₂ and 100 μ M dNTP mix) were all purchased from Thermo Electron (Ulm, Germany) and the nuclease free water from Invitrogen (Paisley, UK). De-salt purified primers were ordered from Sigma Aldrich (Poole, UK). Agarose was purchased from Bioline (London, UK) and the 100 bp ladder from New England Biolabs (Hitchin, UK). The Exo-SAP reagent was bought from USB (Staufen, Germany) and the BigDye Terminator (version 3.1) sequencing kit along with the HiDi formamide was purchased from Applied Biosystems (Warrington, UK).

The RNazol B reagent was procured from Campro Scientific (Birkenhead, UK) and the ImProm-II Reverse Transcription System Kit and oligo dT primers were purchased from Promega (Southampton, UK). Primers for qRT-PCR were ordered from Thermo Electron and were dHPLC purified. The Power SYBR Green master mix was purchased from Applied Biosystems.

2.1.2 – Cell Culture

All cell culture plastic ware including the Transwell permeable supports were purchased from Corning (High Wycombe, UK), except the glass bottom dishes, which were obtained from Ibidi (Munich, Germany). Foetal Bovine Serum (FBS) Gold and the dialysed equivalent along with the G418 sulphate solution were procured from PAA Laboratories (Yeovil, UK). Lipofectamine 2000 transfection reagent was bought from Invitrogen. All other cell culture reagents were obtained from Sigma-Aldrich.

2.1.3 – Protein Reagents

The Complete Mini Protease Inhibitors were purchased from Roche (Welwyn Garden City, UK) and the Dc Protein Concentration Assay Kit from BioRad (Hemel Hempstead, UK). The lyophilysed Bovine Serum Albumin (BSA) was obtained from Sigma-Aldrich, and the polyacrylamide mix was bought from Geneflow (Fradley, UK). The transblot polyvinylidene difluoride (PVDF) membrane (Hybond-P) and ECL Plus western blot detection system kit were procured from GE Healthcare (Amersham, UK). Protein G coupled Dynalbeads and the magnetic block was obtained from Invitrogen. The EZ-link Sulfo-NHS-SS-Biotin was purchased from Thermo Scientific (Loughborough, UK) and the streptavidin-agarose beads from Sigma Aldrich.

2.1.4 – Cloning

Where necessary IMAGE clones were purchased from Geneservice (Cambridge, UK) and the required dHPLC purified PCR primers were ordered from Thermo Electron. The proofreading Platinum Taq Polymerase kit was obtained from Invitrogen. A 2-log DNA ladder, all restriction enzymes, buffers and BSA were procured from New England Biolabs. The T4 DNA ligase and buffer were purchased from Promega. The DH5 α and XL-1 Blue competent cells were purchased from Bioline and Stratagene (Cambridge, UK) respectively. SOC medium was obtained from Invitrogen and plasmid mini and maxi prep kits were purchased from QIAGEN (Crawley, UK). The pEGFP-P75 was a gift from E. Rodriguez-Boulan (Cornell University, New York, NY). The pEGFP-CD63 was a gift from J. Jaiswal and the Rab4, Rab5 and Rab11a constructs were gifts from A. Benmerah and S. Benichou (Institut Cochin, Paris, France). The dominant-negative Rab11a plasmid, pEGFP-DN Rab11a, containing the S25N missense mutation was a gift from F. Barr (University of Liverpool Cancer Research Centre, Liverpool, UK).

2.1.5 – Antibodies and Stains

Monoclonal antibodies against β -actin (clone AC-15) and against the HA (clone HA-7) and myc epitope tags (clone 9E10) were purchased from Sigma-Aldrich. Rabbit polyclonal antibodies against ZO-1 and Claudin-1 and a mouse monoclonal antibody against E-Cadherin were procured from Invitrogen. Rabbit polyclonal antibodies against VPS33B and CEA were respectively purchased from Proteintech Europe (Manchester, UK) and Dako (Ely, UK). The mouse monoclonal antibody against the Na⁺/K⁺ ATPase protein and the rabbit polyclonal antibody against cytokeratin-18 were provided by Millipore (Consett, UK). The mouse

monoclonal antibodies against Rab11a and GM130 were purchased from BD Transduction Laboratories (Oxford, UK). The rat monoclonal antibody against LAMP-1 was purchased from the Hybridoma Bank (Iowa, IA). The rabbit polyclonal antibodies against GFP and β -catenin were purchased from Santa Cruz (Santa Cruz, CA) and Abcam (Cambridge, UK). The rabbit polyclonal antibody against zebrafish E-Cadherin was a kind gift from C.P. Heisenberg (Max Planck Institute, Dresden, Germany). Goat anti-mouse IgG and anti-rabbit IgG conjugates with Alexafluor 488, 546, 568 and 633 secondary antibodies were used. All fluorescent products, including tetramethyl rhodamine isothiocyanate (TRITC)-conjugated phalloidin, the Texas Red-conjugated transferrin and the nuclear stain TOP-RO-3, were purchased from Invitrogen. Cells were mounted in ProLong Gold antifade solution from Invitrogen.

2.1.6 – Zebrafish Reagents

The AB* strain of zebrafish were used for all experiments. The DIG Labelled RNA Probe Synthesis Kit and the alkaline phosphatase-conjugated rabbit anti-DIG antibody were both purchased from Roche. Morpholino oligonucleotides were designed by and obtained from Gene Tools (Philomath, OR). The Message Amp mRNA amplification kit was bought from Ambion (Warrington, UK), and the PED-6 reagent was purchased from Invitrogen.

2.1.7 – General Chemicals

Ethanol, methanol and isopropanol were bought from Fisher (Loughborough, UK) and Phosphate Buffered Saline (PBS) tablets from Oxoid (Basingstoke, UK). All other general laboratory chemicals were purchased from Sigma Aldrich unless otherwise stated.

2.2 – Methods

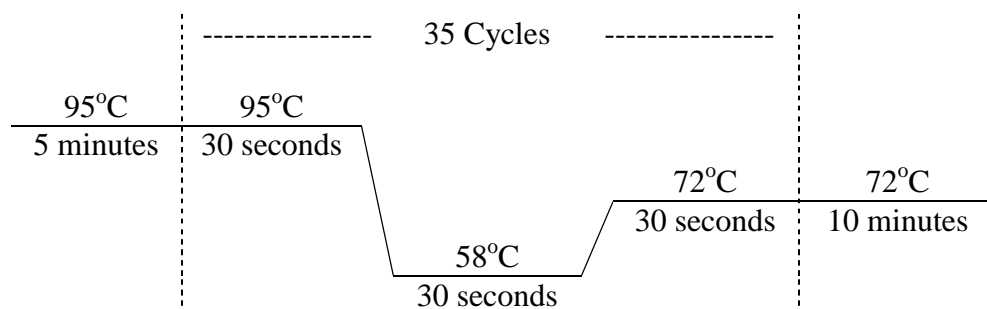
2.2.1 – Sequencing Analysis of ARC Patients

2.2.1.1 – Polymerase Chain Reaction

The Polymerase Chain Reaction (PCR) was carried out to amplify all coding and flanking intronic sequences of *VPS33B* in patients' DNA. *VPS33B* has 23 coding exons and 22 primer pairs were previously designed and are shown in Appendix 1 [1]. The reagents and volumes per reaction are given below.

Reagent	Volume per reaction (μl)
10x PCR buffer	1
dNTP mix (10 μM)	1
MgCl ₂ (25 mM)	0.6
Nuclease Free Water	5.3
Taq. Polymerase (5 units μl ⁻¹)	0.1
Template DNA (50ngμl ⁻¹)	1
Forward Primer (10 μM)	0.5
Reverse Primer (10 μM)	0.5
Total	10

A no template control was run with every primer pair to ensure specificity. The PCR mix was then subjected to the following conditions to allow amplification to occur.



The annealing temperature is variable depending on the melting temperature of the primers used in the reaction. The extension time is also variable and depends on the processivity of the taq polymerase enzyme, which for this enzyme is 1000 base pairs per minute. The primer pairs were designed to have an annealing temperature of 58°C, and the expected product size were all less than 500 base pairs, so an extension time of 30 seconds was adequate

2.2.1.2 – Agarose Gel Electrophoresis

Once the PCR reaction was complete, an agarose gel electrophoresis was carried out on the PCR products to ensure the reaction was successful and specific. A 1% agarose gel was made by dissolving 1% w/v agarose in 1x TBE buffer (90 mM tris-base, 90 mM boric acid, and 2 mM EDTA, pH=8.0) and 10 ngml⁻¹ of ethidium bromide (EtBr). An equal volume of 2x DNA loading buffer (2 mM EDTA, 50% glycerol and 0.1% orange G) was added to 2.5 µl of the PCR product and loaded on the gel. A 100 base pair ladder was added as a size standard, and the electrophoresis was carried out at 120 volts for 30 minutes.

2.2.1.3 – Exo-SAP Reaction

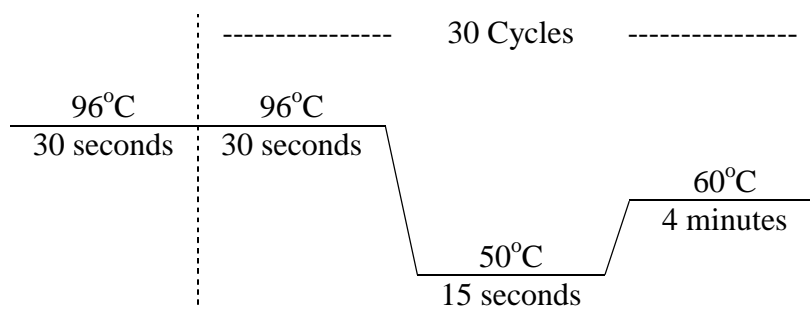
After the PCR reactions have been shown to be successful using agarose gel electrophoresis, the amplified DNA was diluted three fold and 7.5 µl of the diluted DNA samples were added to 2.5 µl of the Exo-SAP reagent. The samples were heated to 37°C for 20 minutes and 80°C for 10 minutes. The reagent contains two enzymes, Exonuclease 1 and Shrimp Alkaline Phosphatase, which removes any primers and dephosphorylates the dNTPs present in the reaction mixture, before the next step in the sequencing protocol.

2.2.1.4 – Sequencing

Direct sequencing of Exo-SAP treated PCR products was carried out using the dideoxy termination method. Each of the patients' DNA was sequenced bi-directionally, therefore from this point the forward and reverse primers were kept separate and two reactions were carried out per patient per PCR product from above. The composition of the reaction is given below.

Reagent	Volume per reaction (µl)
5x Sequencing Buffer	2
PCR Product	4.4
Primer (2 µM)	1.6
Nuclease Free Water	1.5
BigDye	0.5
TOTAL	10

The total reaction mixture was then subjected to the following conditions for the sequencing reaction to occur.



2.2.1.5 – Sequencing Precipitation

Once the sequencing reaction was complete any impurities needed to be removed from the sequencing products, and these included enzymes and any excess fluorescently labelled ddNTPS. The DNA was precipitated by adding 1 µl of 0.25 M EDTA and 32 µl of 100% ethanol, followed by a 10 minute incubation at room temperature. The samples were centrifuged at 4000 x g for 30 minutes at 4°C, and the resulting supernatant was removed by centrifuging the plate upside down at 500 x g for 20 seconds. The DNA pellet was then washed with 125 µl of 70% ethanol and the centrifugation steps repeated as above. The resulting pellet was allowed to air dry for 10 minutes before 10 µl of HiDi formamide was added to each well. The plate was then heated to 95°C for 5 minutes to denature the DNA and cooled immediately on ice.

2.2.1.6 – Sequencing Analysis

The denatured DNA was then sequenced using an ABI 3730 capillary sequencer (Applied Biosystems), and analysed using Chromas v2.23 software (Technelysium, Shannon, Ireland). Any change in the patient sequence compared to the reference sequence was verified bi-directionally and checked for the absence in SNP databases.

2.2.2 – Cell Culture

Control and patients' skin fibroblasts were grown in Dulbecco's Modified Eagle's Medium supplemented with 10% foetal bovine serum, 2 mM L-glutamine, 1x MEM non-essential

amino acid solution and 1x penicillin-streptomycin. Skin fibroblasts from an anonymous patient not affected with ARC were used as a control. Human Embryonic Kidney, HEK293 cells were grown in the same medium as fibroblasts. Murine Inner Medullary Collecting Duct, mIMCD-3 cells (CRL2123; ATCC, Manassas, VA) were grown in a 1:1 mix of DMEM and Ham's F12 medium, supplemented with 10% FBS and penicillin-streptomycin. All cells were passaged using 0.25% trypsin for 5 minutes after being washed twice with pre-warmed PBS. The cells were diluted as necessary in complete growth medium, and all cells were grown at 37°C with 5% CO₂. In order to induce mIMCD-3 cells to fully polarise, cells were seeded onto 0.4 µm pore size transwell permeable supports at a density of 1 x 10⁵ cells per cm². For selection purposes, mIMCD-3 cells were grown in medium containing 1.5 µgml⁻¹ of puromycin, 400 µgml⁻¹ of G418 sulphate, or a combination of both when necessary.

2.2.2.1 – Transfection

HEK293 and mIMCD-3 cells were seeded onto 6-well tissue culture plates and allowed to grow to around 80% confluence before being transfected with plasmid DNA constructs. On the day of transfection the normal medium was removed and replaced with 2ml of antibiotic free medium. A total of 4 µg of DNA and was added to 250 µl of unsupplemented medium, and 12 µl of Lipofectamine 2000 (3x weight of DNA) was added to the same volume in separate tubes. These tubes were incubated at room temperature for 5 minutes. The 2 solutions were mixed together and incubated at room temperature for 20 minutes, after which the resulting mixture was added to the cells, which were incubated at 37°C with 5% CO₂ overnight.

2.2.2.2 – Collagen Culture

To assess mIMCD-3 cell morphogenesis, cells were suspended in type I collagen gels in 96-well plates. Collagen gels were prepared by adding 5×10^5 mIMCD-3 cells to 250 μ l of collagen mix (16 mM HEPES, 32 mM NaHCO_3 , 16% DMEM, and 3.5 mg/ml rat type 1 collagen (all from Sigma Aldrich)). Aliquots of 50 μ l were then seeded into one well of a 96-well plate and allowed to solidify at 37°C, before being overlaid with 100 μ l of complete medium. After 72 hours of culture the tubules were visualised using 10x phase-contrast optics on an Axioplan 2 microscope with images captured on an Axiocam CCD camera (both Carl Zeiss, Welwyn Garden City, UK).

2.2.3 – RNA Analysis

2.2.3.1 – RNA Extraction

The required cells were seeded into 75 cm² flasks and allowed to grow to confluence. The cells were washed twice with ice cold PBS and scraped into 1 ml of RNazol B reagent, after which 100 μ l of chloroform was added, inverted several times and incubated on ice for 10 minutes. The samples were then centrifuged for 15 minutes at 4°C and the clear upper aqueous phase was transferred to a clean tube. An equal volume of isopropanol was added and incubated on ice for 15 minutes before being centrifuged for 30 minutes. The supernatant was discarded and the pellet washed with 1.5 ml of 80% ethanol and centrifuged for 10 minutes. Again the supernatant was discarded and the pellet allowed to air dry before being

re-suspended in 50 µl of nuclease free water. All centrifugation steps were carried out at 4°C and at 4000 x g.

2.2.3.2 – RNA Concentration Quantification

To assess the concentration and quality of RNA obtained from the above procedure, the absorbance values of 70 fold diluted RNA samples were taken at 260 and 280 nm. The ratio between the absorbance values at 260 and 280 should be between 1.8 and 2, which signifies good quality and pure RNA. The concentration of RNA is calculated using the following formula:

$$[\text{RNA}] (\mu\text{g}\mu\text{l}^{-1}) = \frac{\text{Absorbance at 260 nm} \times \text{Dilution Factor} \times 40}{1000}$$

2.2.3.3 – cDNA Synthesis

For cDNA synthesis, 1 µg of total RNA was reverse transcribed using ImProm-II Reverse Transcription Systems and oligo dT primers. The following reagents and volumes per reaction are shown on the next page:

Reagent	Volume per reaction (µl)
5x Buffer	4
MgCl ₂ (25 mM)	4
dNTPs (10 mM)	2
Oligo dT primer (0.5 µgµl ⁻¹)	2
RT enzyme	0.8
RNA (1 µgµl ⁻¹)	1
H ₂ O	6.2
Total	20

The above reaction mixture was incubated at 42°C for 60 minutes followed by 99°C for 5 minutes to inactivate the enzyme. To verify if this reaction was successful, a PCR reaction was carried out as in section 2.2.1.1, using β -actin (*ACTB*), a house keeping gene, as the target and 1 µl of the above reaction mixture as the template. Primer sequences are shown in appendix 1.

2.2.3.4 – Quantitative Real Time PCR

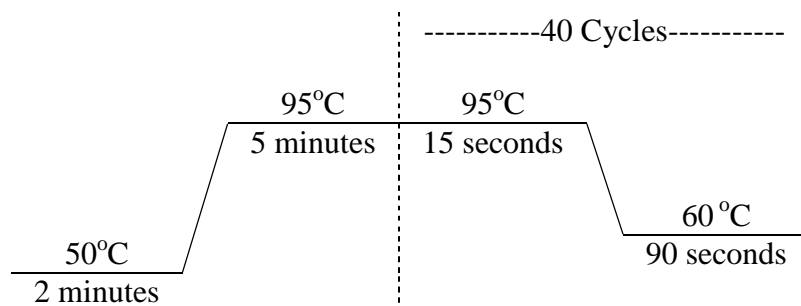
Firstly, PCR primers were designed for human *ACTB*, *VPS33A* and *VPS33B* and mouse *Actb* and *Plrn*, using Primer 3 software available online (<http://frodo.wi.mit.edu>). Primers were designed with an annealing temperature of 60°C, a product size of less than 500 base pairs and preferably with one of the primers spanning an intron so genomic DNA amplification was avoided. The primer sequences generated were run through an nBLAST search to check for specificity to the gene of interest (www.blast.ncbi.nlm.nih.gov). Each primer pair were denaturing HPLC purified and tested by PCR using control cDNA to ensure that they were specific and only one product was amplified at 60°C.

The SYBR green reagents binds to any double stranded DNA molecule, including primer dimers, therefore an optimisation experiment is required to determine the minimum concentration of primer required to amplify the target sequence. A series of standard PCR reactions were carried out with decreasing primer concentrations (1 to 0.05 μM) and the products were electrophoresed on a 4% w/v agarose gel, and assessed for the presence of primer dimers. For all primer pairs designed the required final concentration was 0.1 μM .

Each assay requires a standard curve to be created so that different plates can be compared, and always had β -actin amplified for each sample as a normalising control. For all qRT-PCR reactions the cDNA previously synthesised was diluted 5 fold with nuclease free water. A serial dilution of control cDNA was used for the standard curve, with concentrations of 1 (undiluted cDNA), 0.4, 0.2 and 0.1 being used. No template controls were run with each assay to ensure specificity, and each sample was run in triplicate. The following reagents and volumes per reaction are shown below:

Reagent	Volume per reaction (μl)
SYBR Green Master Mix (2x)	12.5
Forward Primer (10 μM)	0.25
Reverse Primer (10 μM)	0.25
Nuclease Free Water	9.5
cDNA	2.5
Total	25

For an assay 2 master mixes were created, one for the β -Actin and one for the gene of interest. This was aliquotted onto optical 96-well plates, the cDNA added and the plate sealed with optical film. The reaction conditions are given on the next page.



During the reaction, amplicon levels were continuously quantified using an iQ5 instrument (BioRad). After the assay was complete a dissociation curve analysis was carried out, which measures the fluorescence intensity at temperatures between 55°C and 95°C with 0.5°C increments. All samples were run out on a 4% agarose gel to assess the specificity of the reaction and to ensure that no primer-dimers were present.

2.2.4 – Protein Analysis

2.2.4.1 – Protein Extraction

For direct immunoblotting fibroblasts, HEK293 and mIMCD-3 cells were grown to confluence in 75 cm² tissue culture flasks, rinsed twice with ice-cold PBS and scraped into 1 ml of RIPA lysis buffer (50 mM Tris-HCl, 150 mM NaCl, 1 mM EDTA, 1% Igepal CA 630, 0.5% Sodium Deoxycholate, 0.1% SDS and complete mini protease inhibitor cocktail (Roche)). The same lysis buffer was used for mIMCD-3 cells growing on transwell supports, but 250 µl was used instead. For co-immunoprecipitation experiments HEK293 cells were grown on 6-well plates, washed twice with ice-cold PBS and scraped into 250 µl of MRC lysis buffer (50 mM Tris-HCl pH=7.5, 50 mM Sodium Fluoride, 5 mM Sodium Pyrophosphate, 1 mM Sodium Orthovanadate, 1 mM EDTA, 1 mM EGTA, 0.27 M Sucrose,

1% Triton - X - 100 and complete mini protease inhibitor cocktail (Roche)). The resulting solution was centrifuged at 18,000 x g for 15 minutes at 4°C, and the supernatant transferred to a clean tube.

2.2.4.2 – Protein Concentration Quantification

Protein concentrations were assessed using the BioRad Dc Protein Assay kit. For each assay a 2 fold serial dilution of a 3 µgµl⁻¹ BSA standard with the appropriate lysis buffer was made. Lysis buffer alone was also loaded as a blanking control. Reagent A' was prepared by the addition of 10 µl of reagent S and 500 µl of reagent A. Five microlitres of either standard or sample were added to a 96 well plate followed by 25 µl of Reagent A' and 200 µl of reagent B. The plate was then incubated in the dark at room temperature for 10 minutes, after which the absorbance at 690 nm for 1 second per well was read using a Wallac Victor³ fluorometer (Perkin Elmer, Waltham, MA).

2.2.4.3 – Co – Immunoprecipitation

Protein G Dynabeads (Invitrogen) are magnetic beads coupled to Protein G, a molecule that binds to various sub-types of immunoglobulin molecules, with strong binding to mouse IgGs. The magnetic beads are separated from the solution using a magnet block, so no centrifugation steps are necessary. Due to immunoglobulin heavy and light chain interference with the pull-down antibody and the immunoblotting antibody, both of which were raised in the mouse, for over-expressed co-immunoprecipitation experiments the required antibodies were first conjugated to the beads. This prevents their elution at the end of the experiment

and masking the signal of the proteins of interest. All liquids were removed from the beads after 1 minute on the magnetic block and with the tube remaining on the magnet. All solutions were added to tubes not on the magnet to allow mixing to occur. Incubation steps were carried out at room temperature with end over end mixing unless otherwise stated.

2.2.4.3.1 – Antibody Conjugation

For antibody conjugation, 100 µl of homogeneous re-suspended Dynabeads were transferred to a 1.5 ml tube, before being put on the magnet and the supernatant removed. The beads were washed twice with 500 µl of Citrate Phosphate Buffer (24.5 mM Citric Acid and 51.7 mM Dibasic Sodium Phosphate, pH=5.0). Forty micrograms of the required antibody was diluted in 100 µl of PBS, added to dry beads and incubated for an hour. The supernatant was removed and the beads were washed three times with Citrate Phosphate Buffer followed by three washes with 1 ml of 0.2 M Triethanolamine. The antibody and beads were then covalently cross-linked by incubating the mixture for 30 minutes with 20mM Dimethyl Pimelimidate (dissolved in 0.2 M Triethanolamine). The supernatant was removed and the reaction was quenched using 1 ml of 50 mM Tris (pH=7.5) and incubated for 15 minutes, after which the antibody conjugated beads were washed three times with 500 µl PBST (PBS and 0.1% Tween-20). Finally the beads were re-suspended in the 100 µl of PBST and stored at 4°C until required.

2.2.4.3.1 – Immunoprecipitation

HEK293 cells growing on 6-well plates and transfected with a total of 4 µg of plasmid DNA constructs were allowed to recover for 48 hours before the protein was extracted as in section 2.2.4.1. For endogenous co-immunoprecipitation experiments mIMCD-3 cells were grown in 75 cm² flasks and the protein extracted as in section 2.2.4.1. A 50 µg sample of the supernatant was removed so an input western blot could be done. One milligram of protein supernatant was added to 20 µl of antibody conjugated beads, or 20 µg of required antibody and 20µl of beads that were pre-washed three times with 500 µl of Citrate Phosphate Buffer and incubated at 4°C for 3 hours.

The protein, antibody and bead complexes were placed on the magnet for 2 minutes and the liquid transferred to a clean tube and used later as the unbound fraction. The complexes were then washed three times with 500 µl of MRC lysis buffer supplemented with 150 mM NaCl. After the last wash all the liquid was removed and 20 µl of 2x Lamelli sample loading buffer (62.5 mM Tris-HCl (pH=6.8), 25% Glycerol, 2% SDS, 0.5 % β-Mecaptoethanol, 0.5% Bromophenol blue) was added, and the samples boiled for 10 minutes. An equal volume of the 2x Lamelli sample loading buffer was added to the input and unbound fractions, and were loaded onto SDS PAGE gels alongside the eluted proteins for western blot analysis.

2.2.4.4 – Membrane Protein Biotinylation

mIMCD-3 cells were seeded onto 6-well transwell filters at a density of 1 x 10⁵ cells per cm² and allowed to grow for 7 days before the medium was removed and the cells washed once

with ice-cold PBS. The biotinylation reagent, EZ-link Sulfo-NHS-SS-Biotin was dissolved in PBS to a concentration of $250\ \mu\text{gml}^{-1}$, cooled and added to the apical and basal surfaces of the transwell filters at 4°C for 30 minutes. Any remaining unbound biotin was removed by incubating the filters in $250\ \mu\text{l}$ of 1 M ammonium chloride for 2 minutes, after which the cells were washed once using PBS for 2 minutes. The cells were then lysed in $250\ \mu\text{l}$ of MRC lysis buffer as in section 2.2.4.1, and the protein concentration quantified as in section 2.2.4.2.

One-hundred microlitres ($50\ \mu\text{l}$ packed volume) of streptavidin agarose beads per reaction were washed twice using PBS and centrifugation. All centrifugations steps were carried out at $13,000 \times g$ for 1 minute. Two-hundred and fifty micrograms of the protein lysates from above were added to the pre-washed beads and incubated at 4°C for 1 hour with end over end mixing. The biotinylated protein - streptavidin agarose complexes were centrifuged, the supernatants removed and washed three times using $250\ \mu\text{l}$ of MRC lysis buffer. The biotinylated proteins were released from the streptavidin beads by incubating the beads in 2x Lamelli sample loading buffer at 60°C for 30 minutes. This was then centrifuged, the supernatant transferred to another tube and incubated at 95°C for 10 minutes. An equal volume of the 2x Lamelli sample loading buffer was added to the input and unbound fractions, and were loaded onto SDS PAGE gels alongside the eluted proteins for western blot analysis.

2.2.4.5 – Western Blotting

2.2.4.5.1 – SDS – PAGE

Sodium Dodecyl Sulphate PolyAcrylamide Gel Electrophoreses were run to separate proteins according to their molecular mass, for direct immunoblotting of protein samples and after co-immunoprecipitation experiments. The following reagents were mixed together to form the resolving gel, and immediately transferred to 1 mm thick glass plates (BioRad). The smaller percentage gels were used for large proteins and the larger percentage gels were used for smaller proteins.

Reagent	Volume			
	8%	10%	12%	15%
Acrylamide	2.7 ml	3.4 ml	4 ml	5 ml
dH ₂ O	4.5 ml	3.8 ml	3.2 ml	2.2 ml
1.5 M Tris-HCl (pH=8.8)	2.5 ml			
10% Ammonium Persulfate	200 µl			
10% SDS	100 µl			
TEMED	10 µl			

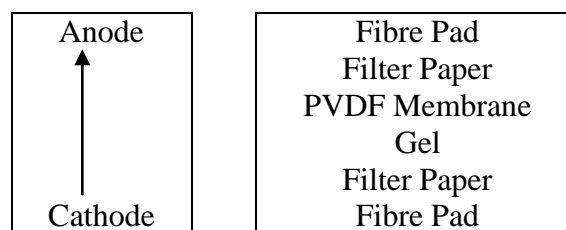
The poured gels were overlayed with isopropanol and allowed to stand for 15 minutes to set, after which the gels were washed and dried. The stacking gel was prepared as shown on the next page and pipetted on top of the resolving gel. Before this gel set, combs were inserted which form the loading wells, and the gel allowed to set for 15 minutes.

Reagent	Volume
Acrylamide	1 ml
0.5 M Tris-HCl (pH=6.8)	1.5 ml
dH ₂ O	3.4 ml
10% Ammonium Persulfate	90 µl
10% SDS	60 µl
TEMED	5 µl

Protein lysates had 2x Lamelli sample loading buffer added and boiled for 5 minutes prior to being loaded onto the gel. A known molecular weight ladder (Page Ruler; Fermentas, York, UK) was also run on the gel, so that later protein sizes could be estimated. The electrophoresis was run in 1x SDS Running Buffer (192 mM Glycine, 250 M Tris-Base and 0.1% SDS) for around 1 hour at 30mA.

2.2.4.5.2 – Transfer

For immunoblotting the above separated proteins were transferred to PVDF (polyvinylidene difluoride) membranes, which were first activated in methanol for 30 seconds. All required materials shown below were equilibrated in 1 x Transfer Buffer (192 mM Glycine, 250 mM Tris-Base and 20% methanol). The blot was created as follows:



The transfer of proteins from the gel to the PVDF membrane was done in 1x Transfer Buffer at 100 mA for 1 hour, with an ice pack and constant stirring.

2.2.4.5.3 – Immunodetection

The membranes were blocked in 10% dried non-fat milk powder (Marvel) dissolved in PBST either overnight at 4°C or for 1 hour at room temperature on a roller. Primary and secondary antibodies were added to an appropriate volume of 5% milk powder in PBST at a concentration determined empirically (see Appendix 2 for antibody dilutions). The secondary antibodies were all Horse Radish Peroxidase (HRP) conjugates, to allow for detection. After blocking, the membranes were incubated with the diluted primary antibody for 1 hour at room temperature on a roller, before being washed three times with PBST for 5 minutes each wash. The membrane was then re-blocked with 5% milk in PBST for 5 minutes, after which it was incubated with the secondary antibody for 1 hour. The membrane was then washed as before and incubated with the enhanced chemo-luminescence plus (ECL+) western blotting detection system reagents (GE Healthcare) at a ratio of 1:40 for reagent A:B for 5 minutes. The bands were detected using X-ray film (Kodak).

2.2.4.5.4 – Membrane Stripping and Re-probing

When a loading control was necessary, the membrane was stripped by first washing the membrane twice in dH₂O for 5 minutes, and twice with 0.2M NaOH for 20 minutes. It was then rinsed twice in dH₂O for 5 minutes before being blocked and immunodetection carried out as before.

2.2.4.5.5 – Densitometry

Western blot films were scanned and imported into LabWorks (Version 2, UVP Corporation, Cambridge, UK). The total absolute intensity was calculated for the band of interest and for β -actin, the loading control. The protein of interest band intensity was normalised to β -actin.

2.2.4.6 – Yeast – 2 – Hybrid Screen

Human *VPS33B* was sub-cloned from pEYFP-VPS33B into the pGBT9 vector using EcoRI and BamHI so that the gene was in frame with the DNA-binding domain of GAL4 for the yeast-2-hybrid screen. The Genomics and Proteomics Core Facility at the Deutsches Krebsforschungszentrum (Heidelberg, Germany) carried out the yeast-2-hybrid screen using human foetal brain and adult kidney cDNA libraries as sources of prey.

2.2.5 – Cloning

2.2.5.1 – IMAGE Clones

Full-length cDNA transcripts were purchased from GeneService UK for various genes, shown on the next page.

Gene	Species	IMAGE ID
PLRN	Human	3920459
Plrn	Zebrafish	7407368
VPS11	Human	6144541
VPS16	Human	6182570
VPS18	Human	2822780
VPS39	Human	3078533
VPS41	Human	4822048

These transcripts were supplied ligated into plasmid shuttle vectors and transformed into bacteria to allow for amplification. The bacteria were grown and the plasmids extracted as detailed in section 2.2.5.9.

2.2.5.2 – Cloning Strategy

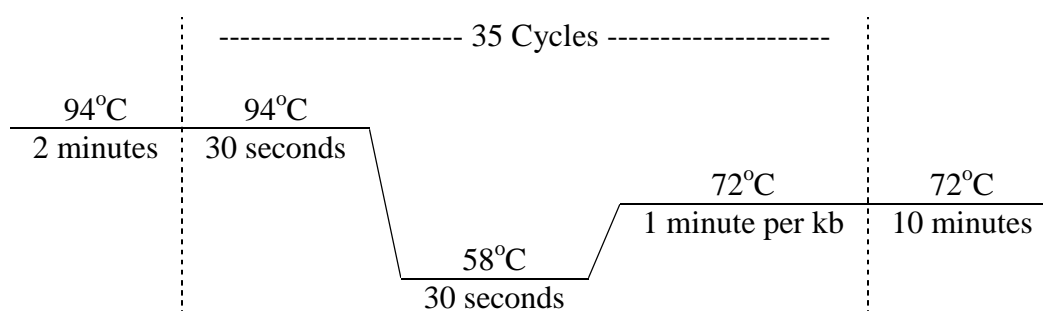
The full-length transcripts were amplified using PCR so that the sequence had restriction sites on the 5' and 3' end to allow for ligation into expression vectors. The required transcript sequence was run through WebCutter 2.0 software available online to identify restriction endonuclease sites within the transcript (www.na.lundberg.gu.se/cutter2). The results of this search was cross-checked with the restriction map of the desired vector, so that a pair of enzymes could be used to for cloning without cutting the transcript. Forward and reverse primers were designed to include the required restriction site tagged onto the native translation initiation (ATG) and stop codons, so that the transcript would be read in frame with the epitope tag in the vector. A cap of CTT was added to the start of each primer to aid restriction digestion. Primer sequences are shown in appendix 1.

2.2.5.3 – Proofreading PCR

Platinum Taq. DNA Polymerase (Invitrogen) was used, as it has proofreading capabilities, which reduces the possibility that errors were incorporated into the PCR product. The reaction was set up as follows, using the IMAGE clone plasmid as the template:

Reagent	Volume per reaction (μl)
10x PCR buffer	2.5
dNTP mix (10 μM)	2
MgCl ₂ (50 mM)	0.75
Nuclease Free Water	17.25
Taq. Polymerase (5 units μl^{-1})	0.5
Template DNA (100ng μl^{-1})	1
Forward Primer (10 μM)	0.5
Reverse Primer (10 μM)	0.5
Total	25

This reaction mixture was then subjected the conditions below to allow amplification to occur.



2.2.5.4 – Agarose Gel Extraction

All of the PCR product from above was loaded onto a 1% agarose gel and electrophoresed as in section 2.2.1.2. A 2-log DNA ladder (100 bp to 10 kb; New England Biolabs) was loaded onto the gel so that the size of the product could be estimated. The correct size band was excised from the gel and extracted from the agarose using the QIAGEN gel extraction kit to purify the PCR product away from the template.

The band of interest was excised from the gel using a clean scalpel, ensuring to minimise the amount of agarose taken from around the band. Three times the weight of the gel slice in volume of Buffer QG was added, and heated at 55°C until the gel had melted after which one volume of isopropanol was added. The resulting solution was applied to the column, centrifuged and the flow through discarded, followed by a 500 µl wash with buffer QG. All centrifugation steps were carried out at 13,000 x g for 1 minute at room temperature. To wash the bound DNA, 750 µl of buffer PE diluted in ethanol was applied to the column, incubated for 5 minutes and centrifuged. The flow through was discarded and the column centrifuged again to remove any remaining liquid. The column was then transferred to a clean tube, had 20 µl of nuclease free water added, incubated for 1 minute and centrifuged to elute the DNA.

2.2.5.5 – Restriction Digestion

The above gel extracted PCR products and appropriate vectors were restriction digested with the necessary restriction enzymes in one reaction to create cohesive ends on both. The enzyme combinations and buffers used are shown on the next page:

Gene	Species	5' Enzyme	3' Enzyme	Vector	Buffer
VPS33A	Human	SalI	NotI	pCMV-HA pEYFP C3	3 + BSA
VPS33B	Human	EcoRI	KpnI	pEYFP C3 pCFP C3	1 + BSA
PLRN	Human	EcoRI	KpnI	PCMV-HA pCMV-myc pEYFP C3 pmCherry C3	1 + BSA
Plrn	Zebrafish	BamHI	EcoRI	pCS2+	EcoRI + BSA
VPS11	Human	EcoRI	XhoI	pCMV-myc	EcoRI + BSA
VPS16	Human	EcoRI	NotI	pCMV-myc	EcoRI + BSA
VPS18	Human	EcoRI	KpnI	pCMV-myc pEYFP C3	1 + BSA
VPS39	Human	SalI	NotI	pCMV-myc	3 + BSA
VPS41	Human	SalI	NotI	pCMV-myc	3 + BSA
P75	Human	ApaI	EcoRI	pmCherry N1	4 + BSA

All restriction digests were carried out in 30 μ l reactions and done at 37°C for 3 hours. The reaction mixture was set up as follows:

Reagent	Volume per reaction	
	Insert	Vector
10x Buffer	3 μ l	3 μ l
100x BSA	0.3 μ l	0.3 μ l
Enzyme 1 (20 unit μ l ⁻¹)	1 μ l	1 μ l
Enzyme 2 (20 unit μ l ⁻¹)	1 μ l	1 μ l
DNA	20 μ l	3 μ l of 1 μ g μ l ⁻¹
H ₂ O	4.7 μ l	21.7
Total	30 μ l	30 μ l

The restriction digest products were then loaded onto a 1% agarose gel using 6x loading buffer and the required bands extracted as in section 2.2.5.4.

2.2.5.6 – Ligation

To ligate the DNA insert into the expression vector the following reaction was set up and incubated at room temperature overnight and at 4°C until required.

Reagent	Volume per reaction (μl)
10x Ligation Buffer	1
T4 DNA Ligase (3 units μl ⁻¹)	1
Insert DNA	3
Vector DNA	1
dH ₂ O	4
Total	10

2.2.5.7 – Transformation

All of the above ligation reaction mixture was added to 50 μl of DH5α E. Coli bacterial cells and incubated on ice for 15 minutes. The cells were then heat shocked to 42°C for 45 seconds, immediately cooled on ice for 2 minutes and had 500 μl of SOC medium (2% tryptone, 0.5% yeast extract, 10mM NaCl, 2.5mM KCl, 10mM MgCl₂ and 20mM glucose) added. The transformed cells were incubated at 37°C with 220 RPM shaking for either 1.5 hours (ampicillin resistance) or for 3 hours (kanamycin resistance). After the incubation the cells were centrifuged at 3000 x g for 1 minute to pellet the cells and 360 μl of the supernatant was removed, leaving 200 μl which was transferred to LB agar plates containing either 100 μgml⁻¹ of ampicillin or 25 μgml⁻¹ of kanamycin. These plates were then incubated at 37°C overnight.

2.2.5.8 – Site Directed Mutagenesis

To introduce the L30P missense mutation into the pCMV-HA-VPS33B construct, two complementary primers were first designed to include the desired nucleotide change surrounded by 15 correct base pairs in either direction. A proofreading PCR was carried out as in section 2.2.5.3 with the original vector used as the template. The entire PCR product was run on a 1% agarose gel and the resulting band excised and purified as in section 2.2.5.4. In order to remove the original un-mutated template, the reaction was digested with Dpn1 as detailed in section 2.2.5.5. This enzyme is methylation specific and will only digest the original template, leaving the mutated products intact. The enzyme was inactivated by heating the reaction mixture to 80°C for 20 minutes, and after cooling 10 µl was transformed into XL-1 Blue competent cells (Stratagene) as in section 2.2.5.7.

2.2.5.9 – Colony Screening

Single colonies were selected off bacterial plates and transferred to 10 ml of Luria Broth containing the appropriate selection antibiotics at the concentration used for plates. These were then allowed to grow overnight at 37°C with shaking at 220 RPM. An 8% glycerol stock of the grown bacteria was made and stored at -80°C until required. The remaining liquid was centrifuged at 5000 x g for 5 minutes to pellet the bacteria. Plasmids were extracted from the bacterial cells using a QIAGEN mini-prep kit. The pellet of bacteria was re-suspended in 250 µl of Buffer P1 (supplemented with RNase and LyseBlue) and lysed in 250 µl of Buffer P2, which contains NaOH and SDS. The alkali was neutralised with Buffer P3, and the resulting solution was centrifuged at 13,000 x g for 10 minutes. All subsequent

centrifugation steps were carried out at room temperature at 13,000 x g for 1 minute. The supernatant was transferred to the spin column, centrifuged and the bound DNA washed with 500 µl of Buffer PB followed by 750 µl of Buffer PE. The column was then centrifuged again to remove any residual liquid, transferred to a clean tube and had 50 µl of nuclease free water added and incubated for 1 minute. The column was spun again to elute the plasmid DNA.

A restriction digest was done on 5 µl of the resulting plasmid using the same enzymes used for the original cloning step. The products were run on a 1% agarose gel alongside the empty vector and undigested plasmids, which identified plasmids that had an insert.

2.2.5.10 – Plasmid Sequencing

Sequencing of plasmids is very similar to the method shown in sections 2.2.1.4 to 2.2.1.6, however the reaction volumes vary slightly as shown below. Plasmid sequencing primer sequences are shown in appendix 1.

Reagent	Volume per reaction (µl)
5x Sequencing Buffer	2
Nuclease Free Water	4.4
BigDye	1
Primer (2 µM)	1.6
Plasmid	1
TOTAL	10

2.2.5.11 – Plasmid Purification

Once the plasmid of interest was shown to contain an insert and be in frame with the epitope tag, the plasmid was amplified in bacteria cells. An inoculation loop was dipped into the glycerol stock of the bacteria containing the plasmid of interest, and transferred to 10 ml of Luria Broth containing the appropriate antibiotics. This was then incubated at 37°C with shaking at 220 RPM for around 6 hours, after which it was diluted to a total of 100 ml and grown overnight.

The following day, plasmids were extracted using the QIAGEN maxi-prep kit. The bacterial suspension was centrifuged at 5000 x g for 10 minutes to pellet the cells, which were then re-suspended in 10 ml of Buffer P1 containing RNase and LyseBlue). The cells were lysed in 10 ml of Buffer P2 (containing NaOH and SDS) and incubated at room temperature for 5 minutes, after which the solution was neutralised with Buffer P3 and immediately transferred to the filtration column. The solution was pushed through the column after a 10 minute incubation and the cleared liquid was retained as this contains the plasmid DNA. To remove the endotoxins from the solution, 2.5 ml of Buffer ER was added and the mixture incubated on ice for 30 minutes. Meanwhile the DNA binding column was equilibrated with 10 ml of Buffer QBT, after which the plasmid solution was added to the column and allowed to pass through under gravity. Bound DNA was washed twice with 30 ml of buffer QC and eluted from the column using 15 ml of Buffer QF. The eluted DNA was precipitated using 10.5 ml of isopropanol and centrifugation at 11,000 x g for 30 minutes at 4°C. The supernatant was removed and the resulting pellet was washed with 5 ml of 70% ethanol and centrifuged again

as before but for 15 minutes. The plasmid DNA pellet was allowed to air dry and re-suspended in 1 ml of nuclease free water.

2.2.5.12 – DNA Concentration Quantification

To assess the concentration of DNA obtained from the above procedure, the absorbance values of 70 fold diluted DNA samples were taken at 260 and 280 nm. The concentration of DNA is calculated using the following formula:

$$[\text{DNA}] (\mu\text{g}\mu\text{l}^{-1}) = \frac{\text{Absorbance at 260 nm} \times \text{Dilution Factor} \times 50}{1000}$$

2.2.6 – Cell Analysis

2.2.6.1 – Immunofluorescence Confocal Microscopy

HEK293 cells were grown on glass coverslips, transfected as in section 2.2.2.1 and allowed to recover for 24h before being fixed in 4% paraformaldehyde (dissolved in PBS, pH=7.0) for 30 minutes at room temperature. The cells were then washed three times in PBS for 5 minutes with shaking and permeabilised with 0.1% Triton-X-100 (diluted in PBS) for 5 minutes. The coverslips were washed in PBS as before, followed by a 30 minute incubation with Blocking Buffer (1% BSA in PBS). Transwell supports containing mIMCD-3 cells had their filters excised and were prepared as above for coverslips, except for immunolabelling for all TJ and AJ proteins, which required ice-cold methanol fixation for 5 minutes and 0.1% saponin permeabilisation.

The filters and coverslips were incubated with the necessary primary antibodies diluted in blocking buffer at the required concentration for 1 hour at room temperature (see Appendix 2 for antibody dilutions). The cells were then washed three times in blocking buffer as before, followed by an hour incubation in the dark with the appropriate fluorophore conjugated secondary antibodies diluted in blocking buffer at the required concentration. Excess secondary antibody was removed by washing three times in blocking buffer as before. Nuclei were stained with TOP-RO-3 diluted 1/500 in Blocking buffer in the penultimate wash. Coverslips and filters were mounted onto microscopy slides using ProLong Gold antifade solution (Invitrogen), sealed and stored in the dark at 4°C until required.

Microscopic images were captured using an inverted Leica TCS SP2 AOBS confocal microscope (Leica, Milton Keynes, UK) with 10x and a 63x oil immersion objectives and the pinhole set to 1 Airy unit. Series of optical sections were collected from the xy plane and merged into maximum projection images. Single optical sections were averages of 3 scans at 1024 x 1024 resolution, and individual fluorophores were scanned sequentially and merged. Single xz plane images were also obtained where necessary.

2.2.6.1.1 – Co-localisation Analysis

Individual xy optical sections with separate images for the green and red channels were used for co-localisation analysis. The puncta in the red channel were selected and the intensity of the fluorescence in the corresponding green channel calculated using MetaMorph software (Molecular Devices, Downingtown, PA). The selections were then shifted to another part of the cell so that they no longer aligned with the red puncta and the intensity of the fluorescence

in the green channel calculated as before. At least 10 puncta were selected for each co-localisation analysis. Mean and standard error values were calculated for aligned and non-aligned fluorescence intensity measurements. All non-aligned values were normalised to their corresponding aligned values and a Student's two-tailed T test was carried out to test the statistical significance of the difference between the values.

2.2.6.1.2 – Live Cell Imaging

HEK293 and mIMCD-3 cells were seeded onto 35mm glass bottom dishes (Ibidi) and transfected as necessary as in section 2.2.2.1. The cells were allowed to recover for 24 hours after transfection and medium changed to phenol-red free medium and overlaid with sterile mineral oil to prevent gaseous diffusion. The confocal microscope as above and cabinet were heated to 37°C before the cells were transferred. The pinhole was opened to 10 airy units and single optical sections were acquired in the *xy* plane over time (*xyt*). For photobleaching experiments, a 3-dimensional area was defined for bleaching and iterations were created to bleach at full laser power for 1 second and acquire images as necessary.

2.2.6.2 – Pulse Chase Experiments

HEK293 cells growing on glass coverslips were transfected with pCMV-myc-PLRN and pEYFP-VPS33B, and allowed to recover for 24 hours before being incubated in serum free medium for 3 hours. Texas Red-conjugated transferrin (Molecular Probes, Invitrogen) was pulsed into serum-starved cells at 1 mgml⁻¹ for 30 minutes, after which the cells were rinsed and incubated with normal medium (chased) for a total of 60 min. The cells were then fixed at

various times (0, 5, 10, 15, 30 and 60 minutes) with 4% paraformaldehyde and processed for immunofluorescence confocal microscopy as in section 2.2.6.1.

2.2.6.3 – shRNA

A pSM2c and a pGIPZ plasmid containing shRNA hairpins were used for Vps33b and Polarin respectively. Non-silencing hairpins were used as controls. Plasmid shRNA constructs (Vps33b; V2MM_91195 and Polarin; V2LMM_9377) were purchased from Open Biosystems (Huntsville, AB). mIMCD-3 cells were transfected with 4 µg of plasmid and allowed to recover for 48 h before transfected cells were selected using 1.5 µgml⁻¹ of Puromycin. Individual clones were selected to reduce variability. Level of knockdown was assessed by western blotting (Vps33b) or quantitative real time PCR (*Plrn*).

2.2.6.4 – Trans-Epithelial Resistance Assay

mIMCD-3 cells treated with non-silencing shRNA and with shRNAs against *Plrn* and *Vps33b* were seeded onto Transwell supports at a density of 1×10^5 cells cm⁻². TER was measured every 24 hours thereafter with an EVOM AC square wave current (+/- 20mA, 12.5Hz) resistance meter (World Precision Instruments, Stevenage, UK). A no cell control was used to compensate for resistance across the filter. TER values for individual cultures were calculated by subtracting the values measured for filters without cells incubated in the same conditions.

2.2.6.5 – Paracellular Diffusion Assay

Non-silencing, *Plrn* and *Vps33b* shRNA treated mIMCD-3 cells were seeded onto transwell filters and allowed to grow for 7 days. After which 1 mgml⁻¹ of each 4kD FITC dextran and 70kD Rhodamine B dextran (Sigma-Aldrich) were dissolved in medium, added to the apical chamber and incubated at 37°C for 3 hours. Diffusion of each molecule to the basolateral compartment was assayed simultaneously using a Wallac Victor³ fluorometer (PerkinElmer). Wavelengths were 485nm and 560nm (excitation) and 535nm and 620nm (emission) for FITC and Rhodamine B respectively.

2.2.6.6 – Calcium Switch Experiments

mIMCD-3 cells treated with non-silencing shRNA and with shRNAs against *Plrn* and *Vps33b* were seeded onto Transwell supports and allowed to grow for 7 days. On day 7 the culture medium was changed for low-calcium medium (Spinner's Culture Medium, Sigma-Aldrich) supplemented with 10% dialysed FBS (PAA Laboratories). The cells were incubated as normal for 24 hours, after which the medium was changed back to normal growth medium. TER and paracellular diffusion assays were carried out before, during and after the calcium switch took place as detailed above.

2.2.7 – Zebrafish Experiments

The day before zebrafish embryos were required, adult zebrafish were separated into male and female, and one of each were placed into separate compartments of mating tanks. After

being left overnight the separator between the fish was removed, and embryos were collected after 10 minutes. These were then either transferred directly to, or injected with morpholino oligonucleotides (MOs) and re-suspended in Hank's Solution (140 mM NaCl, 5.4 mM KCl, 4.2 mM NaHCO₃, 1.3 mM CaCl₂, 1 mM MgSO₄, 440 µM KH₂PO₄, 250 µM Na₂HPO₄). The embryos were cleaned, dechorionated and allowed to further develop in Hank's solution supplemented with 0.1% Methylene blue until required.

2.2.7.1 – In-Situ Hybridisation

2.2.7.1.1 – Probe Synthesis

Ten µg of the pCS2+-Plrn vector was linearised with BamHI (Buffer 3 and BSA) for the antisense probe and EcoRI (Buffer EcoRI and BSA) for the sense probe, as described previously in section 2.2.5.5. The reaction mixture was then loaded and electrophoresed on a 1% agarose gel (2.2.1.2), after which the linearised vector was purified from the gel as in section 2.2.5.4. The concentration of the eluted DNA was assessed as in section 2.2.5.12.

Digoxigenin (DIG)-labeled anti-sense and sense (control) RNA probes were made from 1 µg of linearised pCS2+-Plrn vector, using Sp6 and T7 RNA polymerases respectively, from the DIG Labeled RNA Probe Synthesis Kit (Roche). The reactions were setup as shown on the next page and incubated at 37°C for 2 hours:

Reagent	Volume per Reaction (µl)
10x Transcription Buffer	2
10x DIG Labelling Mix	2
RNase Inhibitor	1
Template (0.5 µgµl ⁻¹)	2
T7/Sp6 Polymerase	2
Nuclease free H ₂ O	11
Total	20

The template DNA was removed by adding 2 µl of RNase free DNase to the reaction and further incubated at 37°C for 15 minutes. The RNA was precipitated by adding 10 µl of 7.5 M ammonium acetate and 75 µl of 100% ethanol to the reaction mixture and incubating at – 80°C for 20 minutes. The resulting mixture was then centrifuged at 12,000 x g for 15 minutes at 4°C. The supernatant was removed and the pellet washed with 1 ml of 80% ethanol. After air-drying, the pellet was re-suspended in 20 µl of Hybridisation Buffer (5x SSC, 9 mM Citric Acid, 50% Formamide, 0.05% w/v Heparin, 0.01% w/v yeast RNA, 0.001% v/v Tween-20). The concentration of the RNA probes were assessed as in section 2.2.3.2 and a sample was run on a 1% agarose gel to check for a single product as in section 2.2.1.2.

2.2.7.1.2 – Hybridisation

For in-situ hybridisation experiments the embryos were grown in Hank's Solution containing 0.2 mM PTU (1-phenyl-2-thiourea) to prevent pigmentation. At 24 hours post fertilisation (hpf) embryos were fixed overnight at 4°C in Fixing Buffer (77 mM Na₂HPO₄, 23 mM NaH₂PO₄, 120 µM CaCl₂, 4% w/v Paraformaldehyde, and 4% w/v Sucrose). Five-day post fertilisation (dpf) embryos were anaesthetised with 0.4% w/v MESAB (Ethyl 3

aminobenzoate MethylSulfonate) and fixed in Fixing Buffer for 15 minutes on ice followed by 75 minutes at room temperature.

The embryos were transferred through increasing concentrations of methanol (25%, 50% and 75% diluted with PBS) for 5 minutes at room temperature to dehydrate the embryos. Finally the embryos were incubated in 100% methanol for at least 2 hours at -20°C . The dehydrated embryos were re-hydrated using decreasing concentrations of methanol (75%, 50% and 25% diluted in PBST) for 5 minutes at room temperature, followed by 2 washes with PBST for 5 minutes.

Permeabilisation was achieved by incubating the embryos in $10\text{ ng}\mu\text{l}^{-1}$ Proteinase K diluted in PBST for 1 minute for 24 hpf embryos and 2 hours for 5 dpf embryos. The embryos were washed once in PBST before being fixed in Fixing Buffer for 20 minutes at room temperature, followed by a further 4 washes in PBST for 5 minutes. The embryos were blocked by incubation in Hybridisation Buffer for at least 3 hours at 65°C , followed by incubation in the DIG labelled RNA probe at a 1 in 500 dilution overnight. The optimal hybridisation temperature was empirically determined to be 65°C .

Unhybridised probe was removed by washing the embryos twice for 40 minutes in Wash Buffer 1 (1x SSC, 50% Formamide and 0.1% Tween-20), once for 15 minutes in Wash Buffer 2 (2 x SSC and 0.1% Tween-20) and twice for 30 minutes in Wash Buffer 3 (0.2x SSC and 0.1% Tween-20). The embryos were then washed in Blocking Buffer (2% Tween-20, 1% DMSO and 0.2% w/v BSA in PBS) once for 5 minutes. The embryos were pre-blocked by incubation in Blocking Buffer for at least 3 hours at room temperature. The rabbit anti DIG

alkaline phosphatase-conjugated antibody was diluted in Blocking Buffer at a concentration of 1 in 400 and pre-blocked in parallel to the embryos. The embryos were then incubated overnight with the antibody at a concentration of 1 in 4000 at 4°C. The unbound antibody was removed by rinsing the embryos once with PBST, followed by 6 washes for 15 minutes each in PBST. The embryos were transferred to 24-well plates for staining.

2.2.7.1.3 – Detection

The probe and antibody bound embryos were then washed twice for 5 minutes with Staining Buffer (100 mM Tris-HCl pH=9.5, 100 mM NaCl, 50 mM MgCl₂ and 0.1% v/v Tween-20). Staining was done by incubating the anti-sense and sense probe hybridised embryos in the dark in Staining Solution (400 µM 5-Bromo 4-chloro 3-indolyl phosphate and 275 µM Nitro Blue Tetrazolium dissolved in Staining Buffer) until staining was observed in the sense control embryos. The staining reaction was quenched by rinsing the stained embryos in PBST and incubating in Fixing Buffer for 15 minutes. For whole-mount images, the stained embryos were taken through a sequential increase in glycerol concentration (25%, 50% and 75% diluted in PBS and 100%) to aid manipulation for visualisation. Staining was visualised on a binocular SMZ800 microscope with a 6.3x objective and captured with a DXM200 CCD camera controlled by ACT-1 (version 2.7) software (Nikon, Kingston Upon Thames, UK). For histological sections, over-stained embryos were incubated for 4 hours in sequential increasing concentrations of sucrose (10%, 20% and 30% diluted in PBS) for cryoprotection. Larvae were oriented in OCT embedding medium in shallow 1 cm x 1 cm moulds, quickly frozen on dry ice, and stored at -80°C until required. Eighteen micrometre transverse sections were taken using a Cryocut cryostat (Bright, Huntingdon, UK) and visualised with an

Axioplan 2 microscope with images captured on an Axiocam CCD camera (both Carl Zeiss, Welwyn Garden City, UK).

2.2.7.2 – Morpholino Oligonucleotide Injections

Morpholino oligonucleotides (MOs) against the transcription initiation (ATG) codon and the splice site for exon 3 of *plrn* were designed by and purchased from Gene Tools. An exon 3 mis-match MO was also used as a specificity control. MO sequences are shown in appendix 1. The ATG, exon 3, and exon 3 mis-match MOs were injected into one-cell embryos in Injection Solution (58 mM NaCl, 5 mM HEPES, 700 μ M KCl, 600 μ M Ca(NO₃)₂, 400 μ M MgSO₄ and 0.1% phenol red) at concentrations of 10, 100, and 100 μ M respectively. The MOs were co-injected with CFP (Cyan Fluorescence Protein) mRNA at a concentration of 0.5 mgml⁻¹, so that the injected embryos could be sorted away from the non-injected embryos at a later stage.

2.2.7.2.1 – mRNA Rescue

Ten μ g of the pCS2+-*Plrn*, CFP and -RFP vector was linearised with NotI (Buffer 3 and BSA) as described previously in section 2.2.5.5. The reaction mixture was then loaded and electrophoresed on a 1% agarose gel (2.2.1.2), after which the linearised vector was purified from the gel as in section 2.2.5.4. The concentration of the eluted DNA was assessed as in section 2.2.5.12.

Polarin, Red Fluorescent Protein (*RFP*) and Cyan Fluorescent Protein (*CFP*) mRNA were produced using T7 RNA polymerase from the Message Amp mRNA amplification kit (Ambion). The reactions were set up as follows and incubated at 37°C for 2 hours:

Reagent	Volume per Reaction (μl)
10x Transcription Buffer	2
dNTP mix (+cap)	10
RNase Inhibitor	1
Template (0.5 μgμl ⁻¹)	2
T7 Polymerase	2
Nuclease free H ₂ O	3
Total	20

The template DNA was removed by adding 2 μl of RNase free DNase to the reaction and further incubated at 37°C for 15 minutes. The RNA was precipitated by adding 115 μl of nuclease free water, 15 μl of 7.5 M ammonium acetate and 150 ml of phenol chloroform mix (50:49:1 Phenol:Cholorofom:Isoamyl Alcohol, pH=4.5). The tubes were shaken vigorously and centrifuged at 7000 x g for 15 minutes at 4°C before the upper clear aqueous layer was removed and transferred to a clean tube. To the transferred liquid 150 μl of chloroform was added and the centrifugation steps carried out as above. The RNA was precipitated by adding 150 μl of isopropanol, incubating the mixture at –80°C for at least 15 minutes and centrifugation at 12000 x g for 15 minutes at 4°C. The supernatant was removed and the resulting pellet was washed with 1 ml of 80% ethanol and centrifuged at 12000 x g for 15 minutes at 4°C. The air-dried pellet was re-suspended in 20 μl of nuclease free water. The concentration of the mRNA was assessed as in section 2.2.3.2 and a sample was run on a 1% agarose gel to check for a single product as in section 2.2.1.2.

When necessary, *plrn* mRNA diluted in Injection Solution at a concentration of 0.5 mgml^{-1} was injected into one-cell embryos already injected with MOs against *plrn* to rescue the phenotype. RFP mRNA was used as a specificity control. RFP mRNA was also injected alongside both the *plrn* and RFP mRNAs as an injected control and to allow sorting at a later stage.

2.2.7.3 – PED-6 Treatment

Liver-function and bile duct assays were carried out by bathing 5 dpf larvae in $2 \text{ }\mu\text{M}$ of PED-6 (Invitrogen) overnight at 28°C . The next day larvae were treated with 0.4% w/v MESAB and transferred to a prepared agarose gel plate containing small wells to allow the correct orientation of the larvae for examination of their gall bladders. Brightfield and PED-6 (green fluorescence) images were visualised using a SMZ1500 binocular microscope with a 10x objective and were captured using a DSQi1Mc CCD camera controlled by NIS Elements (version 3.0) software (all Nikon), which was also used to measure gallbladder area.

2.2.7.4 – Immunostaining

Morpholino and non-injected 5 dpf zebrafish larvae were anaesthetised with 0.4% w/v MESAB and fixed in Fixing Buffer as in section 2.2.7.1.2. The fixed larvae were processed for histological sections as in section 2.2.7.1.3, and $18 \text{ }\mu\text{m}$ sections were taken. The resulting slides were baked at 37°C for 30 minutes, stored at -20°C until needed and required 20 minutes to thaw before use. The required sections were first encircled using a delimiting pen (Dako, Ely, UK) and rehydrated twice for 20 minutes in PBS. The sections were blocked in

2% w/v BSA dissolved in PBST for 90 minutes, after which the sections were incubated with primary antibody diluted in the previous blocking buffer at room temperature for 2 hours. The unbound primary antibody was removed by washing the slides 3 times in PBST for 20 minutes. The appropriate secondary antibody diluted in blocking buffer was added to the sections and incubated at room temperature for 2 hours, after which the slides were washed as before. The sections were sealed and visualised as in section 2.2.6.1.

CHAPTER 3 – MOLECULAR INVESTIGATIONS OF ARC SYNDROME PATIENTS AND DEVELOPMENTAL EXPRESSION OF VPS33 HOMOLOGUES

3.1 – Introduction and Overview

3.1.1 – ARC Patients

Arthrogryposis, Renal dysfunction and Cholestasis syndrome (ARC; MIM# 208085) is an autosomal recessive disorder associated with germline mutations in *VPS33B*. The gene encodes VPS33B protein, one of two (-A and -B) homologues of yeast Vps33 which form part of the HOMotypic Protein Sorting (HOPS) complex involved in assisting SNARE proteins in performing membrane fusion [1]. Characteristic features of ARC include severe failure to thrive, renal tubular acidosis, neonatal cholestasis, ichthyosis and platelet dysfunction. Liver abnormalities (cholestasis, intrahepatocyte deposition of lipofuscin granules and bile duct hypoplasia) are also frequent but the severity of failure to thrive exceeds that expected for the degree of liver and intestinal dysfunction. The identification of mislocalised apical membrane proteins in liver and renal biopsy materials suggests a possibility of a global abnormality in intestinal absorption and renal tubular reabsorption [1;11]. Although arthrogryposis in ARC syndrome appears to be at least partially neurogenic in origin, the degree of arthrogryposis may depend on the foetal position and severity of oligohydramnios [2]. Platelet function abnormalities are likely to be secondary to platelet α -granule biosynthesis defect [12]. Additional features of ARC include corpus callosum dysgenesis (at least 20%) and congenital cardiac defects (~10%).

3.1.2 – Developmental Expression of VPS33 Homologues

The expression pattern of VPS33B, along with other HOPS complex members, has been discerned in adult human tissues using northern blot analysis. These studies revealed an ubiquitous pattern of expression with enrichment in the testis [5;77]. However, the developmental expression of VPS33B has not previously been studied,

The naturally occurring *buff* mouse is a mouse model phenocopy of Hermansky-Pudlak syndrome (HPS), a severe disorder characterised by oculocutaneous albinism and a platelet aggregation defect secondary to a dense-granule defect [82]. The *buff* mouse is a result of a germline missense mutation in *Vps33a*, which causes a glutamic acid to aspartic acid substitution (p.Glu251Asp) in the mutant protein [82]. Thus the *buff* mouse phenotype suggests that Vps33a is involved in the biogenesis of membrane-bound organelles such as melanosomes and platelet dense granules, whereas the ARC syndrome phenotype points to its function in the formation of platelet α -granules and trafficking of the apical membrane proteins in polarised epithelial cells.

3.2 – Aims

In a previous study of ARC syndrome, mutations in *VPS33B* were detected in 77% of patients (48 out of 62 individuals) [2]. Absence of *VPS33B* mutations in patients with a clinical diagnosis of ARC syndrome might result from locus heterogeneity or the presence of *VPS33B* mutations that are not easily detectable by direct sequencing analysis. In order to investigate these possibilities further and to develop additional better methods for detecting ARC

syndrome, VPS33B mRNA and protein analysis in patients with a clinical diagnosis of ARC syndrome was performed. Direct dideoxy sequencing was also carried out on VPS33B for newly referred patients presenting with an ARC syndrome phenotype. This will help to identify common mutations in certain populations, which would aid future mutation screening of ARC patients.

The developmental expression of Vps33 homologues have not previously been studied, and might give an insight into the pathogenesis of both ARC and HPS syndromes. Therefore the objectives of this study were to investigate the level of expression of mammalian homologues of Vps33 at different stages of foetal development, and to gain an insight into the possible embryonic nature of the defects in HPS and ARC.

3.3 – Results

3.3.1 – Mutation Analysis of VPS33B in ARC Patients

Mutation analysis was performed in 16 previously unreported patients with clinical features of ARC syndrome. Eight novel mutations were identified in 12 probands (see Table 3.1).

Strikingly, a splice site mutation (IVS6 ds+2 T>A) was detected in 7 of 9 apparently unrelated patients from South Korea. Although haplotype analysis was not possible (due to insufficient DNA) all the Korean patients were homozygous for the T allele of the rs11073964 SNP (http://www.ensembl.org/Homo_sapiens/snpview?source=dbSNP;snp=rs11073964). This has a prevalence of 100% in the Asian population in contrast to its prevalence of 10-30% in Europeans. Among the novel mutations there were 4 insertions, 1 deletion that resulted in

frameshifting, 1 nonsense substitution, 1 splice site mutation and 1 missense substitution. The c.728C>T (p.Ser243Phe) mutation was not present in 300 control chromosomes. The hydrophilic serine at position 243 is highly conserved in evolution [8] and the change for a strongly hydrophobic phenylalanine may affect protein conformation and subsequently the effect of VPS33B on SNARE complex formation. Four Polish families were analysed and 2 apparently unrelated probands were homozygous for a novel c.1235_1236delCCinsG frameshift mutation. In a further Polish family a c.1594C>T mutation that was previously identified in a large consanguineous UK Pakistani family was detected. None of the missense or splice site mutations identified were detected in 300 ethnically matched chromosomes.

3.3.2 – ARC Patient Expression of VPS33A and VPS33B

To determine the potential diagnostic value of VPS33B mRNA and protein studies in cultured skin fibroblasts, expression was analysed in 9 patients with classical features of ARC (5 with a detectable VPS33B mutation) and one with a milder phenotype (Patient 21). Quantitative RT-PCR (Figure 3.1) and western blotting (Figure 3.2) experiments demonstrated that patients with at least one *VPS33B* mutation had minimal VPS33B protein expression. Of the 4 patients without identified mutations, patient 15 also had minimal VPS33B levels, patient 17 had mRNA levels of <50% compared with the control sample and patient 21 had normal levels of mRNA and protein. Patient 21 initially presented with a triad of typical ARC features as well as some additional clinical characteristics (see section 3.3.2.1); however, his kidney and liver disease appeared transient.

Patient	Ethnicity	Nucleotide alteration	Coding-sequence alteration	Exon	Status
1	Korean		NI		
2	Korean	403+2 T>A		6+2	Het
		1509_1510insG	p.Lys504GluX23	20	Het
3	Korean	740_741delAT	p.Tyr247X	10	Het
4	Korean	403+2 T>A		6+2	Hom
5	Korean	403+2 T>A		6+2	Het
6	Korean	403+2 T>A		6+2	Het
		728C>T	p.Ser243Phe	10	Het
7	Korean	403+2 T>A		6+2	Hom
8	Korean	403+2 T>A		6+2	Het
		1803_1804insA	p.Val602SerX13	23	Het
9	Korean	403+2 T>A		6+2	Hom
10	Polish	1235_1236delCCinsG	p.Pro12ArgX7	17	Hom
11	Polish	1235_1236delCCinsG	p.Pro12ArgX7	17	Hom
12	Polish	1221delA	p.Asp414ValX5	17	Hom
13*	Polish	1594C>T	p.Arg532X	21	Het
14	Turkish	352C>T	p.Gln118X	5	Hom
15*	Thai		NI		
16*	Portuguese	853-2 A>G		12-2	Het
		1519 C>T	p.Arg507X	21	Het
17*	Israeli Arab		NI		
18*	Pakistani	1312C>T	p.Arg438X	18	Hom
19*	Pakistani	1594 C>T	p.Arg532X	21	Hom
20*	Swedish	498+1 G>A		7+1	Het
21*	Afro-Caribbean		NI		
22*	Turkish		NI		

Table 3. 1 – Mutations in VPS33B identified in ARC Patients.

Direct sequencing of VPS33B revealed 8 novel mutations and a common mutation in patients from South Korea. Novel mutations are indicated in bold typeface. Mutation nomenclature is based on GenBank entry NM_018668.3, with +1 corresponding to the A of the translation initiation codon ATG in the cDNA nomenclature. Het - heterozygous, Hom – homozygous, NI- DNA alterations not identified and * - patients whose fibroblasts were used for expression analysis and who were reported previously [1;2]. (Some of the mutations shown here were identified by A. Straatman-Iwanowska, University of Birmingham, UK)

VPS33A is another homologue of yeast Vps33p in mammalian cells, which may bind to HOPS complex proteins in a similar way to VPS33B. As it is not known whether VPS33A can partially substitute for the VPS33B function in ARC patients we, therefore, tested the expression of the -A homologue in VPS33B-deficient cell lines. No change in expression of VPS33A was detected in ARC fibroblasts compared with the control samples (Figure 3.1).

3.3.2.1 – Patient 21

Patient 21 is male, born at term to non-consanguineous Afro-Caribbean parents. He presented with arthrogryposis in both knees, spina bifida (with a lipomeningocele and tethered cord), cholestatic jaundice and renal tubular acidosis. Low γ GT typical of ARC was found and liver biopsy findings were consistent with ARC, including abnormal distribution of apical canalicular markers such as carcinoembryonic antigen and alanyl aminopeptidase. Additional features included bilateral sensorineural deafness, severe diarrhoea, pancreatic insufficiency and malabsorption, which were initially treated with parenteral nutrition. Jaundice resolved by the age of 12 months and the child is now fed enterally with pancreatic enzyme supplementation. He is not facially dysmorphic but has bilateral accessory auricles. He continues to have mild metabolic acidosis, which is treated by sodium bicarbonate supplementation. At the age of 2.5 years the patient growth is parallel to 0.4th percentile for his weight and height. His arthrogryposis has resolved. He has global developmental delay. The results of investigations for ARC included negative mutation screening of *VPS33B*. No abnormalities were found on quantitative real-time PCR and western blotting (see Table 3.1, Figure 3.1 and Figure 3.2).

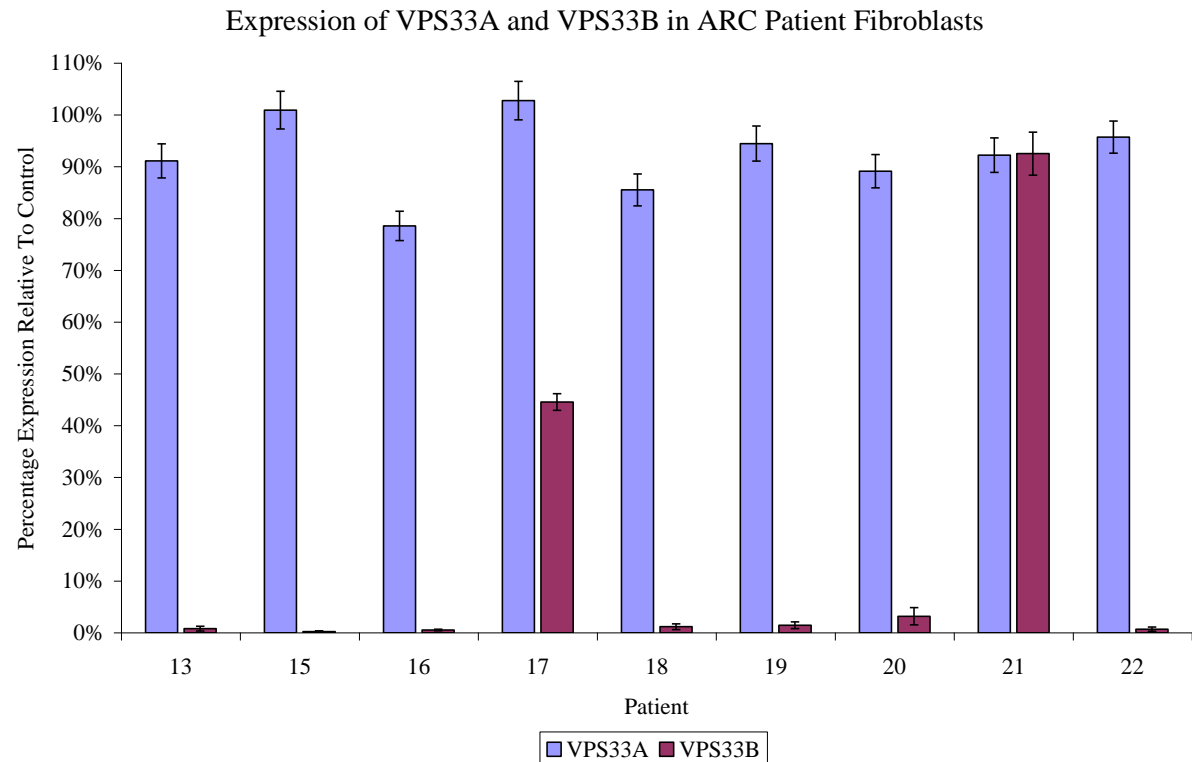


Figure 3.1 – Quantitative Real Time PCR (qRT-PCR) of VPS33A and VPS33B in ARC syndrome patients’ fibroblasts.

Bar chart showing the results from the quantitative real-time PCR experiments. Values shown are mean values of expression levels of the VPS33 homologues normalised to β -actin and relative to a control sample ($n=3$ independent assays run in triplicate for each sample). Error bars represent ± 1 standard error of the mean.

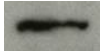








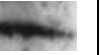










Patient	Control	13	15	16	17	18	19	20	21	22
VPS33B										
β Actin										
OD VPS33B	0.26479	-	-	-	0.10871	-	-	-	0.26089	-
OD β Actin	0.53731	0.5627	0.54747	0.53577	0.53534	0.53489	0.56086	0.54627	0.53386	0.53309
% Expression	49.3 %					20.3 %				48.9%
% Expression to Control	100 %					41.2%				99.1%

Figure 3.2 – Immunoblotting of VPS33B in control and ARC patients' fibroblasts.

Loading was controlled by immunoblotting the same membrane with an anti- β -actin antibody. Densitometry on bands were carried where possible and necessary, and final expression values are normalised to β -actin and relative to the control sample. Results here are consistent with qRT-PCR results shown in Figure 3.1. (Some of the western blots shown here were carried out by A. Straatman-Iwanowska, University of Birmingham, UK)

3.3.3 – ARC Patients’ Cellular Phenotype

The cellular phenotype of skin fibroblasts from patient 13 was assessed by transmission electron microscopy (TEM; Figure 3.3). Multiple heterogeneous granules were identifiable in almost all of the patient’s cells. These granules were found to be osmiophilic in nature and contained multilamellar membranes and multiple vesicular aggregates.

3.3.4 – Developmental Expression of VPS33 Homologues

3.2.4.1 – Human Expression

Analysis of developmental expression of *VPS33A* and *VPS33B* in human kidneys, liver and brain by quantitative real time PCR (Figure 3.4 and 3.5) and immunoblotting of VPS33B (Figure 3.6) revealed a similar pattern of expression for both homologues. In the kidney, the highest expression level can be seen between 11 and 16 weeks gestation with a greater than 4 fold increase for both genes. There is a gradual increase in expression of both genes during foetal liver development, and very low expression of both at all stages in the brain. As is also seen in the mouse in-situ hybridisation (Figure 3.7), during foetal development expression of *VPS33A* is much higher than the B homologue. This pattern is reversed in adult kidney and liver. The highest expression in the liver is seen in the neonatal liver specimen. Foetal samples were not available after 20 weeks gestation, therefore the expression of both VPS33 homologues could not be studied after this stage in development.

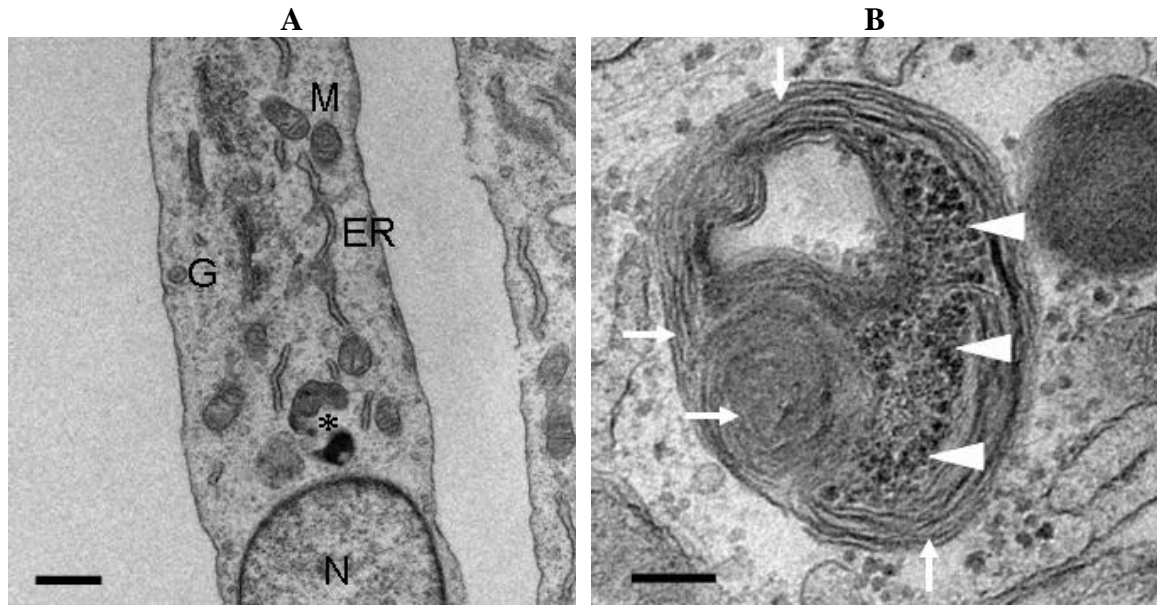


Figure 3.3 – Cellular phenotype of ARC patient fibroblasts.

A, Transmission electron micrograph of patient 13 cultured skin fibroblasts. *N* – nucleus, *G* – Golgi apparatus, *ER* – endoplasmic reticulum and *M* – mitochondria appear normal. Scale bar represents 1 μ m. **B**, An atypical granule enlarged from A (asterisk), filled with lamellar membranes (arrow heads) and vesicular aggregates (arrows). Scale bar represents 200 nm. (Electron microscopy was carried out by R. Sougrat, NIH, Bethesda, MD on fibroblasts grown in Birmingham, UK)

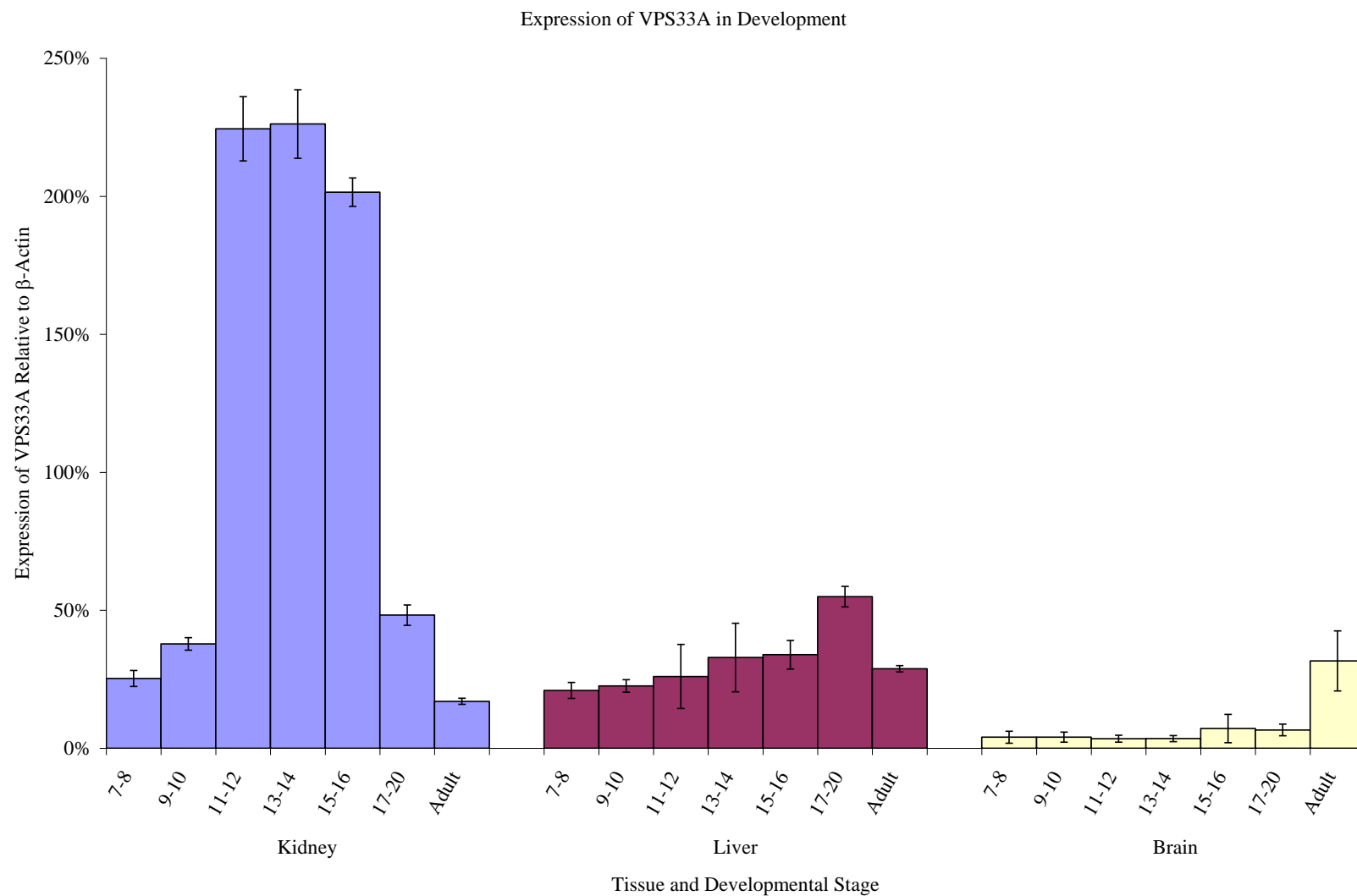


Figure 3.4 – Expression of VPS33A in human foetal and adult kidney, liver and brain samples.
 Values shown are mean values of expression levels of VPS33A normalised to β -actin ($n=3$ independent assays in triplicate for each sample). Numbers on the x-axis represent weeks of gestation. Error bars represent ± 1 standard error of the mean.

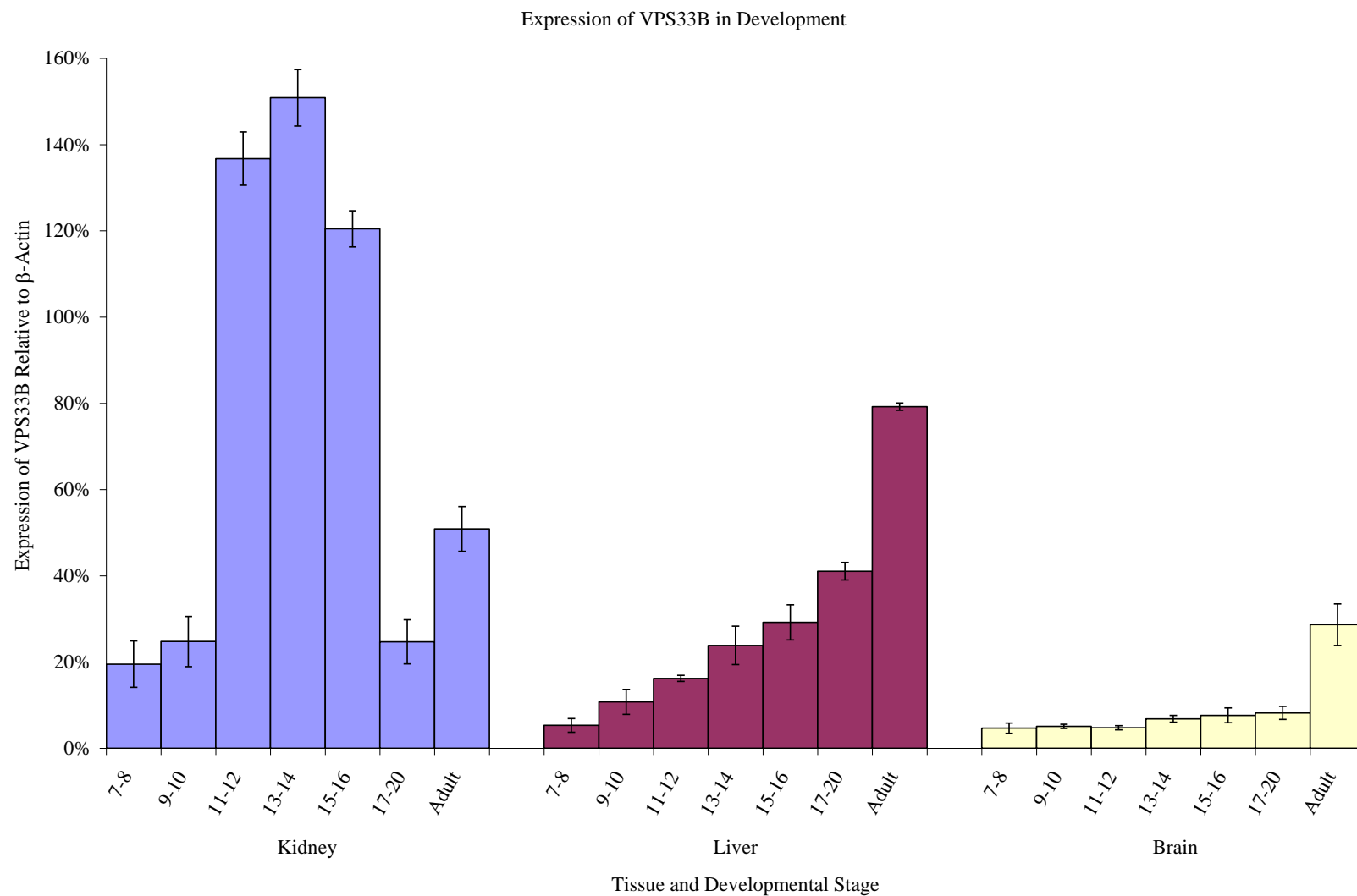


Figure 3.5 – Expression of VPS33B in human foetal and adult kidney, liver and brain samples.
 Values shown are mean values of expression levels of VPS33B normalised to β -actin ($n=3$ independent assays in triplicate for each sample). Numbers on the x-axis represent weeks of gestation. Error bars represent ± 1 standard error of the mean.











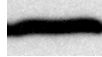
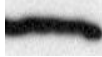








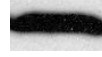



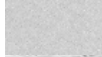













		Developmental Stage							
		7-8	9-10	11-12	13-14	15-16	17-20	Neonatal	Adult
Kidney	VPS33B					NA		NA	
	β Actin					NA		NA	
	% Expression	0.8%	0.6%	69%	51%		4.3%		84%
Liver	VPS33B			NA		NA			
	β Actin								
	% Expression	-	1.2%		3.4%		3.8%	91%	62%
Brain	VPS33B							NA	
	β Actin								
	% Expression	-	-	-	-	-	-		7.9%

Figure 3.6 – Analysis of VPS33B expression in human foetal kidneys, liver and brain by immunoblotting.
Loading was controlled by immunoblotting the same membrane with an anti- β -actin antibody. Developmental stage numbers represent weeks of gestation. Densitometry on bands was carried where possible and necessary, and final expression values are normalised to β -actin. NA - sample not available. Results here are consistent with qRT-PCR results shown in Figure 3.5.

3.3.4.2 – Mouse Expression

Non-radioactive in-situ hybridisation using antisense digoxigenin-labelled RNA probes for Vps33a and Vps33b on sectioned mouse embryos showed that prior to E14.5 expression of both genes is very low being undetectable at E10.5 (data not shown). By E12.5 expression of Vps33a and Vps33b is just apparent in the peripheral nervous system, although Vps33b expression is much lower. By E14.5, low-level widespread expression of Vps33a and Vps33b is readily apparent throughout many embryonic tissues (Figure 3.7). The expression patterns between the two genes seem similar, but Vps33a appears to show higher levels of expression than Vps33b.

On closer examination of Vps33a and Vps33b expression in individual mouse embryonic tissues at E14.5 (Figure 3.8), staining can be seen in various ganglia, including the dorsal root, sympathetic chain, trigeminal and vestibulocochlear ganglia. While noticeable expression of Vps33a can be seen in the neural retina, outer layer of the cortex, pons, medulla, striatum and cerebellar primordium and olfactory epithelium, expression of Vps33b appears much reduced in these tissues. In non-neural tissues, Vps33a shows substantial expression in the kidney (particularly the cortex), adrenal gland, liver, lung, ribs, submandibular gland and thymus. While expression of Vps33b can be discerned in many non-neural tissues, expression is very much lower or absent, for example in the liver.

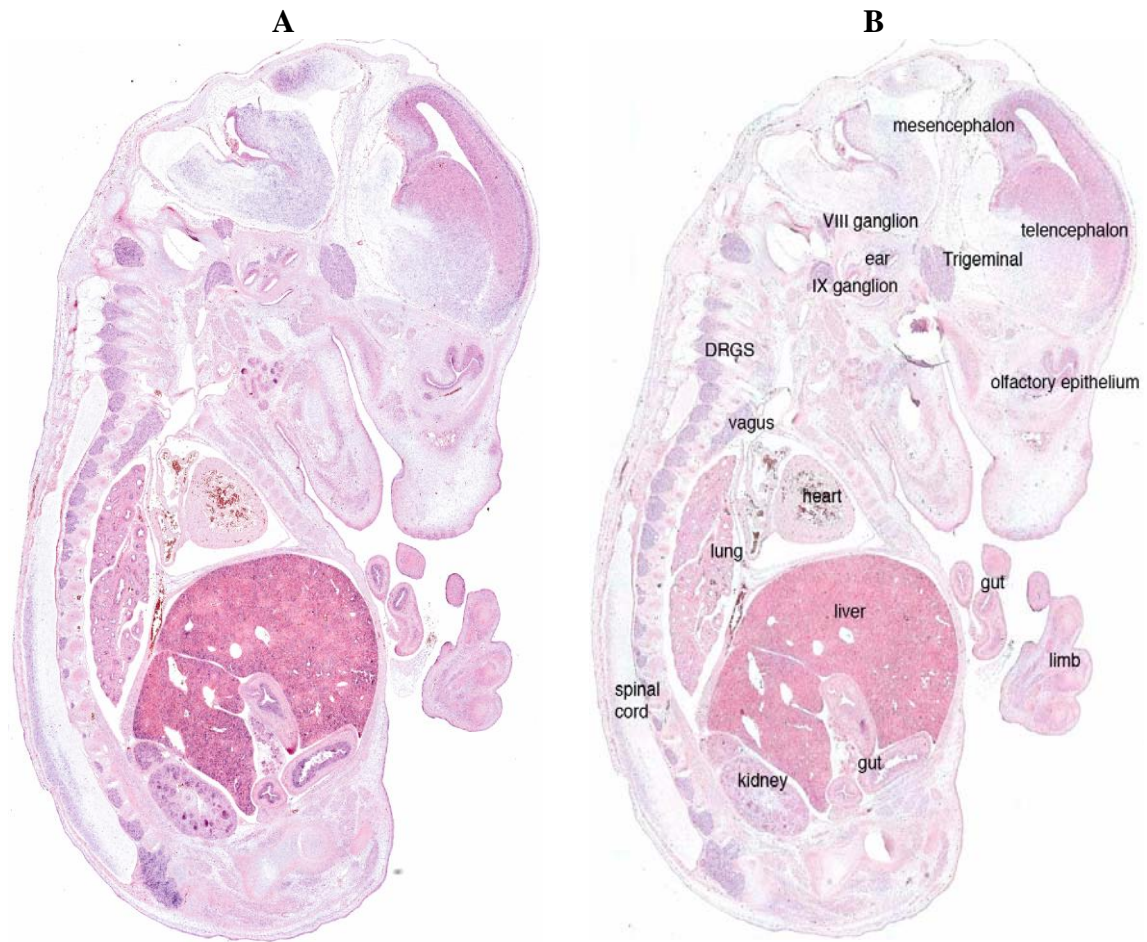


Figure 3.7 – Mouse embryonic expression of Vps33a and Vps33b at E14.5.
Non-radioactive in situ hybridisation using antisense digoxigenin-labelled RNA probes for A, Vps33a and B, Vps33b on sectioned mouse embryos. DRG- Dorsal root ganglia. (In-situ hybridisation carried out by D Tannahil, Cranfield University, UK.)

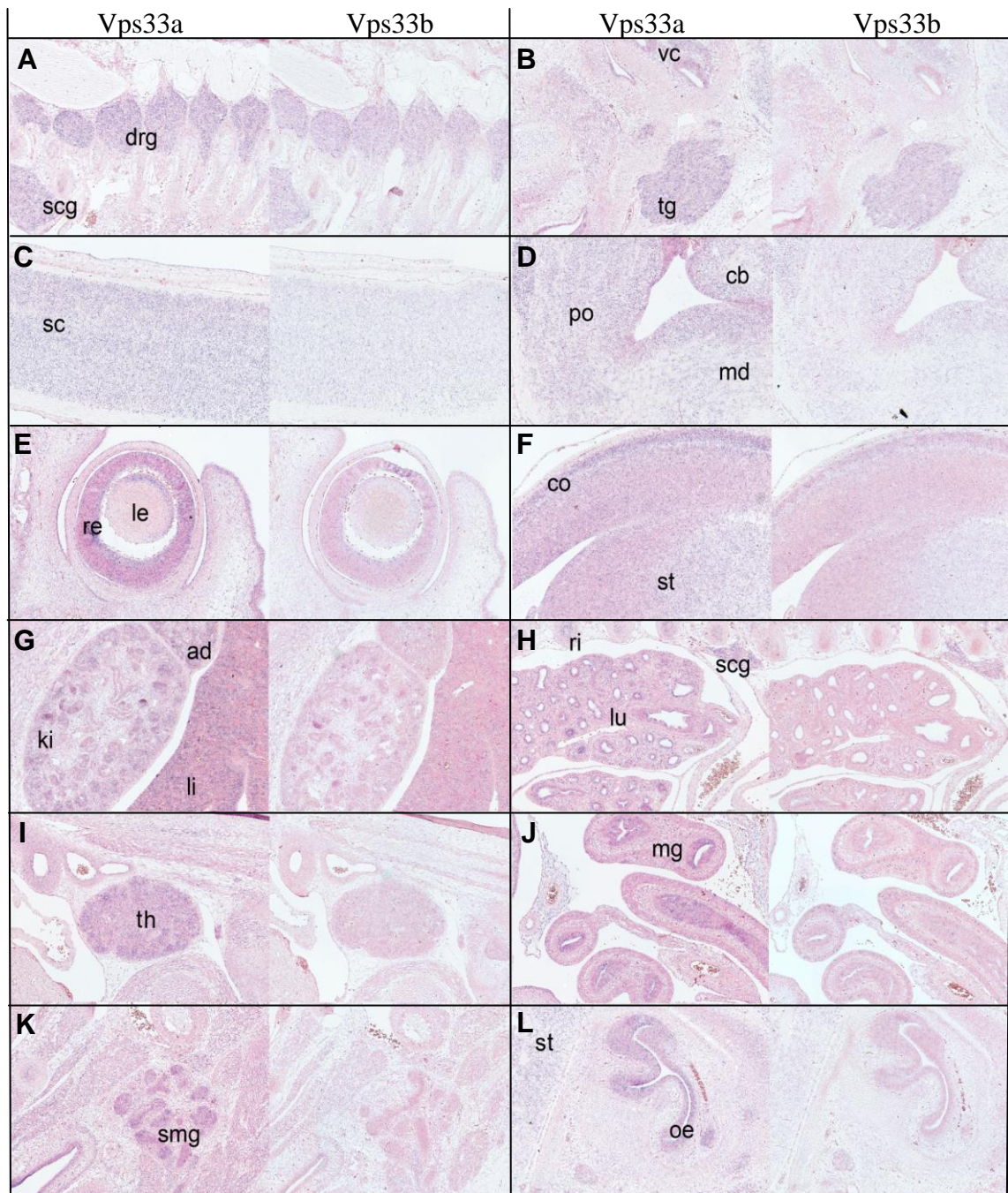


Figure 3.8 – Expression of Vps33a and Vps33b in individual mouse embryonic tissues at E14.5.

Non-radioactive in situ hybridisation using antisense digoxigenin-labelled RNA probes for Vps33a and Vps33b on sectioned mouse embryos. **A**, dorsal root ganglia (drg), sympathetic chain ganglia (scg) **B**, trigeminal and vestibulocochlear ganglia (tg and vc) **C**, spinal cord (sc) **D**, medulla (md), pons (po), cerebellar primordium (cb) **E**, lens (le), retina (re) **F**, cortex (co), striatum (st) **G**, kidney (ki), adrenal (ad), liver (li) **H**, ribs (ri), lung (lu), sympathetic chain ganglia (scg) **I**, thymus (th) **J**, midgut (mg) **K**, submandibular gland (smg) **L**, olfactory epithelium (oe), striatum (st). (In-situ hybridisation carried out by D Tannahil, Cranfield University, UK.)

3.4 – Discussion

3.4.1 – ARC Patients

ARC syndrome is a severe multisystem disorder leading to death in infancy. Early diagnosis is important for correct clinical management. However, the traditional method of diagnosis (liver biopsy) is associated with a substantial risk of morbidity and mortality in ARC syndrome patients due to haemorrhage. Direct sequencing of *VPS33B* is a good method to provide molecular diagnosis in ARC patients. However, in routine clinical practice, mutation analysis results may not be available for months and substantial numbers of patients do not have a detectable mutation. Markedly reduced levels of VPS33B were found in skin fibroblasts from all patients with a classical ARC phenotype and disease course. The only patient with normal VPS33B expression had a milder clinical course and transient liver abnormalities. This child is alive and well on nasogastric tube feeding at 2.5 years despite having an initial clinical diagnosis of ARC syndrome. This suggests that analysis of VPS33B protein expression in cultured fibroblasts may provide a useful initial diagnostic screening investigation to facilitate acute medical management.

Novel mutations were identified in Turkish, South Korean and Polish patients with ARC syndrome. One of the mutations was present in 7 South Korean patients. This is the first report of *VPS33B* mutations in the East European and South East Asian populations.

Identification of population-specific mutations improves the ability to provide rapid molecular diagnosis and makes molecular studies more affordable.

The study of patient skin fibroblasts using transmission electron microscopy identified multiple granules containing lamellar and vesicular structures. Careful examination of their identity using specific organelle markers will provide better insight into the origin of these granules. This finding is in line with the accumulation of hepatocyte lipofuscin granules and skin keratinocyte lamellar bodies in ARC syndrome [148;149] and may reflect abnormal processes of vesicular trafficking and membrane biogenesis.

Low expression of VPS33B may potentially trigger a cellular feedback mechanism and stimulate VPS33A expression as some functional overlap between the 2 homologues was previously suggested. Thus VPS33A mRNA levels in ARC patients' fibroblasts were quantified. Compared to a control there was no discernable change in VPS33A expression, thus suggesting that this mechanism does not spontaneously come into play. However, future attempts at cellular therapies in this disorder may include compensatory overexpression of VPS33A.

3.4.2 – Developmental Expression

Vps33 homologues belong to a family of Sec1/Munc18 proteins, which are thought to provide specificity to the SNARE-complex formation reactions. The phenotypes of their deficiency (ARC syndrome in humans and HPS in mice) suggest their importance to the biosynthesis of lysosome-related organelles such as platelet granules and melanosomes, and also specific apical membrane trafficking of proteins in the liver and kidneys [1;82]. VPS33B is clearly important to the nervous system development as its' deficiency potentially results in hypotonia and congenital joint contractures in ARC syndrome [1].

The analysis of developmental expression of Vps33 homologues showed an upregulation of the expression of both proteins in the kidneys between 11 and 16 weeks gestation in the human foetus, which suggests a possible correlation with active development of renal tubular system that occurs at this point [150;151]. In ARC syndrome, there is a renal tubular defect, thus having defective proteins at this point in development may explain the defect observed. Particularly high neonatal liver expression of VPS33B correlates with the development of biliary ductular structures in the first few weeks of life [152]. In concordance with this expression pattern, a reduced number of bile ducts are found in ARC syndrome patient livers. The foetal liver is predominantly a haemopoietic organ, and does not undertake any polarised epithelial activity until after birth [152]. In light of the expression pattern observed in the foetal and neonatal liver and kidney samples, a role of Vps33b in the epithelialisation of these organs would be expected.

Although low level of expression of both VPS33 homologues was found in human brain, mouse in-situ hybridisations show that there is high expression of both genes in specific ganglia. This may explain the hypotonia in ARC syndrome patients. In line with the expression of Vps33a in the cerebellar primodium, a recent study by Chintala et al. showed that the *buff* mouse mutant had significant motor deficits, specifically grip strength and the righting reflex, which worsened with age [153]. Furthermore, they showed that this was due to cerebellar Purkinje cell loss, a region of the brain responsible for the generation of motor co-ordination and posture [153]. On the other hand, the surprisingly mild renal phenotype in the *buff* mouse may be explained by the relatively weak effect of the genetic alteration on the Vps33a protein product.

The identification of additional and population specific mutations in *VPS33B* in ARC syndrome patients alongside the detection of *VPS33B* expression will help to expedite the diagnostic process for patients and their families. Both the *VPS33* homologues seem to be expressed in similar tissues during human and mouse development, but have different functional effects on cells and on whole organisms. Elucidation of these functions will help identify the pathogenicity of both ARC and HPS syndrome, with the former being examined in the following chapters.

CHAPTER 4 – VPS33B INTERACTING PROTEINS

4.1 – Introduction and Overview

Germline mutations in *VPS33B* are found in approximately 75% of ARC patients [4]. *VPS33B* encodes the VPS33B homologue of yeast class C vacuolar protein sorting (VPS) protein Vps33p, which belongs to the Sec1/Munc18 (SM) family of proteins. SM proteins are thought to modulate Soluble N-ethylmaleimide sensitive factor Attachment REceptor (SNARE) protein interactions and ensure specificity in formation of vesicle- to target-SNARE complexes and in fusion of two apposed membranes [154;155]. Vps33p is unique in that, unlike other SM proteins, it functions as part of the *HO*motypic fusion and vacuole Protein Sorting (HOPS) complex [47]. The HOPS complex includes class C VPS proteins (Vps11, Vps16, Vps18 and Vps33) and also Vps39 and Vps41. It interacts with the yeast Rab7 homologue Ypt7p, and is required for vacuolar biogenesis and for protein trafficking from the Golgi apparatus to the vacuole [76].

The mammalian HOPS complex counterpart is much less well characterised. The human homologues (VPS11, VPS16, VPS18, VPS33A, VPS39 and VPS41) have been shown to localise to the endosome, late endosome and lysosome compartments of cells, and to interact with syntaxin-7 [77;78]. Whether or not VPS33B is a member of this mammalian complex remains unknown. However, over-expression of either VPS18, VPS33B or VPS39 all cause clustering of LAMP-1 positive late endosomes and lysosomes, suggesting that this may be the case [1;80;81].

4.2 – Aims

Although previous studies suggested that the mammalian homologues of class C yeast VPS proteins are involved in intracellular trafficking at the level of early and late endosomes in the endocytic pathway, this work included investigations of only the VPS33A homologue of yeast Vps33p [156]. Furthermore, the HOPS complex, as well as Rab5 and Rab7, have been implicated in the pathway of phagosome maturation during apoptosis [79]. Therefore this chapter describes the investigations performed in order to identify VPS33B interacting proteins and to elucidate its functional pathway.

4.3 – Methodologies

4.3.1 – Yeast–2–Hybrid System

Proteins rarely work alone, and usually form part of a complex network to fulfil their function. Identification of proteins which interact with an uncharacterised protein can often give insight into the biological function, as if an uncharacterised protein interacts with a protein whose role is known, they are likely to have a related function. Co-immunoprecipitation and affinity chromatography can be used to identify protein-protein interactions, but these techniques require the identification of physically interacting proteins by mass spectroscopy [19]. The yeast-2-hybrid system allows the simultaneous isolation of interacting proteins and along with the gene which encodes them [157].

The yeast-2-hybrid system uses a reporter gene to identify protein-protein interactions in the nucleus, and takes advantage of the modular nature of gene activator proteins. The cDNA encoding the target protein or bait is cloned into an expression vector to be in frame with a DNA binding domain using recombinant DNA techniques. The cDNA of putative interacting proteins are ligated into another expression vector with a transcriptional activator domain, producing prey libraries. The libraries are usually produced from reverse transcribed RNA from specific sources, for example human adult kidney [158].

The bait expression vector is introduced into yeast cells, where the fusion protein is produced, which will bind to the regulatory region of the reporter gene. Individual prey expression vectors are also introduced into these yeast cells. If the two proteins interact, the two halves of the transcriptional activator come together, which switches on the expression of the reporter gene, which usually allows the growth of the yeast cells on selective media (Figure 4.1) [157].

The clones of yeast cells that grow on the selective media therefore contain a protein that interacts with the protein of interest. These colonies are scaled up, and the identity of the putative interacting protein is found by sequencing the cDNA inserts in the prey expression plasmids [158]. The yeast-2-hybrid system produces numerous false positives, so any putative interacting protein that is identified must be confirmed using conventional co-immunoprecipitation experiments [19].

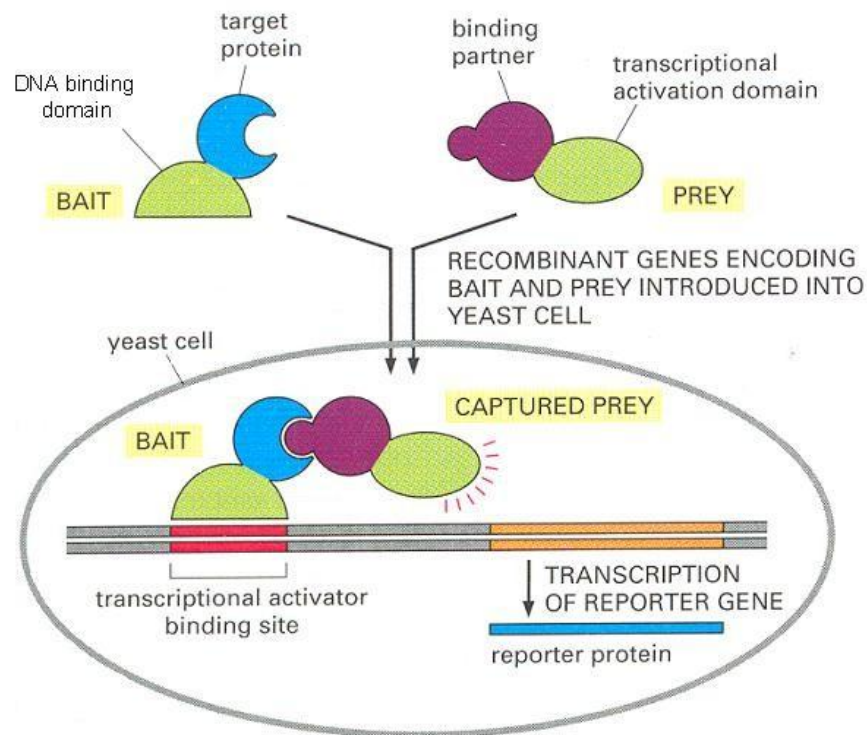


Figure 4.1 – Yeast-2-hybrid method of identifying putative protein-protein interactions. The target or bait protein is fused to a DNA binding domain that localised it to the regulatory region of a reporter gene. When this target protein binds to another specially designed protein in the cell nucleus, their interaction brings together the two halves of the transcription activator, which then switches on the expression of the reporter gene. The reporter gene is often one that will permit growth on a selective medium. Bait and prey fusion proteins are generated by standard recombinant DNA techniques. In most cases, a single bait protein is used to identify interacting proteins among a large collection of prey proteins by ligating DNA encoding the activation domain of a transcriptional activator to a large mixture of DNA fragments from a cDNA library. [19]

4.3.2 – Live Cell Imaging

The use of fluorescent tags for proteins has been widely used to elucidate the function of proteins in living cells. Fluorescent proteins such as Green Fluorescent Protein (GFP) and its' variants (BFP (Blue), CFP (Cyan), YFP (Yellow) and RFP (Red)) can essentially be fused to any protein of interest to analyse protein localisation, movement and chemistry in living cells [159].

Recent advances in fluorescence microscopy methods have allowed the examination of the localisation and kinetic behaviour of fluorescent protein tagged proteins. The most important methods include, 3D – imaging (2 spatial dimensions over time), 4D- imaging (3 spatial dimensions over time), Fluorescence Recovery After Photobleaching (FRAP), and Fluorescence Loss In Photobleaching (FLIP) [159].

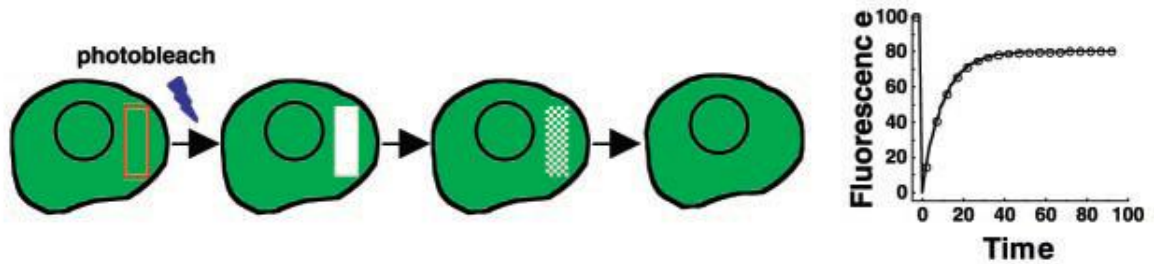
Traditional time lapse live cell imaging techniques involved the collection of images over time and can give information about the steady state localisation and changes in the protein's distribution over time [160]. However, this method does not give information about the protein's kinetic properties, for example, whether the protein is immobilised on a scaffold, free to diffuse or undergoing constant exchange between compartments. To obtain this information, a selected pool of the fluorescently tagged protein is distinguished from the other pool and the fluorescence monitored as the two pools re-equilibrate [159]. This can be accomplished by FRAP and FLIP experiments. For the FRAP technique, a selected region of fluorescence is selected and photobleached using a high intensity laser pulse and the movement of unbleached molecules into the photobleached region (recovery) is assessed

using time-lapse microscopy (Figure 4.2A) [159]. The FLIP technique is similar, however there is repetitive photobleaching of one area of the cell, whilst images are collected for the entire cell using time lapse microscopy (Figure 4.2B) [159]. Making a selected pool of fluorescently labelled protein invisible, using FRAP or FLIP, allows the steady state of the protein to be altered without disrupting protein pathways or creating protein gradients. Photoactivatable GFP, which requires activation at a shorter wavelength before being detectable at the usual wavelength, allows the detection of a protein throughout its' lifetime independently of newly synthesised proteins (Figure 4.2C) [161].

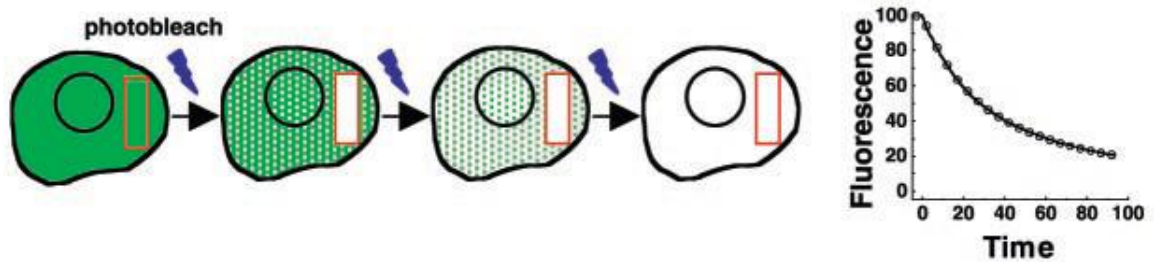
4.3.3 – FRET

GFP and its different colour variants amongst other fluorescent proteins can be used to study protein - protein interactions within cells. The technique called Förster (or Fluorescence) Resonance Energy Transfer (FRET) uses the emission of one fluorophore to excite the other fluorophore. The two proteins of interest are first cloned into expression vectors containing two different and suitable fluorescent proteins. The two fluorophore proteins, or FRET pairs need careful consideration so that the emission spectrum of the first protein overlaps with the excitation spectrum of the second fluorophore. However, at the same time the emission spectrum must be far enough apart so that the light emission from the two fluorophores can be collected separately. Examples of commonly used FRET pairs include BFP and GFP, CFP and YFP or GFP and RFP (or mCherry).

A Fluorescence Recovery After Photobleaching (FRAP)



B Fluorescence Loss in Photobleaching (FLIP)



C Photoactivation

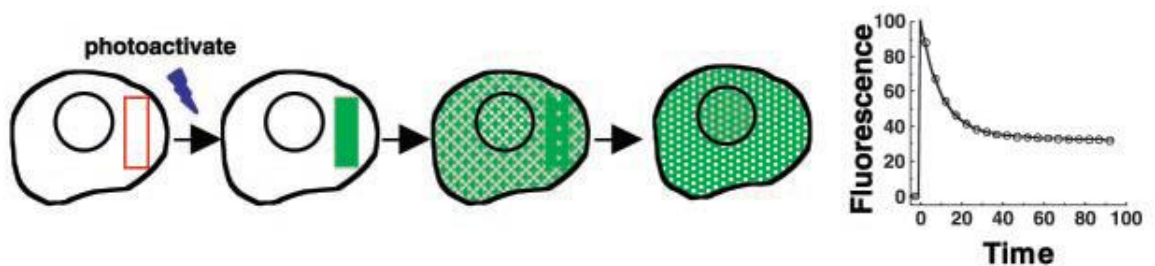


Figure 4.2 – Live cell imaging techniques.

A, FRAP – a region of the cell (indicated in red) is selected and intensively irradiated to photobleach fluorescent molecules. The recovery of fluorescent molecules into that region is assessed quantitatively to determine diffusion coefficients and mobile fractions. B, FLIP – a region of the cell (indicated in red) is repeatedly photobleached. Movement of fluorescent molecules into the region being photobleached results in loss of fluorescence from the area outside of the box and can be used to access the boundaries for a protein's diffusional movement within a cell. C, Photoactivation – selective irradiation of a selected area (indicated in red) leads to the molecules in this region becoming fluorescent. These molecules can then be monitored as they move out of this region and throughout the cell.

[159]

The FRET pair example given in Figure 4.3 is BFP and GFP. BFP requires ultra-violet light for excitation and emits blue light, whereas GFP requires blue light for excitation and emits green light. If protein X coupled to BFP and protein Y coupled to GFP do not interact within the cell, illuminating the sample with ultra-violet light will result in the emission of only blue light. If protein X and Y do interact FRET can occur between the fluorophores, and illuminating the sample with ultra-violet light will excite the BFP whose emission in turn excites the GFP, resulting in the emission of blue and green light from the sample. However, the two fluorophores must be close together, between 1 and 10 nm apart, for FRET to occur. FRET experiments require careful controls to be done such as no transfection and single transfections to be meaningful; however it is a useful way of showing protein-protein interactions within cells.

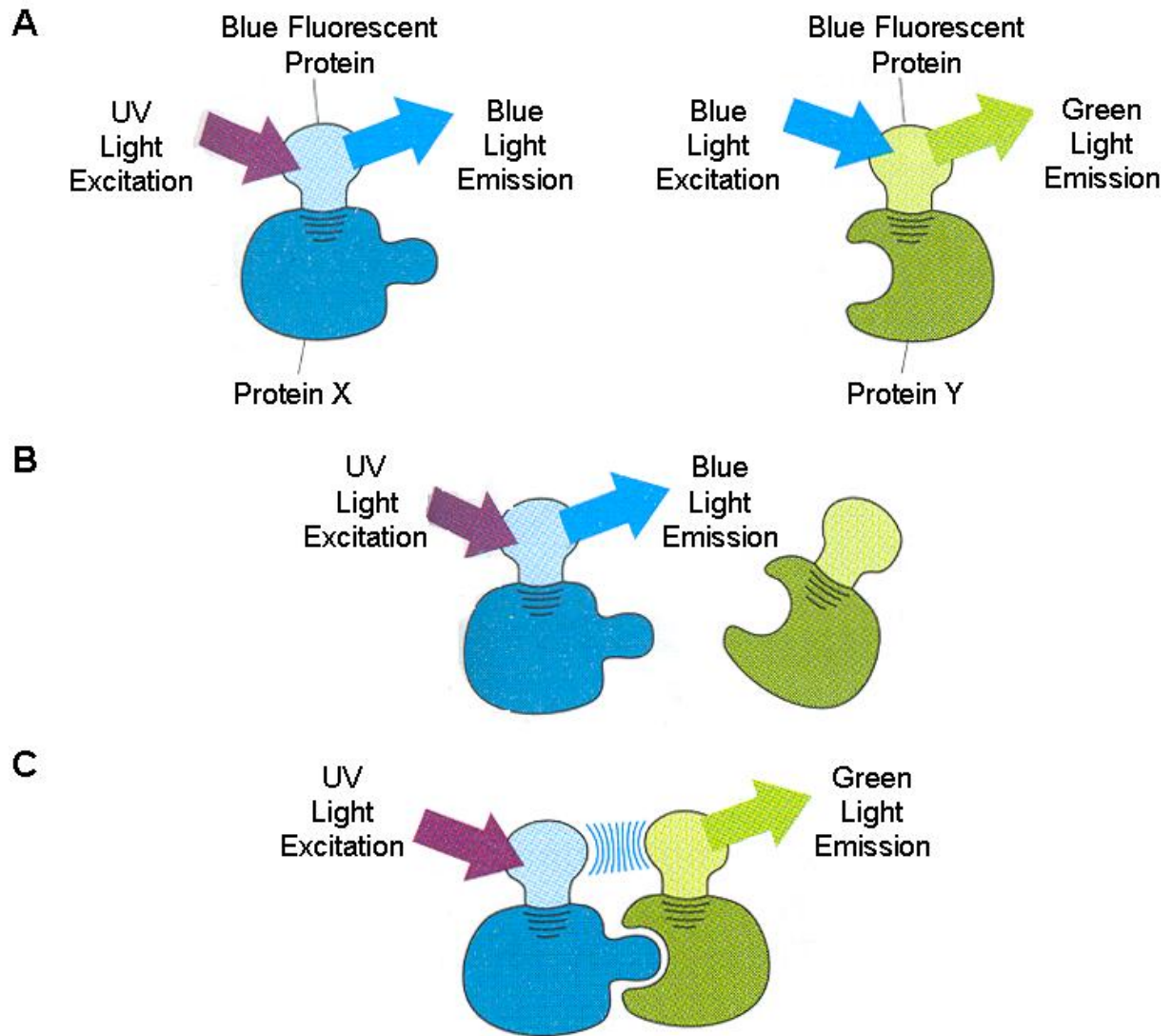


Figure 4.3 – FRET analysis of protein interactions.

To determine whether and when two proteins interact inside the cell, the proteins are first produced as fusion proteins attached to different variants of GFP. **A**, In this example protein X is coupled to blue fluorescent protein (BFP), which is excited by ultraviolet light (370 - 440 nm) and emits blue light (440-480 nm). Protein Y is coupled to green fluorescent protein (GFP), which is excited by blue light and emits green light (510 nm). **B**, If protein X and Y do not interact, illuminating the sample with ultraviolet light yields fluorescence from the BFP only. **C**, When protein X and Y interact, FRET can now occur. Illuminating the sample with ultra-violet light excites the BFP whose emission in turn excites the GFP, resulting in the emission of blue and green light from the sample. The fluorophores must be close together, between 1 and 10 nm apart, for FRET to occur. [Adapted from 19]

4.4 – Results

4.4.1 – Yeast – 2 – Hybrid Screen

Although VPS33A, a homologue of yeast Vps33, is known to interact with the mammalian equivalent of HOPS complex proteins, the functional partners of VPS33B have not been established [79;156]. Therefore a yeast-2-hybrid screen was performed by The Genomics and Proteomics Core Facility at the Deutsches Krebsforschungszentrum (Heidelberg, Germany), to identify VPS33B-interacting proteins. Human foetal brain and adult kidney cDNA libraries were chosen for screening due to the marked renal and CNS phenotype in ARC syndrome. The screen yielded 18 candidates, which were assessed for the likelihood for interaction by the number of times the interaction was observed and the promiscuity rating of that protein (Table 4.1). These proteins were then prioritised on the basis of *in-silico* analysis of their putative functions. Highest priority was given to a novel protein, POLARIN, encoded by the gene *C14orf133* (renamed *PLRN*), due to the number of times this protein was isolated from the yeast-2-hybrid screen and based on similarity to other proteins.

Gene Symbol	Gene Name	Isolation Number	Promiscuity Rating	
C14orf133	chromosome 14 open reading frame 133	16	1	Likely Interactors
C1orf149	chromosome 1 open reading frame 149	2	1	
CDK10	Cyclin-dependent kinase (CDC2-like) 10	1	1	Uncertain Interactors
CCDC22	Coiled-coil domain containing 22	1	1	
CKLF	chemokine-like factor	1	2	
NTF3	Neurotrophin 3	1	2	
MARVELD2	MARVEL domain containing 2	1	3	
MRPL33	mitochondrial ribosomal protein L33	1	3	
SNRPB	small nuclear ribonucleoprotein polypeptides B and B1	7	5	Likely False Positives
FXVD3	FXVD domain containing ion transport regulator 3	1	9	
GH2	growth hormone 2	2	13	
MYBPC1	myosin binding protein C, slow type, transcript variant 1 mRNA.	1	13	
CYB	cDNA: known chromosome:NCBI35:MT:14748:15882:1	1	18	
HBB	Haemoglobin beta mRNA	1	23	
KIF1A	kinesin family member 1A mRNA.	1	38	False Positives
CDCA4	cell division cycle associated 4	2	4	
EIF2AK1	eukaryotic translation initiation factor 2-alpha kinase 1 mRNA.	2	9	
WDR42A	WD repeat domain 42A mRNA	2	29	

Table 4.1 – Yeast–2–hybrid results for VPS33B.

VPS33B was used as bait and human foetal brain and adult kidney cDNA libraries were screened for putative interacting proteins. Highest priority was given to *C14orf133* (renamed *PLRN*) encoding a novel protein, *POLARIN*, due to the number of times this protein was isolated from the yeast-2-hybrid screen.

4.4.2 – *In-silico* Analysis of POLARIN

A species protein alignment for POLARIN homologues revealed conservation through evolution down to multicellular organisms, similar to that for VPS33B (Figure 4.4). A peptide-sequence BLAST search revealed similarity to VPS16 and ClustalW alignments showed 15% identity between the two proteins. Alignments repeated individually for the VPS16 N- and C- terminal domains found proportionate identities of 5% and 16% respectively (Figure 4.5). Bioinformatic analysis of the POLARIN sequence using Pfam and SMART databases found the C-terminal VPS16 domain and a Golgin subfamily A member 5 domain, both in the C-terminal region of POLARIN. Golgin family members are coiled-coil motif-containing proteins known to interact with Rab GTPases [162;163]

Two splice variants have been identified (which differ depending on the presence of exon 16), resulting in proteins of 480 and 493 amino-acid residues long. The larger transcript was used, with a predicted unglycosylated weight of 57 kDa, as the reference sequence for DNA and protein. The reference cDNA and protein sequence along with all other *in-silico* analysis of POLARIN are shown in Appendix 3. Analysis of the amino acid composition of POLARIN revealed that over 32% of the protein is hydrophobic, and that it is predominantly a folded protein, with protein disorder in the N-terminus. Further analysis of the amino acid sequence of POLARIN suggests that the protein is predominantly coiled, most of which being α -helices, and also predicts 2 coiled-coiled regions between amino acids 1-50 and 150-200. The hydrophobicity and the coiled nature of POLARIN suggest that POLARIN is likely to form a stable complex with another protein or other proteins.

Human	1	MNRTKGDEEEYWNSSKFKAFTFDD	DELSQLKESKRAVNSLRD	FVDDDD	-	DDLERSVWSGEPVGSISWS	I	RETAGNSGSGTHEGREQLKS	90												
Rat	1	MNRTKGDEEEYWNSSKFKAFTFDD	DELSQLKESKRAVNSLRD	FVDDDD	-	DDLERSVSWTGEVGSISWS	I	KETAGSSGSGTSEGREQMKG	90												
Mouse	1	MNRTKGDEEEYWNSSKFKAFTFDD	DELSQLKESKRAVNSLRD	I	VDDDD	-	DDLERSVSWTGEVGSISWS	I	KETAGSSGSGTPEGREQLKG	90											
Zebrafish	1	MTRAKPEDDEYWNSSKFKAFTFDD	EDFRLKESKRAVNSI	-	LVDDDD	EDDVEKVSWSGEPVGSISWS	VRETASSIRSGSE	-	QNFPK	87											
Drosophila	1	-MDLQLDSESYWNRSSRAAFS	FDDED	-	-	-	-	EVDLAPDLVSNGLADDT	-	-	-	-	-	-	-	-	-	SVALNLSIKSILS	EEALKLVLQ	EQA	76
Human	91	RNSFSSYAQLPKPTSTYSLSSFFRGRTRPGSFQSLSDALSDTPAKS	YAP	ELGRPKGEYRDYSND	-	-	WSPSDTVRRLRKGVCSL	ERFRSLQ	179												
Rat	91	RNSF--YTQLPKPPSTYSLSSFFRGRTRPGSFQSLSDALSDTPAKT	YSPELGRPKGEYRDYSND	-	-	WLSLSDTVRRLRQGGK	-	-	-	-	-	-	-	-	-	-	-	-	-	-	166
Mouse	91	RNSF--YTQLPKPPSTYSLSSFFRGRTRPGSFQSLSDALSDTPAKS	YAP	ELGRPKGEYRVCSL	ERFRSLQD	KLQLLEEAVS	-	-	-	-	-	-	-	-	-	-	-	-	-	-	169
Zebrafish	88	IDTA--PSLSKQSGSYLSLFLKAKSKPTAFQSFSESFSETSART	YAP	ELRKP	KS	DGKDFVSD	-	LSPEET	IRRMQKGR	AFSMEKFRSLQ	173										
Drosophila	77	LDDR---VLPKGVSP	EEELKLLRRQLQSTLYSPNLEATAQKLLQGKTAPLEMF	KSLHE	-	-	-	-	-	-	-	-	-	-	-	-	-	-	-	-	144
Human	180	DKLQLLEEAVSMH	DGNVITAVLIFLKRTLSKEILFRELEVRQVALRHLIHFLKEIGDQKLLLDLFRFLDRTEELALSHYREHLNIQDP	DKR	270																
Rat	167	-	-	-	-	-	-	-	-	-	-	-	-	-	-	-	-	-	-	-	237
Mouse	170	-	-	-	-	-	-	-	-	-	-	-	-	-	-	-	-	-	-	-	249
Zebrafish	174	DKLLLLDEAVSVY	DGNVITAVLIYLLKKSLSKEILFRELM	PREVALRHYIHYLKEMGEQKLLVELL	KALGRTE	D	MALMQYKEHLNIKDE	GR	264												
Drosophila	145	-	-	-	-	-	-	-	-	-	-	-	-	-	-	-	-	-	-	-	221
Human	271	KEFLKTCVGLP	FSAED	-	-	-	SAHIQDHYTLLERQII	IEANDRHLESAGQTE	IFRKHPRKASILNMPLVTTLFY	SCFYHYTEAEGTFSSPVN	-	357									
Rat	238	KEFLKTCIGLP	FSAED	-	-	-	SAHVQDQYTLLERQII	IEANDRHLESSGQTE	IFRKHPRKASILNMPLVTTLFY	ACFYHYTESEGTTFSSPVN	-	324									
Mouse	250	KEFLKTCIGLP	FSAED	-	-	-	AAHVQDHYTLLERQII	IEANDRHLESSGQTD	IFRKHPRKASILNMPLVTTLFY	ACFYHYTESEGTTFSSPIN	-	336									
Zebrafish	265	RDFLKSLCLSLP	FSD	-	-	-	STHVQDHYTLLERQII	IEASDKKAD	-	-	-	-	TDIFKKFPRKASILNMP	IITLYYSCFYHYGEPEGTFSSPSN	-	347					
Drosophila	222	KKHLQLLV	DAYATAGVGVI	PLYEQVFHAALKMQQLMEKDS	-	-	-	-	-	-	-	-	-	-	-	-	-	-	-	-	298
Human	358	-	-	LKKT	FKIPDKQYVLTALAARAKLRAWNDVDALFTTKN	-	WLGYTKKRAPIGFHRVVEILH	-	-	KNNAPVQILQEYVNLVEDVDTKLNLATK	443										
Rat	325	-	-	LKKT	FKIPDRQYVLTALAARAKLRAWNDVDALFTTK	-	WLGYTKKRAPIGFHRVVEILH	-	-	KNSAPVQILQEYVNLVEDVDTKLNLATK	409										
Mouse	337	-	-	LKKT	FKIPDKQYVLTALAARAKLRAWNDVDALFTTKN	-	WLGYTKKRAPIGFHRVVEILH	-	-	KNSAPVQILQEYVNLVEDVDTKLNLATK	422										
Zebrafish	348	-	-	IRK	TERISEKQYITTALGARAKLSWFDVDSLNTKN	-	WLGYTKKRSP	IAFHRVVDILQ	-	-	KNSAPVQVLQEYVNLIDDPELKL	SVALK	433								
Drosophila	299	QRF	AADQQISPAQYEW	TALNERAQAQAYADLECIF	ERVPSWHP	LKTKQFHISFDLTLAVLR	LYELQAPSTVLQLFLSKMGNSVEKLAL	AQR	389												
Human	444	FKCHDVVIDTY	RD	LKDRQQLLAYRSKVDKGS	AEKEEKIDALLSSSQ	-	IRWKN	-	-	-	-	493									
Rat	410	FKCHDVVIDTC	RD	LKDRQQLLAYRSKVDKGS	AEKEEKIDVILLSSSQ	-	IRWKN	-	-	-	-	459									
Mouse	423	FKCHDVVIDTC	RD	LKDRQQLLAYRSKVDKGS	AEKEEKIDAILSSSQ	-	IRWKN	-	-	-	-	472									
Zebrafish	434	YKCHDII	INTY	RD	LKDRQQLIVYREKLERDSPEYRKIQELLNNGQ	-	IRWKN	-	-	-	-	483									
Drosophila	390	VKCIKAV	ID	AMAGL	KQQQLQQLKDTLPERSEEQFYCENAL	KSLQSKRW	TTDN	IKLKL	-	-	-	447									

Figure 4.4 – Species alignment of POLARIN.

ClustalW amino acid alignment for multicellular organisms with dark shading representing identical amino acids. POLARIN is conserved down to multicellular organisms. The region of POLARIN absent in Rat, Mouse and Drosophila equivalent to human amino acids 159 to 192 correspond to the exon 16 splice variant of PLRN.

POLARIN	MNRTKGDEEEYWNSSKFKAFTFDDDEDELSQLKESKRAVNSLRDFVDDDDDDDLERVSW	60
VPS16_C	-----	0
POLARIN	GEPVGSISWSIRETAGNSGSTHEGREQLKSRNSFSSYAQLPKPTSTYSLSSFFRGRTRPG	120
VPS16_C	-----	0
POLARIN	SFQSLSDALSDTPAKSYAPELGRPKGEYRDYSNDWSPSDTVRRRLRKGVCSLERFRSLQD	180
VPS16_C	-----SYSDIARRAYG--CGRTELAIKLLEYEPRSGEQVPLLLKMKRSKLA-----	44
	: ** .*:.*. *.*: : .: .*: * * * .*	
POLARIN	KLQLLEEAVSMHDGNVITAVLIFLKRTLSKEILFRELEVRQVALRHLIHFLEIGDQKLL	240
VPS16_C	----LSKAIESGDTDLVFTVLLHLKNEINRGDFMTLRNQPMALSLYRQFCKHQ-ELETL	99
	.:.*. * :*: :*:.*. *: : * .: :*: :* .: : *	
POLARIN	LDLFRFLDRTEELALSHYREHLNIQD-PDKRKEFLKTCVGLPFSAEDSAHIQDHYTLER	299
VPS16_C	KDLYNQDDNHQELGSFHIRASYAAEERIEGRVAALQTAADAFYKAKN---EFAAKATED	155
	**:. * .:*. * * : : : * :*.*. .:*. : : *	
POLARIN	QIIIEANDRHLESAGQTEIFRKHPKASILNMPLVTTLFYSCFYHYTEAEGTFSSPVNLK	359
VPS16_C	QMRLLRLQRRLEDELGGQFLDLSLHDT-----VTTLILG-----GHNKRAEQLA	199
	: : ::.*. :*: :*: :*.*. : *	
POLARIN	KTFKIPDKQYVLTALAARAKLRAWNDVDALETTKNWLGYTCKRAPIGFHRVVEILHKNN-	418
VPS16_C	RDERIPDKRLWWLKLTAALADLEDWEELEKFSKSK-----KSPIGYLPFVEICMKQHN	251
	: *:*.*.*. *: * * . * :*: : : .:*	
POLARIN	-APVQILQEYVNLVEDVDTKLNLATKFKCHDVVLDTYRDLKDRQQLLAYRSKVDKGSLEE	477
VPS16_C	KYEAKKYASRVGPEQKVKALLLVGDVAQAADVAIE-HRNEAELSLVLSHCTGATDG-ATA	309
	.: . * . :*.: * :. :. **.*: *: : . :*: : . . * *	
POLARIN	EKIDALLSSSQIRWKN 493	
VPS16_C	DKIQRARAQAQKK--- 323	
	: :. :* :	

Figure 4.5 – Amino acid alignment of POLARIN and VPS16 C- terminal domain.
ClustalW amino acid sequence alignment for POLARIN and VPS16 C-terminal domains. There is 16% identity between the two. Identical amino acids are shaded in dark grey and marked with asterisk. Similar amino acids are shaded in light grey.

4.4.3 – Confirmation of Interaction

Co-immunoprecipitation and immunofluorescence experiments were performed to investigate the reliability of the yeast-2-hybrid findings, and whether there is a redundancy in the interaction between VPS33A and VPS33B homologues and POLARIN and its distant homologue VPS16. Co-immunoprecipitation confirmed that VPS33B interacts with POLARIN but not with VPS16, and in parallel, POLARIN did not interact with VPS33A (Figure 4.6). Both results demonstrate the specificity of the VPS33B-POLARIN interaction and make it unlikely that VPS33B is involved in the conventional HOPS complex function.

As no anti-POLARIN antibody was available for immunofluorescence studies, epitope-tagged VPS33B and POLARIN constructs were used. These, when overexpressed individually in HEK293 cells, displayed a general cytoplasmic localisation with some clusters (Figure 4.7A). Live cell imaging of mIMCD-3 cells transfected with YFP-VPS33B showed a similar general cytoplasmic localisation. However when a FLIP experiment was carried out and hence the free diffusible VPS33B was removed from sight within the cell, discrete clusters of VPS33B could be seen within the cytoplasm (Figure 4.8 and Movie on CD).

Co-overexpression of both proteins strikingly affected their localisation (Figure 4.7B). Wild-type VPS33B and POLARIN colocalised in large discrete cytoplasmic clusters. A specifically constructed VPS33B-L30P mutant protein (modelled on a missense mutation identified in a patient with ARC) did not cluster with POLARIN; both proteins remained generally distributed throughout the cytoplasm. Similarly, no clustering was seen with co-overexpression of POLARIN and VPS33A.

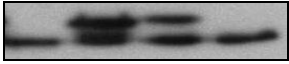
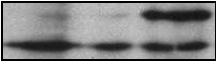
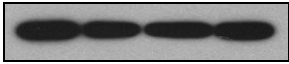
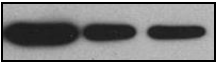
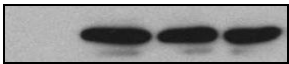

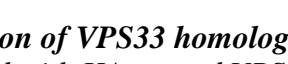
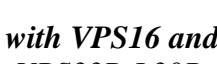
HA-Empty	+				+		
HA-VPS33B		+				+	
HA-VPS33B (L30P)			+				
HA-VPS33A				+			+
myc-POLARIN	+	+	+	+			
myc-VPS16					+	+	+
<hr/>							
IP: α HA							
WB: α myc							
Input							
WB: α HA							

Figure 4.6 – Co-immunoprecipitation of VPS33 homologues with VPS16 and POLARIN.

HEK293 cells were co-transfected with HA-tagged VPS33B, VPS33B-L30P mutant, or VPS33A and with myc-tagged POLARIN or VPS16 constructs. Co-immunoprecipitation experiments show that HA-VPS33B and HA-VPS33B-L30P interact with myc-POLARIN and that HA-VPS33A interacts with myc-VPS16. No interaction is seen between HA-VPS33B and myc-VPS16 or between HA-VPS33A and myc-POLARIN. Quantification revealed that 28.1% (VPS33B), 22.8% (VPS33B-L30P), and 27.7% (VPS33A) of the myc-POLARIN or myc-VPS16 input was recovered.

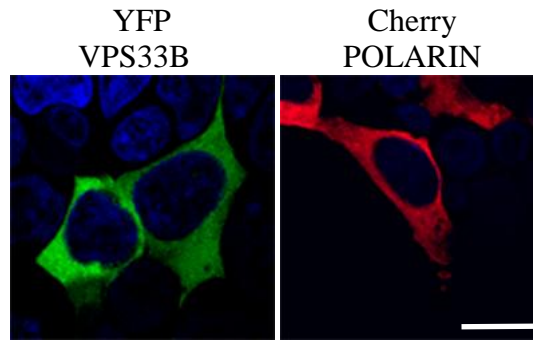
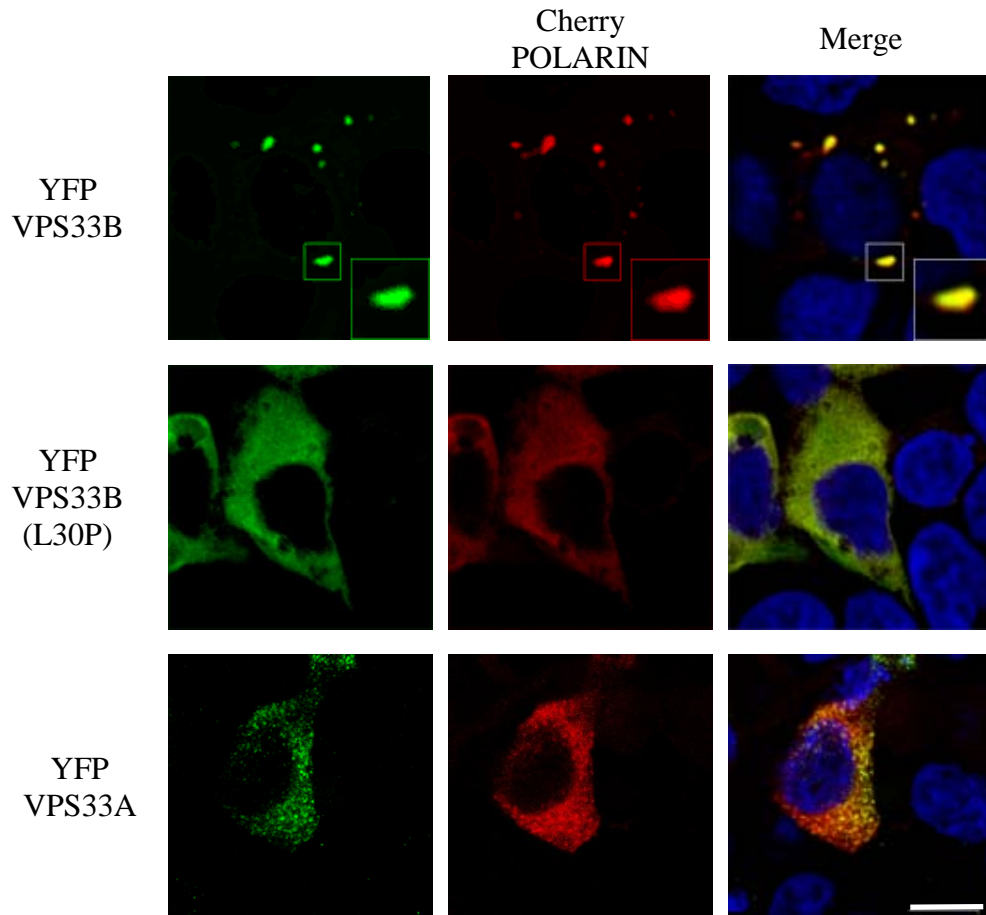
A**B**

Figure 4.7 – Confocal fluorescence photomicrographs of VPS33 homologues with POLARIN

Confocal fluorescence photomicrographs of **A**, HEK293 cells transfected with YFP-VPS33B and Cherry-POLARIN constructs individually and **B**, HEK293 cells co-transfected with both Cherry-POLARIN and YFP-VPS33B, YFP-VPS33B (L30P), or YFP-VPS33A. Nuclei are stained with TO-PRO-3. Scale bar = 10 μ m. When co-overexpressed, Cherry-POLARIN and YFP-VPS33B form cytoplasmic clusters (insert). No clusters are seen when Cherry-POLARIN is co-overexpressed with YFP-VPS33B (L30P) or YFP-VPS33A. (Experiment carried out in collaboration with A Straatman Iwanowska, University of Birmingham, UK)

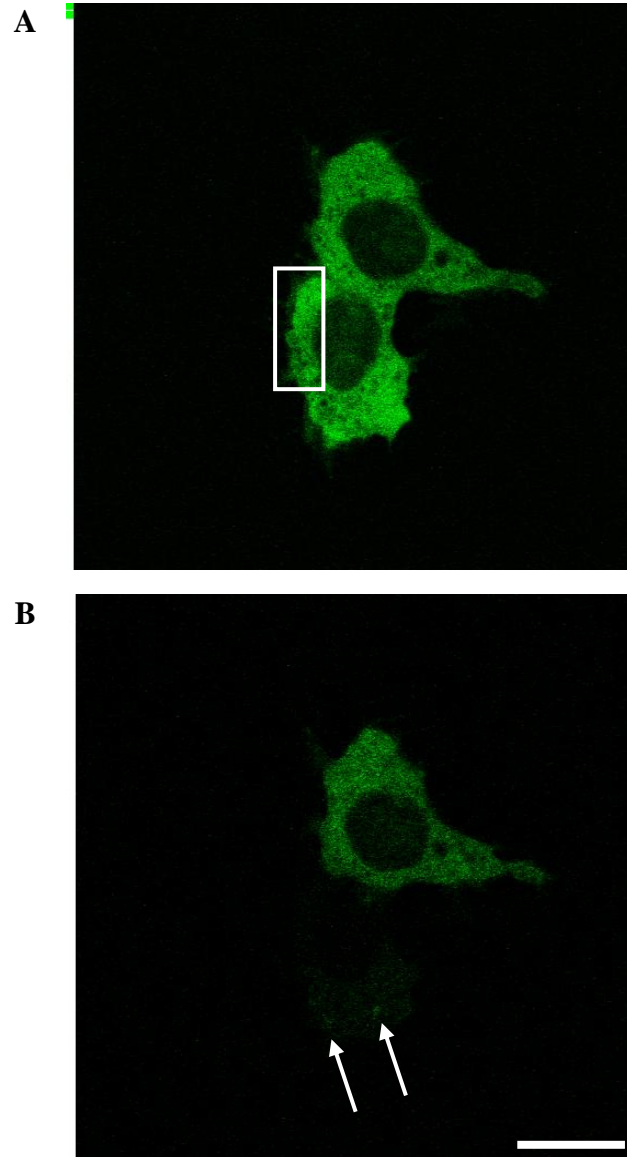


Figure 4.8 – YFP-VPS33B FLIP confocal live-cell microscopy.

*YFP-VPS33B was transfected into mIMCD-3 cells and a Fluorescence Loss In Photobleaching (FLIP) experiment was carried out in live cells. Bleaching was done using a 514 nm laser set to 100% every 5 seconds in an area of one cell (white rectangle), with an image captured every 2.5 seconds for a total of 5 minutes. Images shown are at **A**, $t = 0$ minutes and **B**, $t = 5$ minutes. Scale bar = 10 μm . Removal of the free cytoplasmic YFP-VPS33B pool (by photobleaching) reveals occasional cytoplasmic clusters (white arrows), which are not as pronounced as when VPS33B is co-over expressed with POLARIN, suggesting endogenous interaction with POLARIN.*

4.4.4 – Co-localisation of VPS33B-POLARIN Clusters with Organelle Markers

In the previous section, it was shown that when co-overexpressed in HEK293 cells, VPS33B and POLARIN form large cytoplasmic clusters. In order to determine the sub-cellular localisation of the VPS33B-POLARIN clusters, immunostaining was performed with various organelle markers. For all the following experiments HEK293 cells were transfected with HA-VPS33B and Cherry-POLARIN and either stained or transfected with various organelle markers. Firstly, to ensure the VPS33B-POLARIN cluster was not an artefact of transfection, the transfected cells were stained for GM130, a Golgi membrane marker. No significant co-localisation was observed ($p=0.84$) suggesting that both proteins were released into their native environment (Figure 4.9). Co-localisation was assessed as described previously [164] and in section 2.2.6.1.1

The HOPS complex components have been shown to localise to early and late endosomes and lysosomes within yeast and mammalian cells [74;79]. However in light of the findings that VPS33B specifically interacts with POLARIN and not with VPS16, a HOPS complex member, the VPS33B-POLARIN cluster was assessed for co-localisation with markers of these organelles. No significant co-localisation was observed with Rab5 (early endosome, $p=0.39$), LAMP-1 (late endosome, $p=0.34$) or CD63 (lysosomes, $p=0.22$), further suggesting that VPS33B does not function as part of the conventional HOPS complex (Figure 4.9). However, significant but partial colocalisation was observed with the VPS33B-POLARIN clusters and Rab11a ($p<0.001$), which is present in apical recycling endosomes (AREs), and Rab4a ($p<0.05$), which is thought to be present on some early endosomes and also to be involved in ARE biogenesis [165;166] (Figure 4.10).

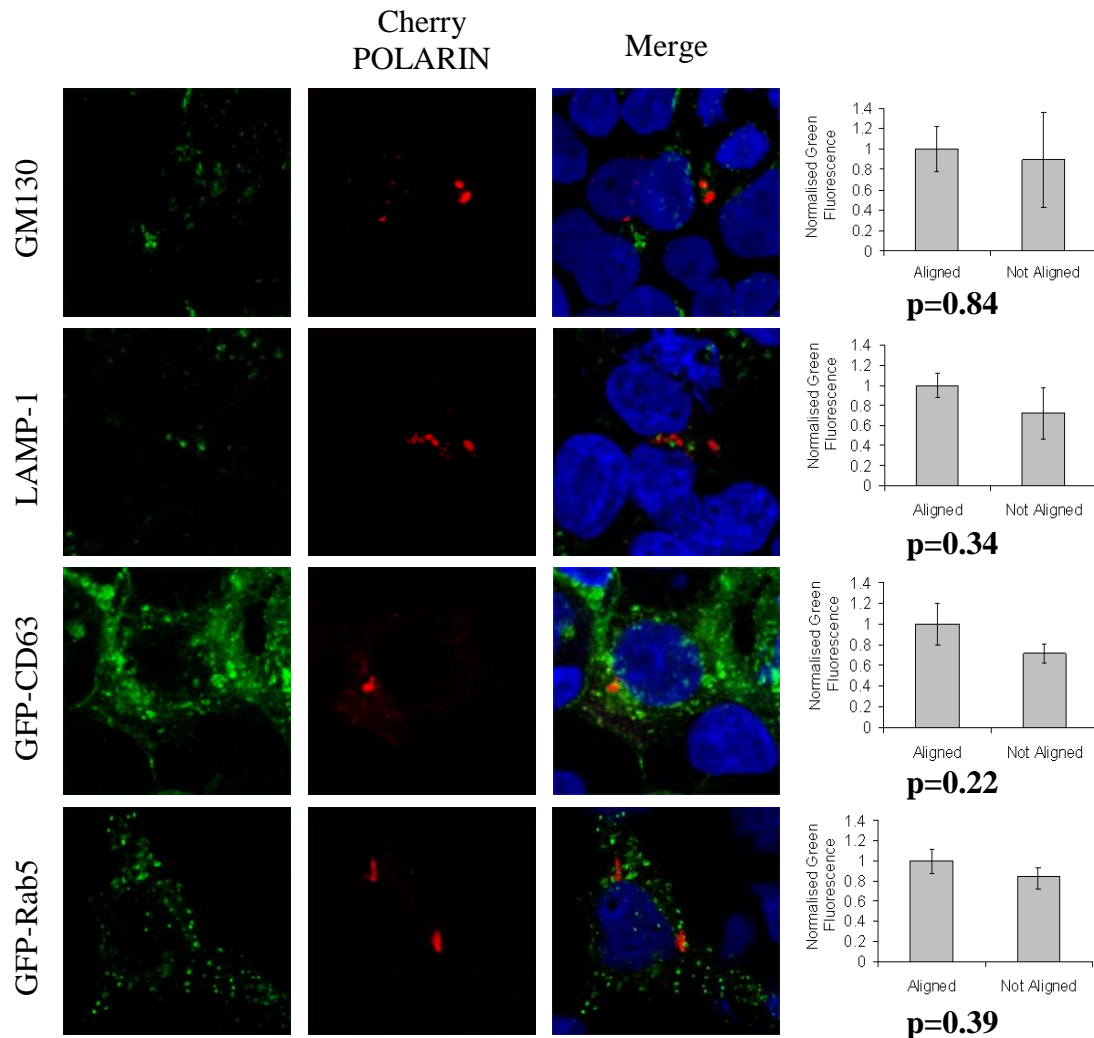


Figure 4.9 – Negative co-localisation of VPS33B-POLARIN clusters with organelle markers.

*HEK293 cells were transfected with HA-VPS33B (not stained) and with Cherry-POLARIN; they were then either immunolabelled (GM130 and LAMP-1) or co-transfected with GFP-tagged organelle markers. Nuclei are stained with TO-PRO-3. Scale bar = 10 μ m. No significant co-localisation (by Student's *T* test) was seen with markers for the Golgi apparatus (GM130), early endosome (Rab5), or late endosome and lysosomes (LAMP-1, CD63). Bar graphs compare the average organelle marker fluorescence per unit area \pm 1 standard error of the mean, in regions within 25 Cherry-POLARIN puncta (in single optical section for each marker) to an equivalent number of regions outside of Cherry-POLARIN spots. (Experiment carried out in collaboration with A Straatman Iwanowska and J. Rappoport, University of Birmingham, UK)*

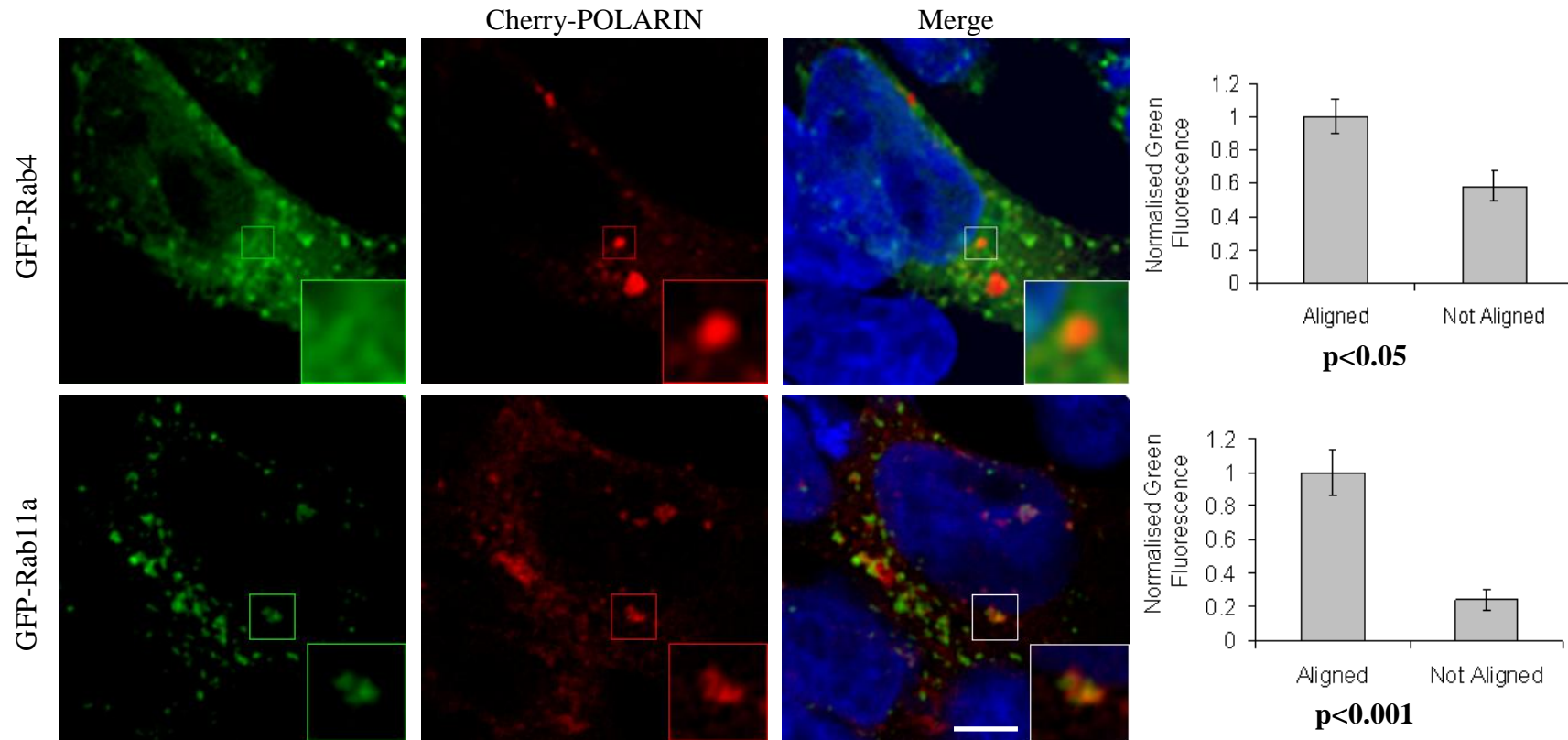


Figure 4.10 - Positive co-localisation of VPS33B-POLARIN clusters with organelle markers.

HEK293 cells were transfected with HA-VPS33B (not stained), Cherry-POLARIN and GFP-Rab4 or GFP-Rab11. Nuclei are stained with TO-PRO-3. Scale bar = 10 μm . Significant co-localisation (by Student's T test) was observed with Rab4 (early endosome) and Rab11a (recycling endosome). Bar graphs compare the average organelle marker fluorescence per unit area ± 1 standard error of the mean, in regions within 25 Cherry-POLARIN puncta (in single optical section for each marker) to an equivalent number of regions outside of Cherry-POLARIN spots. (Experiment carried out in collaboration with A. Straatman Iwanowska and J. Rappoport, University of Birmingham, UK)

4.4.5 – The VPS33B-POLARIN Complex Interacts with Rab11a

The previous co-localisation of the VPS33B-POLARIN clusters with Rab11a was observed with over-expressed proteins, and as antibodies against both VPS33B and Rab11a are commercially available, the co-localisation could be assessed at the endogenous level.

HEK293 and mIMCD-3 cells were stained for both proteins (Figure 4.11). Again significant but partial colocalisation of endogenous VPS33B and Rab11a was also detected in HEK293 cells ($p < 0.001$) and in mIMCD-3 cells ($p < 0.05$).

When Texas Red conjugated transferrin was pulsed into HEK293 cells and chased for a total of 1 hour, no co-localisation was observed at any time point (Figure 4.12). The transferrin receptor is a marker of the basolateral recycling endosomes, and this result suggests that the VPS33B-POLARIN clusters are not present in the basolateral recycling endosomes and furthermore are specifically localised to the apical recycling endosomes [167].

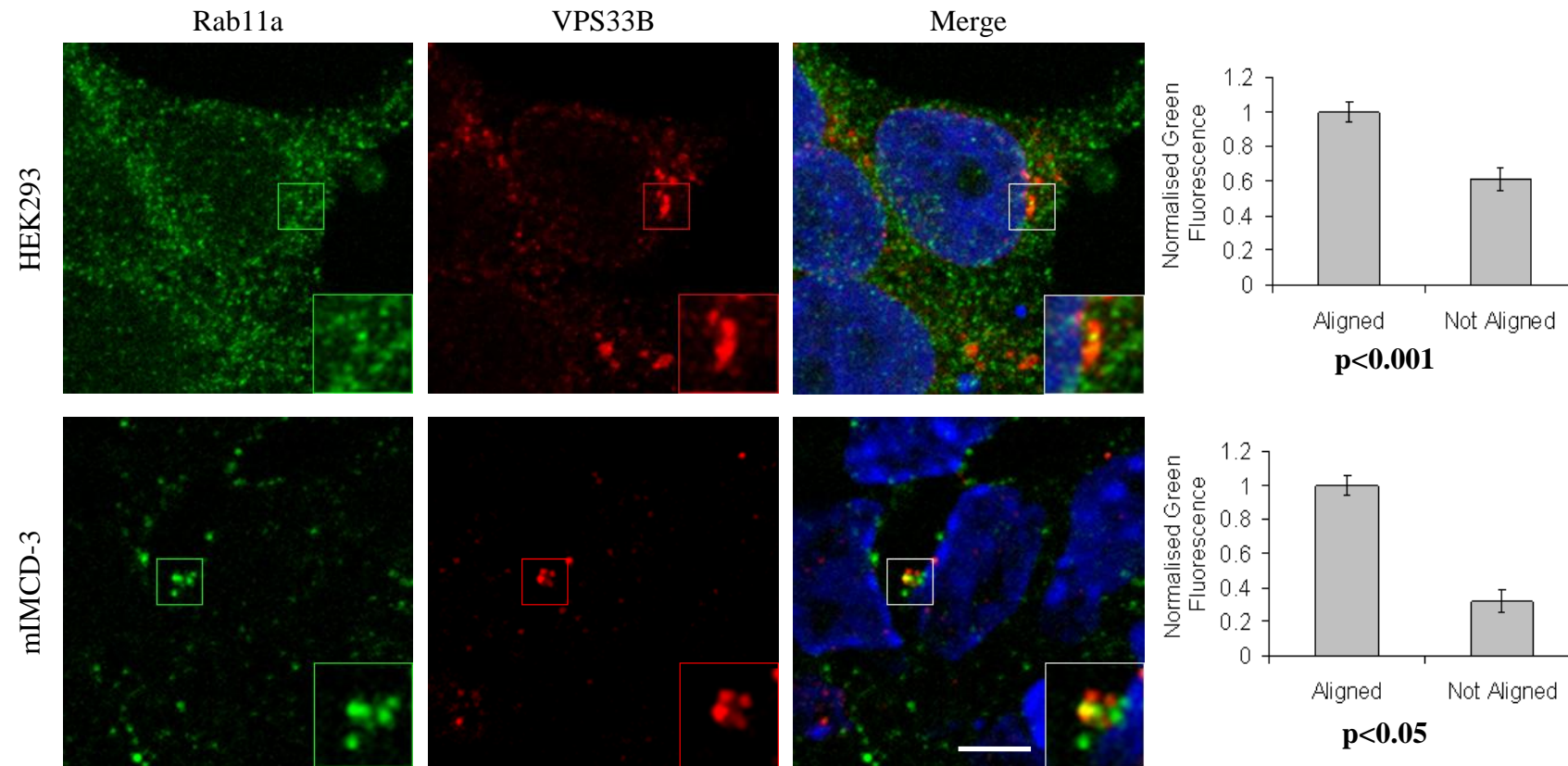


Figure 4.11 – Endogenous co-localisation of VPS33B and Rab11a.

Confocal immunofluorescence photomicrographs of HEK293 and mIMCD-3 cells stained for endogenous Rab11a (green) and VPS33B (red). Nuclei are stained with TO-PRO-3. Scale bar = 10 μm . Partial co-localisation (inserts) of both markers can be seen. Bar graphs comparing the average Rab11a fluorescence per unit area ± 1 standard error of the mean in regions within 25 VPS33B puncta (in single optical section for each marker) to an equivalent number of regions outside of VPS33B spots. (Experiment carried out in collaboration with A Straatman Iwanowska, University of Birmingham, UK)

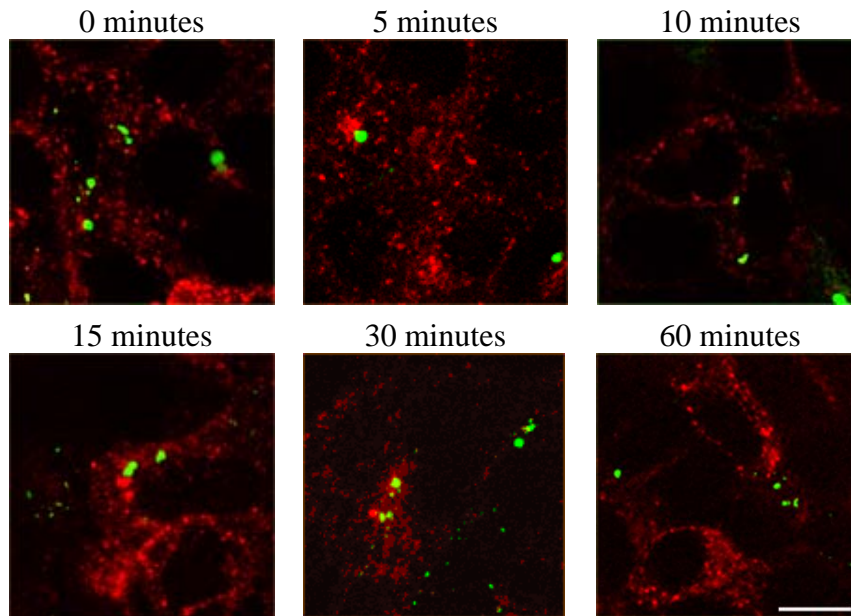


Figure 4.12 – Co-localisation of the VPS33B-POLARIN clusters with the transferrin receptor.

Texas Red-conjugated transferrin was pulsed for 30 minutes into HEK293 cells co-transfected with YFP-VPS33B and myc-POLARIN (not immunostained) and was chased for a total of 60 minutes (scale bar = 10 μ m). No co-localisation was observed at any time. (Experiment carried out in collaboration with A Straatman Iwanowska, University of Birmingham, UK)

Since the VPS33B-POLARIN clusters at both the overexpressed and endogenous level at least partially co-localises with Rab11a, the co-localisation was further investigated using Fluorescence Resonance Energy Transfer (FRET). This technique allows the assessment on how close 2 proteins and their fluorescent tags are to one another, by using light emitted from the first fluorophore (GFP) to excite the next fluorophore (Cherry). For a positive FRET result the 2 fluorophores must be between 1 and 10 nm apart. HEK293 cells were transfected with HA-VPS33B, Cherry-POLARIN (to form clusters) and GFP-Rab11a and a FRET experiment was carried out. Red emission light could be collected from the Cherry fluorophore when the GFP molecule was excited with the 488 nm laser; suggesting that FRET was occurring, and that VPS33B, POLARIN and Rab11a are in close proximity to each other (Figure 4.13). No red emission light was detected in control samples.

The conventional HOPS complex has Rab effector and Rab GEF properties [73;75], so the interaction between this new complex and Rab11a was assessed. VPS33B and Rab11a reciprocally co-immunoprecipitate at the endogenous level in mIMCD-3 cells (Figure 4.14). Furthermore, HEK293 cells were co-transfected with GFP-Rab11a and either HA-VPS33B or myc-POLARIN or both HA-VPS33B and myc-POLARIN together, and co-immunoprecipitation experiments were carried out on these lysates, which revealed a weak interaction between Rab11a, VPS33B and POLARIN (Figure 4.15A). Both VPS33B and POLARIN need to be over-expressed for this interaction to be observed and quantification of the IP revealed only 7.6% (IP α HA) and 7.9% (IP α myc) of the Rab11a input was recovered. However, when the same experiment was carried out with a dominant negative Rab11a (DN-Rab11a) construct carrying a S25N mutation, which locks Rab11a in the Rab-

GDP state, no interaction was observed, suggesting that the newly identified VPS33B-POLARIN complex has Rab effector properties (Figure 4.15B).

4.4.6 – POLARIN Interacts with the HOPS Complex Proteins

Previous work by other groups has shown that VPS33A and VPS16 do indeed interact with the other members of the HOPS complex [79], but the data presented in section 4.4.3 suggests that VPS33B does not interact with VPS16 and VPS33A does not interact with POLARIN. Therefore, whether the newly identified VPS33B-POLARIN complex forms a larger complex with the remaining members of the conventional HOPS complex remains unknown. To address this question, POLARIN was sub cloned into the HA tagged vector and the other members of the HOPS complex (VPS11, VPS18, VPS39 and VPS41) were cloned into the myc tagged expression vector. Co-immunoprecipitation experiments revealed that POLARIN interacts with VPS18 and weakly interacts with VPS11, VPS39 and VPS41 (Figure 4.16). These findings suggest that the VPS33B-POLARIN complex does interact with the remaining members of the HOPS complex. Confocal immunofluorescence microscopy of HEK293 cells transfected individually with myc tagged VPS39 or VPS41 revealed a general cytoplasmic localisation for both proteins, similar to that of VPS33B and POLARIN alone (data not shown). In contrast VPS11 and VPS18 localised to large discrete vesicular structures in the cytoplasm of cells. When HEK293 cells were co-transfected with Cherry-POLARIN and myc-VPS11, VPS39 or VPS41, the localisation observed with single transfections remained unchanged (Figure 4.17). However, when POLARIN was co-transfected with myc-VPS18, POLARIN formed large cytoplasmic clusters which co-localised with VPS18 (Figure 4.17 and 4.18).

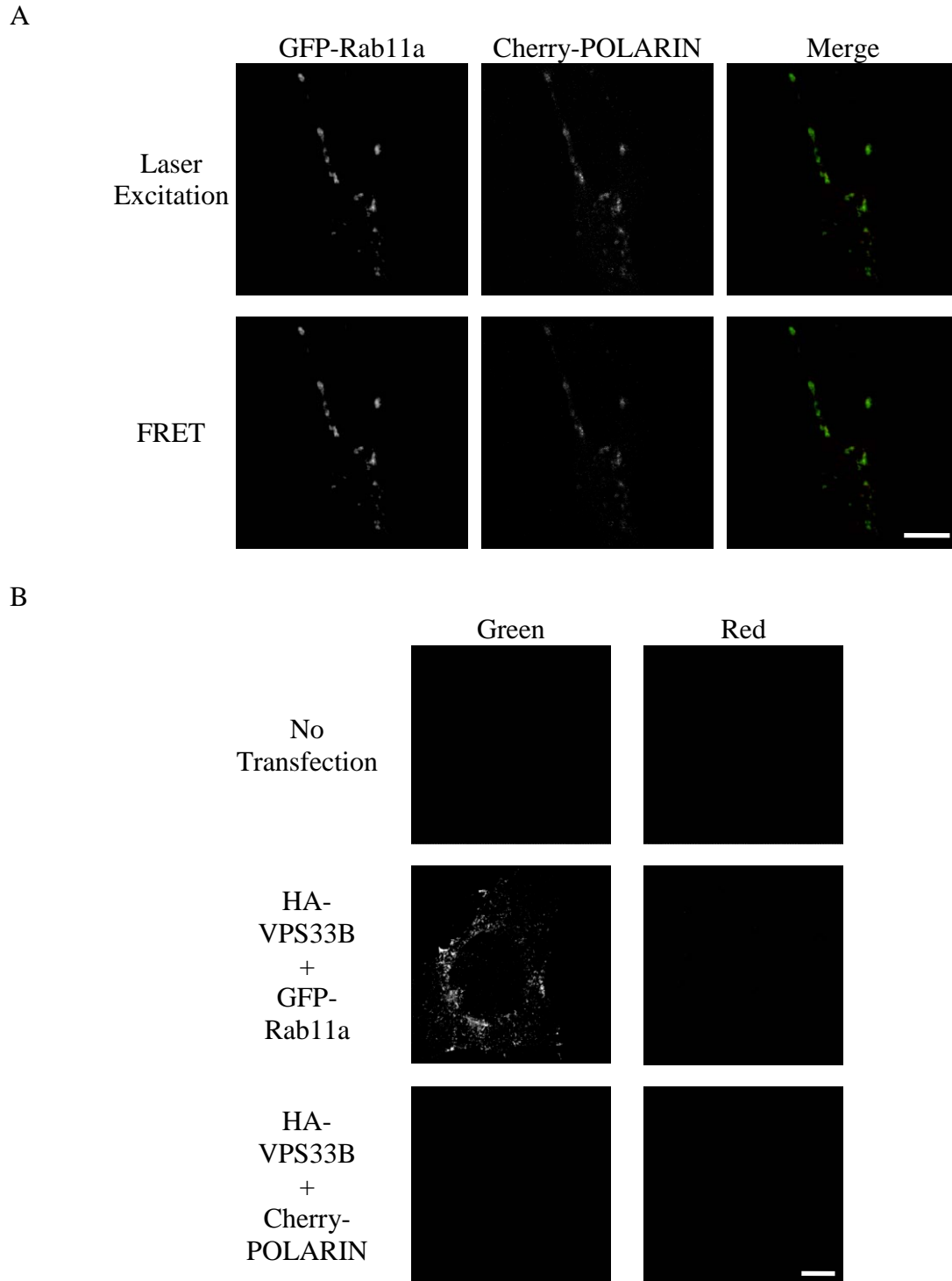
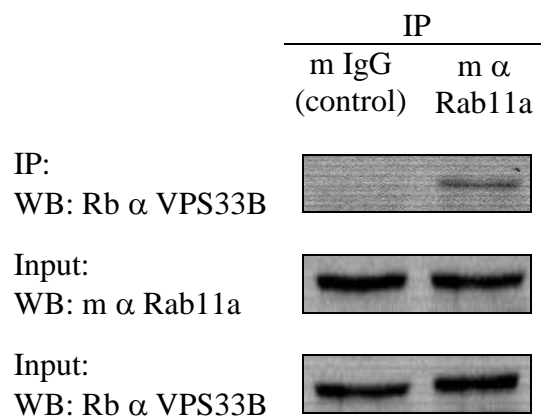


Figure 4.13 – FRET analysis of VPS33B-POLARIN complex and Rab11a.
A, mIMCD-3 cells were triple transfected with HA-VPS33B (not stained), Cherry-POLARIN (red) and GFP-Rab11a (green). The GFP-Rab11a was excited using the 488 laser line and red emission collected using laser excitation and FRET. **B**, Control transfections for FRET experiment in A. The same settings were used as in A, and all red emission light was collected by FRET after excitation using the 488 laser line. No red light was collected in any control sample. Scale bar = 10 μ m.

A



B

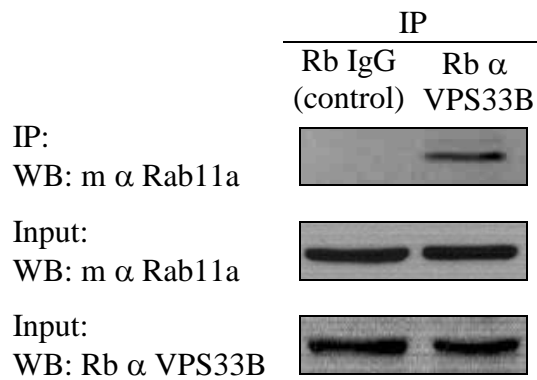


Figure 4.14 - Reciprocal co-immunoprecipitation of endogenous VPS33B and Rab11a. Co-immunoprecipitation of endogenous VPS33B and Rab11a from mIMCD-3 cells after pull-down with **A**, Rab11a antibody and **B**, VPS33B antibody. Control (IgG molecules) failed to pull down the relevant protein despite being present in the lysates.

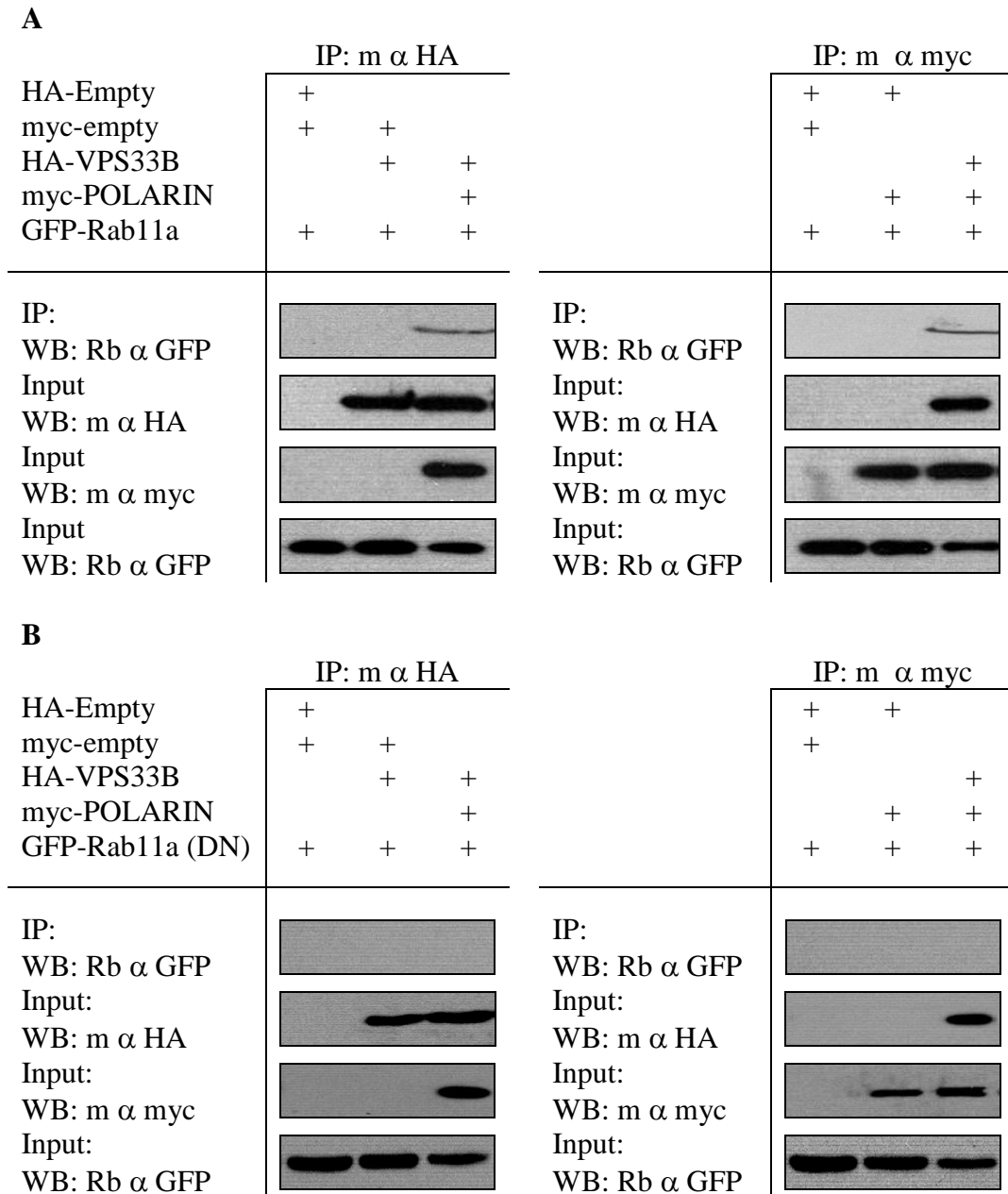


Figure 4.15 – Co-immunoprecipitation of the VPS33B-POLARIN complex and Rab11a.

A, HEK293 cells were co-transfected with HA-tagged VPS33B or empty vector, myc-POLARIN or empty vector, and GFP-tagged Rab11a. Co-immunoprecipitation experiments using HA-VPS33B or myc-POLARIN as bait show that both VPS33B and POLARIN immunoprecipitate in the same complex as Rab11a. Both HA-VPS33B and myc-POLARIN needed to be over-expressed for the interaction with GFP-Rab11a to occur. Quantification of the immunoprecipitation revealed 7.6% (IP α HA) and 7.9% (IP α myc) of the Rab11a input was recovered. **B**, same experiment as in A, but GFP-tagged dominant negative (DN) Rab11a was used. No interaction between the VPS33B-POLARIN complex and the GDP-locked dominant negative Rab11a can be seen.









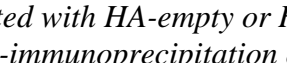
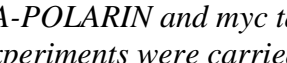

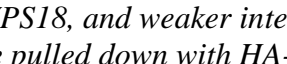
	IP: m α HA				
HA-Empty	+	+	+	+	
HA-POLARIN					+
myc-VPS11	+				+
myc-VPS18		+			+
myc-VPS39			+		+
myc-VPS41				+	+
IP:					
WB: m α myc					
Input					
WB: m α HA					
Input					
WB: m α myc					

Figure 4.16 – Co-immunoprecipitation of POLARIN with the HOPS complex. HEK293 cells were co-transfected with HA-empty or HA-POLARIN and myc tagged VPS11, VPS18, VPS39 or VPS41. Co-immunoprecipitation experiments were carried out, which revealed a strong interaction between POLARIN and VPS18, and weaker interactions with VPS11, VPS39 and VPS41. None of these proteins were pulled down with HA-empty despite being present in the lysates.

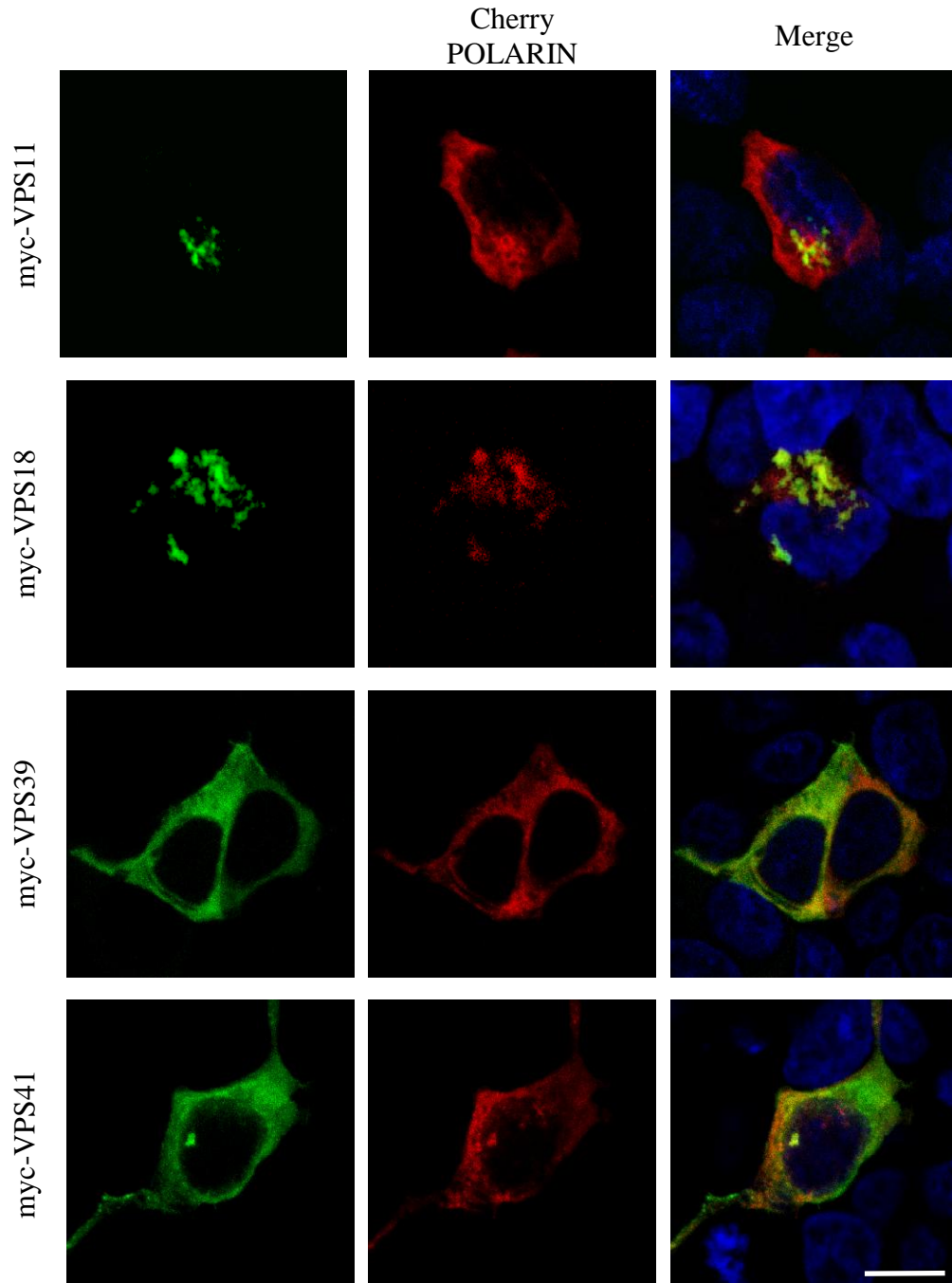










Figure 4.17 – Confocal immunofluorescence of POLARIN with the HOPS complex.
 Confocal immunofluorescence photomicrographs of HEK393 co-transfected with Cherry-POLARIN (red) and myc-VPS11, VPS18, VPS39 or VPS41 (green). Nuclei are stained with TO-PRO-3. Scale bar = 10 μ m. No change in localisation was observed for VPS11, VPS18, VPS39 and VPS41 from their single transfections. POLARIN formed large discrete clusters that co-localised with VPS18 when co-transfected with VPS18. (Experiment carried out in collaboration with A Straatman Iwanowska and Guanmei Luo, University of Birmingham, UK)

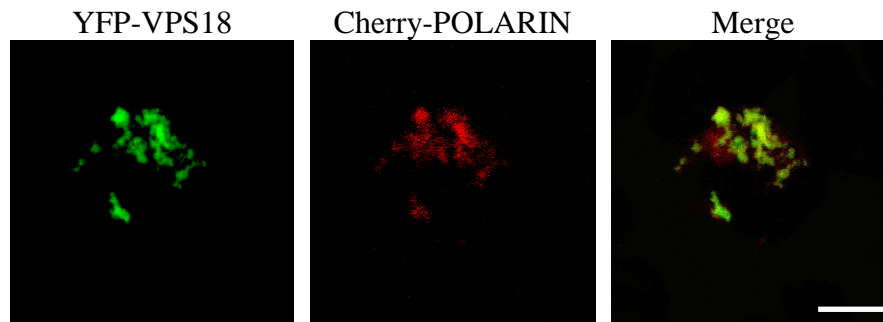
The clustering and co-localisation of POLARIN with VPS18 and the stronger interaction between POLARIN and VPS18 for the co-immunoprecipitation experiment, suggests that this may be a direct interaction. In ARC syndrome, the gene encoding VPS33B is mutated in 75% of patients and there is reduced expression of VPS33B in all patients (chapter 3) [4]. Therefore, assuming the expression levels of POLARIN in these patients are normal, the effect of VPS33B on the interaction between VPS18 and POLARIN needs to be further investigated.

Co-immunoprecipitation was carried out on lysates from HEK293 cells co-transfected with myc-VPS18 and HA-POLARIN with or without the addition of YFP-VPS33B (Figure 4.18A). Confocal immunofluorescence microscopy was also carried out on cells transfected with YFP-VPS18, Cherry-POLARIN with and without the co-transfection with HA-VPS33B (Figure 4.18 B and C). Again, POLARIN strongly interacts and co-localises with VPS18 when VPS33B is not being over-expressed. However, when VPS33B is being over-expressed, the VPS18-POLARIN interaction is greatly reduced, shown by the faint band on the co-immunoprecipitation. Furthermore, the localisation of POLARIN dramatically changes from co-localisation with VPS18 to VPS33B when VPS33B is being over-expressed. In the triple transfected cells, POLARIN predominantly co-localises with VPS33B which are present in completely separate clusters to VPS18, however, there are regions of triple co-localisation.

A

HA-Empty	+		
HA-POLARIN		+	+
YFP-Empty	+	+	
YFP-VPS33B			+
myc-VPS18	+	+	+
<hr/>			
IP: m α HA			
WB: m α myc			
Input			
WB: m α HA			
Input			
WB: Rb α VPS33B			
Input			
WB: m α myc			

B



C

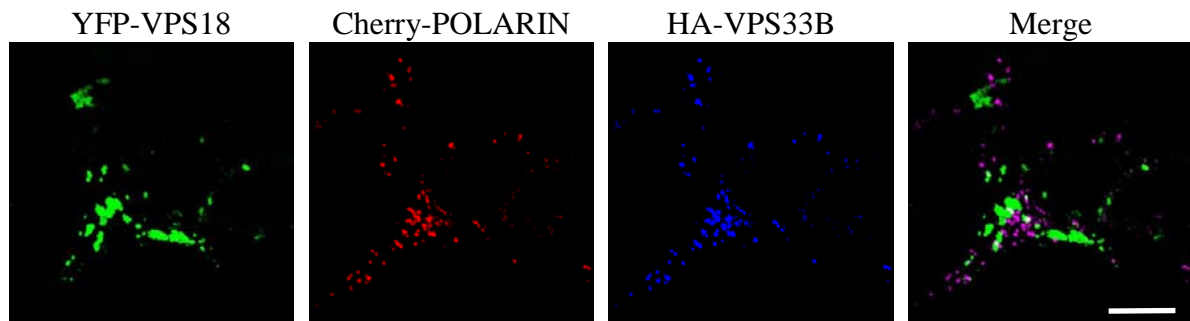


Figure 4.18 – POLARIN interaction with VPS18.

A, HEK293 cells were co-transfected with HA-empty or HA-POLARIN, YFP-empty or YFP-VPS33B and myc-VPS18. A co-immunoprecipitation experiment was carried out, which again revealed a strong interaction between POLARIN and VPS18 when only endogenous levels of VPS33B present. When VPS33B is also over-expressed this interaction diminishes.

B, Confocal fluorescence photomicrographs of HEK393 co-transfected with YFP-VPS18 (green) and Cherry-POLARIN (red), showing clustering and co-localisation of both proteins. **C**, Confocal immunofluorescence photomicrographs of HEK393 co-transfected as in B plus HA-VPS33B (stained using Alexa 633, shown in blue). POLARIN now co-localises with VPS33B (purple in merge image) and not with VPS18. However, there are regions of triple co-localisation (seen as white in the merge image). Scale bars = 10 μ m.

4.4.7 – PLRN Mutation Analysis of ARC Syndrome Patients.

To investigate whether a deficiency in POLARIN may cause clinical features of ARC syndrome, consanguineous families with ARC syndrome in which linkage to the *VPS33B* locus was excluded were analysed. A genomewide linkage screen using 10K and 250K Affymetrix SNP microarrays was performed in 4 unrelated consanguineous patients. Homozygosity for the *PLRN* locus was identified in 3 patients from Turkish and Israeli Arab ethnic backgrounds (data not shown). The genome wide linkages scans were carried out by F. Rahman (University of Birmingham, UK). Mutation screening of all *PLRN* coding exons and flanking intronic sequence was then performed using DNA from all available ARC patients lacking demonstrable *VPS33B* mutations. Eight mutations, 6 nonsense, one frameshift and one missense (changing the start ATG codon to AGG) were detected in 7 unrelated patients (Table 4.2). Mutations were verified by segregation with disease status within the families and by screening at least 200 chromosomes from ethnically matched controls for each mutation. All detected mutations are predicted to cause absence of POLARIN expression.

Patient Number	Ethnic Origin	Nucleotide Alteration	Peptide Alteration	Status
22	Turkish	535C→T	Q179X	Hom *
23	Croatian	748_752delACAGA	T250ArgfsX279	Hom
24	Turkish	658C→T	R220X	Het
		873C→T	Q291X	Het
25	Turkish	1273C→T	Q425X	Hom *
26	Italian	658C→T	R220X	Hom
27	Israeli Arab	808C→T	R70X	Hom *
28	Turkish	2T→G	M1R	Hom *

Table 4.2 – PLRN is mutated in ARC syndrome.

Nucleotides are numbered from the A of the ATG initiation codon. None of these mutations were identified in more than 200 chromosomes from healthy ethnically matched controls.

Patient numbers continue from Table 3.1 (VPS33B mutations). Patient 22 had reduced expression of VPS33B at the RNA and protein level. (= used for genome-wide scan, del = deletion, fs = frameshift, X = stop, hom = homozygous, and het = heterozygous). Mutation screening carried out by A. Straatman-Iwanowska, University Birmingham, UK.*

4.5 – Discussion

The conventional HOPS complex, including VPS33A, was recently found to be involved in the Rab5/Rab7-dependent pathway of phagosome biogenesis during apoptosis in mammalian cells [79]. Another complex, the class C cORE Vacuole/Endosome Tethering (CORVET) complex can be formed by class C VPS proteins in yeast [168]. Unlike other SM proteins, VPS33 homologues require additional proteins to interact with SNARE complexes. Presented here is a novel protein, POLARIN, possessing 16% identity to the C-terminal domain of the HOPS complex member VPS16. However, VPS33B specifically interacts with POLARIN and not with VPS16. Although the experiments shown in this chapter suggest that VPS33B and POLARIN are unlikely to form active parts in the conventional HOPS complex function, there are likely to be other components of the new VPS33B-POLARIN complex. Indeed the VPS33B-POLARIN complex interacts with the remaining members of the HOPS complex (VPS11, VPS18, VPS39 and VPS41). Furthermore, the VPS33B-POLARIN complex is unlikely to function at the early endosome, late endosome or lysosome level, since neither endogenous VPS33B nor co-overexpressed VPS33B-POLARIN clusters significantly co-localised with Rab5, LAMP-1 or CD63. This suggests the presence of a novel complex that possibly utilises members of the conventional HOPS complex, but through the specific action of VPS33B and POLARIN has a different function within cells (Figure 4.19).

In light of the experimental findings it is likely that the VPS33B-POLARIN complex is associated with the Rab4/Rab11 intracellular trafficking pathway in mammalian cells, as evidenced by co-localisation, positive FRET and co-immunoprecipitation. The interaction between VPS33B and POLARIN is required for the complex to interact with Rab11a, and

furthermore the dominant negative (GDP locked) version of Rab11a failed to interact with the complex. This suggests that the newly identified complex has Rab11a effector properties, as Rab11a must be GTP bound for the VPS33B-POLARIN complex to interact [42]. However, this cannot account for the partial co-localisation observed between the VPS33B-POLARIN complex and Rab11a in both HEK293 and mIMCD-3 cells. There are VPS33B-POLARIN clusters that do not contain Rab11a and vice versa. GDP bound Rab molecules are not membrane bound [63], and so should not appear as discrete clusters within the cytoplasm of cells. Rab11a vesicles not containing the newly identified complex can clearly be observed at the over-expressed and endogenous level. Therefore there are likely be other factors regulating the interaction between the VPS33B-POLARIN complex and Rab11a, resulting in a subset of Rab11a vesicles containing the VPS33B-POLARIN complex and vice versa. Furthermore, the interaction between VPS33B-POLARIN and Rab11a is potentially transient, therefore cannot always be seen in fixed cells.

POLARIN is a predominantly coiled protein with 2 predicted coiled-coiled domains, and has similarity to Golgin subfamily A member 5. The Golgin family of proteins are coiled-coil motif-containing proteins known to interact with Rab GTPases [162;163]. Recently another novel protein was identified, SCYL1BP1, which contains a Golgin domain and that specifically binds to the GTP bound form of Rab6 [169]. This is similar to the VPS33B-POLARIN interaction with Rab11a, suggesting a common mechanism of action of Golgin domain containing proteins.

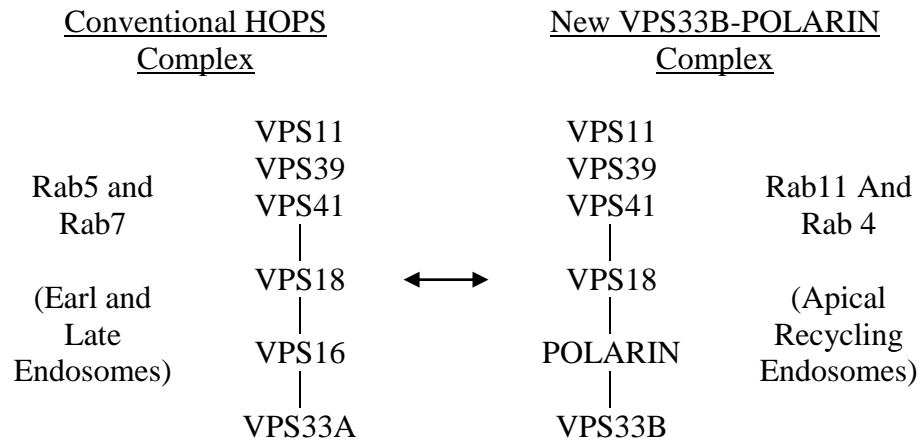


Figure 4.19 – Model for conventional HOPS complex and VPS33B-POLARIN complex.

The conventional HOPS complex contains VPS11, VPS16, VPS18, VPS33A, VPS39 and VPS41, which functions at Rab5 and Rab7 early and late endosomes. The newly identified VPS33B-POLARIN complex utilises VPS11, VPS18, VPS39 and VPS41 from the conventional complex, but replaces VPS33A and VPS16 with VPS33B and POLARIN. This replacement is associated with the newly identified complex's interaction and co-localisation with Rab4 and Rab11a on recycling endosomes.

The weak interaction between POLARIN and VPS11, VPS39 and VPS41 may be due to endogenous limitations of other members of the complex, which must also be over expressed for complete interaction to occur. In contrast, the interaction between POLARIN and VPS18 is much stronger, but only when VPS33B is not being co-overexpressed. This would mimic the effect of reduced expression of VPS33B seen in ARC syndrome patients, as demonstrated in chapter 3. When VPS33B is over-expressed, the POLARIN is predominantly displaced from VPS18 clusters and co-localises with VPS33B, suggesting a competitive binding mechanism of action between POLARIN and VPS33B or VPS18. However, there are regions of triple co-localisation, suggesting the complex can come together under certain and currently unknown circumstances.

The identification of pathogenic mutations in *PLRN*, the gene encoding POLARIN in ARC syndrome patients without detectable VPS33B mutations, is consistent with the idea that VPS33B and POLARIN are required for each other's function in the cell. There are no distinguishable phenotype differences between ARC syndrome patients with *VPS33B* or *PLRN* mutations, further suggesting the 2 proteins co-operate to achieve the same function within cells. However, the exact function of these 2 proteins remains unknown and will be investigated in the next chapter.

CHAPTER 5 – EFFECT OF VPS33B AND POLARIN KNOCKDOWN ON AN EPITHELIAL CELL LINE

5.1 – Introduction and Overview

Epithelial cells contain distinct apical and basolateral plasma membrane domains. Generation of these segregated domains is termed polarisation and is essential for various epithelial functions, including absorption and secretion [85;86]. Epithelial cells form a cohesive layer that acts as a physical ion-selective barrier. This barrier function is highly dependent on the integrity of apical junctional complexes (AJCs), comprising of tight junctions (TJs) and adherens junctions (AJs) that link adjacent epithelial cells [88;89]. TJs, which lie apically to AJs, separate apical and basolateral membrane domains and constitute a partially permeable site of intercellular molecular transport. In the process of epithelial differentiation AJs appear earlier than TJs. AJs form an adhesive belt that encircles each cell and binds the neighbouring epithelial cell membranes [170]. Although the importance of AJCs to generation and maintenance of epithelial polarity is well known, the molecular pathways determining the biogenesis of polarised membranes are not fully characterised. Elucidation of the key pathways for cell polarisation is essential for understanding the development and the molecular and cellular physiology of the many structures, including gut, urinary tract, and central nervous system (CNS), that rely on intact cell polarity for their function [94]. There appears to be a defect in epithelial cell polarisation in ARC syndrome patients. Therefore clarification of these polarisation pathways may help to explain the pathophysiology of ARC syndrome.

Clinical features in ARC syndrome patients differ from the phenotype of hypopigmentation and immune deficiency found in organisms with HOPS complex protein defects [9;171;172]. Furthermore, the data presented in chapter 4 suggests that VPS33B and POLARIN form a

different complex to that of the conventional HOPS complex and does not function at the endosome or late endosome. This suggests that VPS33B is involved in an intracellular trafficking pathway different from the conventional HOPS complex.

5.2 – Aims

We hypothesised that the VPS33B pathway plays an important role in directing the intracellular traffic of apical membrane proteins in hepatocytes, epithelial cells of the renal tubules, and other polarised epithelial cells. To test this hypothesis, clones of mIMCD-3 cells (a mouse polarised epithelial cell line) were created that had a stable reduced expression of either the novel protein Polarin or Vps33b. Characterisation of these knockdown cell lines will be presented in this chapter.

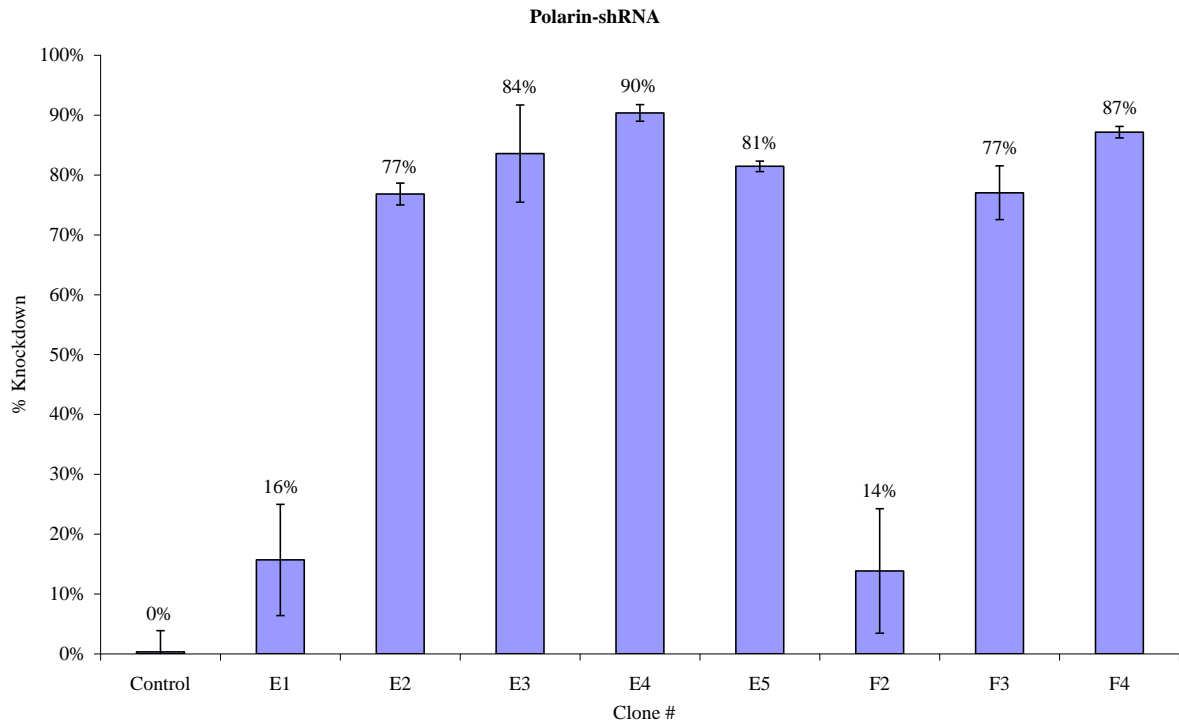
These knockdown cell lines will help elucidate the pathways POLARIN and VPS33B belong to and how these proteins are involved in apical membrane protein trafficking in polarised epithelial cells. Additionally, these knockdown cell lines should mimic the effect of *PLRN* or *VPS33B* mutations seen in ARC syndrome patients' epithelial cells, and thus allow the investigation of molecular pathophysiology of ARC syndrome.

5.3 – Results

5.3.1 – Polarin and Vps33b shRNA in mIMCD-3 cells

In order to investigate further the molecular mechanisms affected by ARC syndrome in polarised epithelial cell models, clones were developed of mouse Inner Medullary Collecting Duct (mIMCD-3) cells stably transfected with silencing shRNAs for Vps33b or Polarin. One hairpin sequence for Vps33b and 2 sequences for Polarin (sequences shown in Appendix I) were individually transfected into mIMCD-3 cells and expression of the shRNA selected for by puromycin resistance. A control shRNA containing a scrambled sequence was used as a specificity control. Several individual clones were grown for each hairpin sequence and the level of knockdown assessed by quantitative real-time PCR (Polarin) or by western blotting (Vps33b, Figure 5.1). No knockdown of either gene was observed in the Control shRNA cells. Clones with the greatest knockdown were used for further experiments. A 90% knockdown was achieved for Polarin (Polarin-shRNA) and a 92% was achieved for Vps33b (Vps33b-shRNA)

Immunostaining of endogenous Vps33b in wild type mIMCD-3 cells, compared with the mIMCD-3 clones with stable Polarin knockdown (Figure 5.2), demonstrated a greatly reduced expression of Vps33b, which supports the hypothesis that Polarin is required for the stabilisation of Vps33b.

A**B**

Clone	WT	1	2	3	4	5	6	Control
Vps33b								
β-Actin								
OD Vps33b	82.200	6.407	50.113	74.432	7.691	55.295	61.609	80.944
OD β-Actin	98.877	98.722	97.757	96.092	97.864	98.733	99.057	97.948
% Expression	83.13%	6.49%	51.26%	77.46%	7.86%	56.00%	62.20%	82.64%
% Knockdown	-	92.19%	38.34%	6.83%	90.55%	32.63%	25.19%	0.59%

Figure 5.1 – Assessment of Polarin or Vps33b knockdown in mIMCD-3 cells.

A, Quantitative Real Time PCR (qRT-PCR) for Polarin. Values shown are mean values of expression levels of the Polarin normalised to β -actin and relative to wild type cells ($n=3$ for each sample). Error bars represent ± 1 standard error of the mean. Two shRNA hairpins were used, E and F. Clone E4 was used for all future experiments, due to greatest level of knockdown of Polarin (90%, renamed Polarin-shRNA). **B**, Western blot for Vps33b. Loading was controlled by immunoblotting the same membrane with an anti- β -actin antibody.

Densitometry on bands was carried out, and final knockdown values are normalised to β -actin and relative to wild type (WT) cells. Clone 1 was used for all future experiments, due to greatest level of knockdown of Vps33b (92%, renamed Vps33b-shRNA). No reduction in either Polarin or Vps33b expression was seen in control-shRNA treated cells.

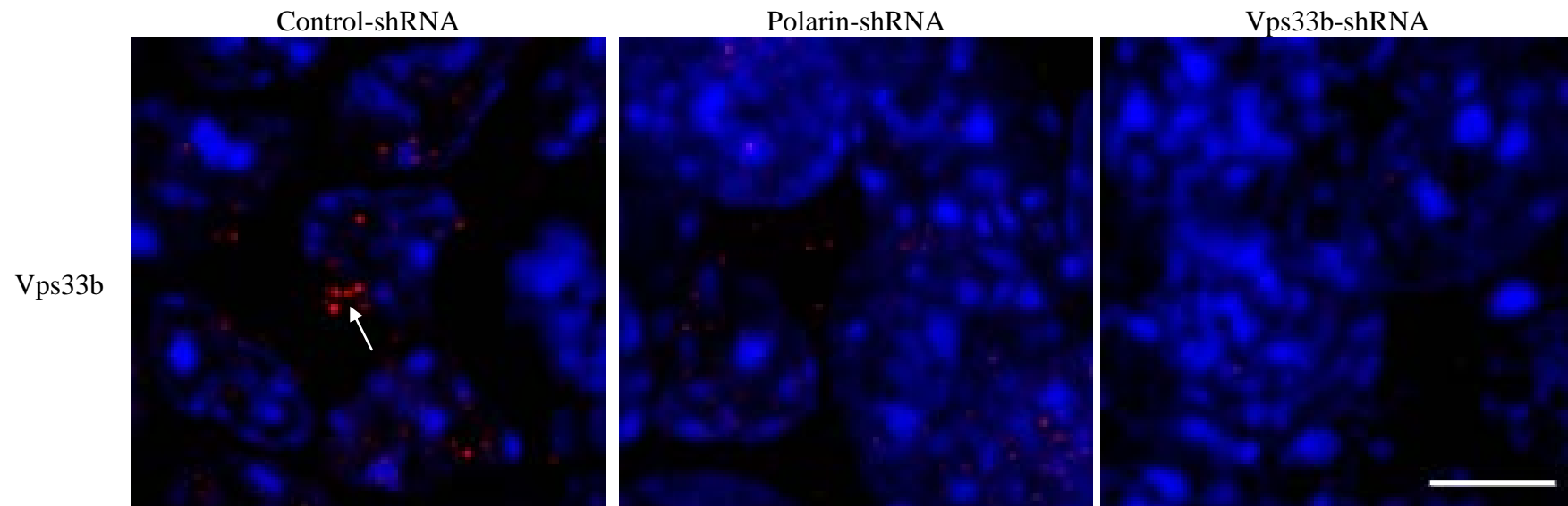


Figure 5.2 – Endogenous Vps33b staining in Control-, Polarin- and Vps33b-shRNA cells.
Confocal immunofluorescence photomicrographs of Control-, Polarin- and Vps33b-shRNA mIMCD-3 cells stained for endogenous Vps33b growing of transwell supports. Large cytoplasmic clusters seen in the wild type cells (arrow) are no longer present in either of the knockdown cell lines. Nuclei are stained with TO-PRO-3. Scale bar = 10 μ m. (Experiment carried out in collaboration with A Straatman Iwanowska, University of Birmingham, UK)

5.3.2 – Mislocalisation of Apical Membrane Proteins

The mislocalisation of apical membrane proteins were observed in liver and kidney biopsies taken from ARC syndrome patients [1;11], therefore, the ability of Polarin- and Vps33b-shRNA cells to maintain correct localisation of apical membrane proteins was tested by immuno-fluorescence confocal microscopy. Obvious loss of specific apical localisation of P75 (exogenous) in both Polarin- and Vps33b-shRNA cell lines was detected. The apical recycling endosome (ARE) marker, Rab11a, also lost its apical localisation in Polarin- and Vps33b-shRNA cells (Figure 5.3). However, the basolateral protein Na/K ATPase maintained its correct basolateral position in the absence of Vps33b or Polarin (Figure 5.3).

The localisation of carcinoembryonic antigen (CEA, endogenous) was also tested as its' apical expression is lost in ARC patients. The fluorescent microcopy did not show a very clear distinction between the control and knockdown cell lines. Therefore, the sulfo-NHS-SS biotin reagent was then used to detect whether CEA was present in the membrane or cytoplasm of the control and knockdown cells. Immunoblotting of CEA on protein lysates from Control-, Polarin and Vps33b-shRNA cells, revealed an absence of the major 180 kDa CEA band in the Polarin and Vps33b deficient cells (Figure 5.4A). The sulfo-NHS-SS biotin reagent binds covalently to the ϵ -amine of lysine residues in proteins, but cannot cross the plasma membrane, and therefore only binds to proteins on the plasma membrane. This reaction is quenched, the cells lysed and the biotinylated proteins separated from the unlabelled (non-membrane) proteins using streptavidin agarose. On closer inspection of the photomicrographs and using a membrane protein biotinylation binding assay, the 180 kDa

protein that was present in the apical membrane of the control cells, corresponded to the band that was undetectable in the knockdown cells (Figure 5.4B).

To investigate whether the Vps33b-Polarin complex may be directly involved in trafficking of CEA and P75, pre-polarised wild type mIMCD-3 cells were immunolabelled for CEA and P75. This revealed that there was co-localisation of the Polarín-Vps33b clusters with the apical membrane markers (P75 and CEA) mislocalised in the shRNA cells (Figure 5.5).

5.3.3 – Apical Junction Complex Defects

A characteristic of all epithelial cells is their ability to maintain an electrochemical gradient across a monolayer of cells [173]. To test whether Polarín and Vps33b-shRNA cells maintained this characteristic, Trans-Epithelial Resistance (TER) experiments were performed by placing electrodes in the apical and basal compartments of transwell supports which had control and knockdown cell lines growing on them, every 24 hours for 12 days (Figure 5.6). Significant reductions (50% for Polarín-shRNA and 75% for Vps33b-shRNA compared with control cells) in maximum TER achieved were detected in both knockdown cell lines, suggesting that a TJ defect and abnormal trafficking of proteins to TJs, as well as to the apical membrane, may account for the overall cellular phenotype.

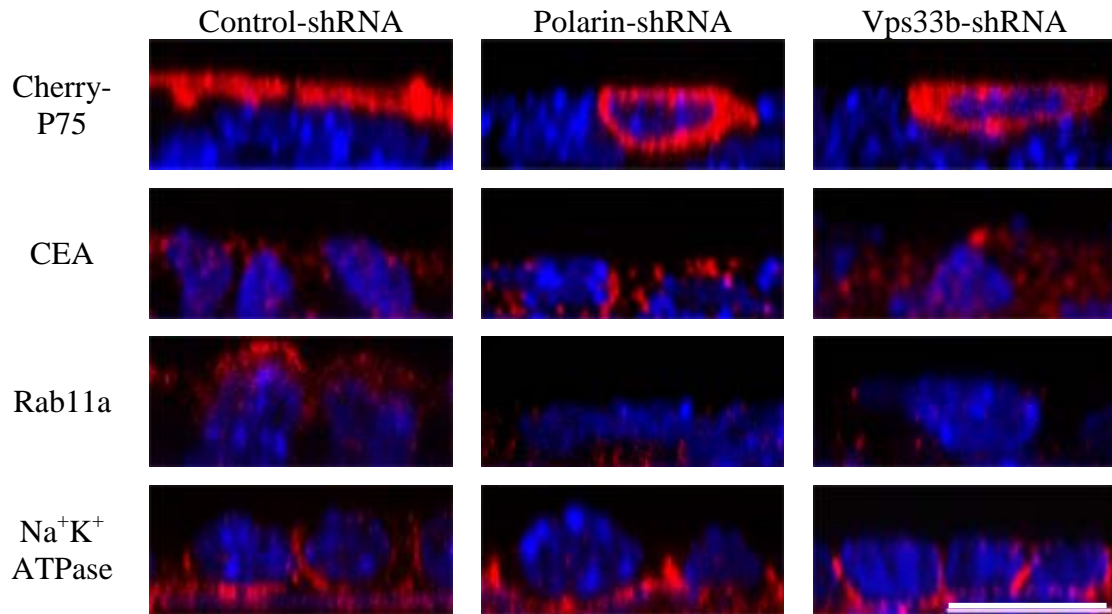
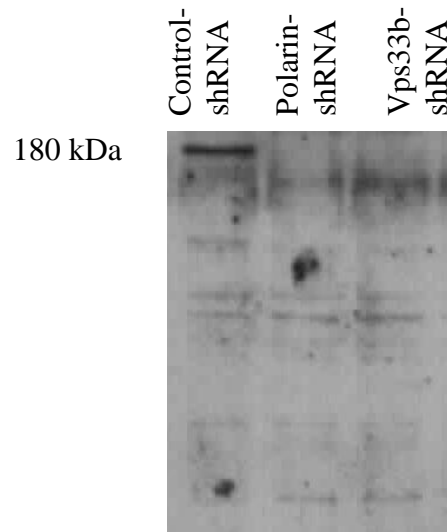


Figure 5.3 – Abnormal localisation of apical markers in Polarin- and Vps33b-shRNA cells.

Confocal immunofluorescence xz plane photomicrographs of transwell support cultured mIMCD-3 cells treated with shRNA (Control-shRNA, Polarin-shRNA and Vps33b-shRNA). As these knockdown cell lines do not grow in monolayers, marker localisation can be difficult.

Only the top layer is shown. Transfected Cherry-P75 and endogenous CEA can be found throughout the basolateral membrane and cytoplasm in Polarin- and Vps33b-shRNA cells, in contrast to their predominantly specific localisation to apical membranes in Control-shRNA cells. The apical recycling endosome marker Rab11a can be seen in the apical region of control-shRNA cells but this localisation is lost in knockdown cells. The basolateral marker Na⁺K⁺ ATPase (endogenous) is correctly localised in all 3 cell types. Nuclei are stained with TO-PRO-3. Scale bar = 10 µm. (Experiment carried out in collaboration with A Straatman Iwanowska, University of Birmingham, UK)

A



B

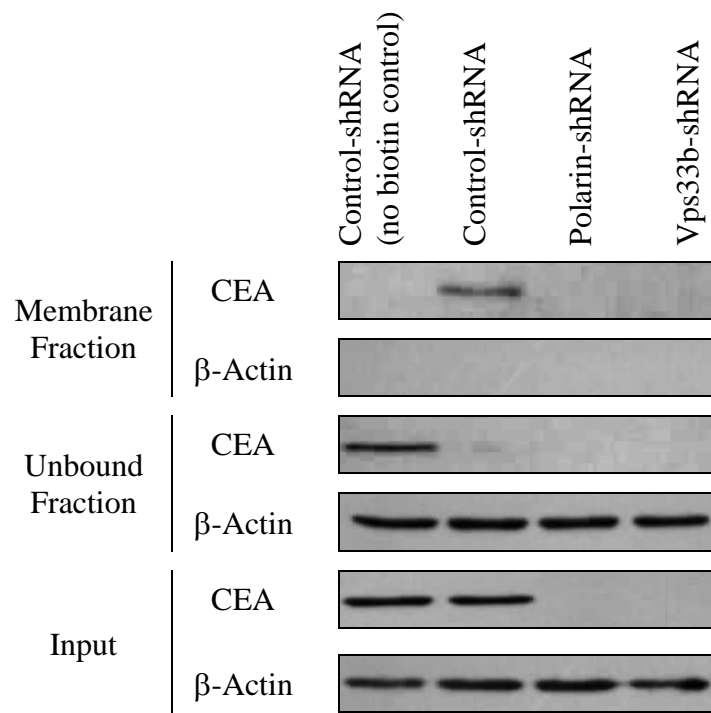


Figure 5.4 - Reduced expression of membrane CEA in Polarin- and Vps33b-shRNA cells
A, Over exposed immunoblot of CEA on protein lysates from Control-, Polarin and Vps33b-shRNA mIMCD-3 cells. In both knockdown cell lines the major 180 kDa CEA band is not detectable, despite the gel being equally loaded (shown by β -actin). **B**, Membrane protein biotinylation assay showing the band absent in A is present in the membrane of control-shRNA cells. No β -actin could be detected in the membrane fraction suggesting the biotin had not got inside the cells, and that the reaction was sufficiently quenched before the cells were lysed. No CEA could be detected in the pulled down membrane protein fraction where no biotin reagent was used, but was seen in the unbound fraction.

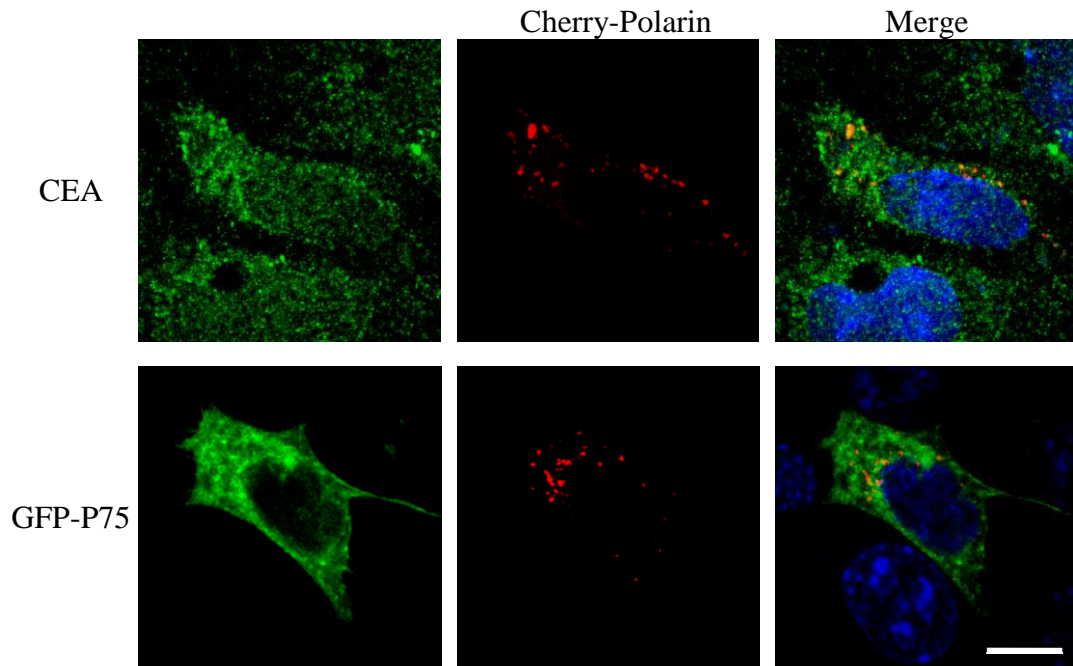


Figure 5.5 – Co-localisation of apical membrane markers with Polarin-Vps33b clusters in mIMCD-3 cells.

Confocal photomicrographs of cultured pre-polarised wild type mIMCD-3 cells transfected with HA-Vps33b (not stained), Cherry-Polarin and GFP-P75 or stained for endogenous CEA. Nuclei are stained with TO-PRO-3. Scale bars = 10 μ m. (Experiment carried out in collaboration with A Straatman Iwanowska, University of Birmingham, UK.)

As functioning TJs are essential to control paracellular flux of macromolecules, fluorescently labelled dextrans were used to test whether Polarin or Vps33b deficiency would lead to a defect in TJ formation and to abnormal barrier function of the mIMCD-3 cell monolayer. Two types of dextran, small and large (4 and 70 kDa), were used for the experiments, which were added simultaneously to the apical chamber of transwell supports and allowed to diffuse through to the basolateral chamber for 3 hours [173]. The ratio of each fluorophore between the apical and basal compartments was measured and the paracellular diffusion of each dextran calculated relative to a transwell filters without cells. Polarin-shRNA allowed twice as much 4kDa dextran, whilst Vps33b-shRNA treated cells allowed 2.5 times as much 4kDa dextran through the monolayer compared to controls. No such significant change was detected for the larger dextran (Figure 5.7)

TJ formation is dependent on the presence of calcium; therefore, to show that the changes in cell layer permeability and polarity are analogous to the physical disruption of TJs, the TER and dextran experiments were performed in cells grown in low-calcium medium [174]. All 3 cell types were cultured in normal growth medium for 6 days, followed by incubation in low calcium medium for 24 hours. After the control mIMCD-3 cells were cultured in low-calcium medium for 24 hours, the values for TER (not shown) and dextran permeability (Figure 5.8) became similar to those for Vps33b-shRNA cells. In Polarin-shRNA cells grown in low calcium medium for 24 hours, the TER decreased and the paracellular permeability increased to similar levels to Vps33b-shRNA cells when grown in normal medium. Both TER and permeability returned to values expected for the Control- and Polarin-shRNA cells after reintroduction of normal-calcium medium, suggesting that these effects were due to loss of functional TJs.

Trans-Epithelial Resistance of mIMCD-3 Cells Grown on Transwell Supports

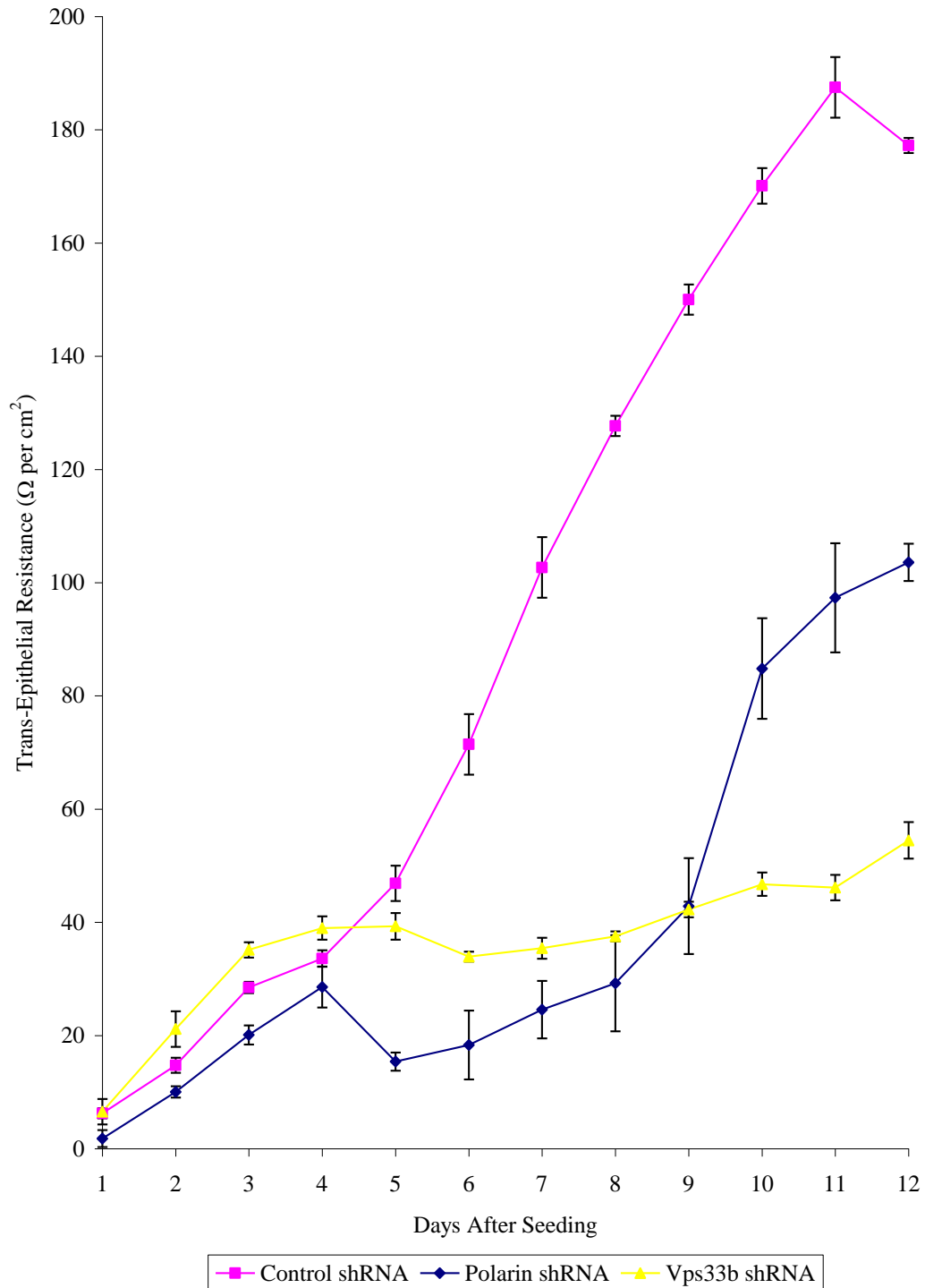


Figure 5.6 – Trans Epithelial Resistance (TER) in Control-, Polarin- and Vps33b-shRNA cells.

Values shown are average trans-epithelial resistance readings every 24 h after seeding the cells onto Transwell supports ($n=4$, error bars = ± 1 standard error of the mean). Polarin- and Vps33b-shRNA cells failed to establish TER to the extent of the control-shRNA cells.

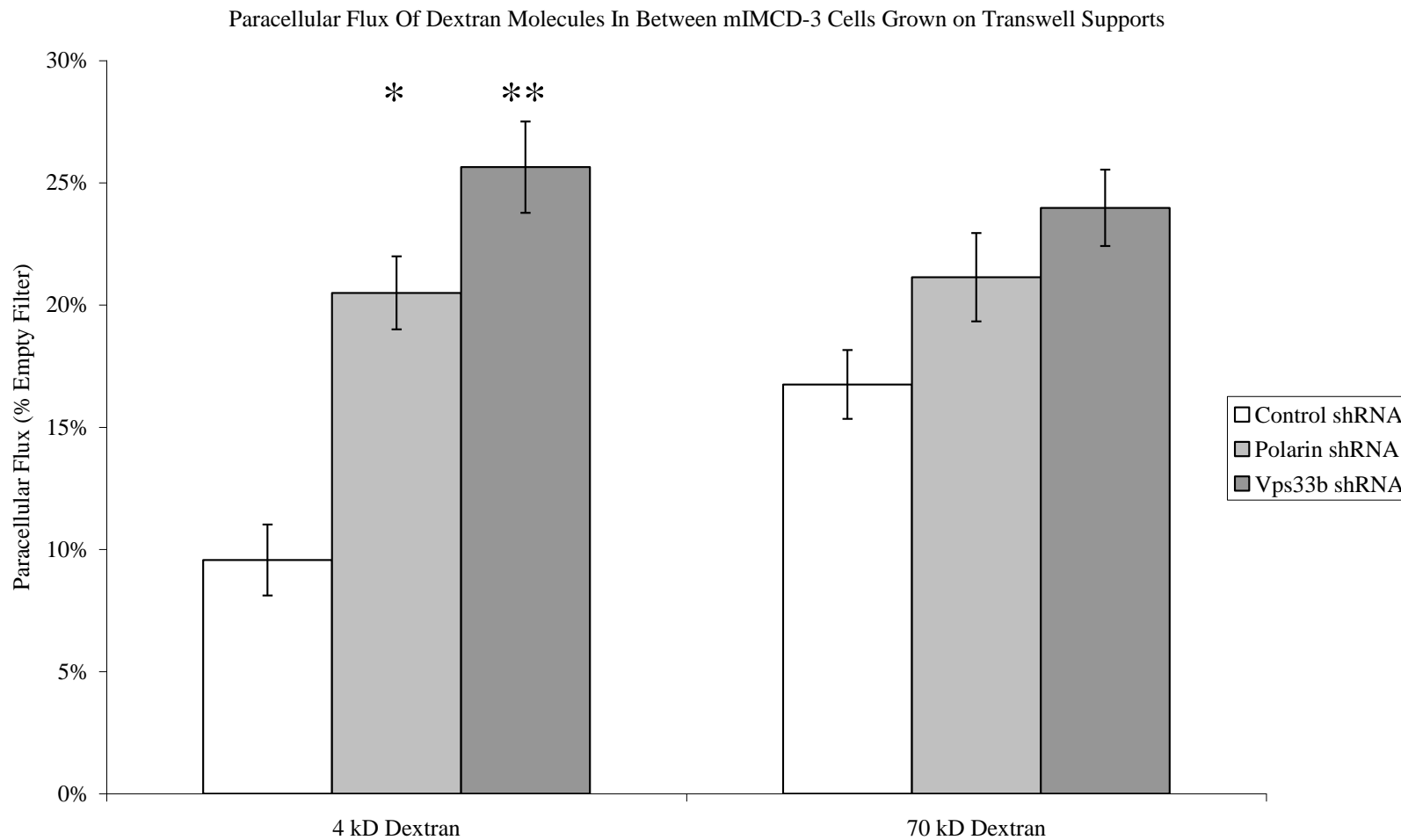


Figure 5.7 – Paracellular diffusion in Control-, Polarin- and Vps33b-shRNA cells.

Paracellular flux of 4 kDa dextran fluorescein isothiocyanate conjugate (FITC), and 70 kDa dextran Rhodamine B conjugate for all 3 cell types. Cells were seeded onto Transwell supports and allowed to grow for 7 days. $n=4$, error bars = ± 1 standard error of the mean, * = $p<0.05$, ** = $p<0.001$ by Student t-test. Polarin- and Vps33b-shRNA cells allowed a significantly greater amount of 4 kDa dextran through the paracellular space. No significant change was seen for 70 kDa dextran.

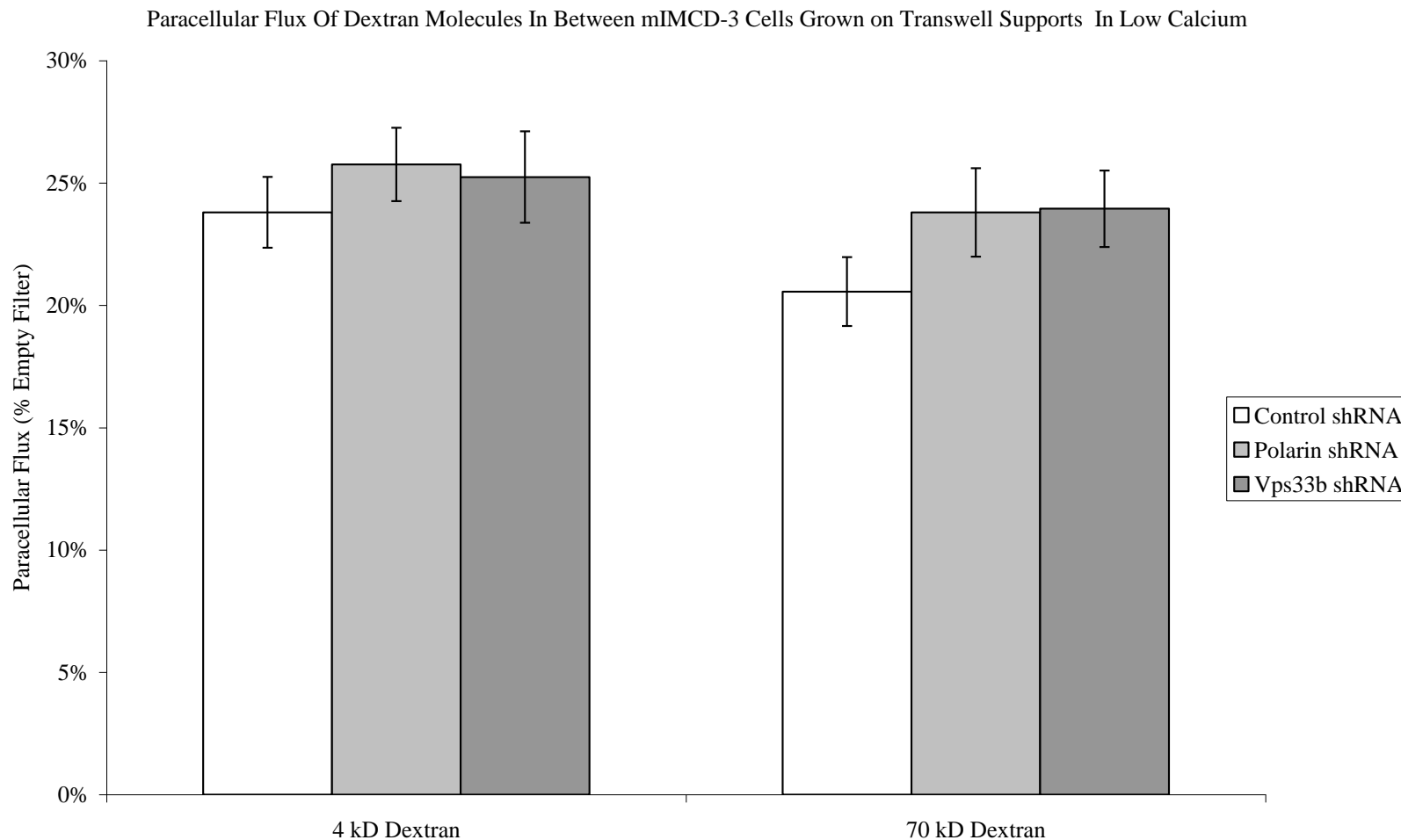


Figure 5.8 – Paracellular diffusion in Control-, Polarin- and Vps33b-shRNA cells grown in low calcium medium. Paracellular flux of 4 kDa dextran fluorescein isothiocyanate conjugate (FITC), and 70 kDa dextran Rhodamine B conjugate for all 3 cell types. Cells were seeded onto Transwell supports and allowed to grow for 6 days in normal medium, after which the medium was changed to low calcium medium 24 hours prior to the experiment. $n=4$, error bars = ± 1 standard error of the mean. No significant difference was observed between the Control-, Polarin-, and Vps33b-shRNA cells as in Figure 5.8 (by Student t-test).

Having demonstrated functional defects of TJs, the effect of decreased expression of Polarin and Vps33b on the localisation of some of the AJC proteins known to be involved in epithelial cell differentiation and human disease were studied. Surprisingly, no mislocalisation was detected on immunostaining of the Polarin-shRNA and Vps33b-shRNA cells for ZO-1, which is normally confined to the cytoplasmic surface of TJs and associates with the actin cytoskeleton (Figure 5.9). More in keeping with the defect in TJ formation, mislocalisation of Claudin-1 to the plasma membranes and cytoplasm was identified in the knockdown cells, whilst in controls Claudin-1 was specifically localised to TJs (Figure 5.9).

E-Cadherin is a calcium-dependent cell adhesion molecule with a functional extracellular domain that forms a part of the AJ adhesive belt. Therefore, following on from the results of the calcium switch dextran assay (Figure 5.7 to 5.8) the effect of decreased Polarin and Vps33b expression on E-Cadherin localisation was analysed. In Polarin- and Vps33b-shRNA cells, E-Cadherin localised predominantly to the cytoplasm whereas in the control cells, E-Cadherin was localised in the lateral membrane (Figure 5.9). Furthermore, it was reported previously that transfection of a dominant-negative Rab11a (DN-Rab11a) construct into Madin-Darby canine kidney (MDCK) cells causes mislocalisation of E-Cadherin and loss of the ability of these cells to form cysts [175]. To further explore the functional relationship between the Polarin-Vps33b complex and Rab11a identified in chapter 4, the phenotype of control mIMCD-3 cells expressing a DN-Rab11a construct was evaluated. mIMCD-3 cells stably transfected with the DN-Rab11a construct failed to polarise, as shown by 75% reduction in maximum achieved TER (similar to Vps33b-shRNA) and by mislocalisation of AJC proteins (Figure 5.9).

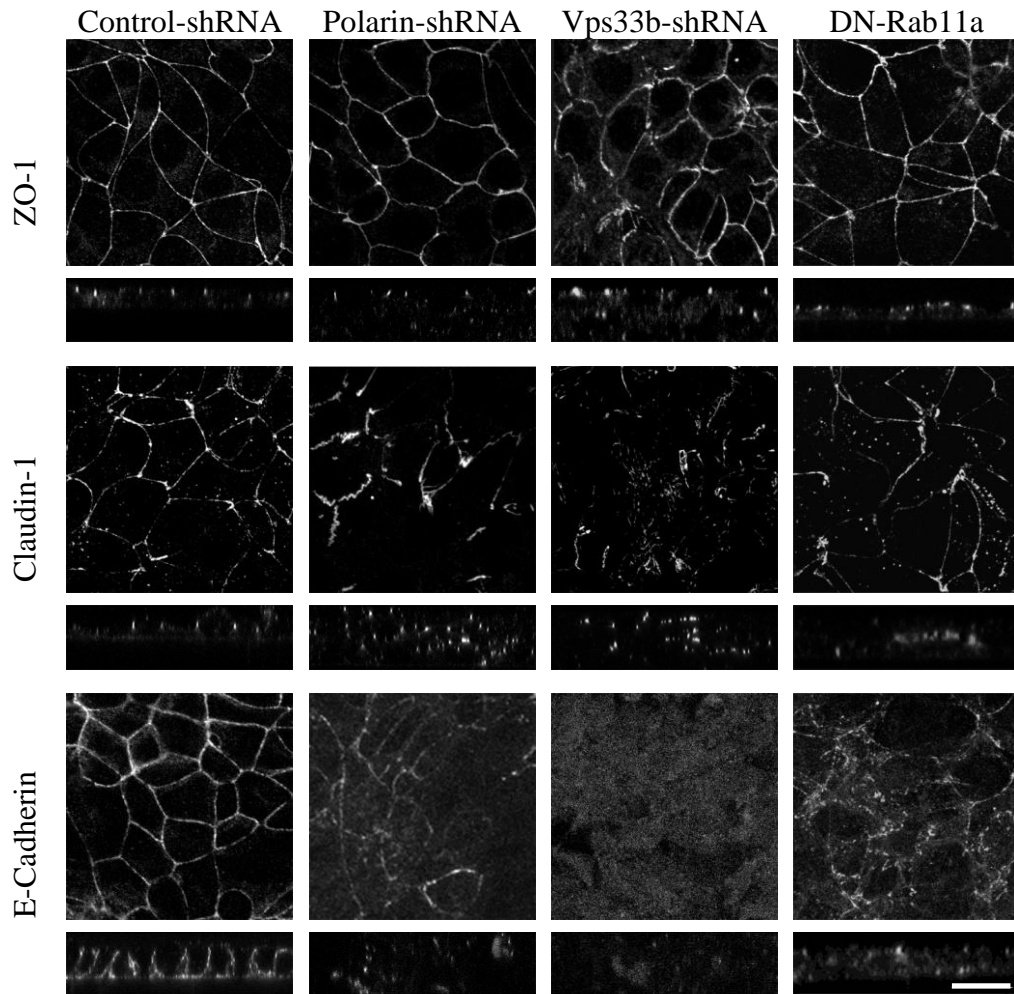


Figure 5.9 – Immunostaining of tight and adherens junction proteins in Control-, Polarin-, Vps33b-shRNA and dominant negative Rab11a cells.

Confocal immunofluorescence photomicrographs in xy and xz planes of ZO-1, Claudin-1, and E-Cadherin in Control-, Polarin-, Vps33b-shRNA and DN-Rab11a cells (scale bar = 10 μ m).

No change is seen for ZO-1 staining in any of the cell types. However, the specific localisation of Claudin-1 and E-Cadherin are lost in the knockdown and dominant negative Rab11a cells. Note the lack of a monolayer in the Polarin- and Vps33b-shRNA cells.

(Experiment carried out in collaboration with A Straatman Iwanowska, University of Birmingham, UK.)

To assess the expression level of these AJC proteins, western blotting was carried out on protein lysates extracted from wild type, Control-, Polarin- and Vps33b-shRNA cells grown on transwell supports for 7 days (Figure 5.10). This revealed a decrease in Claudin-1 with a concomitant increase in ZO-1 expression in the knockdown cells compared to wild type or control cells. The 120 kDa E-Cadherin band was undetectable in the knockdown cells. E-Cadherin that is bound to another E-Cadherin molecule can also bind β -Catenin, which leads to β -Catenin being protected from degradation [99]. With the reduction of E-Cadherin expression detected above, the level of β -Catenin expression could also be altered. However, interestingly β -Catenin expression was comparable to wild-type and control-shRNA cells.

Due to the potential TJ defects identified in Figures 5.6 to 5.10, freeze fracture electron microscopy was used in order to appreciate the three dimensional perspective of the TJs in the knockdown cells (Figure 5.11). This technique allows splitting of the layers of frozen cell membranes into two half-membrane leaflets [176]. The faces of each of the membrane leaflets can then be metal-replicated and visualised by transmission electron microscopy. The extracellular leaflet adjacent to the extracellular space and observed from inside the cell is conventionally called the exoplasmic or “E-face” and the leaflet adjacent to the cytoplasm is the protoplasmic or “P-face” as observed from outside the cell. Examination of the TJs in both Polarin- and Vps33b-shRNA treated cells showed reduced complexity, disturbed P-face association, and an increase of particle-free pores corresponding to overall TJ disruption compared with control cells (Figure 5.11). Vps33b-shRNA cells showed a greater reduction in complexity compared to that of Polarin-shRNA cells. These results were consistent with results of TER and fluorescent dextran studies of TJ function (Figures 5.6 to 5.8).

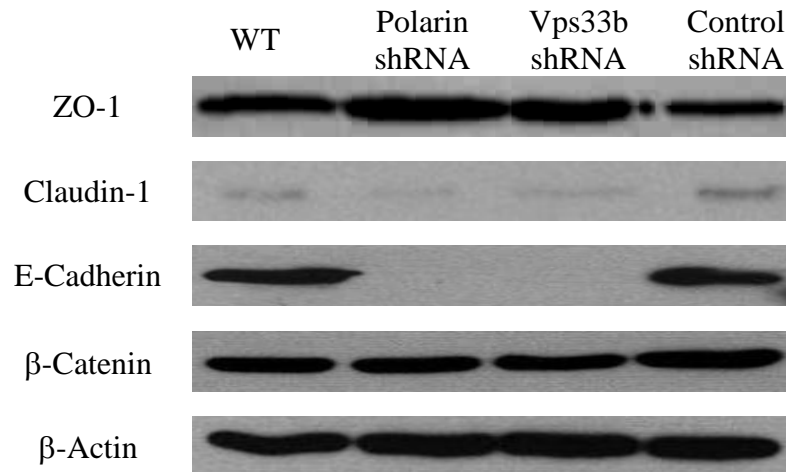
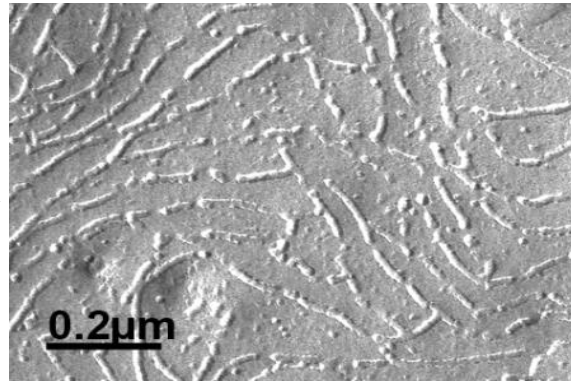


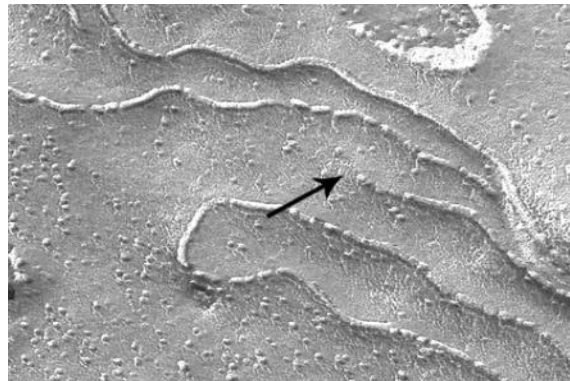
Figure 5.10 – Western blots of tight and adherens junction proteins in wild type, Control-, Polarini-, and Vps33b-shRNA cells.

Immunoblots of the tight junction proteins revealed a reduction in expression of Claudin-1 and an increase in ZO-1 in both knockdown cell lines. E-Cadherin expression is undetectable in these cells. Interestingly there is no change in expression of β-Catenin. Loading was controlled by immunolabelling the same membrane with β-actin.

Control-shRNA



Polarin-shRNA



Vps33b-shRNA

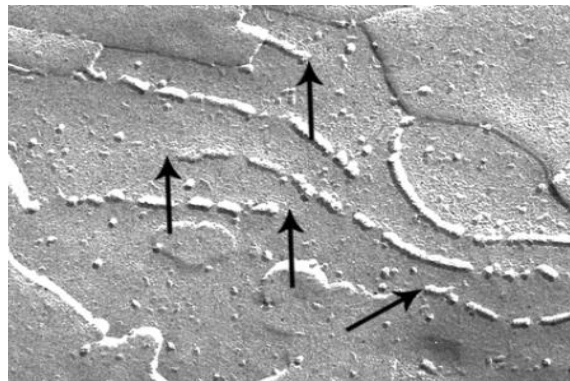


Figure 5.11 – Freeze fracture electron micrographs of Control-, Polarin- and Vps33b-shRNA cells.

Freeze fracture images of Control-, Polarin-, and Vps33b-shRNA cells showing TJ strands (scale bar = 0.2 μm). In Polarin- and Vps33b-shRNA cells, there is a strong decrease of tight junction strand complexity and/or a decrease of the P-face association leading to interrupted and blindly ending strands (arrows) when compared with the control cells. Experiment carried out on cells created in section 5.3.1 by H. Wolburg, University of Tübingen, Tübingen, Germany.

Having detected defects in apical junction complex formation and function in the Polarin and Vps33b deficient cell lines, E-Cadherin was immunostained on ARC syndrome patient liver biopsies (Figure 5.12). This revealed a marked reduction in E-Cadherin expression similar to that observed in the knockdown cell lines (Figure 5.10). The remaining E-Cadherin present in the ARC syndrome patient biopsies also seems to be mislocalised from the basolateral surfaces in the control biopsy to a localisation throughout the membrane and in the cytoplasm. Again this is consistent with the knockdown cell mIMCD-3 cell lines (Figure 5.9)

5.3.4 – Abnormal mIMCD-3 Cell Differentiation and Growth

Observation of mIMCD-3 cell lines' growth in culture and immunofluorescence experiments with antibodies against AJC proteins such as claudin-1 suggested that the knockdown cells failed to maintain epithelial characteristics when grown on Transwell supports. Instead of forming well-defined monolayers, cultured cells formed multilayered structures; cells lost their distinct columnar appearance, becoming flatter. Control-shRNA mIMCD-3 cells start to form cavities after 5 days of culture on Transwell supports (Figure 5.13A) and organise into tubules after 72 hours of growth in collagen gels (Figure 5.13B) [177]. These characteristics were completely lost in Polarin- and Vps33b-shRNA treated cells (Figure 5.13).

After discovering the abnormal morphology in knockdown cells, the effect of decreased expression of Polarin and Vps33b on cell proliferation was analysed. In agreement with other studies that investigated reduced E-Cadherin expression [178], the number of cells detached from transwell supports after 7 days in culture was significantly increased in Polarin- and Vps33b-shRNA cells ($p < 0.05$ by Student's t-test ; Figure 5.14).

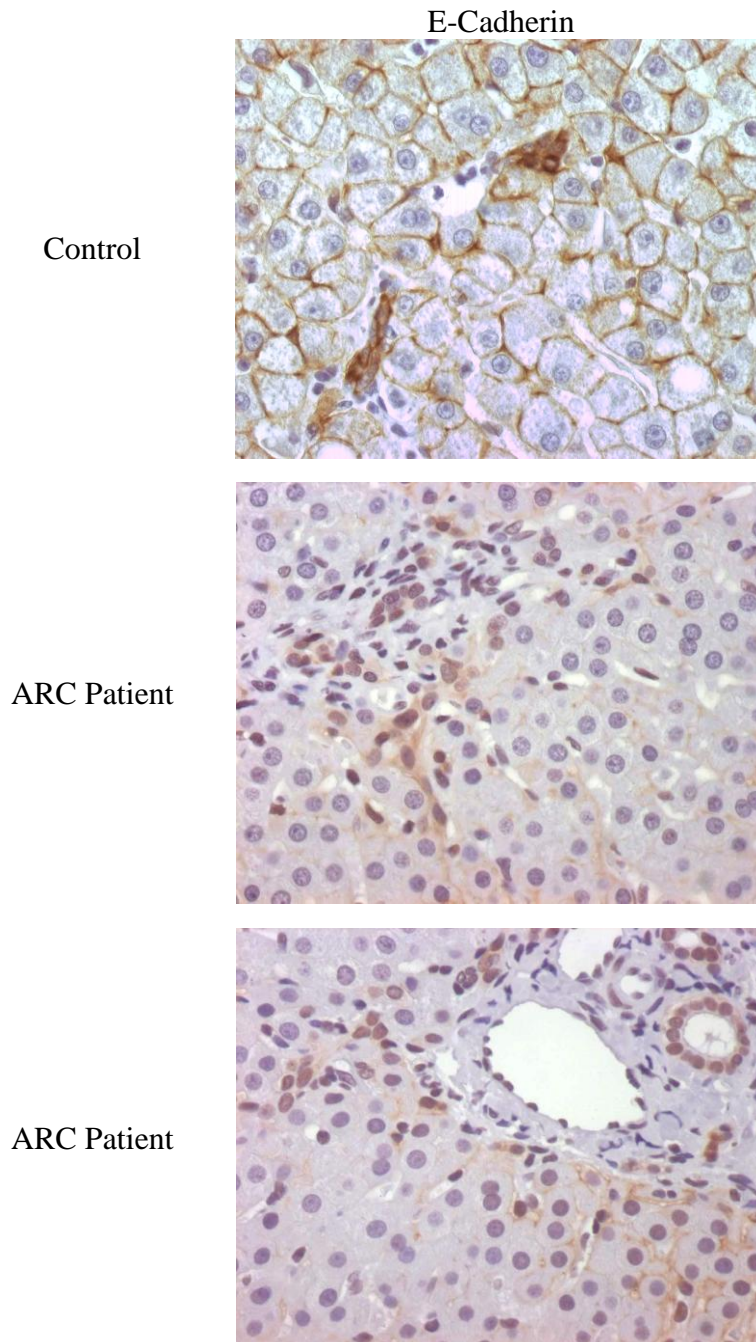
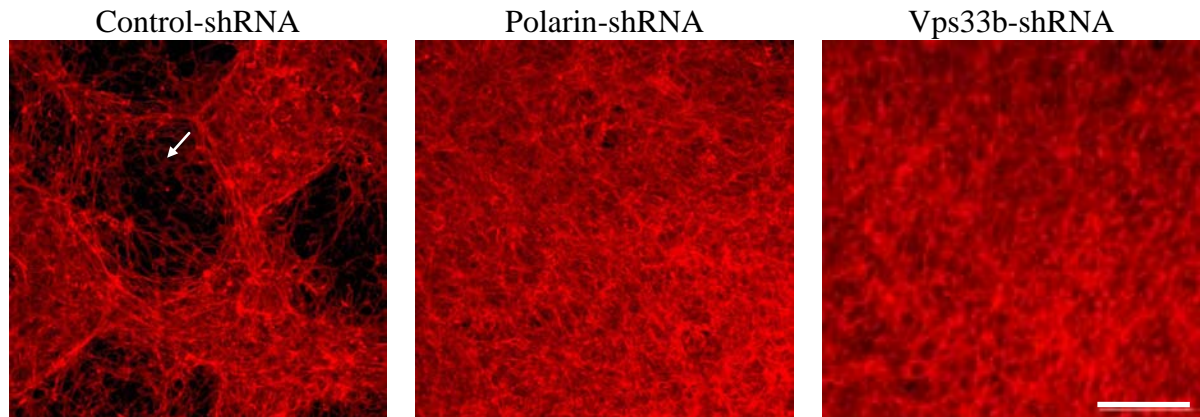


Figure 5.12 – Immunostaining of ARC syndrome patient liver biopsies for E-Cadherin.

Control and ARC syndrome patient liver tissue stained for E-Cadherin (brown staining).

Expression of E-Cadherin is greatly reduced in the ARC syndrome patients biopsies compared to the control biopsy. The remaining E-Cadherin present in the patients' biopsies is also mislocalised to a predominant cytoplasmic localisation, compared to a basolateral localisation in the control sample. A 200x original magnification was used for each, and the specimens were counterstained with haematoxylin. (Experiment carried out by A Straatman Iwanowska, University of Birmingham, UK.)

A



B



Figure 5.13 – Abnormal cell growth of Polarin- and Vps33b-shRNA cells.

A, Control-, Polarin- and Vps33b-shRNA cells grown on Transwell supports were stained for β -actin with phalloidin-TRITC conjugate (scale bar = 100 μ m). Cavitations (arrow) are present only in control cells. **B**, mIMCD-3 cells growing in collagen gels (10x magnification). Control-shRNA cells form highly branched tubules after 3 days in culture, whereas Polarin- and Vps33b-shRNA cells form no tubules.

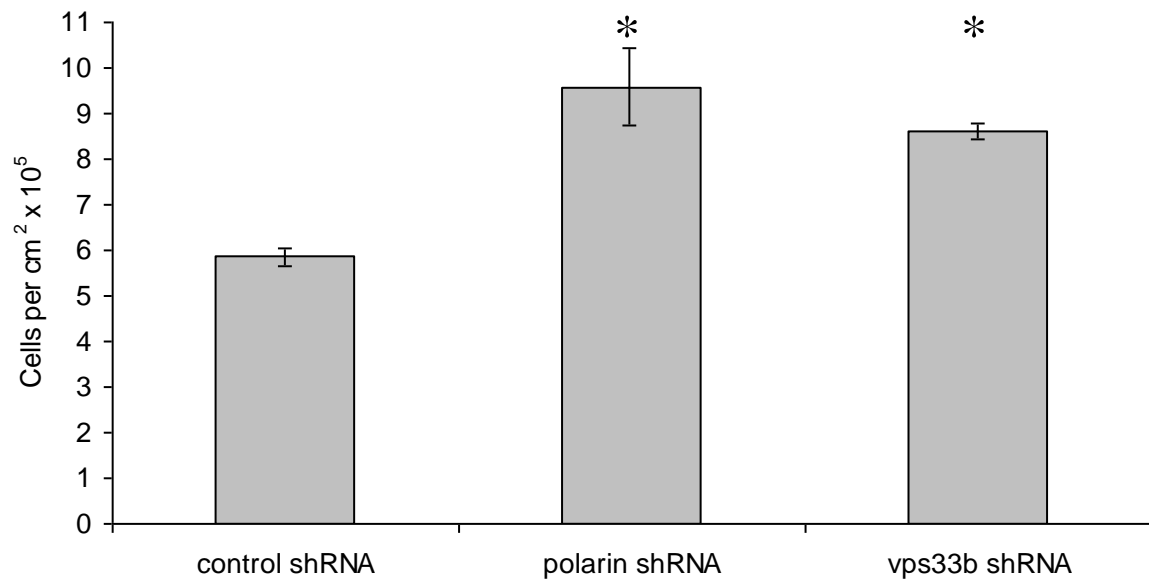


Figure 5.14 – Abnormal cell proliferation in *Polarin*-, and *Vps33b*-shRNA cells
 Values shown are mean number of cells detached, using trypsin, from Transwell supports after 7 days in culture (3 experiments, error bar = ± 1 standard error of the mean, * = $p < 0.05$ by Student's *t*-test). (Experiment carried out in collaboration with A Straatman Iwanowska, University of Birmingham, UK.)

5.4 – Discussion

Abnormal localisation of AJC proteins such as E-Cadherin in Polarin- and Vps33b-shRNA cell lines, like mislocalisation of specific proteins in patient liver biopsy specimens (see below), suggests a disturbance in a Rab11a/Rab4a-dependent trafficking pathway as the major cellular defect in ARC syndrome. Rab11a-expressing AREs may indeed be involved in E-Cadherin trafficking as well as in trafficking of some apical ATP-binding-cassette transporters [97;175;179]. Whilst Rab11a predominantly localised in proximity to the apical membrane in control cells, it was distributed throughout the cytoplasm in Polarin- and Vps33b-shRNA treated mIMCD-3 cells (Figure 5.3). This suggests that the Polarin-Vps33b complex may be involved in directing AREs towards apical membranes, although this finding may be secondary to the generalized loss of polarity in the knockdown cell lines.

Previously, mislocalisation of apical membrane proteins was demonstrated in kidney- and liver-biopsy specimens from patients with ARC syndrome harbouring *VPS33B* mutations [1;11]. Similarly, mislocalisation of apical membrane proteins in ARC syndrome patients harbouring *PLRN* mutations were identified. Furthermore, differences in the immunostaining of two apical membrane transporters were detected. BSEP, which is a major hepatocyte bile salt transporter, was mislocalised in the ARC syndrome patients' livers, whereas another apical membrane transporter, MRP2, was correctly localised (immunostaining performed by AS Knisely, King's College Hospital, London, UK; images shown in Appendix 4 for completeness). This difference is consistent with the suggestion that MRP2 and BSEP are trafficked to the apical membranes via different intracellular routes [180]. BSEP is trafficked

to the apical membrane through Rab11a-positive AREs whereas MRP2 is trafficked to the basolateral membrane first before being transcytosed to the apical membrane [180].

Cultured mIMCD-3 cells with decreased expression of Polarin or Vps33b demonstrated abnormal formation of the apical membrane and of AJCs. Moreover, Polarin- and Vps33b-deficient cell lines failed to polarise as evidenced by reduced TER measurements and by failure of tubule formation in culture. Functional investigations of Polarin and Vps33b in an epithelial cell line suggest that they work synergistically in the trafficking of proteins to the apical membrane and in AJC formation. The requirement of Polarin for Vps33b function and stabilisation is supported by the finding that Vps33b expression and distribution changed in cells with Polarin knockdown.

Immunoblotting of TJ proteins in Polarin- and Vps33b-shRNA cells revealed a decrease in expression of Claudin-1 and an increase in ZO-1 expression. An equivalent result was seen when bile ducts were artificially ligated to mimic the effect of cholestasis, as seen in ARC syndrome [181]. Claudins are the key member of the tight junction complex that regulate the paracellular permeability, and each one of the 24 members, of which Claudin-1 is expressed in kidney IMCD cells, has a different expression and permeability pattern [102;182]. The TJ protein ZO-1, localises correctly in control and knockdown cells, giving a characteristic cobble stone image in the *xy* plane and correct localisation in the *xz* plane. However, the remaining Claudin-1 appears to lose its specific localisation and was present in all plasma membranes in both knockdown cell lines. Claudin-1 is a transmembrane protein, whereas ZO-1 is a cytoplasmic protein that associates with the actin cytoskeleton. This coupled with the mislocalisation of apical membrane proteins gives a possible explanation for the difference in localisation of ZO-1 and Claudin-1.

Inactivating mutations in *CLDN1*, encoding Claudin-1, were found in patients with neonatal sclerosing cholangitis associated with ichthyosis syndrome (NISCH; MIM607626), a syndromic form of cholestasis associated with ichthyosis, two obligate features of ARC syndrome [1;183]. Although NISCH patients survive into adulthood, *Cldn1* knockout mice die on the first day of life with dehydration due to defective skin barrier function [184]. Thus the similarities between the phenotypic features of the two human disorders further support the hypothesis that the defect in AJC formation is a major pathological feature in ARC.

The Polarin- and Vps33b-shRNA cells when grown on transwell supports grow on top of each other and became much shorter, suggesting they have lost their contact inhibition characteristic of epithelial cells. This was never seen in the Control-shRNA treated cells. This effect is usually seen due to epithelial-to-mesenchymal transition (EMT) and is normally brought about by either reduced expression or altered localisation of E-Cadherin [178;185], as seen in ARC syndrome patient liver biopsies and in the Polarin- and Vps33b-shRNA cells. Thus suggesting that an EMT could be occurring in ARC syndrome patients polarised epithelial cells.

Similar results on E-Cadherin and Claudin-1 expression as presented here were recently seen in vascular endothelial cells, where knockdown of VE-Cadherin leads to a decreased expression of Claudin-5 due to the effects of both β -catenin and FOXO1 transcription factors and repressors [99]. The remaining E-Cadherin in both the knockdown cell lines and in ARC syndrome patient liver biopsies is unlikely to be dimerised due to lack of membrane localisation, and therefore unable to bind and hold β -Catenin in the cytoplasm. β -catenin is believed to be the molecular switch between proliferation and polarisation in epithelial cells,

mediated by adherens junction formation leading to a characteristic contact inhibition [185]. Immunoblotting of β -catenin in knockdown cells showed no change in the level of expression (Figure 5.10). Therefore the lack of functional E-Cadherin is likely to cause the down-regulation of Claudin-1 through the action of β -catenin in the nucleus. Consistent with the EMT effect, there was a significant increase in the number of Polarin- and Vps33b-shRNA cells detached from transwell supports, coupled with a dramatic decrease in polarisation in these cells.

The data presented in this chapter advances the knowledge of the molecular pathways determining cell polarity and provides new evidence on the role of intracellular trafficking proteins in formation of functional AJCs and in epithelial polarisation. Furthermore, the fundamental defects in growth and differentiation of epithelial tissues observed in ARC and in Polarin and Vps33b deficient epithelial cell lines emphasise the importance of the Vps33b/Polarin pathway for organ development and function.

**CHAPTER 6 – USE OF MORPHOLINOS
AGAINST *PLRN* IN ZEBRAFISH EMBRYOS
MIMICS THE ARC SYNDROME LIVER
DISEASE**

6.1 – Introduction and Overview

6.1.1 – Zebrafish as a Model Organism

The zebrafish, *Danio rerio*, is a tropical freshwater fish that is native to the streams of the south-eastern Himalayan region. The zebrafish gets its' name from the five uniform, pigmented, horizontal blue stripes on the side of the body, all of which extend to the end of the caudal fin. Male fish have gold stripes between the blue stripes, whereas the females have silver stripes instead of gold. The approximate generation time for the zebrafish is 3 to 4 months. Adult fish rarely grow larger than 4 cm in length in captivity and on average zebrafish live for 2 to 3 years, with a maximum of around 5 years [186].

For the ovulation and spawning of eggs from the female to occur there must be a male present [187]. Females are able to lay eggs as often as every 2 to 3 days with hundreds of eggs being laid in each clutch [186]. Upon release from the female, the first developmental steps will begin; however without the presence of sperm, growth will stop after the first few embryonic cleavages. Once fertilised, the embryos develop rapidly with precursors to all major organs appearing within 36 hours post fertilisation (hpf), and hatching will occur between 48 to 72 hpf [188].

Pioneering work by George Streisinger and his colleagues which began over 40 years ago at the University of Oregon established the zebrafish as a model organism for biomedical research [188]. The zebrafish is a common and useful model organism for studies of vertebrate development and gene function, and may supplement higher vertebrate models,

such as rats and mice. Although the overall generation time of zebrafish is comparable to that of mice, zebrafish embryos develop rapidly, progressing from eggs to larvae in less than three days [186]. The zebrafish model has other advantages over higher vertebrate models, notably that the embryos are large, robust, transparent and develop externally to the mother; characteristics which all facilitate experimental manipulation and observation [186].

A vast majority of the genetic code for the zebrafish has been completed, which further facilitates the use of this animal as a model organism. A common and useful reverse genetics technique is used to reduce gene expression or modify splicing in zebrafish using Morpholino antisense technology [186;188]. Morpholino Oligonucleotides (MOs) are stable, synthetic macromolecules that contain the same nucleotide bases as DNA, and by binding to complementary RNA sequences, reduce the expression of specific genes. MOs are directly injected into one cell of a zebrafish embryo producing an organism in which gene expression is reduced [186]. However there are known common problems with MOs, including off target effects and their occasional inability to knockdown the gene. The latter problem is due to a genome duplication in the zebrafish, and reducing the expression of one gene can lead to the compensation of the other paralogue causing no noticeable phenotype [186]. Nevertheless, with careful controls and screening of the zebrafish genome for these paralogue genes the zebrafish can be a very useful model for biomedical research.

6.1.2 – ARC Syndrome Zebrafish Model Using *vps33b*

Following the identification of mutations in *VPS33B* in the majority of ARC syndrome patients [1;2], Matthews et al. in 2005 investigated the expression pattern of *vps33b* in zebrafish embryos and larvae [189]. The group also examined the effect of knocking down *vps33b* on zebrafish development, and established that *vps33b* functions downstream of the onecut transcription factor *htf6* [189]. Further details of the results from this study will be presented in the following sections

6.1.2.1 – Expression Pattern of *vps33b*

Staged *in-situ* hybridisation in embryonic and larval zebrafish revealed a ubiquitous and widespread expression pattern of *vps33b* at the sphere stage (4 hpf) up until 24 hpf (Figure 6.1A to C). At 48 hpf, *vps33b* expression localised to the brain, retina, ear, liver and proximal intestine (Figure 6.1D). This expression pattern was more pronounced at 72 hpf (Fig 6.1E) and remained detectable through to 5 dpf (not shown). On closer examination of 3 dpf (not shown) and 4 dpf (Figure 6.1F) larvae revealed a reticular pattern of *vps33b* expression in the liver in contrast to the ubiquitous expression pattern of the hepatocyte gene *ceruloplasmin*. This suggested the possibility that *vps33b* is predominantly expressed in the developing biliary epithelial cells. Neither kidney nor spinal cord expression was evident in the wholemount specimens at any stage analysed.

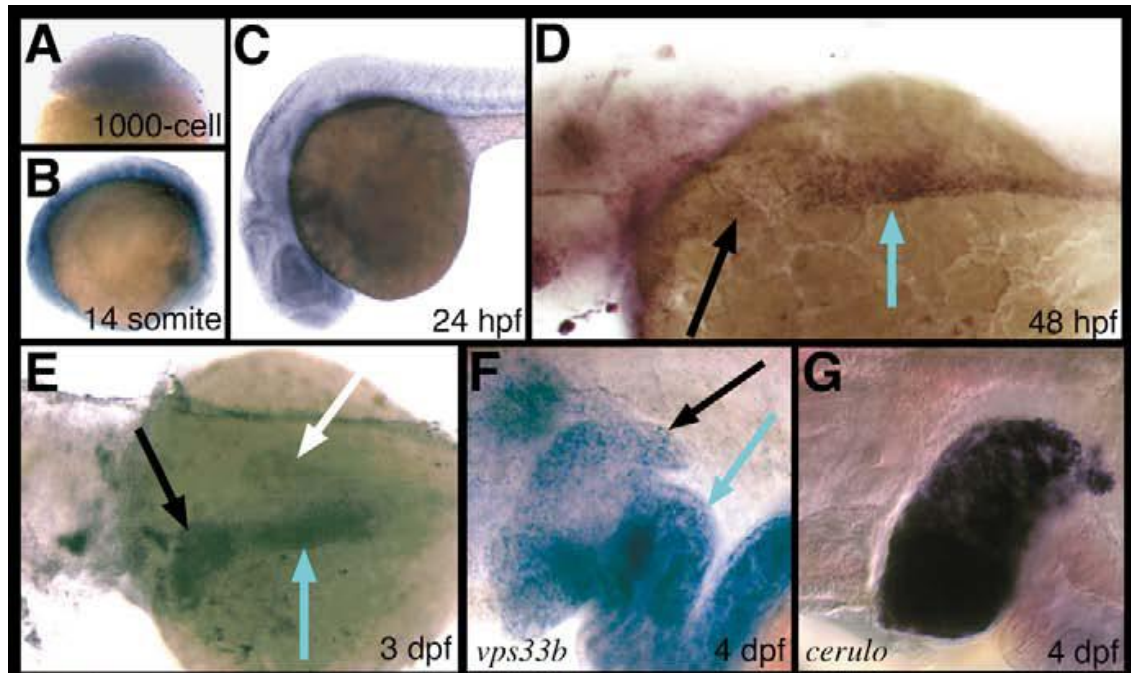


Figure 6.1 – In-situ hybridisation of *vps33b* in zebrafish embryos and larvae.
 Wholemount RNA in-situ hybridisation of **A**, spherical stage, **B**, 10 somites and **C**, 24 hpf show diffuse *vps33b* expression. **D**, *vps33b* expression at 48 hpf is evident in the developing liver (black arrow) and proximal intestine (blue arrow). **E**, Lateral view of a 72 hpf larva showing *vps33b* expression in the liver (black arrow) and proximal intestine (blue arrow). Weak pancreas staining (white arrow) is also evident. High power lateral views of 4 dpf larvae processed for **F**, *vps33b* and **G**, ceruloplasmin whole-mount RNA in-situ hybridisation. **F**, Liver (black arrow) demonstrates a reticular pattern of *vps33b* expression compared with **G**, a homogenous pattern of ceruloplasmin expression. Intestinal *vps33b* expression is also evident (blue arrow, **F**). [Adapted from 189]

6.1.2.2 – Effect of *vps33b* Knockdown on Zebrafish Development

Knockdown of *vps33b* using an ATG and 2 splice site MOs did not affect the overall appearance or liver size of larvae at 5 dpf (Figure 6.2A and B). However, gallbladder fluorescence following ingestion of the quenched fluorescent lipid, PED-6, was reduced in *vps33b* MO injected larvae (Figure 6.2C and D). Transport of this compound to the gallbladder can serve as an indicator of biliary secretion [190], biliary morphology [191] and intestinal lipid absorption [189].

Immunohistochemistry of Cytokeratin-18, a specific marker of the cholangiocytes, on 5 dpf morpholino injected larvae strongly suggest that altered biliary development contributed to the defects of PED-6 processing (Figure 6.2E-G). More precisely the number of intrahepatic bile ducts was reduced compared with control, whereas the extrahepatic biliary tree appeared normal in all of the morpholino-injected larvae. Within the intrahepatic biliary system, defects of the interconnecting and terminal ducts were most pronounced (Figure 6.2H-J) [189]. Ultrastructural analysis revealed cell type specific defects in *vps33b* deficient zebrafish. In the liver, cytoplasmic vesicles were present within *vps33b* deficient biliary epithelial cells, whereas they were absent in the biliary cells of control larvae (Figure 6.3A and B) [189].

In contrast to the biliary defects present in the *vps33b*-deficient larvae, neither renal nor motor axon defects were identified. Normal renal tubular epithelial cell morphology was confirmed histologically and using ultrastructural analyses. Thus, no evidence was given to show that *vps33b* knockdown in zebrafish phenocopies the motor axon and renal defects associated with ARC [189].

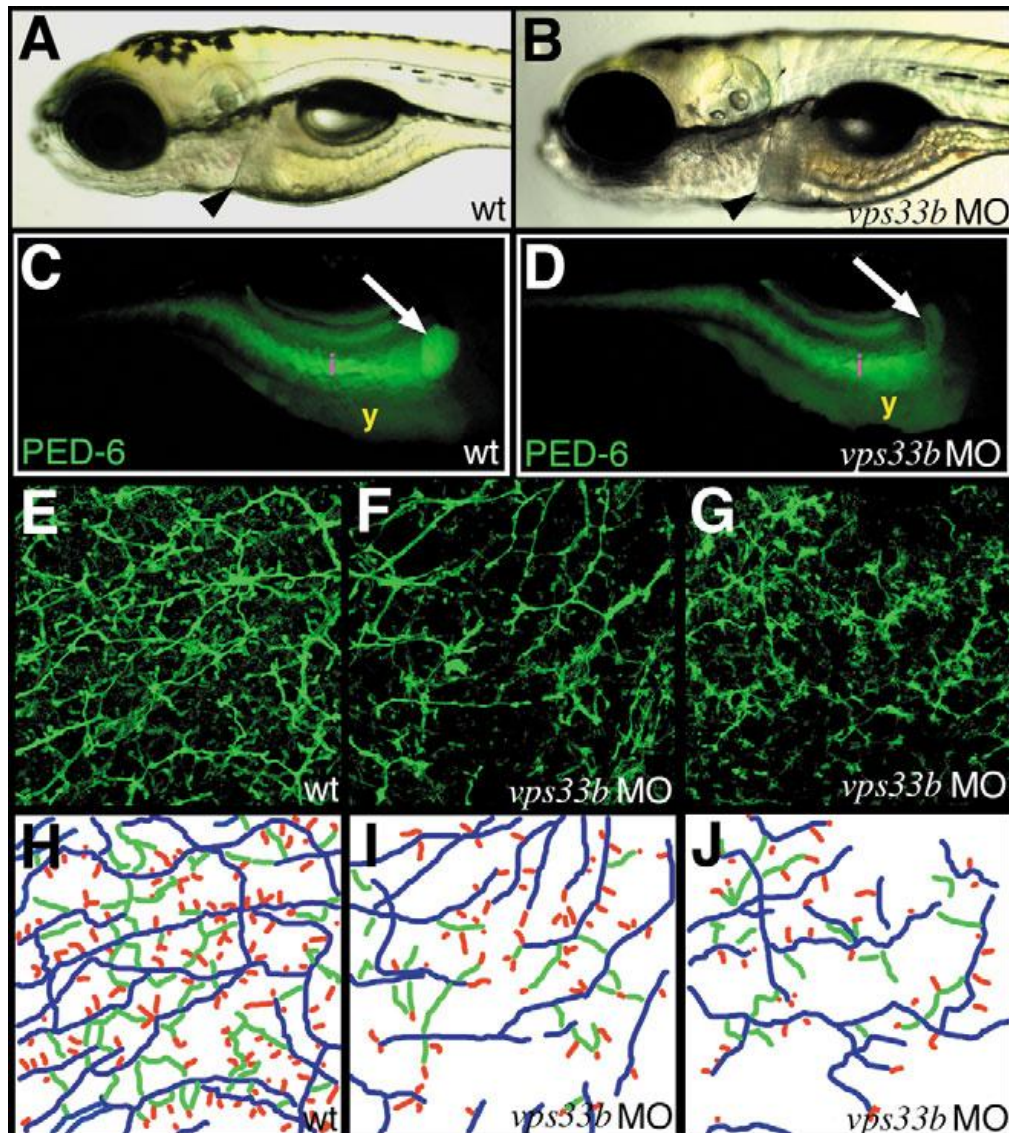


Figure 6.2 – *vps33b* knockdown disrupts zebrafish intrahepatic biliary development.
A and B, Left lateral views of **A**, wild-type and **B**, *vps33b* morpholino-injected 5 dpf larvae. Liver size (black arrowheads) is comparable in these larvae. **C and D**, Right lateral fluorescent images of **C**, wild-type and **D**, *vps33b* morpholino injected 6 dpf larvae following ingestion of the PED-6 lipid reporter. Gallbladder fluorescence (white arrow) is decreased in **D**, morpholino-injected larva relative to **C**, wild-type larva (i - intestinal fluorescence; y - endogenous yolk fluorescence). **E, F and G**, Confocal projections through the liver of **E**, wild-type and **F and G**, *vps33b* 5 dpf larvae processed for keratin 18 immunohistochemistry. There are fewer bile ducts in **F** than in **E**; ducts are sparse, with fewer interconnecting ducts and terminal ductules. **H, I and J**, Coloured schematics of bile ducts from **E, F and G**. Long ducts depicted in blue, interconnecting ducts in green and terminal ductules in red. [189]

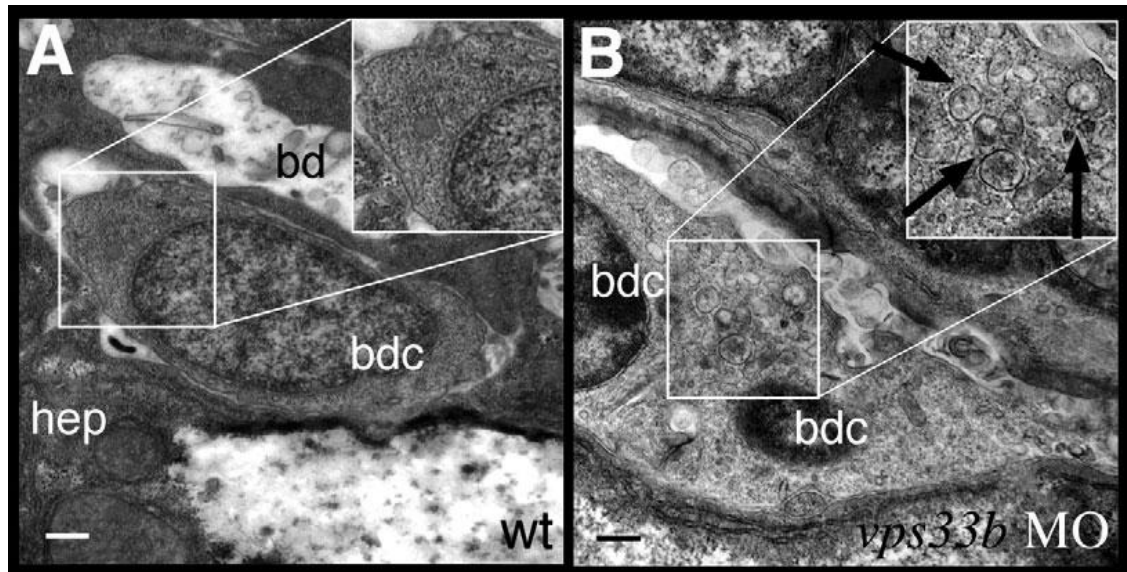


Figure 6.3 – *vps33b* knockdown disrupts the ultrastructure of biliary epithelial cells.
A and B, Electron micrographs of biliary epithelial cells from **A**, wild-type and **B**, *vps33b* morpholino injected 5 dpf larvae. **A**, The wild-type biliary cell cytoplasm has a homogeneous appearance. **B**, A small bile duct comprising two bile duct cells from a *vps33b* morpholino-injected larva. Cytoplasm appears heterogeneously with multiple vesicles (black arrows).
hep - hepatocyte; *bd* - bile duct lumen and *bdc* - bile duct cell. [189]

6.2 – Aims

The data presented in chapter 4 shows that VPS33B interacts with a novel protein, POLARIN and that pathogenic mutations can be identified in the *PLRN* in ARC syndrome patients without *VPS33B* mutations. The cell culture experiments described in chapter 5 implicated VPS33B and POLARIN in epithelial cell differentiation and function. Previously, in an animal model, it was found that MO knockdown of the zebrafish *vps33b* orthologue resulted in abnormal development of the biliary tract [189].

Based on the indistinguishable phenotype of ARC syndrome patients who have mutations in either *VPS33B* or *POLARIN* and the cell culture experiments shown in chapter 5, we hypothesise that polarin will function in the same way as *vps33b* in zebrafish development. To test this hypothesis, RNA *in-situ* hybridisation was carried out on zebrafish embryos and larvae to identify where and when *polarin* is being expressed. Furthermore MO knockdown of polarin in the developing zebrafish was also carried out to identify the effect of reduced expression of polarin in a whole organism.

6.3 – Results

The results of experiments presented in the following chapters was supervised by F. Mueller, and all MO injections were carried out A. Zaucker (both University of Birmingham, UK)

6.3.1 – Expression Pattern of polarin

A full length sense and anti-sense digoxigenin (DIG) labelled RNA probes for *plrn* was transcribed from the pCS2+ vector containing the zebrafish *plrn* orthologue (si:ch211-20b12.1). Staged *in-situ* hybridisation of *plrn* revealed a ubiquitous pattern of expression in 24 hpf embryos (Figure 6.4A) and weak but discrete staining in 5 dpf larvae in the brain, retina, ear, liver and proximal intestine (Figure 6.4B). The sense probe was used to assess overall specificity of the anti-sense probe, and due to the weak expression of *plrn* have been included in Figure 6.4A and B. Neither kidney nor spinal cord expression was evident in the wholemount embryos or larvae at any stage analysed. Histological sections of 5 dpf larvae revealed a reticular pattern of expression in the liver (Figure 6.4C and D). The expression pattern of *plrn* is comparable to that observed for *vps33b* by Matthews et al. [189].

6.3.2 – Effect of polarin Knockdown in Zebrafish

MOs were designed against the zebrafish *PLRN* orthologue (si:ch211-20b12.1) with the intention to reduce the expression of *plrn* in developing embryos and larvae. A MO was designed to target the sequence corresponding to 25 base pairs upstream of the start (ATG) codon to prevent translation and another MO to affect the splicing of exon 3 in the *plrn* transcript. A mis-match MO which differed in 5 nucleotides from the exon 3 splice site MO was purchased, to serve as a specificity control. The concentration of each MO injected into the zebrafish embryos was determined empirically so that either the same concentration of the mis-match MO did not give an observable phenotype (exon 3 MO) or that wild-type *plrn* mRNA could rescue the phenotype (ATG MO).

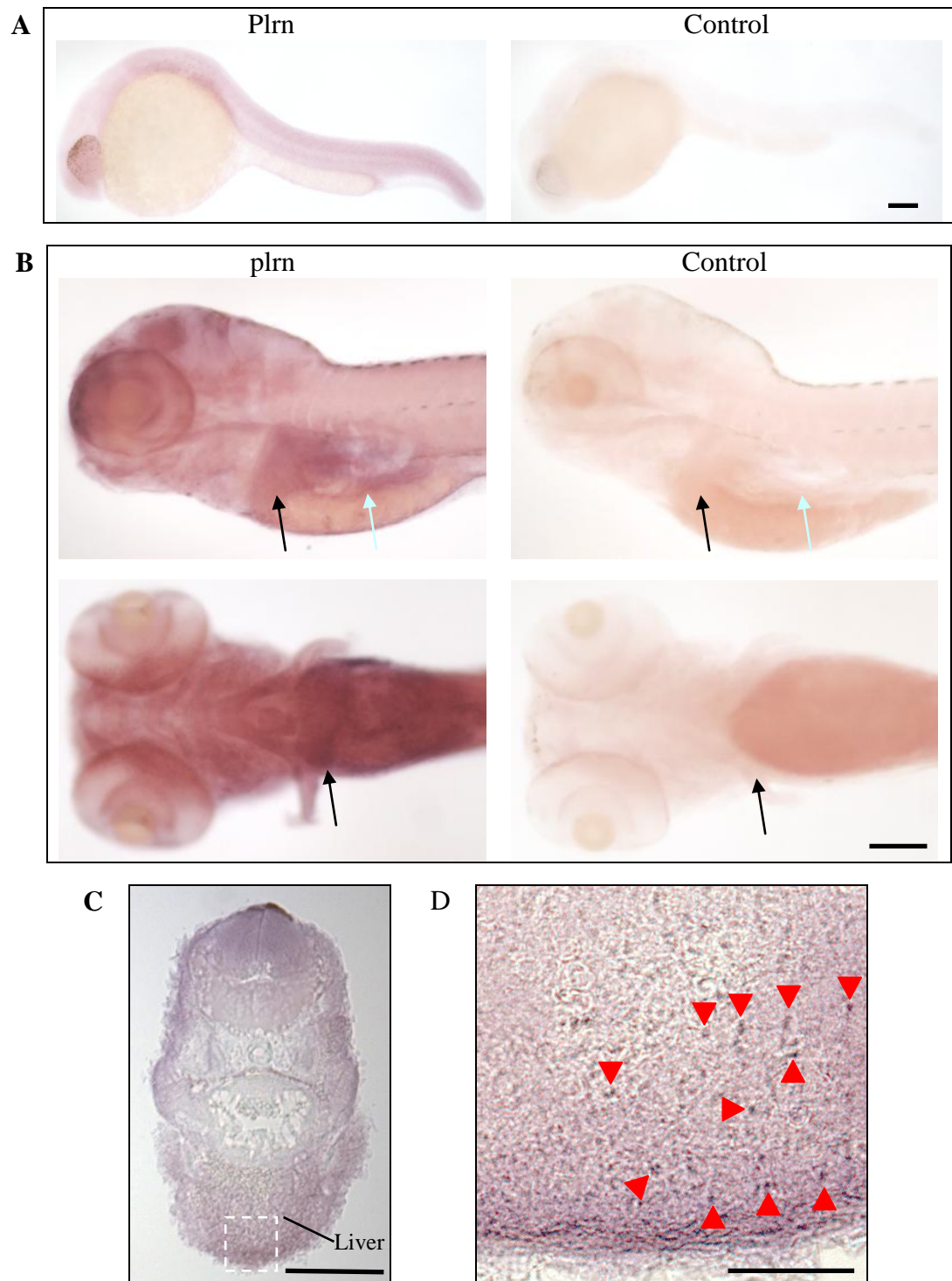
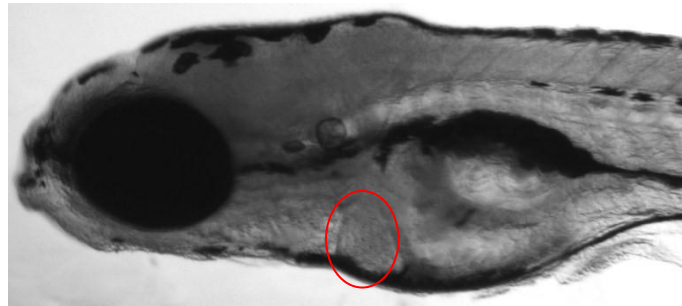


Figure 6.4 – In-situ hybridisation of *plrn* in zebrafish embryos and larvae.

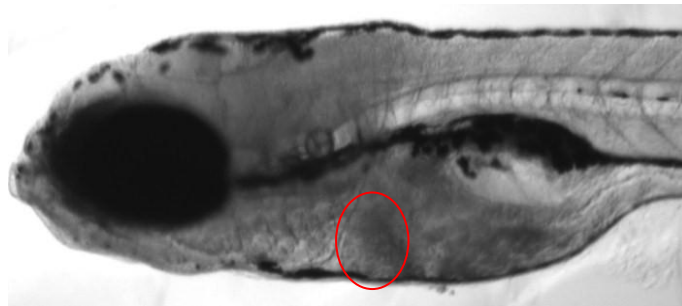
A, Lateral view of 24 hpf embryos and **B**, Lateral and ventral views of 5 (dpf) larvae after in-situ hybridisation using DIG-labelled antisense and sense (control) *plrn* RNA probes. High expression in liver (black arrows) and small intestine (blue arrows) is seen for *plrn* compared with controls. **C and D**, Histological transverse sections of 5 dpf larvae processed for *plrn* whole-mount RNA in-situ hybridisation (**A**, **B** and **C** scale bars = 200 μ m). **D**, Enlarged section shown in white rectangle in **C** reveals a reticular pattern of *plrn* expression in the liver (red arrow heads, scale bar – 20 μ m)

Knockdown of *plrn* in zebrafish embryos by either the ATG or exon 3 MO did not give an easily detectable morphological phenotype up to 5 dpf (Figure 6.5). However, when MO injected 4.5 dpf larvae were incubated with the fluorescent compound PED-6 overnight and visualised at 5 dpf, a significant dose-dependent reduction in gallbladder size, compared with controls, was detected (Figure 6.6). The quenched PED-6 molecule is fed to the zebrafish larvae which they ingest and absorb. In the liver, the molecule is cleaved by phospho-lipase A2 (PLA₂), which removes the quench, allowing the green fluorescence of the PED-6 molecule to be detected in the gall bladder and in the gut [190]. Compared to non-injected controls, ATG and Exon 3 MO injected larvae had an observable decrease in gall bladder size. Quantification of the gall bladder size revealed a significant decrease to a size less than 31% of the non-injected controls (Figure 6.7, 3 separate injections of n=30, p<0.001 by Z-test, raw data shown in Appendix 5). Gall bladder area in one focal plane containing the gall bladder was assessed as described in section 2.2.7.3. This phenotype was not detected in the mismatch control or mRNA rescued larvae. The decrease in gallbladder size and fluorescence after ingestion of the quenched PED-6, in the *plrn* MO injected larvae, coupled with the normal morphology and size of the liver suggests a defect in biliary secretion and morphology [190]. Similar to *vps33b* knockdown in the zebrafish, *plrn* knockdown seems to cause defects in biliary development and function.

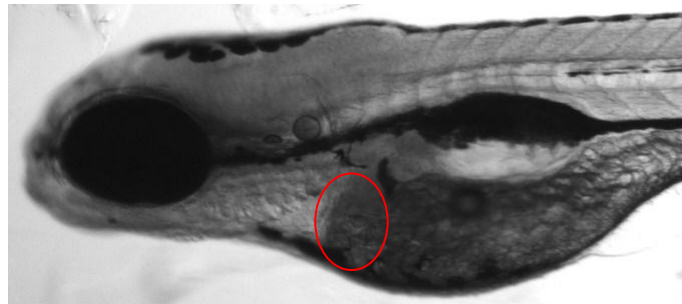
Non
Injected
Control



ATG
Morpholino



Exon 3
Morpholino



Exon 3
Mismatch
Morpholino



Figure 6.5 – Knockdown of *plrn* in the zebrafish does not cause any morphological abnormalities detectable by light microscopy.

Brightfield images of 5 dpf non-injected, ATG, Exon 3 and Exon 3 mismatch MO injected larvae. No obvious morphological abnormalities and no change in liver size (outlined in red) are observed in these larvae. Orientation of larvae is anterior to the left. Scale bar = 150 μ m. MO injections carried out by A. Zaucker, University of Birmingham, UK.

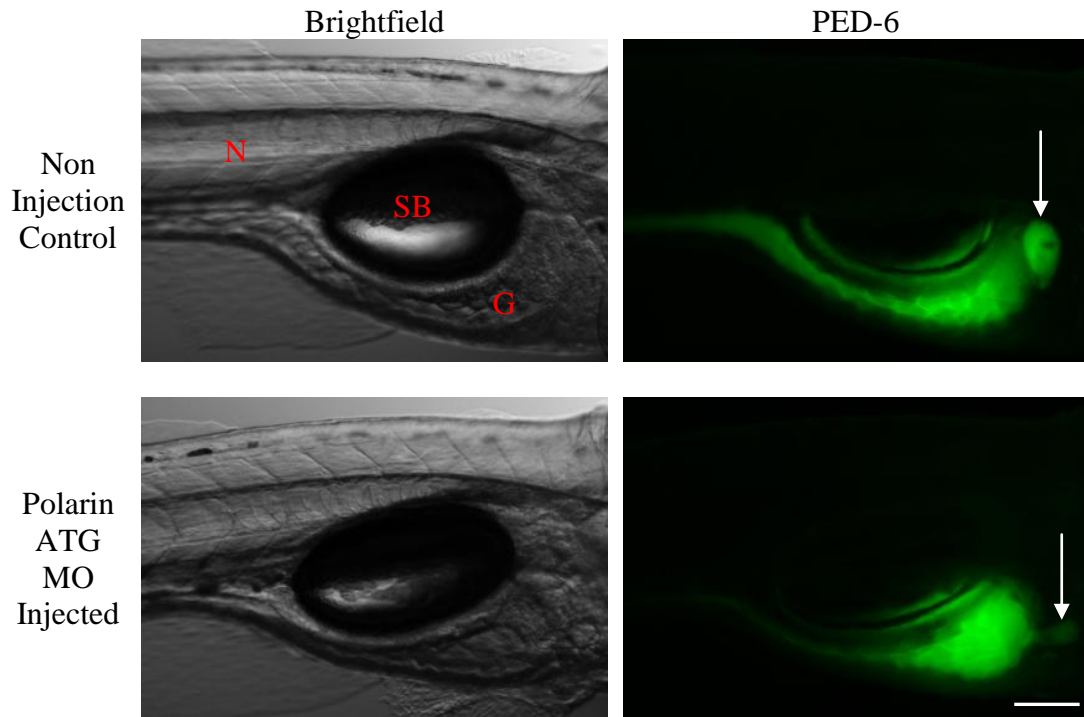


Figure 6.6 – *plrn* deficiency causes a decreased gall bladder size.
*Brightfield and green fluorescence images of PED-6 treated non-injected and *plrn* ATG MO-injected 5-dpf embryos. Gall bladder size is reduced in *plrn* ATG MO injected larvae compared to non-injected control larvae (white arrows). Orientation of larvae is anterior to the right. Scale bar = 200 μ m. Abbreviations; N – Notochord, SB – Swim Bladder, and G - gut. MO injections carried out by A. Zaucker, University of Birmingham, UK.*

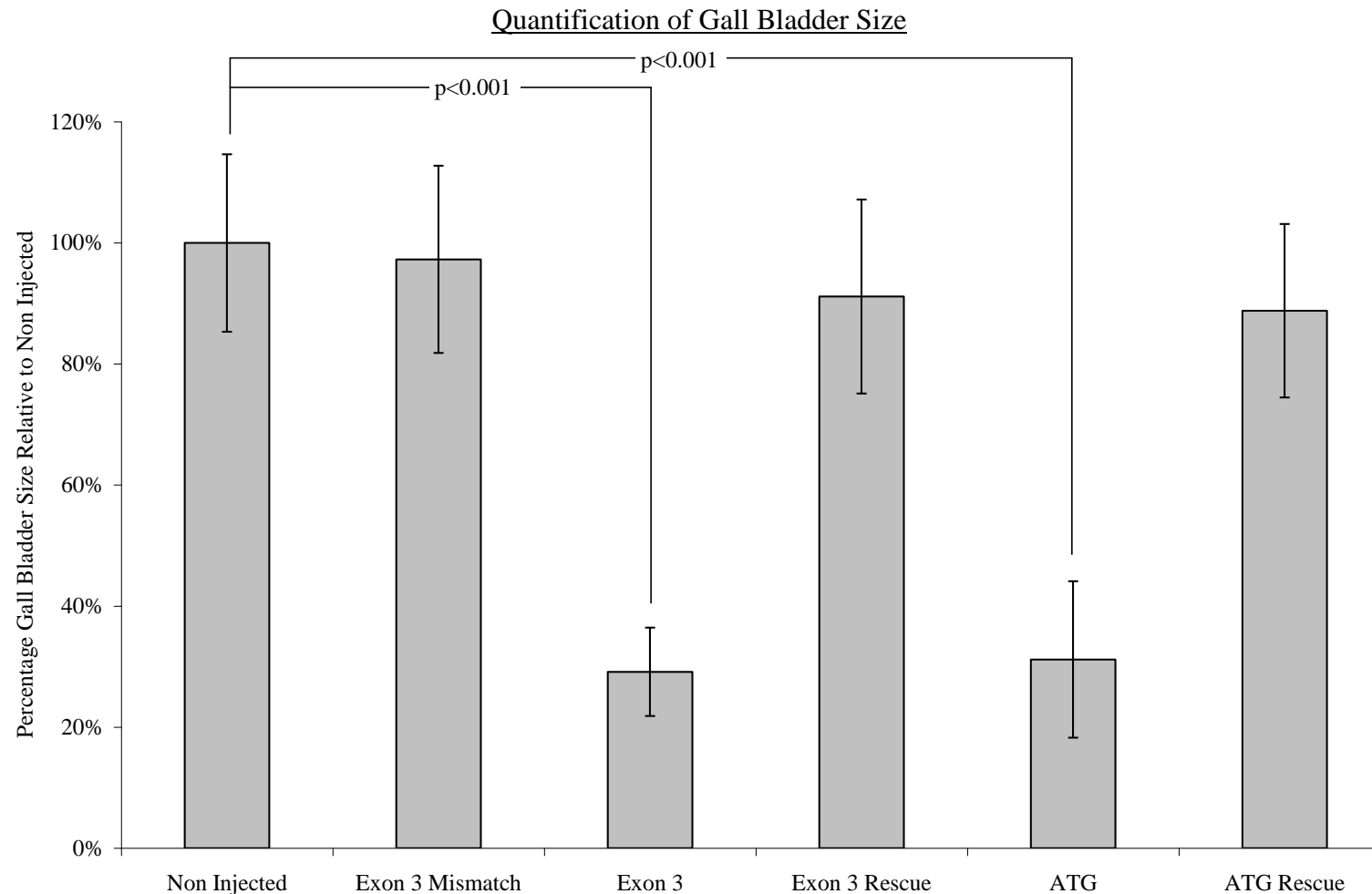


Figure 6.7 – Quantification of gall bladder size in *plrn* deficient zebrafish larvae.

Gallbladder size is significantly reduced in ATG and exon 3 MO-injected larvae compared to non-injected control larvae and to exon 3 mis-match control larvae. Injecting *plrn* mRNA after MO treatment rescued the phenotype. Value shown is average size relative to non-injected control. Errors bars = ± 1 standard deviation ($n = 3$ experiments with 30 larvae in each group, $p < 0.001$ by Z-test). MO injections carried out by A. Zaucker, University of Birmingham, UK.

The data presented in chapter 5 identified the role of both Vps33b and Polarin in apical junction complex formation in polarised epithelial cells. In both the cell culture experiments and ARC syndrome patient's liver biopsies, reduced expression of Vps33b or Polarin lead to a pronounced defect in e-cadherin expression and its' reduced presence in the lateral membrane. To test this result in the zebrafish with reduced expression of polarin, transverse sections of 5 dpf liver were taken and immunostained for e-cadherin. This revealed a significant and striking reduction in e-cadherin expression in all the polarin deficient (ATG and exon 3 MO) larvae inspected ($p=0.02$ by two-tailed Fisher's Exact test, $n=6$ for each treatment group, Figure 6.8).

6.4 – Discussion

The expression pattern of *polarin* corresponded to that of *vps33b* (Figures 6.1 and 6.4) [189], which is consistent with the synergistic action of the two proteins suggested in both chapters 4 and 5. Detailed analysis of the *in-situ* hybridisation in 5 dpf larvae showed a relatively strong reticular pattern of expression of *polarin* in the zebrafish liver. This is again consistent with the pattern of expression seen with *vps33b*, and suggests a function of both *vps33b* and *polarin* in the development of the biliary system in developing zebrafish embryos and larvae.

Morpholino knockdown of the zebrafish *POLARIN* orthologue led to a reduced gallbladder size, as evidenced by decreased PED-6 accumulation (Figure 6.6 and 6.7), thus indicating that *polarin* is active during zebrafish biliary development. Knockdown of *vps33b* is also seen to effect late stages of biliary development in zebrafish larvae, as reflected in the reduction of interconnecting and terminal ducts (Figures 6.2).

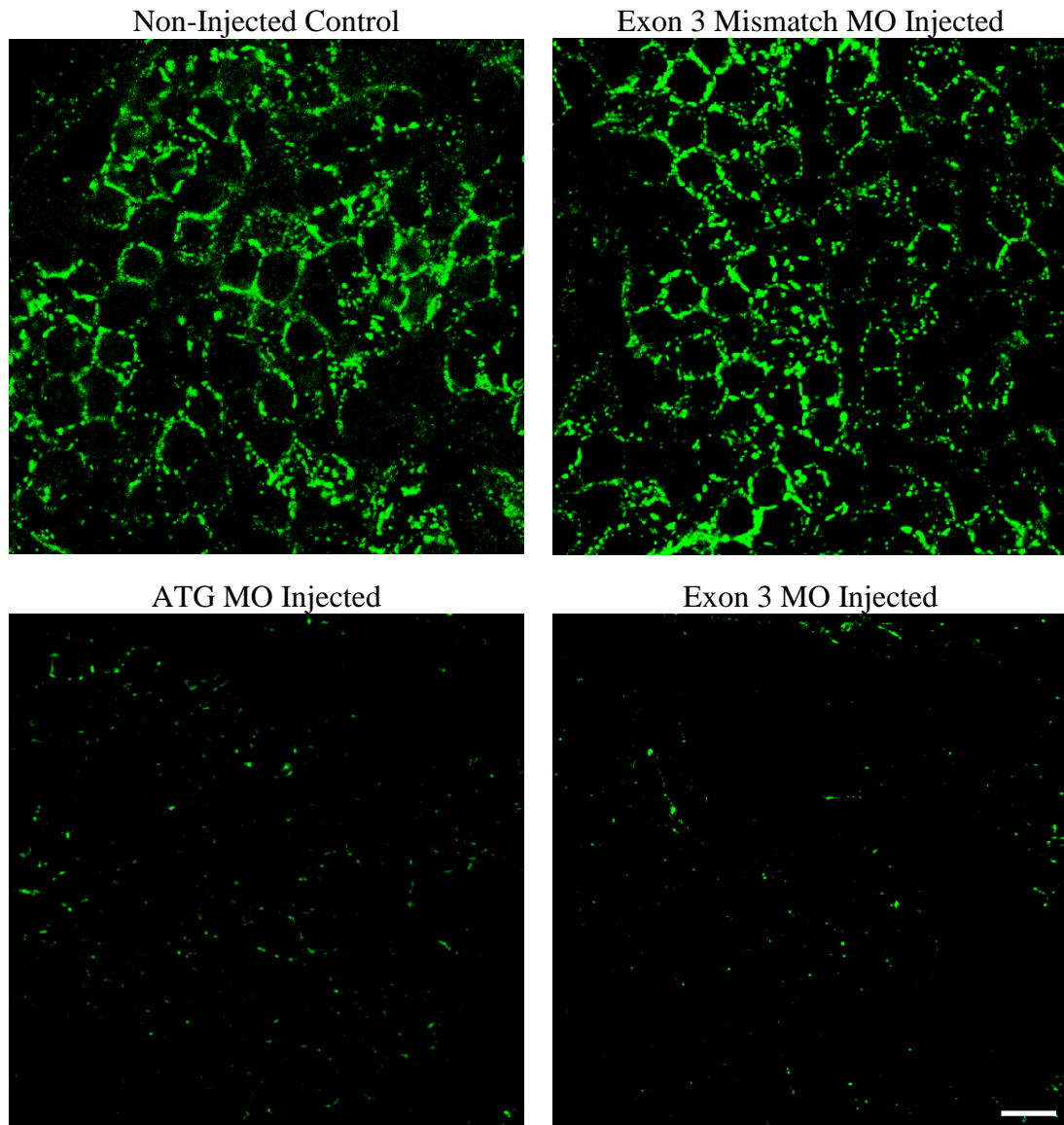


Figure 6.8 – Immunofluorescence confocal micrographs of *e-cadherin* in sections of 5 dpf larvae livers.

*Staining of *e-cadherin* in 2 μm optical sections of 18 μm transverse sections of livers from non-injected, plrn exon 3, exon 3 mismatch control and ATG MO injected 5 dpf larvae. Scale bar = 10 μm . The same excitation and collection settings were used throughout. In the control livers there is strong *e-cadherin* expression and correct localisation, in contrast to the plrn deficient larvae, which have markedly reduced expression ($p=0.02$ by two-tailed Fisher's Exact test, $n=6$ for each treatment group). MO injections carried out by A. Zaucker, University of Birmingham, UK.*

ARC syndrome is one of several heritable disorders that present with cholestasis in infancy, and bile duct paucity in liver biopsies of children with ARC suggests that cholestasis in this syndrome may arise from a primary defect of biliary development [192]. The mechanism of the biliary tract malformation may be explained by the reduction of bile flow due to the mislocalisation of the apical membrane proteins in hepatocytes, such as BSEP in ARC syndrome patients [11]. This reduction in bile flow in turn causes a reduction in size and apparent number of bile duct radicals, as seen in ARC and some other cholestatic disorders [193].

Consistent with the defects with apical junctional complex formation in both cell-culture experiments and ARC syndrome patient liver biopsies presented in chapter 5, there was a striking reduction of e-cadherin expression in livers from 5 dpf larvae (Figure 6.8). Thus, *polarin* MO knockdown in the zebrafish mimics a biochemical feature identified in ARC syndrome and further confirms the cell line results in chapter 5.

Two other major features of ARC syndrome are neurogenic arthrogryposis and renal tubular defect. Neither *vps33b* [189] nor *polarin* expression could be detected in the any part of the nervous system or the kidney. Furthermore, no easily detectable renal or CNS morphological abnormalities were observed in both *vps33b* and *polarin* MO injected embryos and larvae (Figure 6.5). However, further characterisation of the kidney function could not be carried out due to the lack of suitable markers for functional assays. A potential explanation for the lack of phenotype in these tissues may be due to either an unidentified *polarin* paralogue, which fulfils these functions in the zebrafish, or a non-conserved role for *polarin* in nervous system and kidney development.

Nevertheless, the results presented in this chapter confirmed the importance of *polarin*, as well as of *vps33b* orthologues, as proteins active in zebrafish biliary-tract development. Thus, zebrafish models have been created using both *vps33b* [189] and *polarin* that mimic some ARC syndrome phenotypes and biochemical abnormalities. Furthermore these models are suitable for further investigations of liver and biliary development and studies of cholestatic diseases.

CHAPTER 7 – DISCUSSION

7.1 – VPS33B Interacts with a Novel Protein POLARIN

The mammalian HOPS complex, including VPS33A, was recently found to be involved in a Rab5-Rab7 dependent pathway of phagosome biogenesis during apoptosis [79]. The CORVET complex can also be formed by class C VPS proteins in yeast [84]. Unlike other SM proteins, VPS33 homologues require additional proteins to interact with SNARE complexes. In keeping with this idea a conserved novel protein, POLARIN, was identified. It was noted that POLARIN possesses 16% identity to the C-terminal domain of the HOPS complex member VPS16. A POLARIN orthologue has been identified in *D. melanogaster*, which was shown to interact with the Vps33b drosophila orthologue [194]. Although the results of experiments presented in this thesis suggest that VPS33B and POLARIN are unlikely to form an active part in the conventional HOPS complex function, subunits of this complex were shown co-immunoprecipitate with the epitope tagged POLARIN. Thus a novel complex containing POLARIN and VPS33B proteins may interact with VPS11, VPS18, VPS39 and VPS41.

Furthermore, neither endogenous VPS33B nor co-overexpressed VPS33B and POLARIN clusters significantly co-localised with Rab5, LAMP-1 and CD63, markers of early endosomes, late endosomes and lysosomes respectively. These organelles are the sites of action of the conventional HOPS and CORVET complexes [74;84], suggesting another function for the newly identified VPS33B-POLARIN complex. In light of the data presented here, it is likely that the VPS33B-POLARIN complex is associated with the Rab4-Rab11 intracellular trafficking pathway in polarised epithelial cells.

Recently, Zhu et al. identified the *C. elegans* orthologue of human C14orf133, which they named hSpe39 and demonstrated that it interacts with Vps33b [195]. Although *C. elegans* *Spe-39* mutants were initially identified as having abnormal vesicular biogenesis during spermatogenesis, the group also showed that these mutants also have disrupted processing of endocytosed proteins in oocytes [195]. In contrast to the data presented in this thesis, they suggest that both VPS33A and VPS33B interact with hSpe-39. Interestingly, MO knockdown of Vps33a in *C. elegans* did not mimic the phenotype of hSp3-39 mutants whereas Vps33b did [195]. On the other hand, and consistent with the data presented here, the group also showed that Vps33b and hSpe-39 interact with other HOPS complex subunits, and partially co-localise with Rab11a [195].

7.2 – Deficiencies of VPS33B or POLARIN in Development and Disease.

Mutations in *VPS33B* can be identified in around 75% of ARC syndrome patients [1;4]. However, reduced expression of VPS33B at the RNA and protein level could be detected in all ARC syndrome patients with or without detectable VPS33B mutations that could be identified by conventional di-deoxy sequencing. The discovery of pathogenic mutations in the gene encoding POLARIN (*PLRN*) in ARC syndrome patients from different ethnic backgrounds provides further insight into the pathophysiology of human diseases. Reduced expression of VPS33B could be detected in patients with *PLRN* mutations, suggesting that POLARIN is required for the stabilisation of VPS33B. Consistent with the idea that VPS33A functions in a different complex and pathway to that of VPS33B and POLARIN, as evidenced by the data presented in chapter 4, there was no compensatory up-regulation of VPS33A in ARC syndrome patient fibroblasts with reduced expression of VPS33B.

Mislocalisation of apical membrane proteins previously was demonstrated in kidney and liver biopsy specimens from patients with ARC syndrome harbouring *VPS33B* mutations [1;11]. Similar mislocalisation of apical membrane proteins in patients with *PLRN* mutations have now been identified. Furthermore, mislocalisation of BSEP, a major hepatocyte bile salt transporter, was detected in the ARC syndrome patients' livers. This is consistent with the suggestion that BSEP is trafficked to the apical membrane via a Rab11a pathway, since knockdown of either Rab11a or Myosin Vb in WIF-B9 cells, a polarised hepatic cell line, caused the mislocalisation of BSEP [180].

Cultured mIMCD-3 cells with decreased expression of Polar in or Vps33b demonstrated abnormal formation of the apical membrane and of AJCs. Interestingly, some apical and basolateral membrane proteins are correctly localised in ARC syndrome patient liver biopsies and the knockdown cell lines, despite the absence of functional AJCs. This result goes against the central dogma of epithelial cell biology, where TJs are required for the continued separation of apical and basolateral plasma membrane domains, by preventing the inter-mixing of membrane protein pools [88]. However, work by Umeda et al. in 2006 showed that reduced expression of either ZO-1 or ZO-2 in an epithelial cell line did not cause the dimerisation of Claudins in the membrane, since ZO-1 and -2 are required to catalyse the dimerisation of Claudins [103]. Furthermore, and despite the absence of functional TJs, these cells retained their separate apical and basolateral membrane domains [103]. Thus these data show that the processes of epithelial apical-basolateral polarity formation and maintenance are not completely understood.

Furthermore, in the Vps33b and Polarin knockdown mIMCD-3 cell lines, there was a reduction in overall expression of CEA, an apical membrane marker, suggesting a possibility of intracellular CEA degradation. A similar marked reduction in protein expression was observed for E-Cadherin. Moreover, Polarin- and Vps33b-deficient cell lines failed to polarise, as evidenced by reduced TER measurements and by failure of tubule formation in culture. Functional investigations of Vps33b and Polarin suggest that they work synergistically in the trafficking of proteins to apical membrane and formation of AJCs. The requirement of Polarin for Vps33b function is supported by the finding that Vps33b expression was reduced in patients' fibroblasts and in cells with Polarin knockdown.

Morpholino knockdown of the zebrafish POLARIN orthologue led to deficient biliary-tract formation, indicating that polarin is active during zebrafish development. Expression of polarin corresponded to that of vps33b, which is consistent with the synergistic action of the two proteins. The mechanism of the biliary-tract malformation may be explained by reduced bile flow causing reduced size and apparent number of bile duct radicles, as seen in ARC and some other cholestatic disorders [193]. Furthermore a reduced expression of E-Cadherin was detected in the livers of polarin deficient larvae, similar to that observed in the ARC syndrome patient liver biopsies and the cell culture experiments. Thus zebrafish models have been created that are very suitable for further investigations of liver development and disease.

The ultrastructural findings observed in the vps33b ARC syndrome zebrafish model are similar to those found in zebrafish with spontaneous mutations of the yeast class C complex genes *Vps11* and *Vps18* [7;196]. This suggests that the bile duct paucity may arise autonomously in ARC syndrome patients from a defect in vesicle sorting. The accumulation

of intracellular organelles are observed in ARC syndrome patients' fibroblasts and hepatocytes (lipofuscin granules) and in the livers of the *vps33b* deficient zebrafish [148;149;189]. Thus further suggesting a membrane biogenesis defect in the pathophysiology of ARC syndrome

Interestingly, mutation of *vps18* or *vps39* in the zebrafish and *vps11* in medaka causes cutaneous hypopigmentation, hepatocyte defects and bile duct paucity, but neither motor neurone nor kidney defects [172;197-200]. The *buff* mouse, which has a mutation in *Vps33a*, has hypopigmentation as a cardinal feature, and mutation of *VPS33B* in humans and knockdown in the zebrafish causes hepatocyte defects with bile duct paucity [1;82;189]. The partially overlapping phenotypes of *vps11*-, *vps18*-, *vps33b*- and *vps39*-deficient larvae support the idea that in multi-cellular organisms the conventional HOPS complex (VPS33A and VPS16) functions alongside the newly identified VPS33B-POLARIN complex which utilises proteins from the conventional complex. Thus if a member of both complexes, such as VPS11, VPS18, VPS39 or VPS41 is mutated or the expression reduced, a phenotype resulting from the deficiency of both complexes is observed.

Analysis of the developmental expression of VPS33B in human and mouse foetal tissues revealed an upregulation in the human kidney between 11 and 16 weeks gestation and strong expression at 14.5 days in the mouse. At this point in kidney development tubules form and thus there is a requirement for polarised tissues [150;151]. Interestingly, knockout of *Vps33b* or *Polarin* in mIMCD-3 cells reduced polarisation and tubule formation. Furthermore, defects in liver development are observed in zebrafish in which *vps33b* or *polarin* are knocked down.

Taken together, this data demonstrates that VPS33B and POLARIN are critical in the formation of tubular structures such as kidney tubules and biliary ducts.

7.3 – VPS33B and POLARIN Function Through a Rab4-Rab11 Pathway

POLARIN contains a Golgin A5 domain which may be crucial for the interaction of the VPS33B-POLARIN complex with GTP bound Rab11a, similar to the Golgin domain containing SCYL1BP1, which interacts with GTP bound Rab6 [169]. The co-localisation and co-immunoprecipitation of VPS33B along with POLARIN and Rab11a at both the over expressed and endogenous level, suggests that this may be the case. This suggests a common mechanism of action for Golgin domain-containing proteins. Furthermore, mislocalisation of Rab11a was seen in Vps33b and Polarin knockdown mIMCD-3 cells. The VPS33B-POLARIN complex appears to specifically interact with the GTP bound form of Rab11a, suggesting that the newly identified complex may have Rab effector properties, and might facilitate specific SNARE-mediated membrane fusion events in the transport of Rab11a-positive vesicles. Consistent with this idea, mIMCD-3 cells stably transfected with the GDP locked dominant negative Rab11a mimicked some of the phenotype observed in the Vps33b and Polarin deficient cell lines (Figure 5.9).

As VPS33B/POLARIN clusters co-localised with Rab11a and also with Rab4, which is present on endosomes which become Rab11a-positive, one could speculate that the VPS33B-POLARIN complex may function in the maturation or Rab4 early endosomes to Rab11a recycling endosomes, similar to the conventional HOPS complex function of Rab5 to Rab7 conversion on early to late endosomes [74]. However, further experiments are needed to be

carried out to test this hypothesis and which were not possible within the time limits of this project.

In concordance with VPS33B and POLARIN functioning through a Rab11a pathway, there is mislocalisation of apical membrane proteins known to require Rab11a for their correct trafficking to the apical membrane. This is observed in both the ARC syndrome patients' kidney and liver biopsies and the cell culture experiments presented in chapter 5. BSEP is mislocalised in ARC syndrome patients' liver biopsies, whereas a homologue, MRP2, is correctly localised to the apical membrane. It is known that BSEP is stored in Rab11a positive endosomes until required on the canalicular membrane, whereas MRP2 is trafficked to the apical membrane through a transcytotic route [179]. Consistent with the data presented in chapter 5, Desclozeaux et al. observed that functioning Rab11a is required for the correct localisation of E-Cadherin to the lateral membrane and the subsequent cyst formation of MDCK cells [175], a process analogous to tubule formation in mIMCD-3 cells.

The Rab11a pathway and its' interacting protein Myosin Vb has recently been shown to be important in such diverse cellular functions as brain postsynaptic plasticity and small intestinal absorption [201;202]. Inactivation of human *CDH1* (encoding E-Cadherin) is strongly associated with epithelial to mesenchymal transformation (EMT), tumourigenesis, and increased cancer invasiveness [185;203;204]. Interestingly, there is a clear lack of polarisation of the Vps33b and Polarine deficient mIMCD-3 cells, coupled with an increase in proliferation, suggesting that an EMT might be taking place.

7.4 – Conclusions

The gene encoding a novel protein, POLARIN (PLRN) that interacts with VPS33B is mutated in a subset of around 25% of ARC syndrome patients. There is no obvious difference in phenotype between ARC syndrome patients with *VPS33B* or *PLRN* mutations, suggesting a synergistic action of both proteins. Reduced expression of VPS33B can be detected in all ARC syndrome patients irrespective of the gene that is mutated.

The newly identified VPS33B-POLARIN complex is essential for apical junction complex formation and the correct trafficking of some apical membrane proteins. Furthermore, the developmental expression pattern of VPS33B coupled with the phenotype of the Vps33b and Polarin deficient mIMCD-3 cell lines suggests a role of both proteins in the generation and maintenance of polarisation in epithelial cells.

The findings presented in this thesis advance the knowledge of the molecular pathways determining cell polarity and provide new evidence on the role of intracellular trafficking proteins in formation of functional AJCs and in epithelial polarisation. Furthermore, the fundamental defects in growth and differentiation of epithelial tissues observed in ARC and in knockdown cell lines emphasise the importance of the VPS33B-POLARIN pathway for organ development and function.

7.5 – Future Experiments

7.5.1 – Molecular and Cellular Experiments

There is a reduced expression of VPS33B in all ARC syndrome patients' fibroblasts irrespective of the gene that is mutated. However, it is not known whether there is a concordant reduction in POLARIN expression. There is currently no commercially available antibody against POLARIN, but the level of RNA expression could be assessed by qRT-PCR. This could not be assessed in the panel of fibroblasts used in chapter 3 since these cells were lost, and a panel of newly referred ARC syndrome patients' fibroblasts are currently being collected.

If there is no reduction in POLARIN expression in ARC syndrome patients with VPS33B mutations, then the finding that POLARIN completely co-localises and strongly co-immunoprecipitates with VPS18 needs to be further investigated (see chapter 4). The functional effect of POLARIN binding to VPS18 and the proteins in which VPS18 interacts with in the presence and absence of POLARIN should be assessed.

Although the newly identified VPS33B-POLARIN complex interacts with GTP bound Rab11a, the conditions in which the interaction occurs remains unknown. Since there is only a partial co-localisation and a weak interaction between the proteins, it is likely that other proteins or protein complexes are required for the interaction to occur. Consistent with this idea, Rab11a was not identified on the yeast-2-hybrid screen, where only VPS33B is being expressed. Fast two-colour live cell imaging could be used to further assess the interaction.

This will identify if the interaction is always partial or if the two proteins come together, interact then move away from each other

The partial co-localisation of the VPS33B-POLARIN clusters with both Rab4 and Rab11a, and that Rab4 is believed to be a precursor for Rab11a positive endosomes suggests that VPS33B and POLARIN might be required for the maturation to occur. The conventional HOPS complex and the CORVET complex in yeast facilitates the conversion of Rab5 positive early endosomes to and from Rab7 positive late endosomes respectively [74;84]. Therefore, whether the newly identified VPS33B-POLARIN complex can function in a similar manner on Rab4 and Rab11a endosomes could be addressed.

There are numerous pieces of evidence presented in this thesis that imply that VPS33B and POLARIN function synergistically. Therefore, to address these issues of what proteins bind to protein complexes, a Tandem Affinity Purification (TAP) assay could be performed expressing all the proteins of interest together followed by mass spectrometry to identify the interacting proteins of the complex. For example, VPS33B together with POLARIN and POLARIN together with VPS18.

The exact localisation of the VPS33B-POLARIN clusters is still unknown. The data from the TAP assay coupled with further characterisation of the clusters using VPS33B immunogold transmission electron microscopy, will give further biochemical and structural information. Additionally, further characterisation of the atypical granules with lamellar membranes and vesicular aggregates, could also give an insight into how mutations in VPS33B or PLRN causes the generation of such structures.

Another novel protein, C1orf149, was identified using the yeast-2-hybrid screen which has been characterised as a likely interacting protein of VPS33B. Analysis of the amino acid sequence using *in-silico* database searches revealed a likely histone acetyl transferase function. An IMAGE clone and a commercially available antibody are available so the interaction between the two proteins could be either confirmed or ruled out, and further assessed if necessary.

7.5.2 – Animal Models

The experiments suggested above deal primarily with the biochemical interaction of VPS33B and POLARIN at the molecular and cellular level. However, *VPS33B* and *PLRN* are mutated in a human condition, so the effect of reduced expression of either protein in a mammalian animal model would give further information about the pathophysiology of ARC syndrome. The mammalian animal model, usually mice could also be used to assess the role of VPS33B and POLARIN in development. Since ARC syndrome patients have indistinguishable phenotypes irrespective of the gene mutated only one gene needs to be targeted. This can be done using the gene trap method, where a known sequence of DNA is inserted into the genome of Embryonic Stem (ES) cells so that translation of the required transcript is prematurely terminated. Another method is the conditional knockout mouse, which results in tissue-specific inactivation of the gene of interest. This is achieved by breeding mice with recombinase sites introduced into the gene of interest with mice expressing the recombinase enzyme under a tissue specific promoter. The tissue-specific expression of the recombinase allows the inactivation of the gene of interest only in the tissue where the recombinase is expressed. The former method is cheaper than the conditional knockout method, but carries

the risk that knocking out the gene completely can lead to embryonic lethality, and very little information will be obtained. Nevertheless, the mouse model can give a lot of information about the pathophysiology of a human condition, which might not always be obtainable from human samples. Furthermore potential therapeutic agents can be trialled on these mice before clinical trials begin.

APPENDICES

Appendix 1

VPS33B Primer Sequences

Exon	Forward primer	Reverse primer	Product Size
1	CCTTCTCAGAACGAAGGGC	GGAAGAAATGTGCATCCAATG	215
2	CTGCGGAAGCTCATGTGAC	TTGTTTCATCAAAAGAAAACTGC	196
3	TCTTCGTGTCACACTTTGTGC	AGATGAAAGGCAGACGTGC	202
4	GAGACCTGTAGGGCAAATGG	AGGGTCCTTATGGCCAAGG	237
5	GCAGCTTCCCTGTTTCTAGC	CCGGTCCTCAGTCCTGTTC	190
6	TTGTCTTTCACTGGGTTCGG	CCAGGAAAAGAAGGAGCTGG	276
7	TTCCCTCTTAACGTGGAGC	TGGTATTTCTAGCCCTCTGC	254
8	CTAGGGCTAGCCACTTTCC	CAGGGAAAACAGCGTCTGC	225
9	GGAAGTATCACGTGGAAAGG	TAGGGCTGAAAGATGACAGG	228
10	AAGCTGCCCTTGGACATGC	GTCCATCTTGCCAAGATGC	189
11	GTAGGAGAAGTCCTCATTGG	CCCACAGCCTGGTATAAGC	187
12	GAACACCTGAGTACCCTTCC	CTGAGGCAACAAAACAGAGG	217
13	TGGTTTCTCGTGTCTGAGG	GGAGTAATGGTCCTCTGGA	540
14	AGAACCAGGAGTATGTCAGC	TAGAAGCGTGGGCAGTAGC	156
15-16	CCTGTTAGCATAGATGGCAGC	TCACTTCTTCTGTCCCTAAGGC	378
17	GTTCGTTGCTGGTTGATCTG	TGCCAATAACTGCCCTC	187
18	TGACAGTACTAGATGCTCTTTGGAC	ATGCTGCGTGTTGAGAGAAG	256
19	CTGTCGTGTCCTGAATGGTG	CTCCACAATGGAATGAACCC	212
20	TTTAAAGGGTTAGGGAGCTGAG	AAACATTGAGACACGCCAGG	239
21	TGCTGTGCCCTTCCTTTCC	AGGATCAGACCAGATTTCAGC	246
22	CCCTTCCTTTCTTAAGCCTG	GCCCAGCTGACACTTTGTTAC	427
23	TGGAGAGGCTCTATGGGTTG	TGCATCTCACTGAGGAATGTG	211

qRT-PCR Primer Sequences

Species	Gene	Direction	Sequence	Product Size
Human	ACTB	F	CGATTTCCCGCTCGGC	482 bp
		R	GGGGACGAGGCCAGA	
Human	VPS33A	F	CCACAGGACTGCAGAAGAAA	283 bp
		R	TGGGGTTTTACTTCCTTTCA	
Human	VPS33B	F	GGTGGTGTCTTGGGTGGTTGTACATTCTC	249 bp
		R	GGTAGTTGGTGGACACTTGGTTATAGCAGC	
Mouse	Actb	F	AGGTGACAGCATTGCTTCTG	188 bp
		R	GCTGCCTCAACACCTCAAC	
Mouse	Polarin	F	CAGAAGAACTGGCGCTATCC	201 bp
		R	CAGTCTGCCCTGAAGACTCC	

Cloning Primer Sequences

Gene	Direction	Primer Seq
PLRN (human)	F	CTTGAATTCCAATGAATCGGACAAAGGGTGA
	R	CTTGGTACCTTAATTCTTCCATCGAATTT
plrn (zebrafish)	F	CTTGGATCCATGACACGAGCCAAACCTGA
	R	CTTGAATTCTCAGTTTTTCCATCTGATTT
VPS11	F	CTTGAATTCAAATGGCGGCCTACCTGCAGTG
	R	CTTGTCGACGCTTAAGTGCCCCTCCTGGAG
VPS16	F	CTTGAATTCCCATGGACTGCTACACGGCGAAC
	R	CTTGTCGACCCTCACTTCTTCTGGGCTTGTG
VPS18	F	CTTGAATTCCCATGGCGTCCATCCTGGATGAG
	R	CTTGGTAACCTACAGCCAACTGAGCTGCTT
VPS33A	F	CTTGTCGACGATGGCGGCTCATCTGTCCTAC
	R	CTTGCGGCCGCCTAGAAAGGTTTTTCCATCA
VPS39	F	CTTGTCGACCATGCACGACGCTTTCGAGCC
	R	CTTGCGGCCGCTCAAGTGTCTGCTGGGTTTA
VPS41	F	CTTGTCGACCATGGCGGAAGCAGAGGAGCAG
	R	CTTGCGGCCGCCTATTTTTTCATCTCCAAAA

Plasmid Sequencing Primer Sequences

Plasmid	Direction	Sequence
pCMV	F	GTAAAACGACGGCCAGT
	R	CAGGAAACAGCTATGAC
pGFP/YFP	F	CATGGTCCTGCTGGAGTTCGTGACCGC
	R	ATAAGCTGCAATAAACAAGTTAACAAC
pCS2+	F (Sp6)	CCCAAGCTTGATTTAGGTGAC
	R (T7)	AATACGACTCACTATAG
pSM2	F	TGTGGAAAGGACGAAACACC
pGIPz	R	GCATTAAAGCAGCGTATC

shRNA Sequences

Gene	Hairpin	Sequence
Vps33b	-	CCCTGGCCAGTGCTGAAGTATT
Polarin	E	CCCAGCCTTTGAGCACATGTAT
	F	ACCTCGGAAAGGGATATCAGTA

Morpholino Oligonucleotide Sequences

Morpholino	Sequence (5' - 3')
ATG	GTTTGGCTCGTGTTCATCTTCGGAAT
Exon 3	CCAGACAAAGGACTGCGTACTTCCC
Exon 3 Mismatch	CCACACAAACGACTGCCTAGTTGCC
Exon 10	AACAGTGAACCTCACTTCAGTAACTC

Appendix 2

Antibodies and Dilutions Used for Western Blotting

Antibody	Clone	Supplier	Primary Dilution	Secondary Dilution
Rb α VPS33B	-	Protein Tech	1/1000	1/1000
m α β -actin	AC15	Sigma	1/15000	1/20000
m α myc	9E10	Sigma	1/5000	1/20000
m α HA	HA-7	Sigma	1/1000	1/2000
m α Rab11a	47/Rab11	BD Biosciences	1/2000	1/2000
Rb α GFP	-	Santa Cruz	1/2000	1/2000
Rb α CEA	-	Dako	1/1000	1/2000
Rb α ZO-1	-	Invitrogen (Zymed)	1/1000	1/1000
Rb α Claudin-1	-	Invitrogen (Zymed)	1/1000	1/1000
m α E-Cadherin	4A2C7	Invitrogen (Zymed)	1/2000	1/2000
Rb α β -Catenin	-	Abcam	1/4000	1/5000

Antibodies and Dilutions Used for Immunofluorescence Microscopy

Antibody	Clone	Supplier	Primary Dilution	Secondary Dilution
Rb α GM130	-	BD Biosciences	1/100	1/100
Rt α LAMP-1	-	Hybridoma Bank	1/100	1/100
m α Rab11a	47/Rab11	BD Biosciences	1/200	1/200
Rb α VPS33B	-	Protein Tech	1/100	1/100
m α myc	9E10	Sigma	1/200	1/200
Rb α CEA	-	Dako	1/100	1/100
m α Na ⁺ K ⁺ ATPase	C464.6	Millipore	1/100	1/100
Rb α ZO-1	-	Invitrogen (Zymed)	1/100	1/100
Rb α Claudin-1	-	Invitrogen (Zymed)	1/400	1/500
m α E-Cadherin	4A2C7	Invitrogen (Zymed)	1/200	1/200
Rb α E-Cadherin	-	Gift from C.P. Heisenberg	1/400	1.250

Appendix 3

POLARIN Nucleotide and Amino Acid Sequences

```
1 ATGAATCGGACAAAGGGTGATGAGGAGGAGTATTGGAACAGCTCCAAGTTCAAGGCTTTTACCTTTGAC
1 -M--N--R--T--K--G--D--E--E--E--Y--W--N--S--S--K--F--K--A--F--T--F--D-
70 GATGAAGACGATGAGCTTTCACAGTTAAAGGAGTCCAAGCGGGCGGTGAACAGCCTCCGAGACTTCGTG
24 -D--E--D--D--E--L--S--Q--L--K--E--S--K--R--A--V--N--S--L--R--D--F--V-
139 GATGATGATGACGATGATGACCTGGAGCGAGTCAGCTGGAGTGGGGAACCTGTGGGAAGTATCTCATGG
47 -D--D--D--D--D--D--D--L--E--R--V--S--W--S--G--E--P--V--G--S--I--S--W-
208 TCCATCAGAGAGACTGCTGGTAATAGCGGC TCAACC CACGAGGGGCGTGAACAGCTAAAGAGCCGAAAC
70 -S--I--R--E--T--A--G--N--S--G--S--T--H--E--G--R--E--Q--L--K--S--R--N-
277 AGCTTCTCCTCCTATGCACAACTACCCAAGCCTACTTCTACCTACTCCCTGAGCAGCTTTTTTAGAGGT
93 -S--F--S--S--Y--A--Q--L--P--K--P--T--S--T--Y--S--L--S--S--F--F--R--G-
346 AGAAGTAGAAGCTGGAAGTTTCCAGTCCCTTCTGATGCTCTGTCAGACACCTGCCAAAAGCTATGCT
116 -R--T--R--P--G--S--F--Q--S--L--S--D--A--L--S--D--T--P--A--K--S--Y--A-
415 CCAGAGCTG GGGAGACCCAAAAGGGGAGTATAGG GATTACAGCAATGACTGGAGCCCCAGTGATACAGTG
139 -P--E--L--G--R--P--K--G--E--Y--R--D--Y--S--N--D--W--S--P--S--D--T--V-
484 CGACGTCTCCGGAAGGGCAAGGTTTGCTCACTAGAGAGATTCCGCTCCTTACAGGACAACTACAACCTC
162 -R--R--L--R--K--G--K--V--C--S--L--E--R--F--R--S--L--Q--D--K--L--Q--L-
533 CTAGAAGAGGCAGTAAGCATGCATGATGGAAACGTCATTACTGCAGTTCTGATTTTCTCTGAAGAGGACA
185 -L--E--E--A--V--S--M--H--D--G--N--V--I--T--A--V--L--I--F--L--K--R--T-
622 CTGAGCAAAGAGATCCTCTTCCGAGAGCTGGAGGTGCGACAGGTTGCCCTGAGACATCTTATTCACTTC
208 -L--S--K--E--I--L--F--R--E--L--E--V--R--Q--V--A--L--R--H--L--I--H--F-
691 CTTAAGGAAATAGGGGATCAAAAAGTTGCTTTTAGACCTCTTCAGGTTTCCTAGATAGAACAGAAGAGCTT
231 -L--K--E--I--G--D--Q--K--L--L--L--D--L--F--R--F--L--D--R--T--E--E--L-
760 GCGCTATCTCATTATCGAGAGCATTTGAACATT CAGGACCCTGACAAACGAAAAGAATTTCTTAAAACC
254 -A--L--S--H--Y--R--E--H--L--N--I--Q--D--P--D--K--R--K--E--F--L--K--T-
829 TGTGTTGGTTTGCCATTTTCAGCAGAAAGATTCCGCACACATACAGGACCATTACACGCTCCTGGAACGT
277 -C--V--G--L--P--F--S--A--E--D--S--A--H--I--Q--D--H--Y--T--L--L--E--R-
898 CAGATCATTATTGAGGCAAATGATCGCCATCTAGAATCAGCAGGACAGACTGAGATCTTCCGAAAGCAC
300 -Q--I--I--I--E--A--N--D--R--H--L--E--S--A--G--Q--T--E--I--F--R--K--H-
967 CCCCGCAAAGCCTCCATCCTCAACATGCCACTAGTGACAACACTTTTCTACTCCTGCTTCTATCACTAC
323 -P--R--K--A--S--I--L--N--M--P--L--V--T--T--L--F--Y--S--C--F--Y--H--Y-
1036 ACAGAGGCTGAGGGGACATTCAGCAGTCCCGTCAACCTGAAGAAGACATTTAAGATCCAGATAAACAG
346 -T--E--A--E--G--T--F--S--S--P--V--N--L--K--K--T--F--K--I--P--D--K--Q-
1105 TATGTGCTGACAGCCCTGGCTGCTCGTGCCAAGCTTCGAGCCTGGAATGATGTAGATGCCCTATTCACC
369 -Y--V--L--T--A--L--A--A--R--A--K--L--R--A--W--N--D--V--D--A--L--F--T-
1174 ACAAAGAAGCTGGCTGGGCTATACCAAGAAGAGAGCACCATTGGCTTCATCGGGTTGTCGAAATTTTG
392 -T--K--N--W--L--G--Y--T--K--K--R--A--P--I--G--F--H--R--V--V--E--I--L-
1243 CACAAGAACAATGCCCTGTGCAGATATTACAGGAGTATGTCAATCTGGTGGAAGATGTGGACACGAAG
415 -H--K--N--N--A--P--V--Q--I--L--Q--E--Y--V--N--L--V--E--D--V--D--T--K-
1312 TTGAACCTTAGCCACTAAGTTCAAGTGCCATGATGTCGTCAATTGATACCTACCGGGACCTGAAGGATCGT
438 -L--N--L--A--T--K--F--K--C--H--D--V--V--I--D--T--Y--R--D--L--K--D--R-
1381 CAACAGTTGCTAGCATACAGGAGTAAGGTAGATAAAGGATCAGCAGAGGAGGAGAAGATTGATGCTCTT
461 -Q--Q--L--L--A--Y--R--S--K--V--D--K--G--S--A--E--E--E--K--I--D--A--L-
1450 CTCAGCAGCTCGCAAATT CGATGGAAGAATTAA
484 -L--S--S--S--Q--I--R--W--K--N--*-
```

[www.ensembl.org]

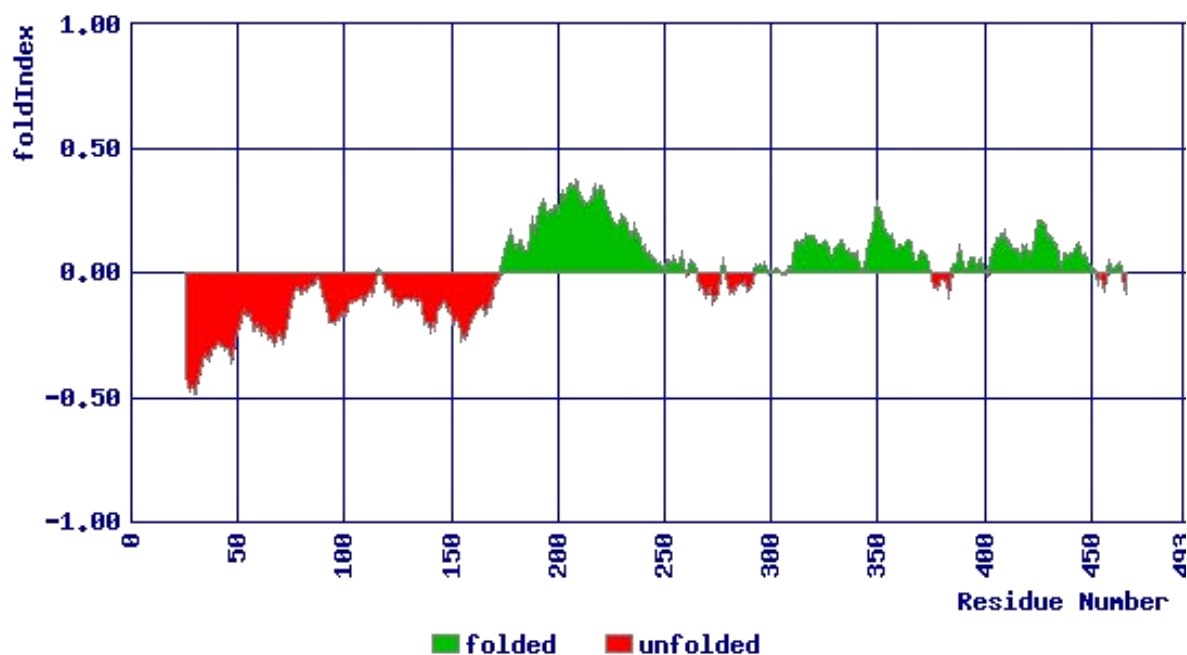
POLARIN Amino Acid Analysis

A - 22 (6.5%)	C - 4 (1.2%)	D - 22 (6.5%)	E - 24 (7.1%)	F - 16 (4.8%)
G - 9 (2.7%)	H - 13 (3.9%)	I - 19 (5.7%)	K - 29 (8.6%)	L - 46 (13.7%)
M - 2 (0.6%)	N - 12 (3.6%)	P - 8 (2.4%)	Q - 14 (4.2%)	R - 25 (7.4%)
S - 18 (5.4%)	T - 19 (5.7%)	V - 21 (6.2%)	W - 3 (0.9%)	Y - 10 (3.0%)

KR - 54 (16.1%)	ED - 46 (13.7%)	AGP - 39 (11.6%)
KRED - 100 (29.8%)	KR-ED - 8 (2.4%)	FIKMNY - 88 (26.2%)
LVIFM - 104 (31.0%)	ST - 37 (11.0%)	

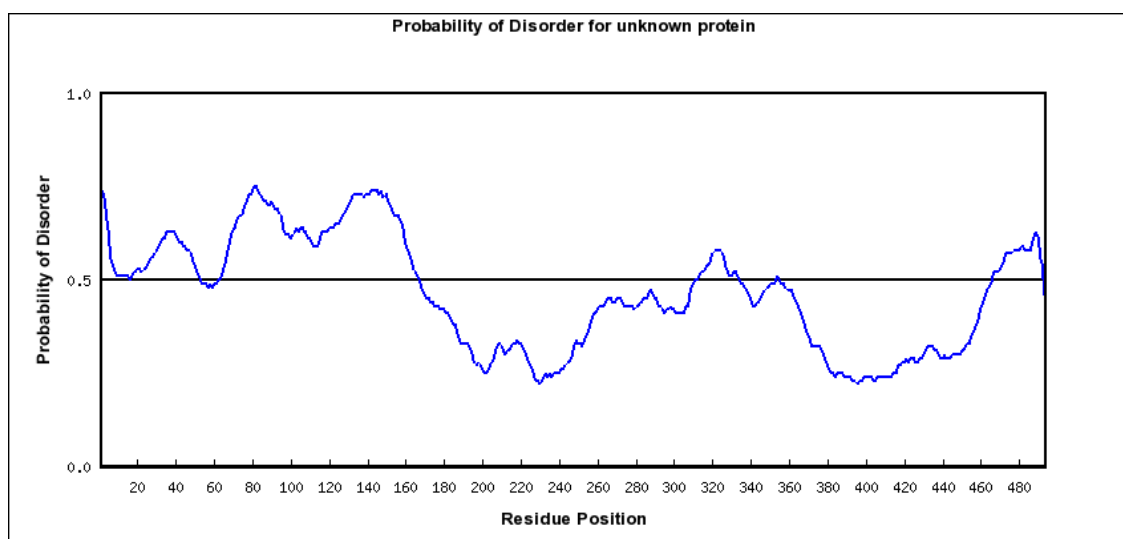
[www.ebi.ac.uk/Tools/saps]

POLARIN Fold Index



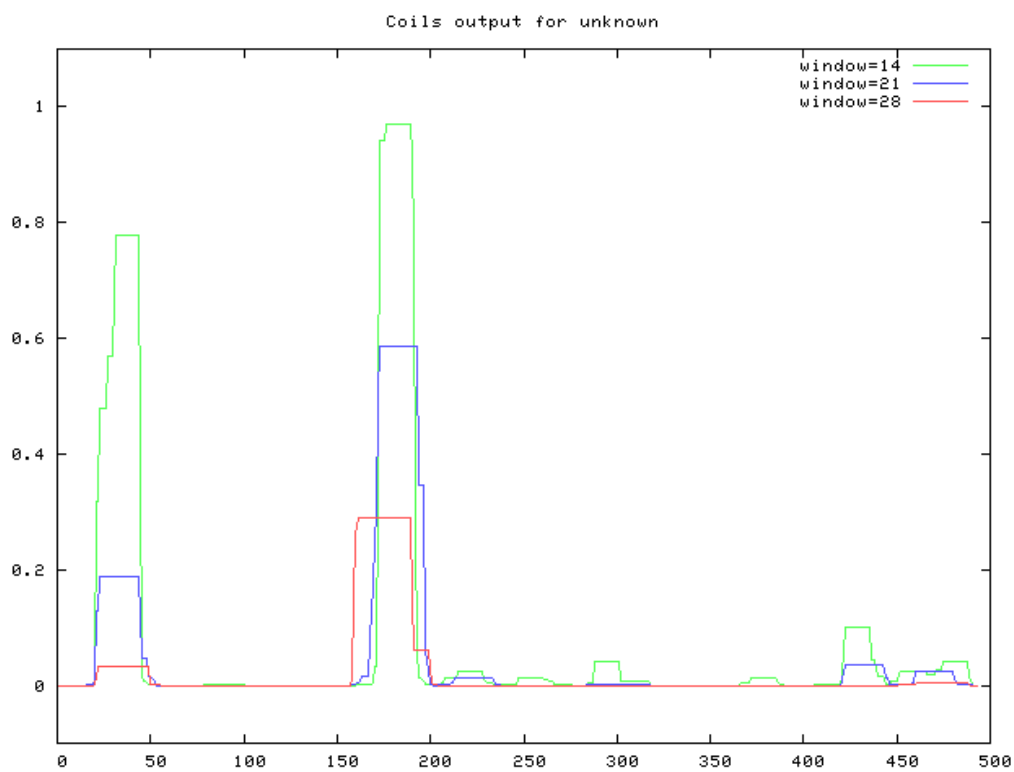
[www.biportal.weizmann.ac.il/fldbin/findex]

POLARIN Disorder Index



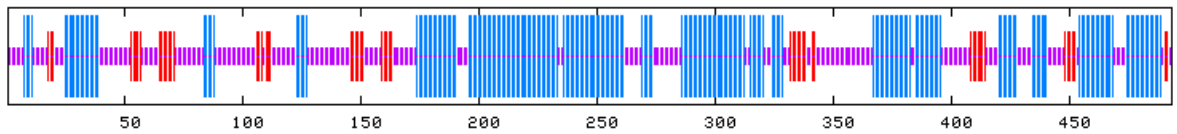
[www.strubi.ox.ac.uk/RONN]

POLARIN Coiled Coil Prediction



[www.ch.embnet.org/software/COILS_form]

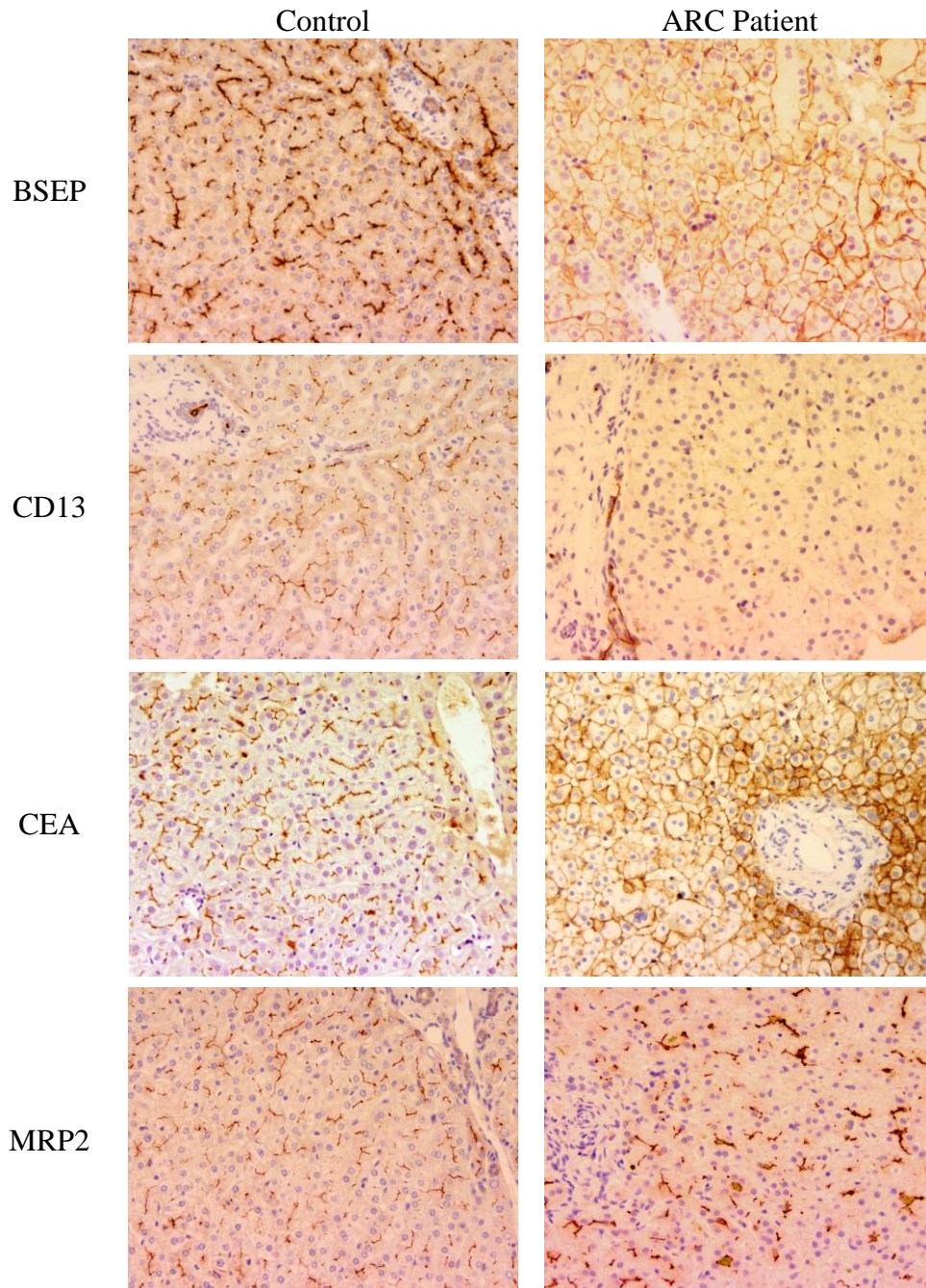
10 20 30 40 50 60 70
 | | | | | | |
 MNRTKGDEEEYWNSSKFKAFTFDDEDELSQLKESKRAVNSLRDFVDDDDDDDLERSVWSGEPVGSISWS
 cccccccchhhhccccceeecccchhhhhhhhhhhhhhhccccccccccccceeeccccccccceee
 IRETAGNSGSTHEGREQLKSRNSFSSYAQLPKPTSTYSLSSFFRGRTRPGSFQSLSDALSDTPAKSYAPE
 eccccccccccccchhhhccccccccccccccccceeeceeeccccccccchhhhcccccccccccc
 LGRPKGEYRDYSNDWSPSDTVRRLRKGVCSLERFRSLQDKLQLLEEAVSMHDGNVITAVLIFLKRTLK
 cccccceeeeeeccccccccceeeccccccccchhhhhhhhhhhhhhhhhccccchhhhhhhhhhhhh
 EILFRELEVRQVALRHLIHFLKEIGDQKLLDLFRFLDRTEELALSHYREHLNIQDPDKRKEFLKTCVGL
 hhh
 PFSAEDSAHIQDHYTLERQIIIEANDRHLESAGQTEIFRKHPRKASILNMPLVTTLFYSCFYHYTEAEG
 cccccchhh
 TFSSPVNLKKTFFKIPDKQYVLTALAARAKLRAWNDVDALFTTKNWLGYTCKRAPIGFHRVVEILHKNNAP
 cccccccccccccccccchhh
 VQILQEYVNLVEDVDTKLNLATKFKCHDVVIDTYRDLKDRQQLLAYRSKVDKGSAAEEKIDALLSSQIR
 hhhhhhhhccccchhhhhhhccccccccceeeecchhhhhhhhhhhhhhhhhhhhhhhhhhhhhhhhh
 WKN
 eec



c = random coil, e = extended strand and h = alpha helix,

[www.npsa-pbil.ibcp.fr/cgi-bin/npsa_automat.pl?page=npsa_gor4]

Appendix 4



Immunohistochemical analysis of membrane transporter protein localisation in an ARC patient with a PLRN mutation.

Control and ARC patient liver tissue stained for BSEP (Bile Salt Export Protein), CD13 (N-aminopeptidase), CEA (Carcino Embryonic Antigen), and MRP2 (Multidrug Resistance Protein 2). In the ARC syndrome patient, BSEP, CEA and CD13 staining loses its specific localisation in the apical (canalicular) membrane, and these markers can also be seen in the basolateral surface. MRP2 retains its' apical membrane localisation in the ARC syndrome patient. A 200x original magnification was used for each, and the specimens were counterstained with haematoxylin. (Images provided by AS Knisely, King's College Hospital, London, UK.)

Appendix 5

Experiment 1

	Gall Bladder Area (μm^2)					
	Non Injected	Exon 3 Mismatch	Exon 3	Exon 3 Rescue	ATG	ATG Rescue
	59684.4	44855.0	24429.1	66589.3	34655.8	72845.7
	60990.2	72007.2	27690.6	52307.1	25150.2	72355.2
	63464.2	68818.5	24250.3	72291.3	25356.4	70807.2
	54075.0	73700.5	31032.9	75550.8	26371.1	71765.2
	70054.0	71042.7	27463.2	64810.1	28895.7	73141.8
	72855.4	68915.5	18049.7	63768.9	39182.8	76779.2
	61134.9	76330.0	16980.3	60663.3	29153.5	69826.6
	54088.5	72123.4	18497.7	76684.0	52025.5	59500.2
	57130.5	78414.2	31491.9	54349.9	38864.5	72409.3
	67339.4	74485.7	26040.9	69930.2	27583.8	62329.1
	59262.4	64049.2	31835.5	74120.0	14468.2	67294.7
	68423.9	71470.8	28004.8	82085.2	39168.0	55962.4
	68215.9	54886.1	19982.9	69581.9	24633.6	63807.1
	64392.4	79729.2	26135.5	82590.5	27564.9	53320.3
	69192.3	62435.4	29104.3	83850.4	23858.0	59814.3
	74765.0	72563.2	28896.9	69525.0	37414.2	69642.9
	86489.3	70819.6	30291.9	64724.6	17401.5	81850.1
	82307.1	69908.6	27021.2	75534.8	15453.8	63232.9
	72291.3	74089.5	21543.3	50734.5	26452.8	70788.2
	75550.8	78705.5	22957.1	76709.5	22566.7	72717.1
	64810.1	73597.4	31517.1	76254.3	35153.5	78595.4
	83768.9	64027.9	18026.9	82318.4	25079.9	57941.9
	90663.3	66158.8	31435.4	80759.2	14710.5	61026.9
	86684.0	61237.6	18617.6	81720.5	25789.9	80445.2
	84349.9	64724.6	30574.6	75589.7	63684.7	59019.5
	79930.2	75534.8	22428.1	60698.8	24186.0	71149.5
	74120.0	87435.5	18117.8	75060.8	58011.1	57561.4
	82035.2	82318.4	29050.9	65387.9	13826.5	60467.8
	89581.9	75589.7	30621.7	65001.8	26891.6	62090.7
	82595.5	75060.8	22562.0	54285.1	23581.4	58074.7
n=	30	30	30	30	30	30
Mean	72008.2	70834.5	25488.4	70115.9	29571.2	66885.4
SD	10892.9	8298.5	4969.8	9598.6	12018.5	7784.4

Experiment 2

Gall Bladder Area (μm^2)						
	Non Injected	Exon 3 Mismatch	Exon 3	Exon 3 Rescue	ATG	ATG Rescue
	92675.0	81347.1	19789.2	52321.4	20040.5	81039.0
	62315.1	72174.7	14316.2	89169.0	18934.7	82534.1
	71197.1	66512.4	18708.5	69160.6	21015.6	65531.7
	91018.2	81148.9	19745.2	61143.7	16446.5	62518.5
	74175.8	98453.7	15205.3	63122.1	17276.8	67729.2
	86794.9	71341.6	18972.4	71451.6	21415.7	91550.7
	77961.1	69789.2	14310.3	80388.9	15709.6	64913.1
	59273.0	59479.1	21735.7	73456.6	14275.2	74740.1
	77630.6	71926.1	14778.1	70508.3	18164.7	51456.6
	74580.1	69630.2	23929.3	92242.5	13357.7	75347.8
	92349.4	86663.0	20423.8	85230.4	18765.0	78518.7
	74968.5	82781.6	15861.1	64170.2	24995.7	62283.6
	92258.4	74562.9	21364.2	72621.3	20759.6	71517.1
	93140.9	99161.1	24538.8	71388.7	28105.0	61696.1
	63634.5	84604.5	17168.4	61216.9	21567.7	71982.5
	66099.6	51589.7	23215.5	51535.9	17011.7	61707.0
	82168.8	91887.8	28858.9	86354.5	14762.5	62546.9
	69661.2	81398.7	30781.9	60533.5	16776.1	61337.3
	67156.2	92657.8	17278.8	76939.3	14322.5	82170.6
	62828.7	79794.9	19257.2	81780.4	24127.4	61548.7
	80350.1	52648.1	16738.7	89188.6	13395.7	82551.3
	61648.5	65758.2	18864.9	71982.5	17282.8	60194.0
	61237.5	53885.6	31879.5	70734.5	17397.6	89779.3
	73655.2	51657.7	19425.6	82473.7	20313.4	76866.2
	92588.4	89158.7	17367.0	81164.7	16838.5	73910.9
	76398.1	53141.3	24721.2	71247.3	24912.8	74310.2
	74646.1	62389.4	18859.3	69139.4	19775.1	72146.0
	78397.2	91151.1	22383.8	61069.2	18013.9	70744.2
	82327.7	62750.7	14749.5	77084.7	18585.6	82377.2
	93505.4	62766.4	26625.3	61342.7	19704.7	56848.5
n=	30	30	30	30	30	30
Mean	76888.0	73740.4	20395.1	72338.8	18801.7	71079.9
SD	11116.2	14426.5	4746.7	10757.9	3567.7	9989.2

Experiment 3

	Gall Bladder Area (μm^2)					
	Non Injected	Exon 3 Mismatch	Exon 3	Exon 3 Rescue	ATG	ATG Rescue
	72199.9	71699.8	16022.1	65579.2	20103.4	51126.7
	64428.8	74943.1	18714.8	58417.1	18928.4	69548.9
	82424.9	59440.7	13713.1	64190.3	32053.9	64643.2
	92201.1	97204.1	23713.1	73104.4	21887.8	81771.4
	82424.9	51535.4	22832.1	52918.4	36663.0	73793.9
	79907.9	66342.6	19660.4	70216.1	19918.0	42994.5
	83857.0	71944.8	13854.2	61861.1	28923.0	64517.8
	52729.6	80272.4	22440.7	85500.3	21176.8	62320.6
	81159.8	59106.2	19678.9	42127.4	17398.0	65841.4
	62540.2	84979.6	13561.7	57320.8	21416.5	57543.3
	79576.2	64505.3	20099.8	72391.0	17414.2	72624.3
	59987.8	71670.3	20131.6	63662.7	15343.5	54838.8
	67282.3	84960.1	22936.8	82149.1	14152.9	79399.5
	89222.3	62879.5	15817.9	72561.6	19500.2	67171.2
	68747.5	72187.4	17090.4	64535.4	19949.1	61944.8
	53890.1	86166.2	23326.3	82967.1	20781.9	51701.8
	81889.8	59410.0	19141.3	59850.5	18796.4	72760.8
	77371.2	74593.1	16179.2	62789.7	16116.4	81341.5
	94843.1	63476.6	20941.8	51151.9	31194.6	41426.2
	69130.0	62978.6	14298.8	52317.8	13961.4	73467.4
	69905.6	62637.6	22141.5	62276.3	17916.8	49740.4
	74789.1	82978.3	19789.2	49342.5	20401.8	41340.3
	64824.4	77004.3	17570.9	64181.5	18430.1	54291.1
	63089.7	70093.6	21347.3	50212.7	16597.3	49395.8
	75479.7	89101.0	21488.5	68302.6	18918.8	53576.5
	92131.7	62010.4	20216.1	52053.6	16672.7	58085.5
	69621.5	91660.6	16336.0	37963.9	22016.6	50706.5
	70266.2	61807.5	19565.7	40677.3	19537.8	42655.2
	88126.2	91785.7	19220.8	42727.4	29236.3	61794.9
	74018.2	74205.7	18138.1	71325.4	21875.2	62012.9
n=	30	30	30	30	30	30
Mean	74602.2	72786.0	18999.0	61155.8	20909.4	60479.2
SD	11105.4	11715.6	2999.1	12423.4	5440.2	11851.0

Summary

	Gall Bladder Area (μm^2)					
	Non Injected	Exon 3 Mismatch	Exon 3	Exon 3 Rescue	ATG	ATG Rescue
Experiment 1	72008.2	70834.5	25488.4	70115.9	29571.2	66885.4
Experiment 2	76888.0	73740.4	20395.1	72338.8	18801.7	71079.9
Experiment 3	74602.2	72786.0	18999.0	61155.8	20909.4	60479.2
Mean	100.00%	97.28%	29.13%	91.14%	31.18%	88.80%
SD	14.66%	15.47%	7.30%	16.01%	12.91%	14.34%

REFERENCES

- [1] Gissen P, Johnson CA, Morgan NV, Stapelbroek JM, Forshew T, Cooper WN, et al. Mutations in VPS33B, encoding a regulator of SNARE-dependent membrane fusion, cause arthrogryposis-renal dysfunction-cholestasis (ARC) syndrome. *Nature Genetics* 2004 Apr;36(4):400-4.
- [2] Gissen P, Tee L, Johnson CA, Genin E, Caliebe A, Chitayat D, et al. Clinical and molecular genetic features of ARC syndrome. *Human Genetics* 2006 Oct;120(3):396-409.
- [3] Abu-Sa'da O, Barbar M, Al Harbi N, Taha D. Arthrogryposis, renal tubular acidosis and cholestasis (ARC) syndrome: two new cases and review. *Clin Dysmorphol* 2005 Oct;14(4):191-6.
- [4] Cullinane AR, Straatman-Iwanowska A, Seo JK, Ko JS, Song KS, Gizewska M, et al. Molecular investigations to improve diagnostic accuracy in patients with ARC syndrome. *Hum Mutat* 2009 Feb;30(2):E330-E337.
- [5] Carim L, Sumoy L, Andreu N, Estivill X, Escarceller M. Cloning, mapping and expression analysis of VPS33B, the human orthologue of rat Vps33b. *Cytogenet Cell Genet* 2000;89(1-2):92-5.
- [6] Gallwitz D, Jahn R. The riddle of the Sec1/Munc-18 proteins - new twists added to their interactions with SNAREs. *Trends Biochem Sci* 2003 Mar;28(3):113-6.
- [7] Peterson MR, Emr SD. The class C Vps complex functions at multiple stages of the vacuolar transport pathway. *Traffic* 2001 Jul;2(7):476-86.
- [8] Gissen P, Johnson CA, Gentle D, Hurst LD, Doherty AJ, O'Kane CJ, et al. Comparative evolutionary analysis of VPS33 homologues: genetic and functional insights. *Human Molecular Genetics* 2005 May 15;14(10):1261-70.
- [9] Sevrioukov EA, He JP, Moghrabi N, Sunio A, Kramer H. A role for the deep orange and carnation eye color genes in lysosomal delivery in *Drosophila*. *Mol Cell* 1999 Oct;4(4):479-86.
- [10] Sriram V, Krishnan KS, Mayor S. deep-orange and carnation define distinct stages in late endosomal biogenesis in *Drosophila melanogaster*. *J Cell Biol* 2003 May 12;161(3):593-607.
- [11] Bull LN, Mahmoodi V, Baker AJ, Jones R, Strautnieks SS, Thompson RJ, et al. VPS33B mutation with ichthyosis, cholestasis, and renal dysfunction but without arthrogryposis: incomplete ARC syndrome phenotype. *J Pediatr* 2006 Feb;148(2):269-71.
- [12] Lo B, Li L, Gissen P, Christensen H, McKiernan PJ, Ye C, et al. Requirement of VPS33B, a member of the Sec1/Munc18 protein family, in megakaryocyte and platelet alpha-granule biogenesis. *Blood* 2005 Dec 15;106(13):4159-66.
- [13] Harrison P, Cramer EM. Platelet alpha-granules. *Blood Rev* 1993 Mar;7(1):52-62.
- [14] Pfeffer SR. Transport vesicle docking: SNAREs and associates. *Annu Rev Cell Dev Biol* 1996;12:441-61.
- [15] Jahn R, Sudhof TC. Membrane fusion and exocytosis. *Annu Rev Biochem* 1999;68:863-911.
- [16] Burd CG, Babst M, Emr SD. Novel pathways, membrane coats and PI kinase regulation in yeast lysosomal trafficking. *Semin Cell Dev Biol* 1998 Oct;9(5):527-33.
- [17] Olkkonen VM, Ikonen E. Genetic defects of intracellular-membrane transport. *N Engl J Med* 2000 Oct 12;343(15):1095-104.
- [18] Gerst JE. SNAREs and SNARE regulators in membrane fusion and exocytosis. *Cell Mol Life Sci* 1999 May;55(5):707-34.

- [19] Alberts B, Johnson A, Lewis J, Raff M, Roberts K, Walter P. *Molecular Biology Of The Cell*. 4th ed. New York: Garland Science; 2002.
- [20] Gissen P, Maher ER. Cargos and genes: insights into vesicular transport from inherited human disease. *J Med Genet* 2007 Sep;44(9):545-55.
- [21] Gruenberg J, Maxfield FR. Membrane transport in the endocytic pathway. *Curr Opin Cell Biol* 1995 Aug;7(4):552-63.
- [22] Mellman I. Membranes and sorting. *Curr Opin Cell Biol* 1996 Aug;8(4):497-8.
- [23] Saksena S, Sun J, Chu T, Emr SD. ESCRTing proteins in the endocytic pathway. *Trends Biochem Sci* 2007 Dec;32(12):561-73.
- [24] Woodman PG, Futter CE. Multivesicular bodies: co-ordinated progression to maturity. *Curr Opin Cell Biol* 2008 Aug;20(4):408-14.
- [25] Futter CE, Pearse A, Hewlett LJ, Hopkins CR. Multivesicular endosomes containing internalized EGF-EGF receptor complexes mature and then fuse directly with lysosomes. *J Cell Biol* 1996 Mar;132(6):1011-23.
- [26] Raymond CK, Howald-Stevenson I, Vater CA, Stevens TH. Morphological classification of the yeast vacuolar protein sorting mutants: evidence for a prevacuolar compartment in class E vps mutants. *Mol Biol Cell* 1992 Dec;3(12):1389-402.
- [27] Vida TA, Huyer G, Emr SD. Yeast vacuolar proenzymes are sorted in the late Golgi complex and transported to the vacuole via a prevacuolar endosome-like compartment. *J Cell Biol* 1993 Jun;121(6):1245-56.
- [28] Babst M. A protein's final ESCRT. *Traffic* 2005 Jan;6(1):2-9.
- [29] Hurley JH. ESCRT complexes and the biogenesis of multivesicular bodies. *Curr Opin Cell Biol* 2008 Feb;20(1):4-11.
- [30] Rothman JE, Warren G. Implications of the SNARE hypothesis for intracellular membrane topology and dynamics. *Curr Biol* 1994 Mar 1;4(3):220-33.
- [31] Sollner T, Whiteheart SW, Brunner M, Erdjument-Bromage H, Geromanos S, Tempst P, et al. SNAP receptors implicated in vesicle targeting and fusion. *Nature* 1993 Mar 25;362(6418):318-24.
- [32] Ungermann C, Langosch D. Functions of SNAREs in intracellular membrane fusion and lipid bilayer mixing. *J Cell Sci* 2005 Sep 1;118(Pt 17):3819-28.
- [33] Jahn R, Scheller RH. SNAREs--engines for membrane fusion. *Nat Rev Mol Cell Biol* 2006 Sep;7(9):631-43.
- [34] Rothman JE. Mechanisms of intracellular protein transport. *Nature* 1994 Nov 3;372(6501):55-63.
- [35] Fasshauer D, Sutton RB, Brunger AT, Jahn R. Conserved structural features of the synaptic fusion complex: SNARE proteins reclassified as Q- and R-SNAREs. *Proc Natl Acad Sci U S A* 1998 Dec 22;95(26):15781-6.
- [36] Weber T, Zemelman BV, McNew JA, Westermann B, Gmachl M, Parlati F, et al. SNAREpins: minimal machinery for membrane fusion. *Cell* 1998 Mar 20;92(6):759-72.
- [37] Sutton RB, Fasshauer D, Jahn R, Brunger AT. Crystal structure of a SNARE complex involved in synaptic exocytosis at 2.4 Å resolution. *Nature* 1998 Sep 24;395(6700):347-53.
- [38] Antonin W, Fasshauer D, Becker S, Jahn R, Schneider TR. Crystal structure of the endosomal SNARE complex reveals common structural principles of all SNAREs. *Nat Struct Biol* 2002 Feb;9(2):107-11.
- [39] Sudhof TC, De Camilli P, Niemann H, Jahn R. Membrane fusion machinery: insights from synaptic proteins. *Cell* 1993 Oct 8;75(1):1-4.

- [40] Mayer A, Wickner W, Haas A. Sec18p (NSF)-driven release of Sec17p (alpha-SNAP) can precede docking and fusion of yeast vacuoles. *Cell* 1996 Apr 5;85(1):83-94.
- [41] Tsui MM, Banfield DK. Yeast Golgi SNARE interactions are promiscuous. *J Cell Sci* 2000 Jan;113 (Pt 1):145-52.
- [42] Zerial M, McBride H. Rab proteins as membrane organizers. *Nat Rev Mol Cell Biol* 2001 Feb;2(2):107-17.
- [43] Toonen RF, Verhage M. Vesicle trafficking: pleasure and pain from SM genes. *Trends Cell Biol* 2003 Apr;13(4):177-86.
- [44] Hu SH, Latham CF, Gee CL, James DE, Martin JL. Structure of the Munc18c/Syntaxin4 N-peptide complex defines universal features of the N-peptide binding mode of Sec1/Munc18 proteins. *Proc Natl Acad Sci U S A* 2007 May 22;104(21):8773-8.
- [45] Brunger AT. Structure and function of SNARE and SNARE-interacting proteins. *Q Rev Biophys* 2005 Feb;38(1):1-47.
- [46] Kauppi M, Jantti J, Olkkonen VM. The function of Sec1/Munc18 proteins – Solution of the mystery in sight? In: Keranen S, Janti J, editors. *Regulatory Mechanisms of Intracellular Membrane Transport*. 10 ed. Heidelberg: Springer; 2004. p. 115-43.
- [47] Seals DF, Eitzen G, Margolis N, Wickner WT, Price A. A Ypt/Rab effector complex containing the Sec1 homolog Vps33p is required for homotypic vacuole fusion. *Proc Natl Acad Sci U S A* 2000 Aug 15;97(17):9402-7.
- [48] Riento K, Kauppi M, Keranen S, Olkkonen VM. Munc18-2, a functional partner of syntaxin 3, controls apical membrane trafficking in epithelial cells. *J Biol Chem* 2000 May 5;275(18):13476-83.
- [49] Wu MN, Littleton JT, Bhat MA, Prokop A, Bellen HJ. ROP, the *Drosophila* Sec1 homolog, interacts with syntaxin and regulates neurotransmitter release in a dosage-dependent manner. *EMBO J* 1998 Jan 2;17(1):127-39.
- [50] Fukuda M. Regulation of secretory vesicle traffic by Rab small GTPases. *Cell Mol Life Sci* 2008 Sep;65(18):2801-13.
- [51] Stenmark H, Olkkonen VM. The Rab GTPase family. *Genome Biol* 2001;2(5):REVIEWS3007.
- [52] Chavrier P, Gorvel JP, Stelzer E, Simons K, Gruenberg J, Zerial M. Hypervariable C-terminal domain of rab proteins acts as a targeting signal. *Nature* 1991 Oct 24;353(6346):769-72.
- [53] Ostermeier C, Brunger AT. Structural basis of Rab effector specificity: crystal structure of the small G protein Rab3A complexed with the effector domain of rabphilin-3A. *Cell* 1999 Feb 5;96(3):363-74.
- [54] Chattopadhyay D, Langsley G, Carson M, Recacha R, DeLucas L, Smith C. Structure of the nucleotide-binding domain of *Plasmodium falciparum* rab6 in the GDP-bound form. *Acta Crystallogr D Biol Crystallogr* 2000 Aug;56(Pt 8):937-44.
- [55] Esters H, Alexandrov K, Constantinescu AT, Goody RS, Scheidig AJ. High-resolution crystal structure of *S. cerevisiae* Ypt51(DeltaC15)-GppNHp, a small GTP-binding protein involved in regulation of endocytosis. *J Mol Biol* 2000 Apr 21;298(1):111-21.
- [56] Stroupe C, Brunger AT. Crystal structures of a Rab protein in its inactive and active conformations. *J Mol Biol* 2000 Dec 8;304(4):585-98.
- [57] Pfeffer S, Aivazian D. Targeting Rab GTPases to distinct membrane compartments. *Nat Rev Mol Cell Biol* 2004 Nov;5(11):886-96.
- [58] Haas AK, Fuchs E, Kopajtich R, Barr FA. A GTPase-activating protein controls Rab5 function in endocytic trafficking. *Nat Cell Biol* 2005 Sep;7(9):887-93.

- [59] Grosshans BL, Ortiz D, Novick P. Rabs and their effectors: achieving specificity in membrane traffic. *Proc Natl Acad Sci U S A* 2006 Aug 8;103(32):11821-7.
- [60] Bock JB, Matern HT, Peden AA, Scheller RH. A genomic perspective on membrane compartment organization. *Nature* 2001 Feb 15;409(6822):839-41.
- [61] Olkkonen VM, Stenmark H. Role of Rab GTPases in membrane traffic. *Int Rev Cytol* 1997;176:1-85.
- [62] Anant JS, Desnoyers L, Machius M, Demeler B, Hansen JC, Westover KD, et al. Mechanism of Rab geranylgeranylation: formation of the catalytic ternary complex. *Biochemistry* 1998 Sep 8;37(36):12559-68.
- [63] Alexandrov K, Horiuchi H, Steele-Mortimer O, Seabra MC, Zerial M. Rab escort protein-1 is a multifunctional protein that accompanies newly prenylated rab proteins to their target membranes. *EMBO J* 1994 Nov 15;13(22):5262-73.
- [64] Dirac-Svejstrup AB, Sumizawa T, Pfeffer SR. Identification of a GDI displacement factor that releases endosomal Rab GTPases from Rab-GDI. *EMBO J* 1997 Feb 3;16(3):465-72.
- [65] Ullrich O, Stenmark H, Alexandrov K, Huber LA, Kaibuchi K, Sasaki T, et al. Rab GDP dissociation inhibitor as a general regulator for the membrane association of rab proteins. *J Biol Chem* 1993 Aug 25;268(24):18143-50.
- [66] Ullrich O, Horiuchi H, Bucci C, Zerial M. Membrane association of Rab5 mediated by GDP-dissociation inhibitor and accompanied by GDP/GTP exchange. *Nature* 1994 Mar 10;368(6467):157-60.
- [67] Carroll KS, Hanna J, Simon I, Krise J, Barbero P, Pfeffer SR. Role of Rab9 GTPase in facilitating receptor recruitment by TIP47. *Science* 2001 May 18;292(5520):1373-6.
- [68] Bonifacino JS, Lippincott-Schwartz J. Coat proteins: shaping membrane transport. *Nat Rev Mol Cell Biol* 2003 May;4(5):409-14.
- [69] Bonifacino JS, Glick BS. The mechanisms of vesicle budding and fusion. *Cell* 2004 Jan 23;116(2):153-66.
- [70] Kirchhausen T. Three ways to make a vesicle. *Nat Rev Mol Cell Biol* 2000 Dec;1(3):187-98.
- [71] Price A, Seals D, Wickner W, Ungermann C. The docking stage of yeast vacuole fusion requires the transfer of proteins from a cis-SNARE complex to a Rab/Ypt protein. *J Cell Biol* 2000 Mar 20;148(6):1231-8.
- [72] Sato TK, Rehling P, Peterson MR, Emr SD. Class C Vps protein complex regulates vacuolar SNARE pairing and is required for vesicle docking/fusion. *Mol Cell* 2000 Sep;6(3):661-71.
- [73] Wurmser AE, Sato TK, Emr SD. New component of the vacuolar class C-Vps complex couples nucleotide exchange on the Ypt7 GTPase to SNARE-dependent docking and fusion. *J Cell Biol* 2000 Oct 30;151(3):551-62.
- [74] Rink J, Ghigo E, Kalaidzidis Y, Zerial M. Rab conversion as a mechanism of progression from early to late endosomes. *Cell* 2005 Sep 9;122(5):735-49.
- [75] Christoforidis S, Miaczynska M, Ashman K, Wilm M, Zhao L, Yip SC, et al. Phosphatidylinositol-3-OH kinases are Rab5 effectors. *Nat Cell Biol* 1999 Aug;1(4):249-52.
- [76] Starai VJ, Hickey CM, Wickner W. HOPS Proofreads the trans-SNARE Complex for Yeast Vacuole Fusion. *Mol Biol Cell* 2008 Jun;19(6):2500-8.
- [77] Huizing M, Didier A, Walenta J, Anikster Y, Gahl WA, Kramer H. Molecular cloning and characterization of human VPS18, VPS 11, VPS16, and VPS33. *Gene* 2001 Feb 21;264(2):241-7.

- [78] Kim BY, Kramer H, Yamamoto A, Kominami E, Kohsaka S, Akazawa C. Molecular characterization of mammalian homologues of class C Vps proteins that interact with syntaxin-7. *J Biol Chem* 2001 Aug 3;276(31):29393-402.
- [79] Kinchen JM, Doukometzidis K, Almendinger J, Stergiou L, Tosello-Trampont A, Sifri CD, et al. A pathway for phagosome maturation during engulfment of apoptotic cells. *Nat Cell Biol* 2008 May;10(5):556-66.
- [80] Caplan S, Hartnell LM, Aguilar RC, Naslavsky N, Bonifacino JS. Human Vam6p promotes lysosome clustering and fusion in vivo. *J Cell Biol* 2001 Jul 9;154(1):109-22.
- [81] Poupon V, Stewart A, Gray SR, Piper RC, Luzio JP. The role of mVps18p in clustering, fusion, and intracellular localization of late endocytic organelles. *Mol Biol Cell* 2003 Oct;14(10):4015-27.
- [82] Suzuki T, Oiso N, Gautam R, Novak EK, Panthier JJ, Suprabha PG, et al. The mouse organellar biogenesis mutant buff results from a mutation in Vps33a, a homologue of yeast vps33 and *Drosophila* carnation. *Proc Natl Acad Sci U S A* 2003 Feb 4;100(3):1146-50.
- [83] Chintala S, Li W, Lamoreux ML, Ito S, Wakamatsu K, Sviderskaya EV, et al. Slc7a11 gene controls production of pheomelanin pigment and proliferation of cultured cells. *Proc Natl Acad Sci U S A* 2005 Aug 2;102(31):10964-9.
- [84] Peplowska K, Markgraf DF, Ostrowicz CW, Bange G, Ungermann C. The CORVET tethering complex interacts with the yeast Rab5 homolog Vps21 and is involved in endo-lysosomal biogenesis. *Dev Cell* 2007 May;12(5):739-50.
- [85] Rodriguez-Boulan E, Nelson WJ. Morphogenesis of the polarized epithelial cell phenotype. *Science* 1989 Aug 18;245(4919):718-25.
- [86] Shin K, Fogg VC, Margolis B. Tight junctions and cell polarity. *Annu Rev Cell Dev Biol* 2006;22:207-35.
- [87] Schuck S, Simons K. Polarized sorting in epithelial cells: raft clustering and the biogenesis of the apical membrane. *J Cell Sci* 2004 Dec 1;117(Pt 25):5955-64.
- [88] Anderson JM, Van Itallie CM, Fanning AS. Setting up a selective barrier at the apical junction complex. *Curr Opin Cell Biol* 2004 Apr;16(2):140-5.
- [89] Hartsock A, Nelson WJ. Adherens and tight junctions: structure, function and connections to the actin cytoskeleton. *Biochim Biophys Acta* 2008 Mar;1778(3):660-9.
- [90] Ceteci F, Ceteci S, Karreman C, Kramer BW, Asan E, Gotz R, et al. Disruption of tumor cell adhesion promotes angiogenic switch and progression to micrometastasis in RAF-driven murine lung cancer. *Cancer Cell* 2007 Aug;12(2):145-59.
- [91] Wan H, Winton HL, Soeller C, Tovey ER, Gruenert DC, Thompson PJ, et al. Der p 1 facilitates transepithelial allergen delivery by disruption of tight junctions. *J Clin Invest* 1999 Jul;104(1):123-33.
- [92] Wapenaar MC, Monsuur AJ, van Bodegraven AA, Weersma RK, Bevova MR, Linskens RK, et al. Associations with tight junction genes PARD3 and MAGI2 in Dutch patients point to a common barrier defect for coeliac disease and ulcerative colitis. *Gut* 2008 Apr;57(4):463-7.
- [93] Izaddoost S, Nam SC, Bhat MA, Bellen HJ, Choi KW. *Drosophila* Crumbs is a positional cue in photoreceptor adherens junctions and rhabdomeres. *Nature* 2002 Mar 14;416(6877):178-83.
- [94] Wang Q, Margolis B. Apical junctional complexes and cell polarity. *Kidney Int* 2007 Dec;72(12):1448-58.

- [95] Pokutta S, Herrenknecht K, Kemler R, Engel J. Conformational changes of the recombinant extracellular domain of E-cadherin upon calcium binding. *Eur J Biochem* 1994 Aug 1;223(3):1019-26.
- [96] Bryant DM, Stow JL. The ins and outs of E-cadherin trafficking. *Trends Cell Biol* 2004 Aug;14(8):427-34.
- [97] Lock JG, Stow JL. Rab11 in recycling endosomes regulates the sorting and basolateral transport of E-cadherin. *Mol Biol Cell* 2005 Apr;16(4):1744-55.
- [98] Capaldo CT, Macara IG. Depletion of E-cadherin disrupts establishment but not maintenance of cell junctions in Madin-Darby canine kidney epithelial cells. *Mol Biol Cell* 2007 Jan;18(1):189-200.
- [99] Taddei A, Giampietro C, Conti A, Orsenigo F, Breviario F, Pirazzoli V, et al. Endothelial adherens junctions control tight junctions by VE-cadherin-mediated upregulation of claudin-5. *Nat Cell Biol* 2008 Aug;10(8):923-34.
- [100] Theard D, Steiner M, Kalicharan D, Hoekstra D, Van IJendoorn SC. Cell polarity development and protein trafficking in hepatocytes lacking E-cadherin/beta-catenin-based adherens junctions. *Mol Biol Cell* 2007 Jun;18(6):2313-21.
- [101] Yu AS, McCarthy KM, Francis SA, McCormack JM, Lai J, Rogers RA, et al. Knockdown of occludin expression leads to diverse phenotypic alterations in epithelial cells. *Am J Physiol Cell Physiol* 2005 Jun;288(6):C1231-C1241.
- [102] Balkovetz DF. Claudins at the gate: determinants of renal epithelial tight junction paracellular permeability. *Am J Physiol Renal Physiol* 2006 Mar;290(3):F572-F579.
- [103] Umeda K, Ikenouchi J, Katahira-Tayama S, Furuse K, Sasaki H, Nakayama M, et al. ZO-1 and ZO-2 independently determine where claudins are polymerized in tight-junction strand formation. *Cell* 2006 Aug 25;126(4):741-54.
- [104] Shin K, Margolis B. ZONing out tight junctions. *Cell* 2006 Aug 25;126(4):647-9.
- [105] Niessen CM. Tight junctions/adherens junctions: basic structure and function. *J Invest Dermatol* 2007 Nov;127(11):2525-32.
- [106] Chung S, Andrew DJ. The formation of epithelial tubes. *J Cell Sci* 2008 Nov 1;121(Pt 21):3501-4.
- [107] Nelson WJ. Adaptation of core mechanisms to generate cell polarity. *Nature* 2003 Apr 17;422(6933):766-74.
- [108] Mostov K, Su T, ter Beest M. Polarized epithelial membrane traffic: conservation and plasticity. *Nat Cell Biol* 2003 Apr;5(4):287-93.
- [109] Gassama-Diagne A, Yu W, ter Beest M, Martin-Belmonte F, Kierbel A, Engel J, et al. Phosphatidylinositol-3,4,5-trisphosphate regulates the formation of the basolateral plasma membrane in epithelial cells. *Nat Cell Biol* 2006 Sep;8(9):963-70.
- [110] Martin-Belmonte F, Gassama A, Datta A, Yu W, Rescher U, Gerke V, et al. PTEN-mediated apical segregation of phosphoinositides controls epithelial morphogenesis through Cdc42. *Cell* 2007 Jan 26;128(2):383-97.
- [111] Martin-Belmonte F, Mostov K. Regulation of cell polarity during epithelial morphogenesis. *Curr Opin Cell Biol* 2008 Apr;20(2):227-34.
- [112] Baas AF, Kuipers J, van der Wel NN, Batlle E, Koerten HK, Peters PJ, et al. Complete polarization of single intestinal epithelial cells upon activation of LKB1 by STRAD. *Cell* 2004 Feb 6;116(3):457-66.
- [113] Wang Q, Chen XW, Margolis B. PALS1 regulates E-cadherin trafficking in mammalian epithelial cells. *Mol Biol Cell* 2007 Mar;18(3):874-85.
- [114] Munson M, Novick P. The exocyst defrocked, a framework of rods revealed. *Nat Struct Mol Biol* 2006 Jul;13(7):577-81.

- [115] Wang S, Hsu SC. The molecular mechanisms of the mammalian exocyst complex in exocytosis. *Biochem Soc Trans* 2006 Nov;34(Pt 5):687-90.
- [116] Kreitzer G, Schmoranz J, Low SH, Li X, Gan Y, Weimbs T, et al. Three-dimensional analysis of post-Golgi carrier exocytosis in epithelial cells. *Nat Cell Biol* 2003 Feb;5(2):126-36.
- [117] Ang AL, Taguchi T, Francis S, Folsch H, Murrells LJ, Pypaert M, et al. Recycling endosomes can serve as intermediates during transport from the Golgi to the plasma membrane of MDCK cells. *J Cell Biol* 2004 Nov 8;167(3):531-43.
- [118] Hoekstra D, Tyteca D, Van IJendoorn SC. The subapical compartment: a traffic center in membrane polarity development. *J Cell Sci* 2004 May 1;117(Pt 11):2183-92.
- [119] Thompson A, Nessler R, Wisco D, Anderson E, Winckler B, Sheff D. Recycling endosomes of polarized epithelial cells actively sort apical and basolateral cargos into separate subdomains. *Mol Biol Cell* 2007 Jul;18(7):2687-97.
- [120] Harris BZ, Lim WA. Mechanism and role of PDZ domains in signaling complex assembly. *J Cell Sci* 2001 Sep;114(Pt 18):3219-31.
- [121] Mostov KE, Verges M, Altschuler Y. Membrane traffic in polarized epithelial cells. *Curr Opin Cell Biol* 2000 Aug;12(4):483-90.
- [122] Bastaki M, Braiterman LT, Johns DC, Chen YH, Hubbard AL. Absence of direct delivery for single transmembrane apical proteins or their "Secretory" forms in polarized hepatic cells. *Mol Biol Cell* 2002 Jan;13(1):225-37.
- [123] Ranganathan R, Ross EM. PDZ domain proteins: scaffolds for signaling complexes. *Curr Biol* 1997 Dec 1;7(12):R770-R773.
- [124] Mostov KE, de Bruyn KA, Deitcher DL. Deletion of the cytoplasmic domain of the polymeric immunoglobulin receptor prevents basolateral localization and endocytosis. *Cell* 1986 Nov 7;47(3):359-64.
- [125] Casanova JE, Apodaca G, Mostov KE. An autonomous signal for basolateral sorting in the cytoplasmic domain of the polymeric immunoglobulin receptor. *Cell* 1991 Jul 12;66(1):65-75.
- [126] Brewer CB, Roth MG. A single amino acid change in the cytoplasmic domain alters the polarized delivery of influenza virus hemagglutinin. *J Cell Biol* 1991 Aug;114(3):413-21.
- [127] Hunziker W, Fumey C. A di-leucine motif mediates endocytosis and basolateral sorting of macrophage IgG Fc receptors in MDCK cells. *EMBO J* 1994 Jul 1;13(13):2963-9.
- [128] Wehrle-Haller B, Imhof BA. Stem cell factor presentation to c-Kit. Identification of a basolateral targeting domain. *J Biol Chem* 2001 Apr 20;276(16):12667-74.
- [129] Matter K, Hunziker W, Mellman I. Basolateral sorting of LDL receptor in MDCK cells: the cytoplasmic domain contains two tyrosine-dependent targeting determinants. *Cell* 1992 Nov 27;71(5):741-53.
- [130] Boehm M, Bonifacino JS. Adaptins: the final recount. *Mol Biol Cell* 2001 Oct;12(10):2907-20.
- [131] Folsch H, Ohno H, Bonifacino JS, Mellman I. A novel clathrin adaptor complex mediates basolateral targeting in polarized epithelial cells. *Cell* 1999 Oct 15;99(2):189-98.
- [132] Simmen T, Honing S, Icking A, Tikkanen R, Hunziker W. AP-4 binds basolateral signals and participates in basolateral sorting in epithelial MDCK cells. *Nat Cell Biol* 2002 Feb;4(2):154-9.

- [133] Rodriguez-Boulan E, Kreitzer G, Musch A. Organization of vesicular trafficking in epithelia. *Nat Rev Mol Cell Biol* 2005 Mar;6(3):233-47.
- [134] Lisanti MP, Sargiacomo M, Graeve L, Saltiel AR, Rodriguez-Boulan E. Polarized apical distribution of glycosyl-phosphatidylinositol-anchored proteins in a renal epithelial cell line. *Proc Natl Acad Sci U S A* 1988 Dec;85(24):9557-61.
- [135] Lisanti MP, Caras IW, Davitz MA, Rodriguez-Boulan E. A glycopospholipid membrane anchor acts as an apical targeting signal in polarized epithelial cells. *J Cell Biol* 1989 Nov;109(5):2145-56.
- [136] Scheiffele P, Peranen J, Simons K. N-glycans as apical sorting signals in epithelial cells. *Nature* 1995 Nov 2;378(6552):96-8.
- [137] Yeaman C, Le Gall AH, Baldwin AN, Monlauzeur L, Le Bivic A, Rodriguez-Boulan E. The O-glycosylated stalk domain is required for apical sorting of neurotrophin receptors in polarized MDCK cells. *J Cell Biol* 1997 Nov 17;139(4):929-40.
- [138] Marmorstein AD, Csaky KG, Baffi J, Lam L, Rahaal F, Rodriguez-Boulan E. Saturation of, and competition for entry into, the apical secretory pathway. *Proc Natl Acad Sci U S A* 2000 Mar 28;97(7):3248-53.
- [139] Vagin O, Kraut JA, Sachs G. Role of N-glycosylation in trafficking of apical membrane proteins in epithelia. *Am J Physiol Renal Physiol* 2009 Mar;296(3):F459-F469.
- [140] Kamiya Y, Kamiya D, Yamamoto K, Nyfeler B, Hauri HP, Kato K. Molecular basis of sugar recognition by the human L-type lectins ERGIC-53, VIPL, and VIP36. *J Biol Chem* 2008 Jan 25;283(4):1857-61.
- [141] van Meer G, Simons K. Lipid polarity and sorting in epithelial cells. *J Cell Biochem* 1988 Jan;36(1):51-8.
- [142] Simons K, Ikonen E. Functional rafts in cell membranes. *Nature* 1997 Jun 5;387(6633):569-72.
- [143] Lipardi C, Nitsch L, Zurzolo C. Detergent-insoluble GPI-anchored proteins are apically sorted in fischer rat thyroid cells, but interference with cholesterol or sphingolipids differentially affects detergent insolubility and apical sorting. *Mol Biol Cell* 2000 Feb;11(2):531-42.
- [144] Allan VJ, Thompson HM, McNiven MA. Motoring around the Golgi. *Nat Cell Biol* 2002 Oct;4(10):E236-E242.
- [145] Yildiz A, Tomishige M, Vale RD, Selvin PR. Kinesin walks hand-over-hand. *Science* 2004 Jan 30;303(5658):676-8.
- [146] Apodaca G. Endocytic traffic in polarized epithelial cells: role of the actin and microtubule cytoskeleton. *Traffic* 2001 Mar;2(3):149-59.
- [147] Sheff DR, Kroschewski R, Mellman I. Actin dependence of polarized receptor recycling in Madin-Darby canine kidney cell endosomes. *Mol Biol Cell* 2002 Jan;13(1):262-75.
- [148] Horslen SP, Quarrell OW, Tanner MS. Liver histology in the arthrogryposis multiplex congenita, renal dysfunction, and cholestasis (ARC) syndrome: report of three new cases and review. *J Med Genet* 1994 Jan;31(1):62-4.
- [149] Hershkovitz D, Mandel H, Ishida-Yamamoto A, Chefetz I, Hino B, Luder A, et al. Defective lamellar granule secretion in arthrogryposis, renal dysfunction, and cholestasis syndrome caused by a mutation in VPS33B. *Arch Dermatol* 2008 Mar;144(3):334-40.
- [150] Saxen L. Organogenesis of the kidney. Cambridge University Press: Cambridge, UK; 1987.

- [151] Karp SL, Molitoris SA. Establishment of polarity in epithelial cells of the developing nephron. In: Vize PD, Woolf AS, Bard J, editors. The kidney: From normal development to congenital disease. Burlington, MA: Academic Press; 2003. p. 211.
- [152] Zorn AM. Liver development. Cambridge, MA: Harvard University Press; 2008.
- [153] Chintala S, Novak EK, Spornyak JA, Mazurchuk R, Torres G, Patel S, et al. The Vps33a gene regulates behavior and cerebellar Purkinje cell number. *Brain Res* 2009 Apr 17;1266:18-28.
- [154] Subramanian S, Woolford CA, Jones EW. The Sec1/Munc18 protein, Vps33p, functions at the endosome and the vacuole of *Saccharomyces cerevisiae*. *Mol Biol Cell* 2004 Jun;15(6):2593-605.
- [155] Togneri J, Cheng YS, Munson M, Hughson FM, Carr CM. Specific SNARE complex binding mode of the Sec1/Munc-18 protein, Sec1p. *Proc Natl Acad Sci U S A* 2006 Nov 21;103(47):17730-5.
- [156] Richardson SC, Winistorfer SC, Poupon V, Luzio JP, Piper RC. Mammalian late vacuole protein sorting orthologues participate in early endosomal fusion and interact with the cytoskeleton. *Mol Biol Cell* 2004 Mar;15(3):1197-210.
- [157] Fields S, Song O. A novel genetic system to detect protein-protein interactions. *Nature* 1989 Jul 20;340(6230):245-6.
- [158] Gietz RD, Triggs-Raine B, Robbins A, Graham KC, Woods RA. Identification of proteins that interact with a protein of interest: applications of the yeast two-hybrid system. *Mol Cell Biochem* 1997 Jul;172(1-2):67-79.
- [159] Lippincott-Schwartz J, Patterson GH. Development and use of fluorescent protein markers in living cells. *Science* 2003 Apr 4;300(5616):87-91.
- [160] Hammond AT, Glick BS. Raising the speed limits for 4D fluorescence microscopy. *Traffic* 2000 Dec;1(12):935-40.
- [161] Patterson GH, Lippincott-Schwartz J. A photoactivatable GFP for selective photolabeling of proteins and cells. *Science* 2002 Sep 13;297(5588):1873-7.
- [162] Satoh A, Wang Y, Malsam J, Beard MB, Warren G. Golgin-84 is a rab1 binding partner involved in Golgi structure. *Traffic* 2003 Mar;4(3):153-61.
- [163] Burguete AS, Fenn TD, Brunger AT, Pfeffer SR. Rab and Arl GTPase family members cooperate in the localization of the golgin GCC185. *Cell* 2008 Jan 25;132(2):286-98.
- [164] Rappoport JZ, Lipkowitz MS, Abramson RG. Localization and topology of a urate transporter/channel, a galectin, in epithelium-derived cells. *Am J Physiol Cell Physiol* 2001 Dec;281(6):C1926-C1939.
- [165] Ward ES, Martinez C, Vaccaro C, Zhou J, Tang Q, Ober RJ. From sorting endosomes to exocytosis: association of Rab4 and Rab11 GTPases with the Fc receptor, FcRn, during recycling. *Mol Biol Cell* 2005 Apr;16(4):2028-38.
- [166] Cresawn KO, Potter BA, Oztan A, Guerriero CJ, Ihrke G, Goldenring JR, et al. Differential involvement of endocytic compartments in the biosynthetic traffic of apical proteins. *EMBO J* 2007 Aug 22;26(16):3737-48.
- [167] Deborde S, Perret E, Gravotta D, Deora A, Salvarezza S, Schreiner R, et al. Clathrin is a key regulator of basolateral polarity. *Nature* 2008 Apr 10;452(7188):719-U3.
- [168] Peplowska K, Markgraf DF, Ostrowicz CW, Bange G, Ungermann C. The CORVET tethering complex interacts with the yeast Rab5 homolog Vps21 and is involved in endo-lysosomal biogenesis. *Dev Cell* 2007 May;12(5):739-50.

- [169] Hennies HC, Kornak U, Zhang H, Egerer J, Zhang X, Seifert W, et al. Gerodermia osteodysplastica is caused by mutations in SCYL1BP1, a Rab-6 interacting golgin. *Nat Genet* 2008 Dec;40(12):1410-2.
- [170] Knust E, Bossinger O. Composition and formation of intercellular junctions in epithelial cells. *Science* 2002 Dec 6;298(5600):1955-9.
- [171] Suzuki T, Oiso N, Gautam R, Novak EK, Panthier JJ, Suprabha PG, et al. The mouse organellar biogenesis mutant buff results from a mutation in Vps33a, a homologue of yeast vps33 and Drosophila carnation. *Proc Natl Acad Sci U S A* 2003 Feb 4;100(3):1146-50.
- [172] Schonthaler HB, Fleisch VC, Biehlmaier O, Makhankov Y, Rinner O, Bahadori R, et al. The zebrafish mutant lbk/vam6 resembles human multisystemic disorders caused by aberrant trafficking of endosomal vesicles. *Development* 2008 Jan;135(2):387-99.
- [173] Matter K, Balda MS. Functional analysis of tight junctions. *Methods* 2003 Jul;30(3):228-34.
- [174] Aijaz S, Sanchez-Heras E, Balda MS, Matter K. Regulation of tight junction assembly and epithelial morphogenesis by the heat shock protein Apg-2. *Bmc Cell Biology* 2007 Nov 20;8.
- [175] Desclozeaux M, Venturato J, Wylie FG, Kay JG, Joseph SR, Le HT, et al. Active Rab11 and functional recycling endosome are required for E-cadherin trafficking and lumen formation during epithelial morphogenesis. *Am J Physiol Cell Physiol* 2008 Aug;295(2):C545-C556.
- [176] Liebner S, Kniesel U, Kalbacher H, Wolburg H. Correlation of tight junction morphology with the expression of tight junction proteins in blood-brain barrier endothelial cells. *Eur J Cell Biol* 2000 Oct;79(10):707-17.
- [177] Dawe HR, Smith UM, Cullinane AR, Gerrelli D, Cox P, Badano JL, et al. The Meckel-Gruber Syndrome proteins MKS1 and meckelin interact and are required for primary cilium formation. *Human Molecular Genetics* 2007 Jan 15;16(2):173-86.
- [178] Cavey M, Rauzi M, Lenne PF, Lecuit T. A two-tiered mechanism for stabilization and immobilization of E-cadherin. *Nature* 2008 Jun 5;453(7196):751-U2.
- [179] Wakabayashi Y, Kipp H, Arias IM. Transporters on demand: intracellular reservoirs and cycling of bile canalicular ABC transporters. *J Biol Chem* 2006 Sep 22;281(38):27669-73.
- [180] Wakabayashi Y, Lippincott-Schwartz J, Arias IM. Intracellular trafficking of bile salt export pump (ABCB11) in polarized hepatic cells: Constitutive cycling between the canalicular membrane and Rab11-positive endosomes. *Molecular Biology of the Cell* 2004 Jul;15(7):3485-96.
- [181] Maly IP, Landmann L. Bile duct ligation in the rat causes upregulation of ZO-2 and decreased colocalization of claudins with ZO-1 and occludin. 2008 Mar;129(3):289-99.
- [182] Colegio OR, Van Itallie C, Rahner C, Anderson JM. Claudin extracellular domains determine paracellular charge selectivity and resistance but not tight junction fibril architecture. *Am J Physiol Cell Physiol* 2003 Jun;284(6):C1346-C1354.
- [183] Hadj-Rabia S, Baala L, Vabres P, Hamel-Teillac D, Jacquemin E, Fabre M, et al. Claudin-1 gene mutations in neonatal sclerosing cholangitis associated with ichthyosis: a tight junction disease. *Gastroenterology* 2004 Nov;127(5):1386-90.
- [184] Furuse M, Hata M, Furuse K, Yoshida Y, Haratake A, Sugitani Y, et al. Claudin-based tight junctions are crucial for the mammalian epidermal barrier: a lesson from claudin-1-deficient mice. *J Cell Biol* 2002 Mar 18;156(6):1099-111.

- [185] Yang J, Weinberg RA. Epithelial-mesenchymal transition: at the crossroads of development and tumor metastasis. *Dev Cell* 2008 Jun;14(6):818-29.
- [186] Nüsslein-Volhard C, Dahm R. Zebrafish. 1st ed. New York: Oxford University Press; 2002.
- [187] Spence R, Gerlach G, Lawrence C, Smith C. The behaviour and ecology of the zebrafish, *Danio rerio*. *Biol Rev Camb Philos Soc* 2008 Feb;83(1):13-34.
- [188] Bradbury J. Small fish, big science. *PLoS Biol* 2004 May;2(5):E148.
- [189] Matthews RP, Plumb-Rudewiez N, Lorent K, Gissen P, Johnson CA, Lemaigre F, et al. Zebrafish vps33b, an ortholog of the gene responsible for human arthrogryposis-renal dysfunction-cholestasis syndrome, regulates biliary development downstream of the onecut transcription factor hnf6. *Development* 2005 Dec;132(23):5295-306.
- [190] Farber SA, Pack M, Ho SY, Johnson ID, Wagner DS, Dosch R, et al. Genetic analysis of digestive physiology using fluorescent phospholipid reporters. *Science* 2001 May 18;292(5520):1385-8.
- [191] Matthews RP, Lorent K, Russo P, Pack M. The zebrafish onecut gene hnf-6 functions in an evolutionarily conserved genetic pathway that regulates vertebrate biliary development. *Dev Biol* 2004 Oct 15;274(2):245-59.
- [192] Eastham KM, McKiernan PJ, Milford DV, Ramani P, Wyllie J, van't Hoff W, et al. ARC syndrome: an expanding range of phenotypes. *Arch Dis Child* 2001 Nov;85(5):415-20.
- [193] Yehezkeley-Schildkraut V, Munichor M, Mandel H, Berkowitz D, Hartman C, Eshach-Adiv O, et al. Nonsyndromic paucity of interlobular bile ducts: report of 10 patients. *J Pediatr Gastroenterol Nutr* 2003 Nov;37(5):546-9.
- [194] Pulipparacharuvil S, Akbar MA, Ray S, Sevrioukov EA, Haberman AS, Rohrer J, et al. Drosophila Vps16A is required for trafficking to lysosomes and biogenesis of pigment granules. *Journal of Cell Science* 2005 Aug 15;118(16):3663-73.
- [195] Zhu GD, Salazar G, Zlatic SA, Fiza B, Doucette MM, Heilman CJ, et al. SPE-39 family proteins interact with the HOPS complex and function in lysosomal delivery. *Mol Biol Cell* 2009 Feb;20(4):1223-40.
- [196] Rieder SE, Emr SD. A novel RING finger protein complex essential for a late step in protein transport to the yeast vacuole. *Mol Biol Cell* 1997 Nov;8(11):2307-27.
- [197] Golling G, Amsterdam A, Sun Z, Antonelli M, Maldonado E, Chen W, et al. Insertional mutagenesis in zebrafish rapidly identifies genes essential for early vertebrate development. *Nat Genet* 2002 Jun;31(2):135-40.
- [198] Yu JF, Fukamachi S, Mitani H, Hori H, Kanamori A. Reduced expression of vps11 causes less pigmentation in medaka, *Oryzias latipes*. *Pigment Cell Res* 2006 Dec;19(6):628-34.
- [199] Sadler KC, Amsterdam A, Soroka C, Boyer J, Hopkins N. A genetic screen in zebrafish identifies the mutants vps18, nf2 and foie gras as models of liver disease. *Development* 2005 Aug;132(15):3561-72.
- [200] Maldonado E, Hernandez F, Lozano C, Castro ME, Navarro RE. The zebrafish mutant vps18 as a model for vesicle-traffic related hypopigmentation diseases. *Pigment Cell Res* 2006 Aug;19(4):315-26.
- [201] Wang Z, Edwards JG, Riley N, Provance DW, Jr., Karcher R, Li XD, et al. Myosin Vb mobilizes recycling endosomes and AMPA receptors for postsynaptic plasticity. *Cell* 2008 Oct 31;135(3):535-48.

- [202] Muller T, Hess MW, Schiefermeier N, Pfaller K, Ebner HL, Heinz-Erian P, et al. MYO5B mutations cause microvillus inclusion disease and disrupt epithelial cell polarity. *Nat Genet* 2008 Oct;40(10):1163-5.
- [203] Perl AK, Wilgenbus P, Dahl U, Semb H, Christofori G. A causal role for E-cadherin in the transition from adenoma to carcinoma. *Nature* 1998 Mar 12;392(6672):190-3.
- [204] Guilford P, Hopkins J, Harraway J, McLeod M, McLeod N, Harawira P, et al. E-cadherin germline mutations in familial gastric cancer. *Nature* 1998 Mar 26;392(6674):402-5.

PEER REVIEWED PUBLICATIONS

1. Dawe HR, Smith UM, **Cullinane AR**, Gerrelli D, Cox P, Badano JL, Blair-Reid S, Sriram N, Katsanis N, Attie-Bitach T, Afford SC, Copp AJ, Kelly DA, Gull K, Johnson CA. The Meckel-Gruber Syndrome proteins MKS1 and meckelin interact and are required for primary cilium formation. Hum Mol Genet 2007 Jan; 16(2):173 – 186.
2. Khaddour R, Smith U, Baala L, Martinovic J, Clavering D, Shaffiq R, Ozilou C, **Cullinane A**, Kyttälä M, Shalev S, Audollent S, d'Humières C, Kadhon N, Esculpavit C, Viot G, Boone C, Oien C, Encha-Razavi F, Batman PA, Bennett CP, Woods CG, Roume J, Lyonnet S, Génin E, Le Merrer M, Munnich A, Gubler MC, Cox P, Macdonald F, Vekemans M, Johnson CA, Attié-Bitach T; SOFFOET. Spectrum of MKS1 and MKS3 mutations in Meckel syndrome: a genotype-phenotype correlation. Human Mutat 2007 May; 28(5): E523-E536
3. Taha D, Khider A, **Cullinane AR**, Gissen P. A novel VPS33B mutation in an ARC syndrome patient presenting with osteopenia and fractures at birth. Am J Med Genet A 2007 Dec 1;143A(23):2835-7.
4. **Cullinane AR**, Straatman-Iwanowska A, Seo JK, Ko JS, Song KS, Gizewska M, et al. Molecular investigations to improve diagnostic accuracy in patients with ARC syndrome. Hum Mutat 2009 Feb;30(2):E330-E337.
5. **Cullinane AR**, Straatman-Iwanowska A, Zaucker A, Wakabayashi Y, Bruce C, Luo G, Rahman F, Gurakan F, Utine E, Ozkan TB, Denecke J, Vukovic J, Di Rocco M, Mandel H, Cangul H, Matthews R, Thomas SG, Rappoport J, Arias IM, Wlburg H, Knisely AS, Kelly DA, Mueller F, Maher ER, Gissen P. Polarin is critical to epithelial polarization and apical junction complex formation. Nat Genet 2009 (In review)